UC Riverside
UC Riverside Electronic Theses and Dissertations

Title
A Lipid Biomarker Investigation Tracking the Evolution of the Neoproterozoic Marine Biosphere and the Rise of Eukaryotes

Permalink
https://escholarship.org/uc/item/86p25344

Author
Zumberge, John Alexander

Publication Date
2019

Peer reviewed|Thesis/dissertation

eScholarship.org Powered by the California Digital Library
University of California

UNIVERSITY OF CALIFORNIA
RIVERSIDE

A Lipid Biomarker Investigation Tracking the Evolution of the Neoproterozoic Marine Biosphere and the Rise of Eukaryotes

A Dissertation submitted in partial satisfaction
of the requirements for the degree of

Doctor of Philosophy

in

Geological Sciences

by

John Alexander Zumberge

September 2019

Dissertation Committee:
Dr. Gordon Love, Chairperson
Dr. Tim Lyons
Dr. Andrey Bekker

Copyright by
John Alexander Zumberge
2019

The Dissertation of John Alexander Zumberge is approved:

Committee Chairperson

University of California, Riverside

ACKNOWLEDGEMENTS

This doctoral research was predominantly supported by grants from the NASA Astrobiology Institute and NASA Exobiology programs. Additional support came from grants and fellowships from the American Association of Petroleum Geologists, the National Science Foundation and Royal Dutch Shell. Thank you to my dissertation committee, including Tim Lyons, Andrey Bekker and my advisor Gordon Love for their helpful advice, constructive feedback and insightful questions. I'm deeply indebted to Gordon's commitment to my progress as an organic geochemist during my time at UC-Riverside. Gordon's guidance, expert advice and enduring patience over the years were critical to my success and his role as both a mentor and friend made the whole process an immensely enjoyable endeavor. Thanks to all the collaborators that were involved, in one way or another, in my various projects through the years. I especially thank Paco Cárdenas who supplied over 100 sponge specimens and was critical to my research involving the steroid assays of modern Porifera. Thanks to Don Rocher for holding onto and supplying vital Chuar Group rocks as well as Noah Planavsky, Alan Rooney, Susanna Porter and Carol Dehler who guided me during field work when collecting samples from the Visingsö Group (Sweden). Assistance with sample preparation, biomarker analyses, conference goings, beer drinking and the many other general situations/circumstances that arise in the life of a grad student in the Love Lab came from Megan Rohrssen, Carina Lee, Aaron Martinez, Kelden Pehr, Rosemarie Bisquera and Nathan Marshall. Special acknowledgment to the 'golf crew' over the years including Dalton Hardisty, Charlie Diamond, Scott Evans, Gordon Love and 'Uncle' Rob Raiswell. You all provided me with

an integral outlet from school/work and instead of stressing about lab work or impending manuscript deadlines, you forced me to focus on the many problems with my golf swing! Huge thanks to GeoMark Research for allowing me to continue to work remotely from the "GeoMark Riverside Division". I look forward to being back in the office full time. Lastly, thanks to my family, near and far, for all the love and support over the years. Mom, Dad, Tori, Kayte, Jed, Jaclyn, Jackson, Ashely, Iles, Julie, Steve, Marilyn, Lexi, Porter, Alyssa, Evelyn, Eloise, Jace and Zoey. Special thanks to Mom & Dad for all you have done for me: from the encouragement and support in all facets of my life to the endless love. You two set the bar high for the kind of parent I strive to be with my own kids.

DEDICATION

To Ashley,

for dropping everything and moving to Riverside, for the boundless support,

for the laughter, for the patience, for all the late nights, for raising our

beautiful children, for always telling me I can do it, for the love

and

to Evelyn and Zoey (and all my future babies),

for showing me a new meaning to life and the word ‘joy’,

for always putting a smile on my face, for the love.

ABSTRACT OF THE DISSERTATION

A Lipid Biomarker Investigation Tracking the Evolution of the Neoproterozoic Marine Biosphere and the Rise of Eukaryotes

by

John Alexander Zumberge

Doctor of Philosophy, Graduate Program in Geological Sciences
University of California, Riverside, September 2019
Dr. Gordon Love, Chairperson

The transition from simple, single cellular eukaryotes to more complex multicellular organisms, including animals, represents one of life's most profound evolutionary advances. Yet, the temporal dynamics and natural selection pressures which led to the evolution of animals remains enigmatic. A detailed investigation of the evolutionary history of the domain Eukaryota can offer valuable insights and an enhanced resolution of this momentous transition. This includes an examination of pivotal events such as the first recorded appearance of eukaryotes in the microfossil record during the Mesoproterozoic, versus the temporal lag associated with the rise of eukaryotes to ecological dominance during the Neoproterozoic Era as shown by lipid biomarker geochemistry. Steroid biomarkers were employed to track the evolution, expansion, diversification and the ecological rise of eukaryotes relative to bacteria in the geologic rock record.

We used multiple lipid biomarker proxies to track the evolution of the marine biosphere with carefully selected sedimentary rock targets that had undergone a mild thermal history

and that were not adversely affected by organic contaminants. The findings described here include i) the oldest kerogen-bound sterane signals ever reported from thermally well-preserved Tonian rocks (ca. 780-729 Ma.), prior to the first (Sturtian) Neoproterozoic glaciation event, ii) a new C_{30} ancient metazoan steroid biomarker recovered from the Cryogenian-Ediacaran rock record and classification of the equivalent sterol precursors in a number of modern demosponge species and iii) a systematic investigation of the biosynthetic pathways involved in the production of conventional and unconventional sponge sterols that yield attractive ancient biomarker targets. The unique analytical approaches in this study, including the analysis of covalently bound biomarkers recovered from the kerogen-bound phase of organic matter, push the boundary of our understanding of the timing of eukaryotic diversification and expansion in the Neoproterozoic marine biosphere. For modern sponge taxa, a combination of intact sterol analyses and hydrogenation of sterols to sterane derivatives allowed for the identification of several novel C_{29} and C_{30} ancient sponge sterane biomarkers and provided a better understanding of the steroid biosynthetic pathways and product-precursor relationships.

Table of Contents

Chapter 1: Demosponge Steroid Biomarker 26-methylstigmastane (26-mes) Provides Evidence for Neoproterozoic Animals

Abstract 1

Introduction 2

Geologic Setting 4

Materials and Methods 6

Catalytic hydropyrolysis of sponge biomass 6

Lipid biomarker analysis of ancient rocks and oils 7

Extraction and analysis of sterols in modern sponge cells 9

Instrumental Analysis 11

Sterane analysis using Multiple Reaction Monitoring-Gas Chromatography-Mass Spectrometry (MRM-GC-MS) 11

Sterane analysis by GC-triple quadrupole (QQQ)-MS 12

Results and Discussion 14

Structural identification of 26-mes and self-consistency checks for syngenicity 18

26-mes steranes as specific biomarkers for demosponges 29

HyPy of extant biomass allows screening of the sterane core content of steroids 33

The enigma of strongylosterol and host sponge association in some previous reports 36

Jaspis wondoensis versus *Rhabdastrella wondoensis* 37

Plausible sponge sterane biomarkers predating the Sturtian glaciation (>717 Ma) 38

Conclusions.....40

Chapter 2: Free and Kerogen-Bound Biomarkers from Tonian Sedimentary Rocks Record Abundant Eukaryotes in Early Neoproterozoic Marine Communities

Abstract 51

Introduction.....52

Materials and Methods.....59

Samples 59

Extraction and separation.....61

Hydropyrolysis (HyPy) of extracted rocks 62

Instrumental Analysis 64

Multiple Reaction Monitoring-Gas Chromatography-Mass Spectrometry (MRM-GC-MS) of the saturate hydrocarbon fractions 64

Full scan GC-MS of the saturate and aromatic hydrocarbons 65

GC-MS/MS (QQQ) of the saturate and aromatic hydrocarbons 65

Results and Discussion 66

Total organic carbon (TOC) and thermal maturity 66

Total aliphatic hydrocarbon distributions 70

Sterane assemblages in the Chuar Group.....71

Sterane assemblages in the Visingsö Group 78

Hopane assemblages in the Chuar and Visingsö Groups.....81

Sterane/Hopane relationships.....87

Conclusions.....92

Chapter 3: Patterns of Steroid Synthesis in Modern Demosponges and the Identification of Novel Fossil Sterane Biomarker Targets

Abstract.....95

Introduction.....96

Materials and Methods.....102

Sponges (Porifera) 102

Extraction and analysis of sterols in modern sponge cells 103

Catalytic hydropyrolysis of sponge biomass 104

Instrumental Analysis 107

Extracted sterol analysis by Gas Chromatography-Mass Spectrometry (GC-MS) 107

Sterane analysis using Multiple Reaction Monitoring-GC-MS (MRM-GC-MS) 108

Sterane analysis by GC-triple quadrupole-MS (GC-QQQ-MS).....109

Background.....111

Sterol biosynthesis in eukaryotes.....111

Other putative sources of Neoproterozoic-Cambrian C_{30} steranes 114

Sponge sterol naming conventions 115

Sterol identification and elucidation from the solvent extracts of extant sponges.....116

Results and Discussion 119

Sterol distributions from the solvent extracts of extant sponges 119

Conventional sterol biosynthesis patterns in Porifera.....120

Unconventional sterol biosynthesis patterns in Porifera.....126

Other putative occurrences of unconventional sterols in Eukaryota 130

Inferred unconventional sterols in the geologic rock record 130

Relative abundances of unconventional sterols in Porifera 131

Consistency within the sterol assays of the same species across multiple localities 132

Sequence-selective bioalkylation patterns in Porifera 134

Sterane distributions from the HyPy pyrolysates of extant sponges.....137

Novel C_{29}-C_{31} steranes found in this study.....142

Conclusions.....146

References.....149

Appendix A: Mass Spectral Library for Sterols Identified in this Study.....166

Appendix B: HyPy-generated Sterane Distributions of Sponge Biomass.....195

Appendix C: Sterol (TMS-ether) Distributions of Sponge Biomass.....228

List of Figures

Figure 1. C_{30} sterane assemblages: modern demosponges vs the ancient rock record 15

Figure 2. Conversion of 26-mes precursor sterols to 26-mes 17

Figure 3. Sterol distributions of four different specimens of *R. globostellata*.....17

Figure 4. Mass spectrum of Stelliferasterol from *R. globostellata* PC922 19

Figure 5. Mass spectra of 26-methylstigmastane and stigmastane 20

Figure 6. Ediacaran/Early Cambrian oils & modern sponge co-elution experiments 21

Figure 7. Increased C_{30} sterane resolution via slow GC temperature ramp.....22

Figure 8. Extracted sterols vs HyPy-generated steranes for G. hentscheli (GhII).....35

Figure 9. Co-occurrence of 24-ipc & 26-mes during the Neoproterozoic-Cambrian.....39

Figure 10. Proterozoic Biomarker Record 55

Figure 11. Tonian paleography 59

Figure 12. Thermal maturity differences between the Chuar & Visingsö Groups 68

Figure 13. Total ion chromatograms for samples from the Chuar & Visingsö Groups....71

Figure 14. *Free* vs *kerogen-bound* sterane distributions from SWE2 (Chuar Gp.) 73

Figure 15. C_{28} sterane distributions in the Chuar & Visingsö Groups.....74

Figure 16. C_{30} sterane distributions in the Chuar & Visingsö Groups.....77

Figure 17. Solvent extractable (*free*) steranes from v12 (Visingsö Gp.) 79

Figure 18. Solvent extractable (*free*) hopanes from SWE2 vs. v12.....84

Figure 19. TOC vs. S/H in the Chuar & Visingsö Groups.....90

Figure 20. Proof of concept for sterol to sterane conversions 99

Figure 21. C_{30} sterane vs. sterene distributions after HyPy of sponge biomass 106

List of Figures (cont.)

Figure 22. C_{27}-C_{30} sterane distributions: MRM-GC-MS vs. GC-QQQ-MS.....110

Figure 23. C-24 alkylation criteria in unconventional sterols.....128

Figure 24. Sterol distributions of six specimens of *R. globostellata* 133

Figure 25. Conventional & Unconventional C_{29} & C_{30} steranes 143

Figure 26. Resolution of five different C_{30} steranes from MRM-GC-MS.....144

List of Tables

Table 1. Biomarker ratios (*free*) from the South Oman Salt Basin.....43

Table 2. Biomarker ratios (*kerogen-bound*) from the South Oman Salt Basin.....45

Table 3. C_{30} steranes in a selection of rocks and oils through geologic time.....46

Table 4. Taxonomic assignments for the sponges used in Chapter 1 47

Table 5. HyPy-generated C_{30} sterane patterns from sponges used in Chapter 1.....48

Table 6. GC retention time offsets for various αααR steranes using MRM-GC-MS 50

Table 7. TOC & Rock-Eval pyrolysis data for the Chuar & Visingsö Groups.....70

Table 8. Maturity & source sensitive biomarker ratios for the Chuar & Visingsö. 85

Table 9. Taxonomic affinities of the Porifera used in Chapter 3 119

Table 10. Unsaturation patterns in downstream sterols when 26-methylenecholesterol was the primary sterol constituent 121

Table 11. HyPy-generated sterane distributions from sponge biomass 138

List of Charts

Chart I. Conventional vs Unconventional vs Unsaturated steroid side chains.....42

Chart II. Conventional vs Unconventional steroid side chains (extended).....118

Chart III. Steroid core nuclei 118

Chart IV. C_{27}-C_{30} conventional sterane biomarkers.....118

List of Schemes

Scheme I. Steroid Biosynthetic Pathway: Squalene to Lanosterol/Cycloartenol.....125

Scheme II. Conventional Steroid Biosynthetic Pathway 125

Scheme III. Unconventional Steroid Biosynthetic Pathway.....136

CHAPTER 1: DEMOSPONGE STEROID BIOMARKER 26-METHYLSTIGMASTANE (26-MES) PROVIDES EVIDENCE FOR NEOPROTEROZOIC ANIMALS

Abstract

Sterane biomarkers preserved in ancient sedimentary rocks hold promise for tracking the diversification and ecological expansion of eukaryotes. The earliest proposed animal biomarkers from demosponges (Demospongiae) are recorded in a ca. 100-Myr-long sequence of Neoproterozoic-Cambrian marine sedimentary strata from the Huqf Supergroup, South Oman Salt Basin. This C_{30} sterane biomarker, informally known as 24-isopropylcholestane (24-ipc), possesses the same carbon skeleton as sterols found in some modern-day demosponges. However, this evidence is controversial because 24-ipc is not exclusive to demosponges since 24-ipc sterols are found in trace amounts in some pelagophyte algae. Here we report a new fossil sterane biomarker that co-occurs with 24-ipc in a suite of late Neoproterozoic-Cambrian sedimentary rocks and oils, which possesses a rare hydrocarbon skeleton that is uniquely found within extant demosponge taxa. This sterane is informally designated as 26-methylstigmastane (26-mes), reflecting the very unusual methylation at the terminus of the steroid side-chain, and is the first animal-specific sterane marker detected in the geological record which can be unambiguously linked to precursor sterols only reported from extant demosponges. These new findings strongly suggest that demosponges, and hence multicellular animals, were prominent in some late Neoproterozoic marine environments at least extending back to the Cryogenian Period.

Introduction

The transition from unicellular protists to multicellular animals constitutes one of the most intriguing and enigmatic events in the evolutionary history of life, largely due to the absence of unambiguous physical fossils for the earliest fauna. The Neoproterozoic rise of eukaryotes (Brocks et al., 2017), including demosponges (Love et al., 2009), in marine environments can be discerned from lipid biomarker records preserved in ancient sedimentary rocks which have experienced a mild thermal history. Molecular phylogenies commonly show that sponges (Porifera) are the sister group of other animals (Simion et al., 2017) and molecular evidence for Neoproterozoic animal life was first proposed based on the occurrence of unusual C_{30} demosponge-derived steranes informally known as 24-ipc steranes (24-isopropylcholestane) in sedimentary rocks and oils of that age (McCaffrey et al., 1994; Love et al., 2009). These steranes are the hydrocarbon remains of 24-isopropylcholesterols and structurally related sterols (Hofheinz & Oesterhelt 1979). The record of 24-ipc steranes commences in Cryogenian-aged sediments in South Oman (ca. 717-635 Myr (Love et al., 2009; Rooney et al., 2015)) and then occurs continuously through the Ediacaran-Cambrian formations of the Huqf Supergroup of the South Oman Salt Basin. Notably, these steroids also occur as covalently-bound constituents fixed within the immobile kerogen phase of the same rocks, which is an important confirmation that these are not younger contaminant compounds that migrated into the rocks (Love et al., 2009).

Demosponges are the only known extant taxon that can biosynthesize 24-ipc precursors as their major sterols. High relative absolute abundances of 24-ipc steranes have now been reported in many other late Neoproterozoic-early Cambrian rocks and oils (McCaffrey et al., 1994; Peters et al., 1995; Grosjean et al., 2009; Love et al., 2009; Kelly et al., 2011). These 24-ipc occurrences—if interpreted correctly—reflect an early presence of Porifera and provide a conservative minimum time estimate for the origin of animal multicellularity and the sponge body plan. Others have hypothesised that the 24-ipc steranes could be derived from unicellular animal ancestors or have an algal origin (Antcliffe 2013) since the parent sterols have been reported in trace amounts in some extant pelagophyte algae (Love et al., 2009). The claim that poribacterial sponge symbionts from the candidate phylum *Poribacteria* can make 24-ipc steroids (Siegl et al., 2011) has since been shown to be erroneous due to a genome assembly error (Love & Summons 2015; Gold et al., 2016).

Currently, two chromatographically resolvable series of ancient C_{30} steranes are known: 24-npc (24-n-propylcholestane) and 24-ipc (24-isopropylcholestane). Demosponges are the most plausible Neoproterozoic-Cambrian source of 24-npc as well as 24-ipc because both are produced by extant demosponges (Love et al., 2009). Foraminifera are another possible source of 24-npc (Grabenstatter et al., 2013). Pelagophyte algae likely account for the 24-npc steranes that are found in Devonian and younger marine sediments and their derived oils (Gold et al., 2016). Various recent findings support a pre-Ediacaran origin of animals/sponges and arguably reinforce the validity of the 24-ipc biomarker record, including: i) steroid assays and genomic analyses of extant taxa (Gold et al., 2016), which

suggest that sponges were the most likely Neoproterozoic source biota for 24-ipc steranes and ii) nuclear and mitochondrial gene molecular clock studies which consistently support a pre-Ediacaran origin of animals and Neoproterozoic demosponges (Erwin et al., 2011; dos Reis et al., 2015; Dohrmann & Wörheide 2017; Schuster et al., 2018). The discovery of other sponge biomarkers to augment the 24-ipc sterane record would greatly strengthen evidence for the presence of animals prior to the appearance of the Ediacara fauna, since the efficacy of the standalone 24-ipc sterane record for tracking early demosponges has been contested (Antcliffe 2013; Love & Summons 2015).

Geologic Setting

Huqf Supergroup, South Oman Salt Basin

The Huqf Supergroup provides one of the best preserved, most continuous successions of late Neoproterozoic through earliest Cambrian strata (ca. 713-540 Myr) within subsurface sedimentary basins of the South Oman Salt Basin (SOSB). A description of the geological settings and the different formations, with radiometric age constraints, have been described in detail previously (Grosjean et al., 2009; Love et al., 2009). Briefly, the record of both 26-mes and 24-ipc steranes commences in Cryogenian-aged sedimentary rocks of the Huqf Supergroup of the SOSB (Ghadir Manquil Formation, ca. 717-635 Myr; and more likely better constrained from Sturtian termination dates as between ca. 660 and 635 Myr) and is apparently continuous into the Early Cambrian. While a zircon age of 645 Myr reported from Lahan-1 core from dropstone-bearing siltstones does not help refine our oldest depositional age, since zircons were recovered from just 9 m below the cap dolostone and

are likely associated with the top of the Marinoan diamictite, it does support the assignment of the cap dolostone in SOSB strata as being Marinoan in age (Love et al., 2009). Furthermore, these zircons were isolated from a different drill core to our two interglacial biomarker samples so the relative stratigraphic positions of these to the zircons is uncertain. The Ghadir Manquil Fm. sediment from GM-1 core was a lime mudstone found approximately 150 meters below the base of a diamictite that we interpret as Marinoan age because of the stratigraphic position directly beneath both the Nafun Gp. sedimentary package and the underlying (Marinoan) cap carbonate. The MQR-1 sedimentary rock was a siltstone/sandstone also found below the same sedimentary units in this well.

Petroleum exploration and production activities of Petroleum Development of Oman allowed us to access numerous deep (1-5 km) sediment cores and cuttings through the Huqf Supergroup as well as oils produced from these thermally well-preserved sediments. The sediments deposited within the Ara Group are commonly called intra-salt rocks, whereas rocks deposited before, including those of the Nafun Group, are referred to as pre-salt rocks. Ara source rocks deposited in the Athel Basin are commonly referred to as Athel intra-salt rocks, as opposed to the Ara carbonate stringers.

64 SOSB source rocks were acquired in total (Tables 1 and 2) and were selected to provide extensive stratigraphic coverage of all formations of the Huqf Supergroup in SOSB. Most of the samples were cutting composites in order to more completely characterize the geochemistry of source rock intervals but some core material was also used. Rocks

analyzed had total organic contents (TOCs) of 0.2 to 11 wt.% and the sedimentary organic matter was thermally well preserved, with Hydrogen Indices (HIs) measured from Rock-Eval pyrolysis in the range of 250-700 mg/g TOC (Grosjean et al., 2009). These HI values are typical of marginal- to middle-oil window source rock maturity and SOSB rocks represent amongst the least thermally altered Neoproterozoic-Cambrian age sediments used to date for molecular biomarker work (Grosjean et al., 2009).

Material and Methods

Catalytic hydropyrolysis of sponge biomass

Continuous-flow hydropyrolysis (HyPy) experiments were performed on 30-150 mg of catalyst-loaded sponge biomass at UC-Riverside as described previously (Love et al., 2005; 2009). Freeze-dried sponge biomass was initially impregnated with an aqueous methanol solution of ammonium dioxydithiomolybdate [$(NH_4)_2MoO_2S_2$] to give a give a nominal loading of 3-10 wt.% catalyst. Ammonium dioxydithiomolybdate reductively decomposes *in situ* under HyPy conditions above 250 ^oC to form a catalytically-active molybdenum sulfide (MoS_2) phase.

The catalyst-loaded samples were heated in a stainless steel (316 grade) reactor tube from ambient temperature to 250 ^oC at 100 ^oC/min immediately followed by 250 ^oC to 460 ^oC at 8 ^oC/min while maintaining constant hydrogen pressure of ~150 bar. A hydrogen sweep gas flow rate of 6 L/min, measured at ambient temperature and pressure, through the reactor bed ensured that the residence times of volatiles generated was the order of only a few

seconds. Products were collected on a silica gel trap cooled with dry ice and recovered for subsequent fractionation using silica gel adsorption chromatography.

HyPy products (hydropyrolysates) of sponge biomass were separated by silica gel adsorption chromatography into aliphatic (alkane + alkene), aromatic and polar (or N, S, O) compounds by elution with *n*-hexane, *n*-hexane:dichloromethane (1:1 v/v) and dichloromethane:methanol (3:1 v/v), respectively. For hydropyrolysates, solvent-extracted activated copper turnings were added to concentrated solutions of aliphatic hydrocarbon fractions to remove all traces of elemental sulfur, which is formed from disproportionation of the catalyst during HyPy. Aliphatic fractions were further purified to a saturated hydrocarbon fraction by the removal of any unsaturated products (alkenes) via silver nitrate impregnated silica gel adsorption chromatography and elution with *n*-hexane.

Lipid biomarker analysis of ancient rocks and oils

Detailed methods for extraction and analysis of sedimentary rocks and oils at UCR were described previously (Rohrssen et al., 2013; 2015; Haddad et al., 2016) and data is shown in Table 3. Rock pieces were first trimmed with a water-cooled rock saw to remove outer weathered surfaces (at least a few mm thickness) and to expose a solid inner portion and sonicated in a sequence of ultrapure water, methanol, dichloromethane (DCM), and hexane before a final rinse with DCM prior to powdering and bitumen extraction. Rock fragments were powdered in a zirconia ceramic puck mill in a SPEX 8515 shatterbox, cleaned between samples by powdering two batches of fired sand (850 ^{o}C overnight) and rinsing

with the above series of solvents. Typically, 5 g of crushed rock was extracted in a CEM Microwave Accelerated Reaction System (MARS) at 100 °C in a DCM:methanol (9:1 v/v) mixture for 15 minutes. Full laboratory procedural blanks with combusted sand were performed in parallel with each batch of rocks to ensure that any background signals were negligible in comparison with biomarker analyte abundances found in the rocks (typically by at least three orders of magnitude). Saturated hydrocarbon and aromatic fractions for rock bitumens and oils were obtained by silica gel column chromatography; the saturate fractions were eluted with hexane and the aromatic fractions with DCM:hexane (1:1 v/v).

The procedures for ancient biomarker analyses from sedimentary rocks from Huqf Supergroup of the SOSB performed at MIT (results reported in Tables 1 and 2) were similar to those described above for UCR protocols, including MRM-GC-MS methods (see below) which were described in detail previously (Grosjean et al., 2009; Love et al., 2009). Analytical errors for absolute yields of individual hopanes and steranes are estimated at ± 30%. Average uncertainties in hopane and sterane biomarker ratios are ± 8% as calculated from multiple analyses of a saturated hydrocarbon fraction from AGSO and GeoMark standard oils (n = 30). Full procedural blanks with combusted sand were ran in parallel with each batch of samples to quantify any low background signal. Tables 1 and 2 contain original data from Love et al., 2009; but now also with 26-mes sterane data added. The yields and ratios verify that significant abundances of 26-mes were detected in all these samples at a similar order of magnitude abundance to those of 24-ipc steranes.

Extraction and analysis of sterols in modern sponge cells

Eighteen modern sponge samples were acquired for solvent extraction to monitor their free sterol contents as trimethylsilyl (TMS) ethers. Sponge specimens were supplied by Paco Cárdenas (Uppsala University) and Erik Sperling (Stanford University) and their colleagues; including Jean Vacelet, Ute Hentschel, Kevin Peterson, Ted Molinski, Thierry Pérez, Hans Tore Rapp, Alexander Plotkin, Jae-Sang Hong, Yusheng M. Huang, Sven Rohde, Scott Nichols, Barbara Calcinai, Jose V. Lopez, Gulia Gatti, Bartek Ciperling, João-Pedro Fonseca, Luís Magro, Francesca Azzini, Allen G. Collins and the Bedford Institute of Oceanography (Dartmouth, Canada). Sponge biomass arrived immersed in ethanol or freeze-dried. Combined ethanol washings for each sample were filtered to remove suspended particulates, concentrated into a small volume and then transferred to a pre-weighed glass vial and blown down carefully under dry N_2 gas. Freeze-dried sponge biomass was extracted via sonication for 25 minutes in DCM:methanol (3:1 v/v) to recover the total lipid extract. Multiple rounds of solvent extractions were performed, typically until no more color was observed.

Total lipid extracts (TLEs) were separated into 3 fractions, based on polarity, by gravity flow silica gel absorption chromatography. Approximately, 1-5 mg of TLE was adsorbed on the top of a 10 cm silica gel pipette column and then sequentially eluted with 1.5 column volumes of *n*-hexane (fraction 1), 2 column volumes of DCM (fraction 2) and 3 column volumes of DCM:methanol (7:3 v/v) (fraction 3). The alcohol products, including sterols, typically eluted in fraction 2 and approximately 20-50 µg of this fraction was derivatized

with 10-20 µl of bis(trimethylsilyl)trifluoroacetamide (BSTFA) in 10-20 µl of pyridine and heated at 70 ºC for 30 minutes.

Alcohol fractions were then analyzed by GC-MS as trimethylsilyl (TMS) ethers within 36 hours of derivatization in full scan mode at UC-Riverside using gas chromatography-mass spectrometry (GC-MS) on an Agilent 7890A GC system coupled to an Agilent 5975C inert MSD mass spectrometer. Sample solutions were volatilized via programmed-temperature vaporization (PTV) injection onto a DB1-MS capillary column (60 m × 0.32 mm, 0.25 µm film thickness) and helium was used as the carrier gas. The oven temperature program used for GC for the derivatized alcohol fraction consisted of an initial temperature hold at 60 °C for 2 min, followed by an increase to 150 °C at 20 °C/min, and then a subsequent increase to 325 °C at 2 °C/min and held for 20 min. Data was analyzed using ChemStation G10701CA (Version C) software, Agilent Technologies. C_{30} sterol identifications for the three 26-mes precursors (stelliferasterol (structure **B13** in CHART I), isostelliferasterol (**B14**) and strongylosterol (**B15**); plus see Fig. 2) in certain *Rhabdastrella* and *Geodia* sponge species were identified from published mass spectral features and relative retention times (Bortolotto et al., 1978; Theobald & Djerassi 1978; Theobald et al., 1978; Stoilov et al., 1986; Cho et al., 1988). Stelliferasterol was the dominant C_{30} sterol in *Rhabdastrella globostellata* (PC922), while strongylosterol, stelliferasterol and isostelliferasterol were found in *Geodia parva* (GpII).

Instrumental Analysis

Sterane analysis using Multiple Reaction Monitoring-Gas Chromatography-Mass Spectrometry (MRM-GC-MS)

Saturated hydrocarbon fractions from ancient rocks and oils as wells as from modern sponge HyPy pyrolysates were analyzed by Multiple Reaction Monitoring-Gas Chromatography-Mass Spectrometry (MRM-GC-MS) conducted at UCR on a Waters Autospec Premier mass spectrometer equipped with an Agilent 7890A gas chromatograph and DB-1MS coated capillary column (60 m x 0.25 mm, 0.25 μm film) using He for carrier gas. Typically, one microliter of a hydrocarbon fraction dissolved in hexane was injected onto the GC column in splitless injection mode. The GC temperature program consisted of an initial hold at 60 °C for 2 min, heating to 150 °C at 10 °C/min followed by heating to 320 °C at 3 °C/min and a final hold for 22 min. Analyses were performed via splitless injection in electron impact mode, with an ionization energy of 70 eV and an accelerating voltage of 8 kV. MRM transitions for C_{27}–C_{35} hopanes, C_{31}–C_{36} methylhopanes, C_{21}–C_{22} and C_{26}–C_{30} steranes, C_{30} methylsteranes and C_{19}–C_{26} tricyclic terpanes were monitored in the method used. Procedural blanks with pre-combusted sand yielded less than 0.1 ng of individual hopane and sterane isomers per gram of combusted sand (Haddad et al., 2016). Polycyclic biomarker alkanes (tricyclic terpanes, hopanes, steranes, etc.) were quantified by addition of a deuterated C_{29} sterane standard [d_4-ααα-24-ethylcholestane (20R)] to saturated hydrocarbon fractions and comparison of relative peak areas. In MRM analyses, this standard compound was detected using 404→221 Da ion transition. Cross-talk of non-sterane signal in 414→217 Da ion chromatograms from C_{30} and C_{31} hopanes was < 0.2%

of 412→191 Da hopane signal [mainly 17α,21β(H)-hopane, which is resolvable from C_{30} steranes] and <1% of the 426→191 Da signal, respectively (Rohrssen et al., 2015).

Peak identifications of sponge steranes were confirmed by comparison of retention times with an AGSO oil saturated hydrocarbon standard and with Neoproterozoic oils from Eastern Siberia (McCaffrey et al., 1994; Kelly et al., 2011) and India (Peters et al., 1995) which were reported previously to contain significant quantities of 24-isopropylcholestane and which we have now demonstrated contain significant quantities of 26-methylstigmastane (Table 3). Polycyclic biomarkers were quantified assuming equal mass spectral response factors between analytes and the d_4-C_{29}-ααα-24-ethylcholestane (20R) internal standard. Analytical errors for absolute yields of individual hopanes and steranes are estimated at ± 30%. Average uncertainties in hopane and sterane biomarker ratios are ± 8% as calculated from multiple analyses of a saturated hydrocarbon fraction prepared from AGSO and GeoMark Research standard oils (n = 30 MRM analyses).

Sterane analysis by GC-triple quadrupole (QQQ)-MS

To confirm the presence of the new 26-methylstigmastane peak and investigate the retention time of the analyte peaks compared with other C_{30} steranes (24-npc and 24-ipc), the saturated hydrocarbon fractions from sponge HyPy products and oils from Eastern Siberia and India (Table 3) were run on a different instrument employing a different GC column to that used in the MRM-GCMS instrument at UCR. GC-QQQ-MS was performed at GeoMark Research (Houston, TX) on an Agilent 7000A Triple Quad interfaced with an

Agilent 7890A gas chromatograph equipped with a J&W Scientific capillary column (DB-5MS+DG: 60 m x 0.25 mm i.d., 0.25 μm film thickness, 10 m guard column). Using helium as carrier gas, the flow was programmed from 1.2 mL/min to 3.2 mL/min. The GC oven was programmed from 40 °C (2 min) to 325 °C (25.75 min) at 4 °C/min. Saturated hydrocarbon fractions were spiked with a mixture of 7 internal standards (Chiron Routine Biomarker Internal Standard Cocktail 1). Samples were concentrated without being taken to dryness & were injected in cold splitless mode at 45 °C with the injector temperature ramped at 700 °C/min to 300 °C. The MS source was operated in EI-mode at 300 °C with ionization energy at -70 eV. A number of molecular ion to fragment transitions were monitored throughout the run; dwell time was adjusted as needed to produce 3.5 cycles/second. Exact chromatographic co-elution (with identical retention time in the C_{30} sterane analytical window) of the αααR diastereoisomer of 26-mes sterane in our ancient oils with the equivalent peak from the modern sponges was demonstrated in 414→217 Da ion transitions (the parent molecular mass to daughter fragment ion transition for regular (4-desmethyl) C_{30} sterane compounds).

Results and Discussion

Here we report the presence of a new C_{30} sterane designated 26-methylstigmastane (26-mes) in a suite of Neoproterozoic-Cambrian rocks and oils (Fig. 1, Tables 1-3). Further, we attribute this biomarker to demosponges since these are the only known organisms amongst extant taxa to produce sterols with the same carbon skeleton. The abundance of 26-mes sterane biomarkers is of comparable magnitude to 24-ipc and 24-npc (Fig. 1), although the relative proportions of the three main C_{30} sterane compounds can vary from sample to sample (Fig. 1, Tables 1 and 2, with summed C_{30} steranes being typically 1-4% of the total C_{27}-C_{30} sterane signal in South Oman rocks although higher contents >5% can also be found). Our analyses confirm the presence of 26-mes along with 24-ipc steranes in the Neoproterozoic-Cambrian rock extracts and kerogen pyrolysates from South Oman reported previously (Grosjean et al., 2009; Love et al., 2009) as well in Ediacaran-Cambrian sourced oils from Eastern Siberia (Kelly et al., 2011) and India (Peters et al., 1995), for which representative samples are shown in Fig. 1 (also, see Table 3). When 26-mes is detectable in Cryogenian to Cambrian age rocks and oils, it is found alongside both the 24-ipc and 24-npc sterane compounds. These three different sterane series constitute only a small subset of all the structural possibilities for C_{30} sterane compounds, which are feasible from adding three additional carbons to a cholestane (C_{27}) side-chain, and they correspond with three of the most commonly occurring sterane skeletons for C_{30} sterols found in extant demosponges (Fig. 1). In contrast, 26-mes abundance is typically lower or absent for the small suite of Phanerozoic oils and rocks analysed thus far but can be detected, along with 24-ipc and 24-npc, in some samples but not in the procedural blanks.

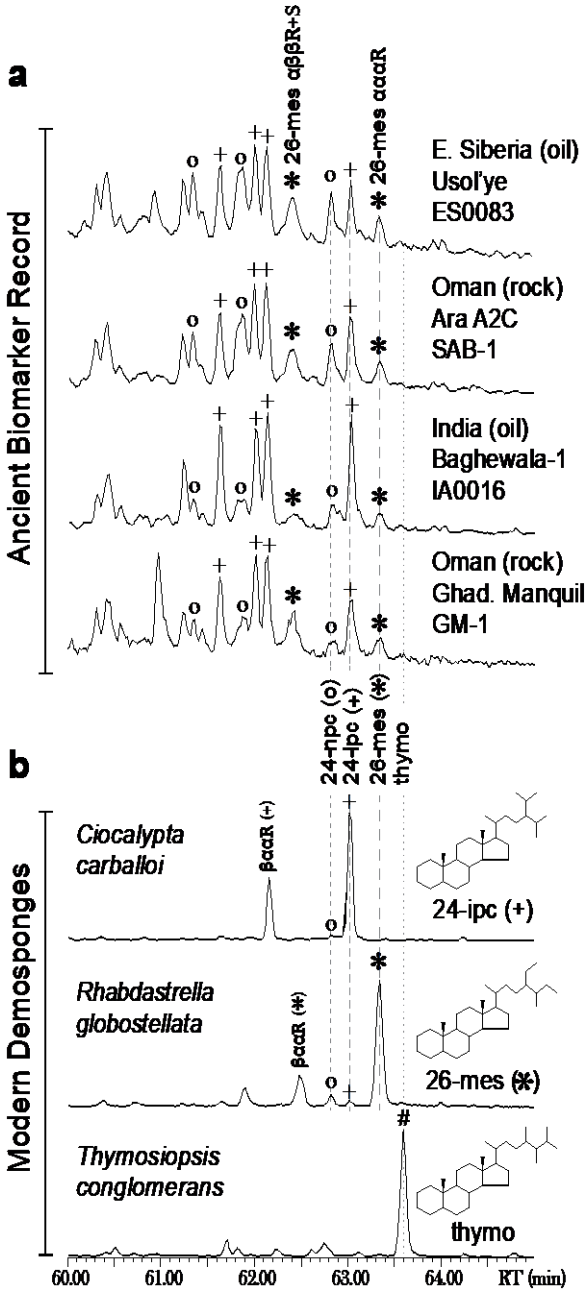

Figure 1. MRM-GC-MS ion chromatograms of C_{30} sterane distributions (414 Da → 217 Da ion transitions) from **a**. Neoproterozoic-Cambrian rock bitumens and oils and from **b**. the HyPy products from cells of three modern demosponges (see Table 4 for taxonomic assignments). Ancient samples, having undergone protracted burial and alteration, exhibit a more complex distribution of diastereoisomers compared to modern sponge biomass. Four regular sterane diastereoisomers can be found in ancient samples of oil window-maturity (αααS, αββR, αββS, αααR) while two diastereoisomers (βααR and αααR) result from laboratory hydrogenation of individual Δ^5-sterols in modern sponge biomass. The signal peak for the αααS geoisomer of 26-mes often co-elutes with other C_{30} steranes though and so this one isomer peak is usually obscured in chromatograms. Direct correlation with modern sponges uses the αααR isomer as shown by the dashed lines. The αββ(R+S) isomers show expected enhancement of signal in 414 Da → 218 Da ion chromatograms relative to ααα stereoisomers (not shown here). Examples from the Proterozoic rock record show three distinct resolvable sterane series co-occurring together (24-npc, 24-ipc and 26-mes). The rock from Ghadir Manquil Fm., South Oman, was deposited during the Cryogenian period (likely ca. 660-635 Myr ago) and is the oldest example known with 24-ipc and 26-mes co-occurring in the rock record. The new 26-mes sterane biomarker was detected in significant amounts in the South Oman rock extracts and kerogen pyrolysates reported previously (Love et al., 2009) (Tables 1 and 2). The oil from the Usol'ye Fm., Eastern Siberia, is likely Ediacaran to Early Cambrian in source age (Kelly et al., 2011) as is the Baghewala-1 oil from India (Peters et al., 1995). [24-npc(o) = 24-n-propylcholestane; 24-ipc(+) = 24-isopropylcholestane; 26-mes(*) = 26-methylstigmastane; thymo = thymosiosterane = 24,26,26'-trimethylcholestane]

To unequivocally confirm the assignment of the newly identified ancient sterane series as 26-mes, we compared the C_{30} sterane distributions of Neoproterozoic rocks and oils with sterane products derived from steroids of modern sponges comprising demosponges, hexactinellids, homoscleromorphs and calcisponges (Tables 4 and 5). We applied catalytic hydropyrolysis (HyPy), a mild reductive technique employing high pressure hydrogen, to convert sterols from sponge biomass into steranes with minimal structural and stereochemical disturbance (Love et al., 2005). Only three possible parent C_{30} sterols, with an identical side-chain skeleton, are currently known in extant taxa (Fig. 2), and these were the likely precursors to the sedimentary 26-mes described above. *Rhabdastrella globostellata* was used as a model sponge species for initial investigations since its sterols have been previously well characterized (Theobald & Djerassi 1978; Theobald et al., 1978) and it contains stelliferasterol as the major C_{30} sterol constituent, which was verified for multiple specimens in our collection (Fig. 3). We generated a simple C_{30} sterane distribution as expected from the HyPy conversion of the *R. globostellata* sterols, dominated by 26-mes stereoisomers βααR and αααR (Fig. 4). These products were used as a sterane standard to unequivocally test for presence or absence of the 26-mes biomarker in modern and ancient samples. The identification of the fossil 26-mes sterane series was verified by observing co-elution of the 5α,14α,17α(H)-20R stereoisomer with the same isomer produced from *R. globostellata* and other extant demosponges (Fig. 1). This co-elution was further confirmed using two different GC-MS techniques in two different laboratories using different GC column stationary phases.

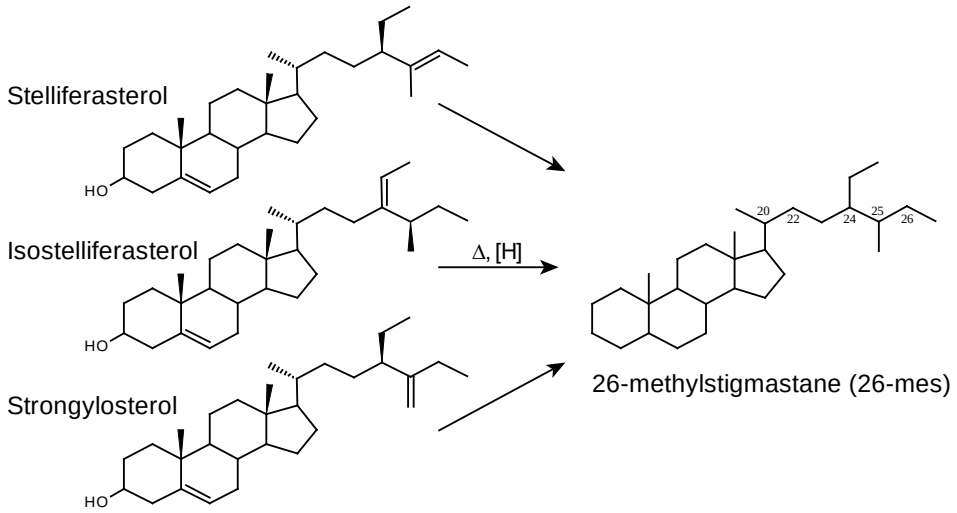

Figure 2. Chemical structures of stelliferasterol, isostelliferasterol and strongylosterol which are the three known natural sterol precursors of the 26-mes sterane biomarker (Bortolotto et al., 1978; Theobald & Djerassi 1978; Theobald et al, 1978; Stoilov et al., 1986; Cho et al., 1988). These are found only in certain demosponges but not detected in other groups of eukaryotes. Note i) the methyl-substituent at the terminal position of the sterol side chain remains preserved at C-26 in 26-mes and ii) the unusual double bond positions in the side chains of stelliferasterol and strongylosterol. The biological configuration is 20R for all three sterols, 24R for strongylosterol and stelliferasterol, and 25S for isostelliferasterol. Three stereogenic carbon atoms exist in the side-chain of 26-methylstigmastane (chirality at C-20, C-24 and C-25) but only C-20 stereoisomers give separate compounds peaks, producing up to four regular stereoisomers of 26-mes (αααS, αββR, αββS, αααR) in ancient rocks and oils as also found for other sterane compounds.

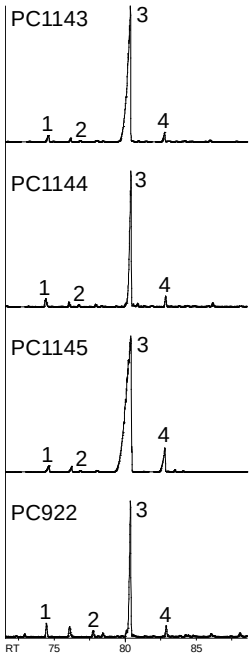

Figure 3. Total ion current (TIC) chromatograms showing the distribution of sterols in the alcohol fractions from total lipid extracts of four different specimens of *Rhabdastrella globostellata* from Taiwan. Sterols were derivatized and analyzed as trimethylsilyl (TMS) ethers. Peak assignments 1: C_{27} Δ^5 cholesterol; 2: C_{28} $\Delta^{5,25}$ codisterol; 3: C_{29} $\Delta^{5,24(28)}$-dehydroaplysterol; 4: C_{30} $\Delta^{5,25}$ stelliferasterol. See Table 4 for specimen identification.

Structural identification of 26-mes and self-consistency checks for syngenicity

The structural identification of the 26-mes sterane series was carefully verified by observing perfect co-elution of the peak signal for the αααR diastereoisomer standard produced by HyPy of extant sponges (that contained 26-mes sterols as their major C_{30} sterol constituents) with the αααR diastereoisomer resolvable within the equilibrium mixture in the Neoproterozoic rocks and oils samples (the least altered 5α,14α,17α(H)-20R or αααR sterane form; which is present as the major sterane peak in extant eukaryotes and is one of four abundant regular sterane stereoisomers in ancient geological samples (Fig. 1)). To recover the steranes generated from mild reductive conversion of sponge sterols, HyPy was performed on demosponges containing at least one of the three different known 26-mes sterol precursors (stelliferasterol, isostelliferasterol and strongylosterol; Fig. 2). In all cases for the demosponges in which stelliferasterol/isostelliferasterol/strongylosterol were the most abundant C_{30} sterol constituents, the major C_{30} sterane product was 26-mes (in the form of two resolvable peaks: βααR and a more abundant αααR isomer; e.g. Fig. 4c), facilitating a direct correlation with the ancient steranes using the αααR compound peak (Fig. 1). Various co-injection experiments with subsequent analysis with MRM-GC-MS show conclusively that the αααR sterane product generated by HyPy conversion of these modern sponges exactly matches the αααR isomer from the new sterane series found in the Neoproterozoic-Cambrian rocks and oils and that this is 26-methylstigmastane beyond any reasonable doubt (Figs. 4-7).

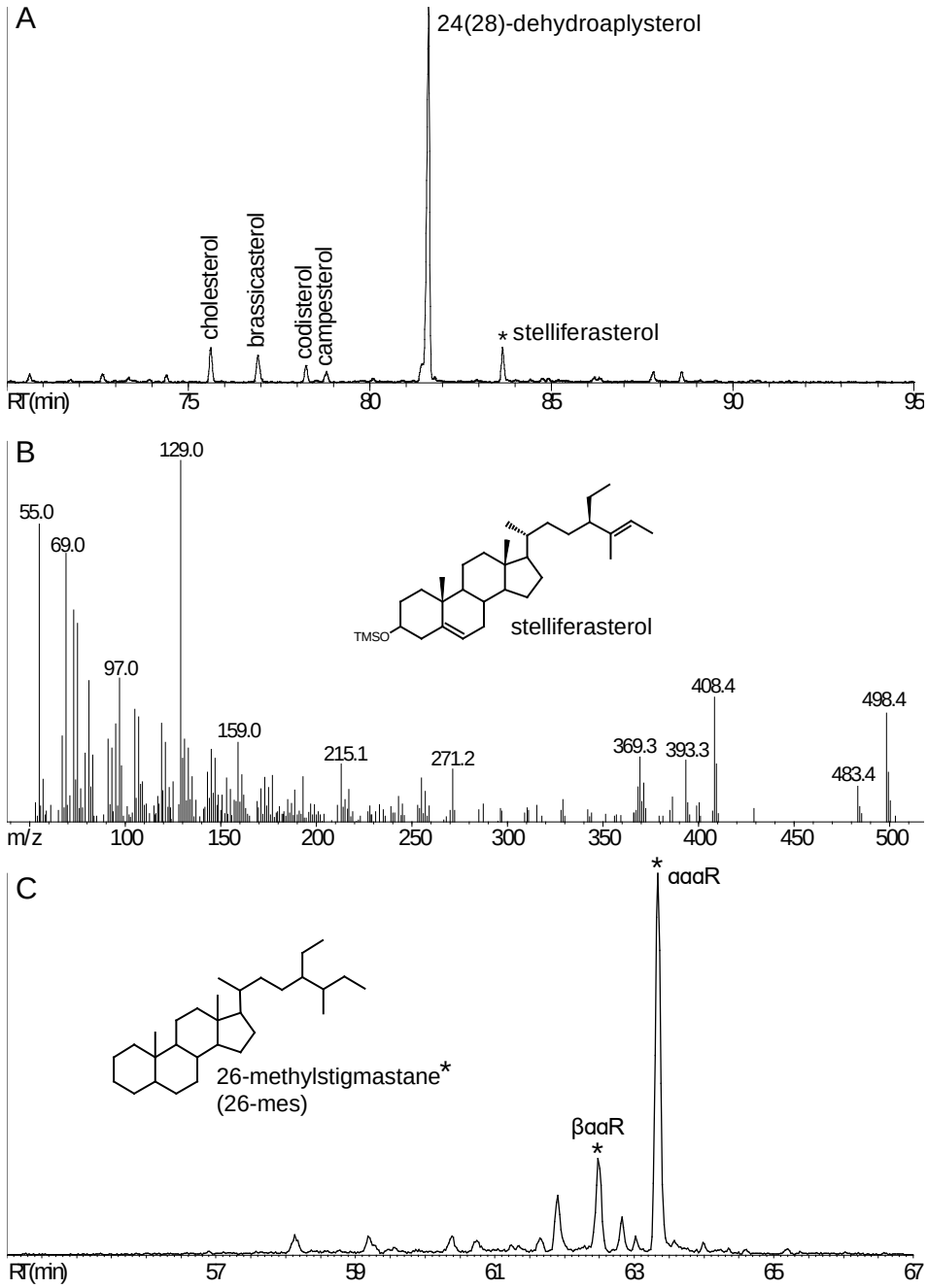

Figure 4. A. Selected ion chromatogram (m/z 129) from GCMS of a sponge sterol extract shows the sterol distributions (as TMS ethers) of *Rhabdastrella globostellata* PC922 and **B.** the associated mass spectrum of the main C_{30} sterol, stelliferasterol (*). Major fragment ions and fragment ion abundances for stelliferasterol from our sponge *R. globostellata* PC922 are in close agreement with previously published spectra of stelliferasterol (Theobald & Djerassi 1978; Theobald et al., 1978; Cho et al., 1988), and prior full spectroscopic characterization confirm its structure and stereochemistry as 26-methylstigmasta-5,25(26)-dien-3b-ol which yields **C.** 26-methylstigmastane (βααR and αααR) as the dominant C_{30} sterane from HyPy; MRM-GC-MS 414→217 ion Da transition.

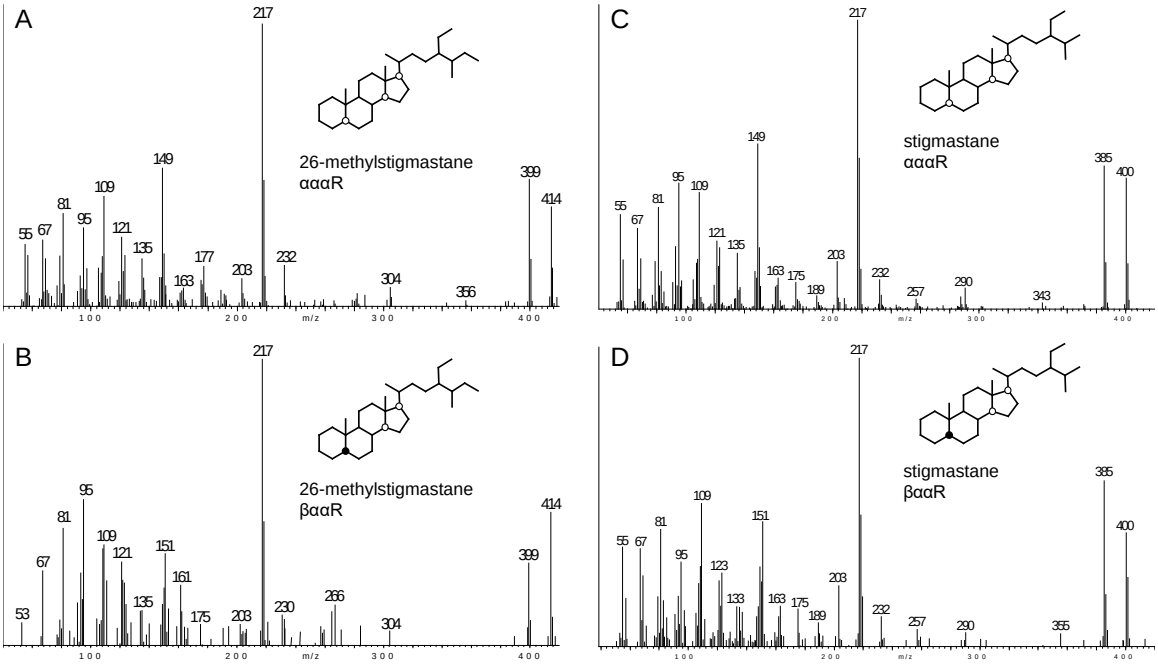

Figure 5. Mass spectra of the two major sterane isomers (5β,14α,17α(H),20R; βααR and 5α,14α,17α(H),20R; αααR) of stigmastane and 26-mes generated from HyPy of modern sponges (Table 5). Mass spectra **A** and **C** show characteristic fragment patterns of αααR isomers of 26-mes and stigmastane from GC-MS using electron ionization (70 eV), respectively. Mass spectra **B** and **D** show characteristic fragment patterns of βααR 26-mes and stigmastane, respectively, and exhibit elevated 151 Da relative to 149 Da fragment response for the βααR stereoisomer for both compounds, as expected. Designation of α (below the plane) and β (above the plane) hydrogen configurations are shown using open and closed circles, respectively.

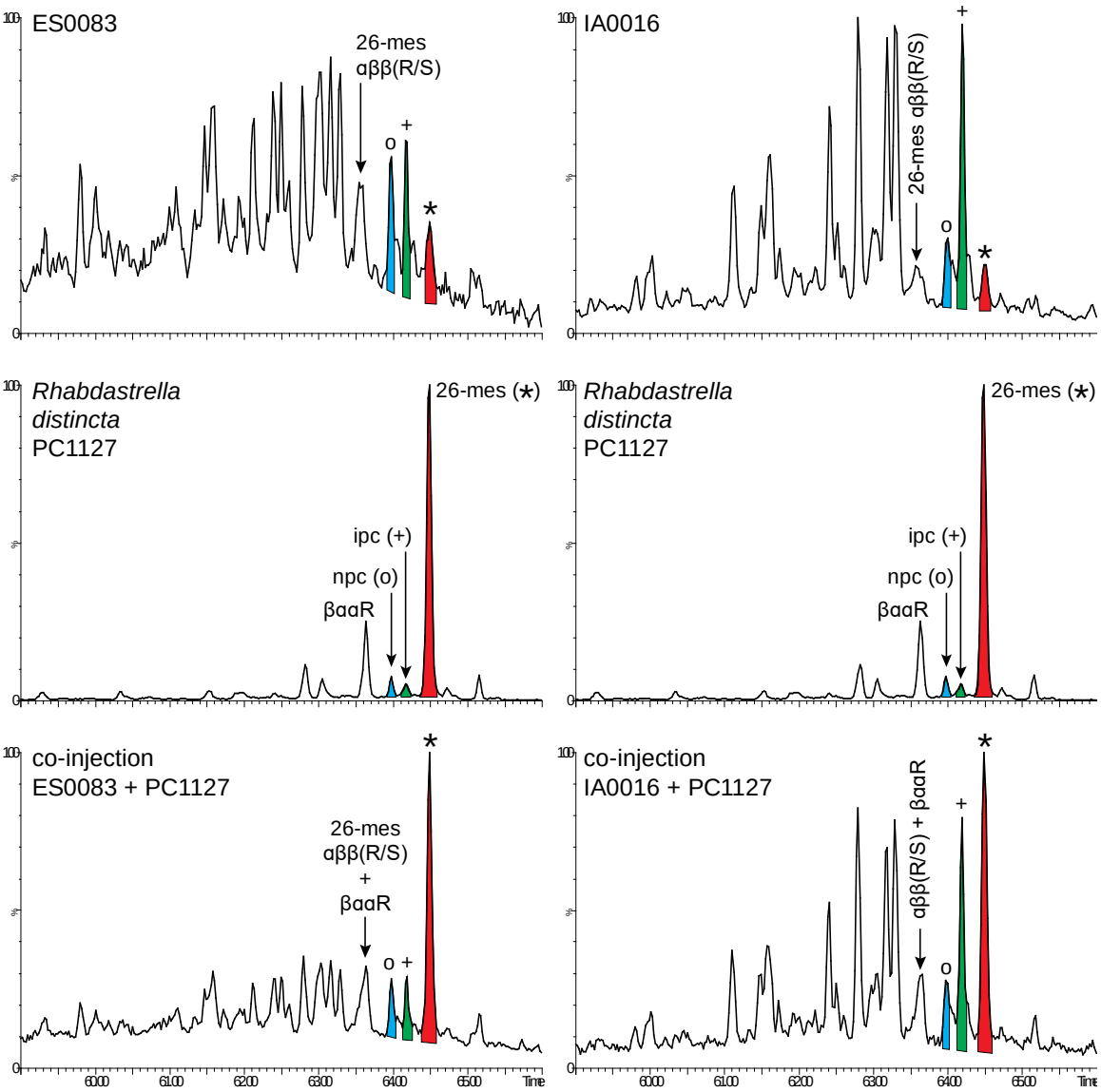

Figure 6. MRM-GC-MS (414→217 Da) chromatograms of (*top*) two Ediacaran-Cambrian oils with different C_{30} sterane distributions that show a mature/geologic distribution of regular sterane isomers (αααS, αββR, αββS, αααR) and (*middle*) a sponge from our dataset that produces 26-mes as its major C_{30} sterane with an immature distribution of sterane isomers (only βααR and αααR) (see Tables 3 and 4 for sample info). The (*bottom*) co-injection of the immature sterane series from the sponge with the mature sterane series from the two oils confirms the presence of 26-mes in rock bitumens and oils ranging from Cryogenian to Early Cambrian in age (red 26-mes αααR peak becomes greatly enhanced). Consistent with first principle elution patterns, this co-injection experiment shows that the immature 26-mes βααR peak elutes slightly *after* the mature 26-mes αββ(R+S) doublet as a right shoulder peak; a feature similar to our observations for other sterane compounds (e.g. stigmastane and 24-ipc). C_{30} sterane series assignments: 24-npc (o/blue peak); 24-ipc (+/green peak); 26-mes (*/red peak).

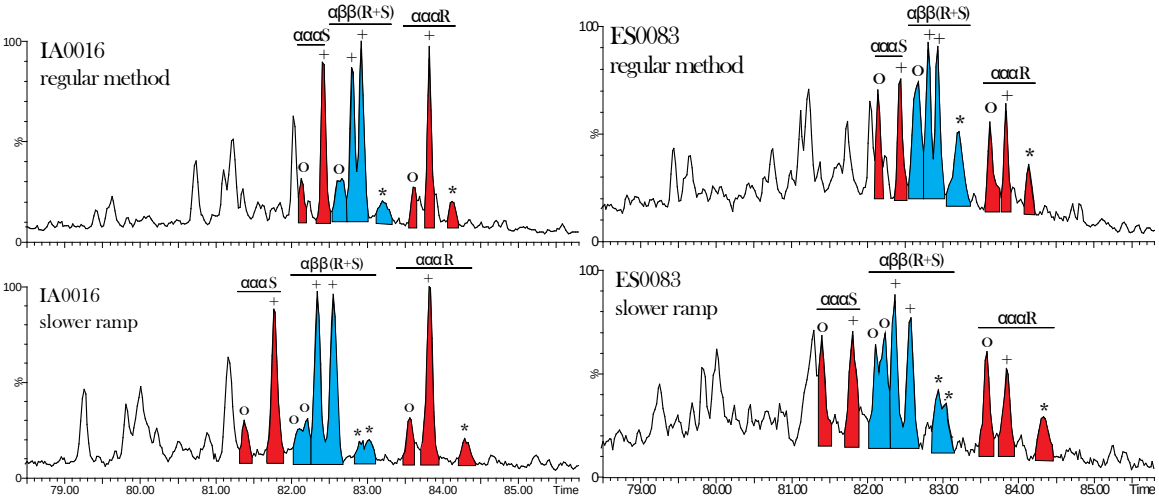

Figure 7. MRM-GC-MS (414→217 Da) chromatograms of the C_{30} regular sterane distributions for two Ediacaran-Cambrian oils used in this study employing two different heating methods (see Table 3 for sample details). The regular method (*top*) with a temperature ramp of 3 °C/min to 320 °C results in only weakly resolved αββ(R+S) peaks for *both* 24-npc and 26-mes. A revised GC method (*bottom*) with a slower temperature ramp of 2 °C/min to 320 °C greatly enhances the separation of the αββ(R+S) doublet for *both* 24-npc and 26-mes. C_{30} sterane series assignments: 24-npc (o); 24-ipc (+); 26-mes (*). Blue shaded peaks; αββ(R+S) stereoisomers. Red shaded peaks; ααα(S+R) stereoisomers.

From a large set of modern sponges (Table 4) used for investigation in our study, we identified *Rhabdastrella globostellata* (specimen PC922, Tables 4 and 5) as a model system for a 26-mes sterol producing organisms since it contains one dominant C_{30} sterol that can be unambiguously identified as stelliferasterol (Theobald & Djerassi 1978; Theobald et al., 1978; Cho et al., 1988) as well as lower amounts of isostelliferasterol (although this Great Barrier reef sponge was mistakenly called *Jaspis stellifera* in these classic papers, the identity of the sponge was later confirmed as *Rhabdastrella globostellata* from detailed sponge taxonomy (Kennedy 2000)). The *Rhabdastrella globostellata* (specimen PC922, along with others from Taiwan) from our collection contains $\Delta^{24(28)}$-dehydroaplysterol (**B11**) as the main sterol constituent, as we confirmed (Figs. 3 and 4), which is the known biosynthetic C_{29} sterol precursor of stelliferasterol, isostelliferasterol and strongylosterol (Stoilov et al., 1986). **B11** is also found as the major sterol which makes appreciable amounts of two other 26-mes precursor sterols: stelliferasterol and isostelliferasterol (Cho et al., 1988). Strongylosterol was first reported many years ago as the main sterol constituent of the sponge *Strongylophora* (aka *Petrosia*) *durissima* (Bortolotto et al., 1978; Stoilov et al., 1986).

Stelliferasterol has undergone complete structural and stereochemical elucidation and the NMR and mass spectral details were published previously (Theobald & Djerassi 1978; Theobald et al., 1978; Cho et al., 1988). The basic biosynthetic pathway which requires a concerted triple bioalkylation of the cholesterol (**B1**) sidechain has been studied in detail. Stelliferasterol has been confirmed as 26-methylstigmasta-5,25(26)E-dien-3b-ol which

contains 26-methylstigmastane as the basic sterane skeleton (Fig. 2). The efficacy of the HyPy systematics for the reductive conversion of sterols to steranes with minimal structural and stereochemical alteration has been previously demonstrated unequivocally from decades of prior work using model sterol compounds and algal cultures from the published literature (Love et al., 2005; 2009; Sephton et al., 2005; Meredith et al., 2006). So, the major C_{30} sterane products from HyPy conversion of PC922 sponge biomass is undoubtedly 26-methylstigmastane (see Fig. 1, 3 and 4). The proof of concept for sterol to sterane conversions via HyPy of sponge biomass is consistent across C_{27}-C_{30} sterol and stanol compound classes. We have observed that aplysterols/dehydroaplysterols yield aplysterane (βααR and αααR isomers; **A7**; Table 5), 24-methylenecholesterol yields ergostane (βααR and αααR isomers; **A2**), 24-ipc sterols yield 24-ipc steranes (βααR and αααR isomers; **A5**; Fig. 1) and thymosiosterol (**C12**) yields thymosiosterane (αααR only since there is no double bond at C-5 and 5α(H) is the configuration in the sterol precursor; **A8**; Fig. 1).

The co-elution of the 5α,14α,17α(H)-20R (αααR) diastereoisomer was confirmed by two different GC-MS techniques performed independently in two different laboratories. Using 414→217 Da ion transitions to detect regular (4-desmethyl) C_{30} steranes, MRM-GC-MS was performed at UCR on a 60 m capillary column with a DB-1MS stationary phase while QQQ-MS was performed at GeoMark Research on a 60 m column with a DB-5MS stationary phase (see **Materials and Methods**). With both GC columns, the 26-mes (**A10**) series elutes later than both the 24-npc (**A4**) and 24-ipc (**A5**) sterane series. The

chromatographic elution order of the different C_{30} sterane compounds (see Fig. 1 and Table 6) is consistent with chromatographic first principles: compounds with all three additional carbon atoms positioned in the interior of the sterane side-chain at position C-24 (i.e. 24-npc and 24-ipc) will elute *before* compounds with extra carbons in terminal sites (i.e. 26-mes and thymosiosterane). Since 26-mes contains two extra mid-chain carbons through an ethyl-substituent at C-24 and a terminal methyl-substituent at C-26, the predicted elution time is between 24-ipc (no extra terminal carbon) and thymosiosterane (two terminal methyl groups both attached at C-26), as is observed (Fig. 1, Table 6). Three series of C_{30} steranes are present (24-npc, 24-ipc and now 26-mes) in Neoproterozoic rocks and oils whereas thymosiosterane has not been confirmed as yet from the geological record (Fig. 1). Additionally, partially resolved peaks for the αββR and αββS diastereoisomer forms of ancient 26-mes steranes correctly eluted with the retention times predicted for C_{30} steranes; near but immediately before the immature βααR diastereoisomer from the sponge HyPy products, also consistent with their identities as 26-mes diastereoisomers (Fig. 6).

Other than the 24-ipc steranes, no other diagnostic animal molecular biomarkers have been applied to the geological record, till now, that are resolvable from the conventional steroids found as abundant membrane lipids of extant microbial eukaryotes. This is surprising but largely reflects only an emerging knowledge concerning the variety, abundance and taxonomic distributions of unconventional steroids made predominantly or exclusively by animals that can be preserved as detectable and resolvable ancient sterane markers. Other recalcitrant lipids could expand the molecular biomarker repertoire significantly in the

search for early animal fossil evidence. Reactive functional moieties, particularly alkene and alcohol groups, associated with sterols do not survive the protracted processes of sedimentary diagenesis and catagenesis and so any diagnostic structural features must be preserved over hundreds of millions of years of burial as an integral part of the recalcitrant hydrocarbon core structure. Animal steroids containing unusually alkylated side-chains offer a high potential in this regard, since a subset of demosponges are known to make a diverse array of these unconventional steroids as secondary metabolites (Kerr & Baker 1991). 26-mes steroids are such an example of "unconventional" steroids which possess distinctive methylation at the terminus of the steroid sidechain (**A10**), and other structural varieties of these steroids represent promising targets for novel animal markers being detected in the ancient geological record. As more demosponge genomes and transcriptomes are sequenced, future studies may reveal an evolutionary phylogeny for key enzymes involved in biosynthesis of steroids with unusual extended side-chains (i.e. **A8** and **A9**).

The parallel analysis of kerogen-bound products, containing abundant covalently bound 24-ipc and 26-mes (Table 2), alongside conventional solvent-extractable biomarkers (Table 1) adds significant confidence that these sponge biomarkers are indigenous and syngenetic with the host sediment and have not simply migrated from other, possibly younger, strata. The bound biomarker pool exhibits a slightly less mature distribution of hopanes and steranes than the corresponding solvent extracts for any particular rock, including noticeably less amounts of rearranged hopanes and sterane isomers, such as

neohopanes and diasteranes (Murray et al., 1998; Love et al., 2005). This distinguishes the HyPy products from any residual rock bitumen components which may have escaped solvent extraction or any migrated petroleum and confirms that the HyPy-generated biomarkers were predominantly covalently-linked into kerogen. Furthermore, the kerogen-bound biomarker distributions confirm that kerogen was largely formed early during stages of diagenesis. It is an important self-consistency check that confirms that the three series of C_{30} sterane compounds detected (24-npc, 24-ipc and 26-mes) are genuine Neoproterozoic-Cambrian biomarker compounds and we can rule out any significant contaminant contributions.

In order to better constrain the taxonomic distribution of 26-mes, we supplemented literature reports with targeted analyses of extant sponges using HyPy to directly convert sterols into steranes (Table 5). Species of *Rhabdastrella* and *Geodia* both produced appreciable amounts of 26-mes after the reductive conversion of sterols to steranes via HyPy treatment (1-9% of total $C_{27\text{-}30}$ steranes, Table 5). Apart from *Geodia hentscheli*, which only makes conventional sterols for which alkylation is restricted to the C-24 position, 26-mes was the predominant C_{30} sterane product in our *Rhabdastrella* and *Geodia* specimens. Molecular phylogenetic results indicate these species are closely related within Geodiidae (order Tetractinellida). Additionally, we also detected trace amounts of 26-mes steranes along with 24-ipc and 24-npc in four species of *Aplysina* and *Verongula* (order Verongiida) and one species of *Cymbaxinella* (order Agelasida) (Table 5). No 26-mes precursors were detected in a *Jaspis* sp., where stelliferasterol and isostelliferasterol were

supposedly originally discovered (Theobald & Djerassi 1978; Theobald et al., 1978). This is consistent with the belief that the Great Barrier Reef '*Jaspis stellifera*' specimens were mis-identified and were in fact *Rhabdastrella globostellata* (Kennedy 2000). Our HyPy results for three specimens of *R. globostellata* confirmed that 26-mes sterol precursors were present, as well as in two other *Rhabdastrella* species. Other than the Geodiidae, another known major source of 26-mes steroids is *Petrosia* (*Strongylophora*) cf. *durissima* (Bortolotto et al., 1978) (order Haplosclerida) which can synthesize strongylosterol as its dominant single sterol (Fig. 2). As not all demosponges make 26-mes, Geodiidae and *P. (S.)* cf. *durissima* may have retained the ancestral capacity to make terminally methylated C_{30} steroids as major membrane lipids, which has been lost in other demosponge groups.

Our new findings of 26-mes production in *Geodia*, *Rhabdastrella*, *Aplysina* (aspiculate), *Verongula* (aspiculate) and *Cymbaxinella* species suggest that a wider range of demosponge groups might possibly make 26-mes, as well as other terminally methylated steroids, but have not yet been identified. These demosponge species and others can make various unusual C_{29} and C_{30} sterols with terminal methylation in the side-chain. For example, *Thymosiopsis conglomerans* (order Chondrillida) makes a distinctive C_{30} sterol (Vacelet et al., 2000) yielding a different sterane skeleton which has not been detected in the ancient record (Fig. 1). The finding of this extra terminal carbon atom in a variety of sterols from diverse extant demosponges suggests that the capability for 26-methylated sterol side-chains likely has a deep origin within the clade. In the case of both 24-ipc (Love et al., 2009) and 26-mes (this study), the ability to make these sterols is phylogenetically widespread within demosponges. Notably, the known extant demosponge species which

contain 26-mes as the dominant hydrocarbon core of their C_{30} steroids are different from those that make 24-ipc as major steroids. Specifically, the demosponge family Halichondriidae (*Ciocalypta (=Collocalypta), Halichondria*, *Epipolasis),* and the genus *Topsentia* make 24-ipc amongst their most abundant sterols (Love & Summons 2015) while 24-ipc constitutes >99% of sterols in *Cymbastella coralliophila* (=*Pseudoaxynissa* sp. in the original publication), family Axinellidae (Hofheinz & Oesterhelt 1979).

26-mes steranes as specific biomarkers for demosponges

Unlike the case for 24-isopropylcholesterol (**B5**) and related 24-ipc sterols with different unsaturation patterns which have been found in trace amounts in some (but not all) published sterol assays from pelagophyte algae (Love et al., 2009; Love & Summons 2015), no plausible precursor sterols for 26-methylstigmastane have been reported in any extant taxa *other than* from a subset of demosponges. This is despite decades of research in lipid natural products and detailed sterol assays of all major groups of algae (Volkman 1986; 2003; Volkman et al., 1994; 1998; Love et al., 2005; Kodner et al., 2008; Giner et al., 2009) and unicellular animal outgroups (Kodner et al., 2008; Gold et al., 2016). In contrast to demosponges, previous investigations into the sterol constituents of 20 hexactinellid sponges and 20 calcarean sponges did not reveal the presence of any unconventional steroid structures with unusual side-chain chemistry (Blumenberg et al., 2002; Hagernann et al., 2008) and the authors concluded that the main sterols in hexactinellids were derived predominantly from dietary uptake. Nor did we find any detectable 26-mes steranes, even in trace amounts, in this study from MRM-GC-MS

analysis of the HyPy products of a hexactinellid sponge, two homoscleromorphs and a calcisponge (Table 5).

There has been no report of appropriate 26-mes precursor sterols from any eukaryote lineage, other than from demosponges, despite the finding of these three C_{30} sterol compounds going back 40 years. These sterols (stelliferasterol, isostelliferasterol and strongylosterol) were discovered and their structures and stereochemistries were characterized in detail (Bortolotto et al., 1978; Theobald & Djerassi 1978; Theobald et al., 1978). Mass spectra and other spectroscopic attributes were clearly described and published in these papers. If 26-mes precursor sterols were significant sterol constituents of other eukaryotic lineages, then it is puzzling why no reports have followed these papers through this 40-year time lapse given that the information needed to identify these was published and available in established chemistry journals.

More steroid assays are needed on heterotrophic protists, animal outgroups (e.g. Kodner et al., 2008; Gold et al., 2016) and other classes of sponges (e.g. Blumenberg et al., 2002; Hagernann et al., 2008) but an important feature of all these sterol distributions is already recognized. Namely, that no other sponge class (other than the demosponges) or unicellular animal outgroup contains unconventional steroid structures possessing unusual side-chain chemistry (such as terminal methyl groups) of any variety. Only an array of conventional sterols with common straight chain alkylated sidechains (hydrogen, methyl, ethyl, or

propyl substituents at C-24) have thus far been found in hexactinellid sponges, calcarean sponges and unicellular animal outgroups.

Our results show that certain species of demosponges from genera *Rhabdastrella* and *Geodia* (family Geodiidae, order Tetractinellida), from shallow tropical to deep arctic waters, make significant amounts of the appropriate precursor sterols with methylation at C-26 in the sterol side-chain amongst their major C_{30} sterols (Bortolotto et al., 1978; Theobald & Djerassi 1978; Theobald et al., 1978; Stoilov et al., 1986) and correspondingly generated 26-mes as their major C_{30} steranes from HyPy treatment (Table 5; Figs. 3 and 4). The three precursor sterols (Fig. 2) for 26-methylstigmatane are stelliferasterol (**B13**), isostelliferasterol (**B14**) and strongylosterol (**B15**). Additionally, we found low but detectable amounts of 26-mes in HyPy products (Table 5) from species within genera *Aplysina* and *Verongula* (family Aplysinidae, order Verongiida) as well as one species from genus *Cymbaxinella* (order Agelasida). This suggests that there are likely more demosponge species, within these orders or from different taxonomic groups, that can produce terminally alkylated sterols.

A diverse array of unconventional steroids found in demosponges may reflect necessary membrane structural modifications that accompanied the divergence of this class of poriferans (Hofheinz & Oesterhelt 1979; Itoh et al., 1983; Rambabu et al., 1987; McCaffrey et al., 1994). The precise role that these unusual sterols, with structural modifications to the side-chain or steroid nucleus, serve in demosponge cell membranes is admittedly not

known but it has been suggested that they may (i) fulfill a purely structural role by providing improved conformational alignment of cell membrane molecules, including other unusual sponge lipids and proteins, or alternatively, (ii) be involved in modulating a variety of physiological regulatory processes (Lawson et al., 1988). Similarly, the synthesis of steroids in sponges is not fully understood despite decades of research into sponge natural products and the sterols may be derived from one of (or a combination of) three end-member sources: i) synthesized by the host sponge *de novo,* ii) by-products of unique symbiotic relationships between the sponge and specific microbes that it hosts and iii) obtained from dietary uptake and/or are alteration products from a primary stock of sterols. Our view is that the uniformity of unsaturation patterns (double bond positions) across the major sterol constituents in the sponge extracts suggests a host control on the overall assemblage of downstream sterols, though some upstream sterol precursors may be routed from the diet rather than exclusively made *de novo* by the host. This is particularly pertinent to side-chain chemistry and demosponges are now thought to contain "promiscuous" SMT genes that allow them to modify the sterol side-chain (Gold et al., 2016).

From a comprehensive database of steroid assays performed on extant organisms from decades of lipid research, alongside our targeted assays here, 26-mes precursor sterols are found only in certain demosponges (Bortolotto et al., 1978; Theobald & Djerassi 1978; Theobald et al., 1978) but have never been yet reported to our knowledge from any other group of eukaryotes. This evidence of absence includes for diverse groups of algae (Volkman 2003; Love et al., 2005; Kodner et al., 2008), hexactinellid sponges

(Blumenberg et al., 2002; this study), calcisponges (Hagernann et al., 2008; Love et al., 2009; this study), homoscleromorphs (this study), and unicellular animal outgroups (Gold et al., 2016). Indeed, only steroids possessing conventional side-chains (with methyl, ethyl or propyl- groups or a hydrogen substituent at C-24) have been reported for other sponge classes, heterotrophic protists and these unicellular animal outgroups (Blumenberg et al., 2002; Hagernann et al., 2008; Grabenstatter et al., 2013; Gold et al., 2016), but not steroids with unconventional side-chains of any variety (CHART I). Thus, the finding of 26-mes together with the 24-ipc steranes in Neoproterozoic rocks and oils is most parsimoniously explained by an origin from demosponges living in marine settings.

HyPy of extant biomass allows screening of the sterane core content of steroids

Continuous-flow HyPy was used to reductively convert sterols (and any other functionalized steroids) from sponge cells into steranes (and some sterenes) to facilitate comparison of extant and fossil lipids in the same analytical window. HyPy generation of extant biomass is a useful and rapid means of assessing the diversity and relative abundance of lipid hydrocarbon skeletons (Love et al., 2005; 2009). The key features of the HyPy methodology ensure that covalent bonds can be cleaved at the lowest possible temperatures in the heating cycle (typically between 250 ^{o}C and 450 ^{o}C) and a high hydrogen sweep gas flowrate continuously flushes products from the hot zone of the reactor bed, minimizing rearranged by-product compounds. This combination of factors results in excellent preservation of structural and stereochemical features of hydrocarbon products in comparison to other analytical pyrolysis techniques. Cholesterol (**B1**), cholestanol and

other lipid model compounds were previously investigated under the standardized HyPy conditions to monitor the level of side-chain cleavage and stereochemical rearrangement during pyrolysis (Meredith et al., 2006). The amount of side-chain scission which occurred was found to be very low while excellent retention of the biologically inherited stereochemistry was observed in the sterane products (e.g. 5α,14α,17α(H)-20R isomer of cholestane (**A1**) was the dominant product from 5α,14α,17α(H)-20R cholestenol (**B1**); while both 5β,14α,17α(H)-20R and 5α,14α,17α(H)-20R isomers are generated from sterols possessing Δ^5 unsaturation). Additionally, cholestane products yielded individual $\delta^{13}C$ signatures that matched those of the precursor sterols within analytical error (Sephton et al., 2005).

As an example, comparing the extracted sterol and HyPy sterane profiles of *Geodia hentscheli* shows the efficacy of sterol → sterane conversion from HyPy treatment, retaining the core stereochemical and structural integrity of the hydrocarbon core skeleton with little side-chain cracking and with 5β,14α,17α(H)-20R and 5α,14α,17α(H)-20R isomers generated (Fig. 8). *Geodia hentscheli* produced ergostane (**A2**) as its major sterane from HyPy conversion (Table 5). GC-MS analysis of the derivatized sterols (as TMS ethers using BSTFA) in the total lipid extracts independently confirmed that the same specimen contained 24-methylenecholesterol (a conventional C_{28} sterol) as its major sterol component and that the total relative abundance of each steroid class ($C_{27}/C_{28}/C_{29}$) agrees between the two analytical approaches (Fig. 8). This illustrates the effective conversion of the biological precursor sterol to the saturated sterane 'core skeleton' after HyPy treatment

and provides the basis for comparisons between modern and ancient sponge-derived biomarkers since both contain the αααR diastereoisomer peak (e.g. Fig. 1).

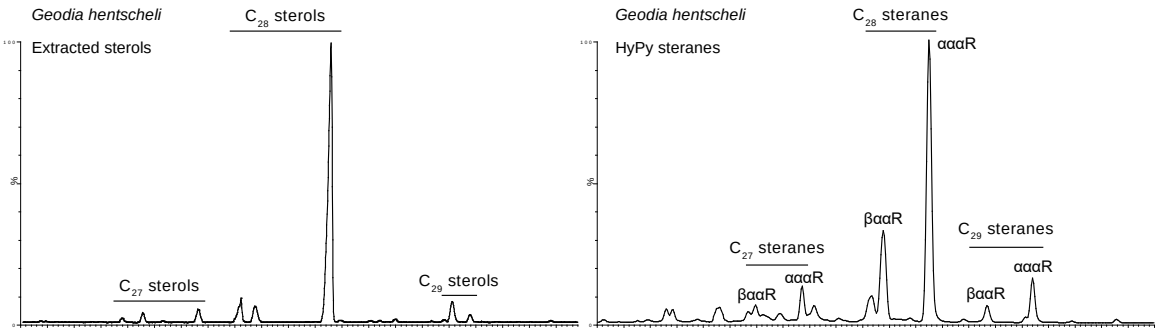

Figure 8. Extracted sterols (as TMS ethers) vs HyPy-generated sterane distributions for the same demosponge specimen: *Geodia hentscheli* (GhII). The similar abundance patterns between the intact sterols and their sterane products highlights the efficacy of HyPy conversion of precursor steroids in extant sponge biomass to immature steranes with minimal thermal cracking and rearrangements (forming predominantly βααR and αααR diastereoisomers from Δ^5-sterols).

The major patterns of HyPy-generated sterane distributions from a variety of modern sponge species (Table 4) are represented by the data displayed in Table 5. The HyPy approach allows a very sensitive screening for any individual sterane compounds using MRM-GC-MS of HyPy products, down to sub-ng quantities. This allows us to assess the sterane core content of steroids in biomass by a rapid and reproducible process (Love et al., 2005), particularly in this case to identify sponges that contain significant quantities of 26-mes steroids (Table 5) and allows for a direct comparison with ancient steranes in the geological record (Fig. 1). Sponges in our collection that contained either stelliferasterol (**B13**), isostelliferasterol (**B14**) and/or strongylosterol (**B15**) (e.g. *Geodia parva*, *Rhabdastrella globostellata*, *Geodia phlegraei*) as major Δ^5-unsaturated C_{30} sterols gave 26-methylstigmastane (**A10**) as the major HyPy C_{30} sterane product (0.5 to 9.3% of total

C_{27}-C_{30} steranes) in every case, without exception (Table 5). As expected, the 26-mes sterane peaks from these three sponges produced two major stereoisomer peaks from the reduction of the double bond at C-5 in each precursor sterol: βααR and αααR. These are the two main sterane diastereoisomers produced from the reduction of any conventional or unconventional sterols with unsaturation at C-5 position (Fig. 5). The same pattern is seen from HyPy of sponges that yield conventional sterols and steranes (e.g. *Geodia hentscheli*, Fig. 8). Furthermore, HyPy screening of microalgal cultures has yet to produce any C_{30} sterane series consistent with a 26-mes source, and conventional steroids dominate the HyPy products with sterane carbon number patterns generally matching the sterol patterns reported in the literature (Love et al., 2005).

The enigma of strongylosterol and host sponge association in some previous reports

Strongylosterol was first isolated from a sponge specimen collected on Laing island, 35 meters water depth (Papua New Guinea) and identified by Dr. P. A. Thomas as *Petrosia (Strongylophora) durissima* (Bortolotto et al., 1978). However, when we investigated another specimen of *P. (S.) durissima* from Indonesia (PC1068), we could not detect 26-mes in the HyPy products [as expected if it produced strongylosterol in high amounts, as suggested by Bortolotto et al., 1978]. Furthermore, we obtained the same result from the holotype of *Petrosia (Strongylophora) durissima* (NHM 1907.2.1.37) from Sri Lanka. We can therefore assume that strongylosterol was isolated from a different species, mis-identified as *P. (S.) durissima* by Dr. Thomas. Unfortunately, no voucher has been kept from the previous study (Bortolotto et al., 1978), so we cannot be sure of that. Therefore,

we consider that Bortolotto *et al.* (1978) worked on a species that we call *P. (S.)* cf. *durissima* in the present study.

The chemist J. C. Braekman had given pieces of the whole Papua New Guinea sponge collection to Dr. Thomas to identify. Dr. Thomas described this sponge collection in a subsequent series of papers. Thomas (1991) describes from this collection *Strongylophora durissima* along with a new species, *Strongylophora septata*. Both species have identical spicules but different external shapes. Thomas (1991) unfortunately does not mention which one had been studied by Bortolotto *et al.* (1978) but according to our results, we can assume that strongylosterol was originally isolated from *P. (S.) septata* and not *P. (S.) durissima*. Again, we cannot formally conclude due to the absence of vouchers left from Bortolotto *et al.* (1978).

Jaspis wondoensis *versus* Rhabdastrella wondoensis

Jaspis is a contentious group of sponges currently belonging to the Ancorinidae family, Tetractinellida order (Cárdenas et al., 2011). *Jaspis wondoensis* (Sim & Kim 1995) was described from the shallow waters of Geomun islands (locality of Wondo), Jeju Strait, South Korea. In this study we examined material from the Jeju Strait, Yeoseo Island (courtesy of Dr. Jae-Sang Hong, Inha University, Republic of Korea). *Jaspis* species are characterized by oxeas of different sizes (notably microxeas on the surface) with a paratangential arrangement; euasters are without a centrum. However, we observed spicules (rare large spherasters in the cortex, no microxeas) and spicule arrangement (radial

organization) suggesting that this species should be reallocated to the genus *Rhabdastrella*, as *Rhabdastrella wondoensis* comb. nov. The absence of triaenes in *R. wondoensis*, is not uncommon in some *Rhabdastrella* species (e.g. *R. globostellata*). Molecular phylogeny studies further suggest that the tropical *Rhabdastrella* genus belongs to the Geodiidae family, and not to the Ancorinidae family (Cárdenas et al., 2011).

Plausible sponge sterane biomarkers predating the Sturtian glaciation (>717 Ma)

In terms of possible older occurrences of sponge biomarkers, robust evidence for steranes has been reported in some 800-700 Myr Neoproterozoic rocks (Brocks et al., 2015; Adam et al., 2018) from the Chuar Group (USA) and Visingsö Group (Sweden). These rocks contain an unusual C_{28} sterane, 26-methylcholestane, informally designated as cryostane (Fig. 9), which has been proposed as a possible ancient sponge or unicellular stem metazoan marker (Brocks et al., 2015). Cryostane is also characterized by the unusual methylation at C-26, making it a structural analogue of 26-mes and adding credence to the case for cryostane being a plausible ancient sponge biomarker. However, possible precursor sterols for cryostane containing a cryostane core structure (aka "cryosterol") have not yet been found in any extant organisms, despite the discovery of a wide variety of other unconventional steroid structures in modern sponges. The Chuar and Visingsö Group rocks, like all pre-Sturtian-aged samples reported so far, contain C_{27} steranes as their major steranes (Summons et al., 1988; Vogel et al., 2005; Brocks et al., 2015; Adam et al., 2018) and are devoid of 24-ipc, 24-npc and 26-mes steranes. Here we note that 24-ipc and 26-mes (C_{30} steranes) are found in rocks/oils that often exhibit a C_{29} sterane dominance

(Grosjean et al., 2009; Love et al., 2009; Kelly et al., 2011; this study). This carbon number relationship (n+1 versus n) may be from heterotrophic modification (n+1) of primary steroids (n) in these ancient marine environments systems and suggests dietary modification of sterol feedstocks as a possible early transformation mechanism to make unconventional steroids. Thus, cryostane cannot currently be applied as a robust animal biomarker until more is known about its biological origins and whether the biosynthetic capacity to make unconventional 26-methylated steroids (CHART I) is restricted to demosponges or otherwise. The origins of cryostane are intriguing and a bridging of the cryostane and 26-mes/24-ipc records may signify a continuity of sponge markers persisting through the two Neoproterozoic glaciation events (Fig. 9), but this requires further investigation.

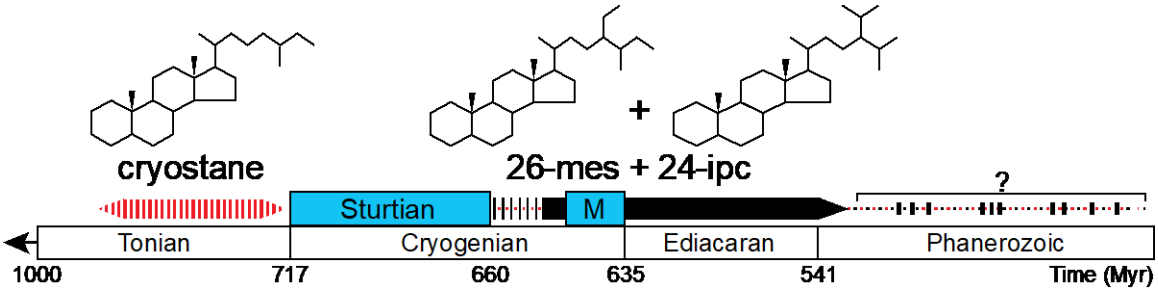

Figure 9. A revised Neoproterozoic-Cambrian timeline showing co-occurrences of 26-mes and 24-ipc sterane biomarkers. The South Oman record commences in the Cryogenian period (>635 Myr) after the Sturtian glaciation (terminating at ca. 660 Myr; Rooney et al., 2015) and continues throughout the Ediacaran period into the Early Cambrian for Huqf Supergroup rocks (Tables 1 and 2). Other Ediacaran oils also contain the C_{30} steranes series (Table 3) but some Ediacaran rocks are devoid of the C_{30} sterane series although they contain predominantly algal steranes with a C_{29} dominance (Pehr et al., 2018). The distribution and abundance patterns of the C_{30} sterane, 26-mes, have yet to be fully established for the Phanerozoic rock record however it can be detected in some Phanerozoic rocks and oils (see Table 3). Cryostane (26-methylcholestane) is a potentially older biomarker for sponges or unicellular protists, and it has been detected in pre-Sturtian rocks in the 717-800 Myr age range (Brocks et al., 2015). Cryostane is a C_{28} sterane analogue of 26-mes but corresponding sterol precursors for cryostane have never been reported from any extant taxa despite the identification of 26-mes demosponge sterols many decades ago (Bortolotto et al., 1978; Theobald & Djerassi 1978; Theobald et al., 1978).

Conclusions

The co-occurrence of 24-ipc and 26-mes steranes constitutes the earliest robust biomarker evidence for Neoproterozoic animals, first detected in the Cryogenian period (>635 Myr) after the Sturtian glaciation (beginning at <717 Myr and terminating at ca. 660 Myr) (Love et al., 2009; Rooney et al., 2015). This suggests that Metazoa first achieved ecological prominence in Neoproterozoic marine paleoenvironments most likely between 660 and 635 Myr which is consistent with recent molecular clock predictions for the first appearance of demosponges (Erwin et al., 2011; dos Reis et al., 2015; Dohrmann & Wörheide 2017; Schuster et al., 2018). This view from molecular clocks and biomarkers remains to be reconciled with the fossil spicule record, which suggests a later (Cambrian) origin (Botting & Muir et al., 2018). Future sampling of modern taxa may reveal other sources of 26-mes steroids, but multiple possibilities for taphonomic mega-bias of early sponge body fossils have been identified (Muscente et al., 2015), perhaps related to sparse biomineralization and/or silica dissolution and reprecipitation in low-oxygen marine conditions (Berelson et al., 2005), despite overall higher Proterozoic oceanic silica levels. The records could also be reconciled if demosponge spicules evolved convergently in the Cambrian or if aspiculate demosponges were dominant producers of Neoproterozoic 26-mes and 24-ipc.

All available current data indicates that 26-mes steranes are made by diverse species of modern demosponges, and apparently not by any other sponge class (Hexactinellida, Homoscleromorpha, Calcarea) or other extant eukaryote, implying that Neoproterozoic total-group demosponges were the most probable source biota for these biomarkers. As

demosponges are derived within Porifera, these data consequently predict the presence of sponges at this time irrespective of whether sponges (Simion et al., 2017) or ctenophores (Whelan et al., 2017) are the sister group of all other animals. Thus, this new Neoproterozoic steroid biomarker evidence for demosponges provides a conservative minimum time estimate for the origin of animal multicellularity and the sponge body plan involving feeding with a water canal system.

CHART I

Conventional | Unconventional | Unsaturated

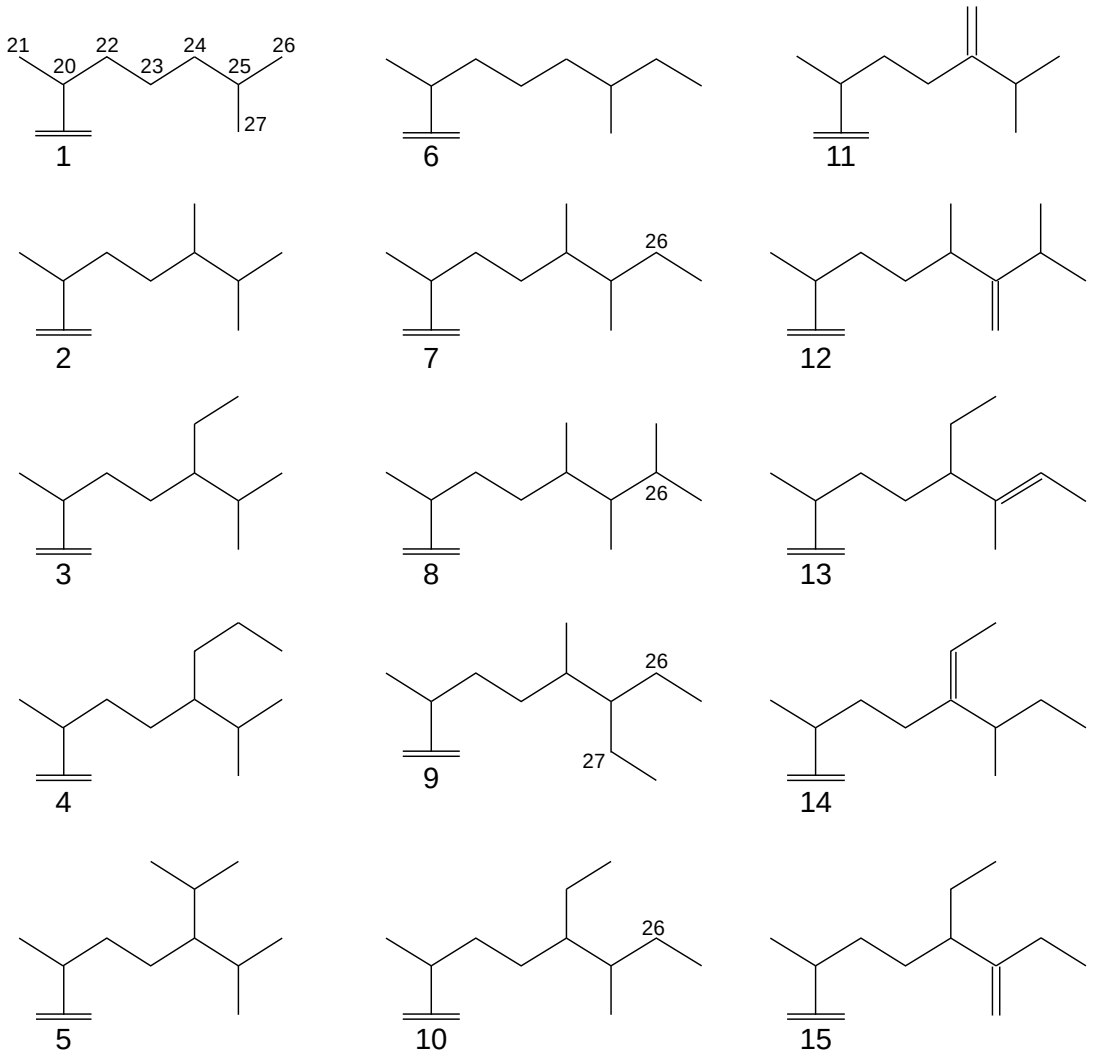

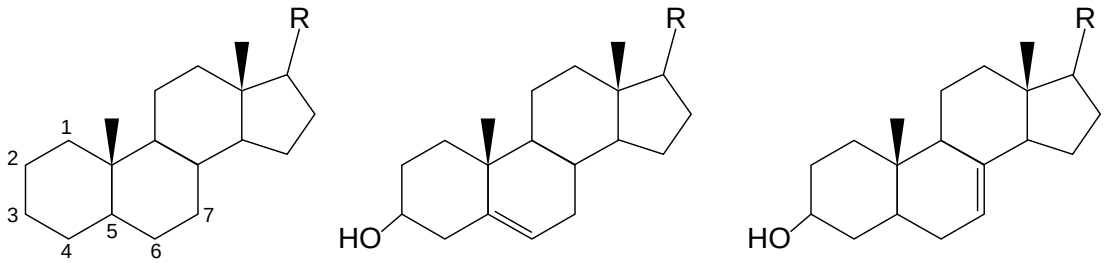

A B C

Table 1: Selected biomarker ratios and yields obtained from free saturate fractions of sediment cores and cuttings

Well ID	Minimum Depth (m)	Stratigraphy	TOC wt.%	Lithology/Facies	S/H[a]	%C_{26} st[b]	%C_{29} st[c]	%C_{30} st[d]	ipc/ npc[e]	ipc[e] ppm	26-mes[f] ppm	26-mes/ ipc[f]
MKS-2	1648	A6	n.d.	Shale band above A5C stringer	0.82	6.46	58	2.05	1.15	138.7	126.5	0.91
SAR-2	3838	A6*	n.d.	Siliciclastics above A5C stringer	0.21*	6.88*	69	6.69*	1.95	65.6	37.9	0.58
AJB-1	3588	A5C*	n.d.	Carbonate stringer-saline*	0.22*	9.96*	62	1.89*	0.95	13.0	4.7	0.36
OMR-1	2851	A5C	0.44	Carbonate stringer	0.85	6.62	69	1.93	1.55	23.5	10.8	0.46
OMR-1	2853	A5C	1.05	Carbonate stringer	0.82	4.81	69	2.02	1.67	17.7	6.5	0.37
BB-3	2928	A4C	1.06	Carbonate, sapropelic laminite	0.91	4.86	70	2.11	1.49	7.2	5.0	0.69
BB-3	2930	A4C	0.95	Carbonate stringer	1.05	6.26	68	2.45	1.36	11.6	7.8	0.67
BB-5	3009	A4C	1.92	Carbonate stringer	0.99	4.36	66	1.95	1.39	9.2	6.0	0.65
BB-2	2927	A3C	0.53	Carbonate stringer	0.96	4.73	75	2.10	1.49	13.5	8.4	0.62
BBN-1	3785	A3C	0.13	Carbonate stringer	0.79	5.92	70	2.02	1.38	49.0	16.7	0.34
BBN-1	3787	A3C	0.72	Carbonate stringer	0.87	12.7	69	2.31	1.46	11.8	7.1	0.61
BBN-1	3789	A3C	0.40	Carbonate stringer	0.78	5.36	71	2.10	1.66	23.9	10.0	0.42
BBN-1	3790	A3C	0.19	Carbonate stringer	0.82	3.92	70	2.10	1.67	25.5	12.5	0.49
DRR-1	2969	A3C	0.19	Carbonate, crinkly laminite	0.82	4.77	70	2.00	1.45	55.0	26.2	0.48
DRR-1	2990	A3C	0.46	Carbonate, crinkly laminite	0.78	4.56	70	2.07	1.60	62.5	32.4	0.52
BBN-1	4204	A2C	1.90	Carbonate stringer	0.96	6.03	75	2.13	1.52	9.5	5.3	0.55
RF-1	3547	A2C*	n.d.	Carbonate stringer- saline*	0.57	12.9*	70	3.56*	1.17	39.9	16.1	0.40
RF-1	3577	A2C*	n.d.	Carbonate stringer- saline*	0.59	10.1*	72	4.65*	1.48	57.7	28.8	0.50
SAB 1	2399	A2C	1.19	Carbonate stringer	0.93	4.46	75	1.90	1.69	11.9	5.3	0.45
SJT-1	5033	A2C	0.86	Carbonate, pustular laminite	0.72	4.94	52	2.84	1.26	27.4	7.8	0.29
SJT-1	5053	A2C	1.39	Carbonate, thrombolite	0.83	4.74	61	3.39	1.77	33.9	11.5	0.34
DHS-3	2997	A1C	1.22	Carbonate stringer	0.72	4.52	73	1.80	1.92	78.6	30.9	0.39
MIN-1	3400	A1C*	n.d.	Carbonate stringer-saline*	0.52*	9.88*	73	4.75*	1.42	59.4	24.8	0.42
MIN-1	3430	A1C*	n.d.	Carbonate stringer- saline *	0.54*	9.62*	71	5.20*	1.49	116.7	48.7	0.42
AMSE-1	2345-2375	Buah	1.6	Carbonate	0.76	4.07	73	1.66	0.86	5.8	5.4	0.93
SB-1	1569-1602	Buah	2.3	Marlstone?	0.74	8.04	72	1.33	0.77	10.9	11.0	1.01
TRF-2	4411	Buah	3.1	Marlstone	0.84	7.39	67	1.74	0.70	8.7	10.2	1.17
ATH-1	2016-2019	Buah	11.0	Organic-rich marlstone	1.06	9.16	64	1.82	0.55	21.3	27.6	1.29
ZFR-1	1905-1940	Shuram	3.4	Mudstone/siltstone	0.61	6.27	71	2.33	1.78	92.6	43.5	0.47
ATH-1	2379	Shuram	1.5	Mudstone/siltstone	0.56	3.02	77	2.01	0.81	109.1	49.6	0.45
ATH-1	2053-2121	Shuram	1.3	Mudstone/siltstone	0.96	3.81	68	2.12	0.92	14.0	10.1	0.72
ATH-1	2424.5-2447	Shuram	3.0	Mudstone/siltstone	0.66	2.86	70	2.19	1.10	6.8	6.2	0.91
ATH-1	2449-2452	Shuram	3.6	Mudstone/siltstone	0.70	6.68	65	2.50	1.41	8.0	4.5	0.57
TF-1	2247.5-2250	Shuram	n.d.	Mudstone/siltstone	1.06	6.17	65	1.87	1.07	34.3	31.2	0.91
TM-6	2350	Shuram	2.4	Mudstone/siltstone	1.00	5.63	70	2.18	0.92	35.6	28.8	0.81
TM-6	2685-2740	Shuram	3.9	Mudstone/siltstone	0.80	6.15	70	2.00	1.33	26.1	19.6	0.75
TM-6	2800	Shuram	9.2	Lower Shuram black shale	0.84	5.17	73	2.02	1.27	43.5	15.4	0.35
TM-6	2830	Khufai	3.2	Carbonate	0.49	6.02	72	3.34	1.43	72.3	41.3	0.57
RNB-1	3125-3143	Masirah B	1.7	Mudstone/siltstone	0.49	6.84	58	3.53	3.98	14.5	6.8	0.47
ZFR-1	2280-2295	Masirah B	3.8	Mudstone/siltstone	0.73	5.18	84	12.61	16.1	245.7	24.9	0.10
SRS -1	4230-4385	Masirah B	0.4	Mudstone/siltstone	0.70	5.70	64	2.25	1.49	6.1	3.1	0.51

TM-6	2895-2910	Masirah B	4.9	Mudstone/siltstone	0.70	4.49	69	3.16	1.35	12.1	6.9	0.57
MWB-1	2628-2724	Masirah B	n.d.	Mudstone/siltstone	0.73	4.86	60	2.44	1.52	16.5	8.2	0.50
GM-1	2420-2446	Ghad. Manquil	0.59	Laminated lime mudstone	0.90	7.18	72	2.65	3.26	61.0	25.3	0.41
MQR-1	4370	Ghad. Manquil	n.d.	Siltstone	0.43	4.32#	56#	3.72#	0.52#	n.d.	n.d.	0.16
Athel Group												
AML-9	1731	Thuleilat	2.2	Black shale	0.95	11.4	60	2.78	1.34	79.3	41.6	0.52
ATH-1	1000-1102	Thuleilat	8.0	Black shale	0.62	5.74	67	3.34	1.36	18.3	16.1	0.88
MAR-248	2068-2084	Thuleilat	10.4	Mudstone/silicylite transitional	1.29	5.41	71	1.91	1.37	34.8	25.0	0.72
TLT-2	1417.5-1483	Thuleilat	6.4	Black shale	0.81	4.86	71	2.23	1.35	24.9	24.9	1.00
TLT-2	1520-1547	Thuleilat	2.5	Mudstone	0.91	5.16	73	2.27	1.56	35.4	31.5	0.89
ATH-1	1198-1425	Silicylite	3.4	Finely laminated quartz	0.79	4.06	74	1.85	1.39	62.6	37.6	0.60
MAR-248	2104-2120	Silicylite	3.4	Upper silicylite- laminated quartz	1.50	4.78	72	1.93	1.42	28.6	18.3	0.64
MAR-248	2240-2352	Silicylite	2.3	Lower silicylite- laminated quartz	1.02	4.93	76	1.84	1.87	61.0	25.5	0.42
TLT-2	1551-1602	Silicylite	4.3	Finely laminated quartz	1.21	6.11	74	2.41	2.13	90.0	35.6	0.40
TLT-2	1628-1742	Silicylite	2.6	Finely laminated quartz	0.87	21.4	75	2.25	2.44	103.5	38.9	0.38
ATH-1	1425-1527	U shale	3.5	Black shale	0.85	7.73	66	2.37	1.11	17.2	12.2	0.71
ATH-1	1527	U shale	4.9	Black shale	1.00	4.69	61	2.64	0.93	10.0	8.9	0.89
ATH-1	1773-1872	U shale	5.7	Black shale	0.91	19.7	61	2.63	0.78	4.3	3.3	0.77
MAR-248	2420-2460	U shale	6.4	Black shale	0.79	7.24	60	2.90	1.35	8.7	5.4	0.62
TLT-2	1751-1833	U shale	4.0	Black shale	0.89	9.87	65	2.20	1.41	27.9	15.7	0.56

a: ratio of (C_{27}-C_{29} steranes)/(C_{27}+C_{29-35} hopanes)
b: ratio of (21-nor- +27-norcholestanes)/Σ(C_{26}-C_{29} steranes), for C_{26} desmethylsteranes (C_{27}-C_{29} 21-norsteranes peak areas were not included)
c: ratio of C_{29} steranes to the total sum of C_{27}-C_{29} steranes
d: ratio of (24-*n*-propylcholestanes+24-isopropylcholestanes)/Σ(C_{27}-C_{30} steranes), for C_{30} desmethylsteranes
e: ratios and compound yields were calculated from summing peak areas of all 4 regular isomers of each compound (αααS, αββR, αββS, αααR)
f: ratios and compound yields for 26-methylstigamstane were calculated from the peak area of the αααR isomer
#: affected by contamination from marine Phanerozoic-sourced petroleum drilling fluids, hence the lower ratios of %C_{29} sterane and iso-C_{30}/n-C_{30} sterane
*: saline marine facies, hence lower sterane/hopane ratio and apparently higher %C_{26} and %C_{30} steranes (as C_{28} and C_{29} 21-norsteranes, prominent at higher salinity, are not included in the calculation)
n.d.: not determined
Analytical errors for absolute yields of 27-norcholestanes and 24-isopropylcholestanes absolute yields are estimated at ± 30%. Average uncertainties in hopane and sterane biomarker ratios are ± 8% as calculated from multiple analyses of a saturated hydrocarbon fraction prepared from an AGSO standard oil (n = 30 MRM analyses).
Rock-Eval pyrolysis data for these samples is given in Grosjean et al., (2009).

Table 2: Selected biomarker ratios and yields obtained from hydropyrolysis of kerogens/extracted sediments

Well ID	Minimum Depth (m)	Stratigraphy	TOC wt.%	Lithology/Facies	S/H[a]	%C_{26} st[b]	%C_{29} st[c]	%C_{30} st[d]	ipc/ npc[e]	ipc[e] ppm	26-mes[f] ppm	26-mes/ ipc[f]
OMR-1	2851	A5C	0.44	Carbonate stringer	0.89	5.62	59	2.27	0.83	61.8	30.5	0.49
BB-3	2928	A4C	1.06	Carbonate stringer	0.84	8.27	53	3.60	0.73	14.7	13.8	0.94
DRR-1	2990	A3C	0.44	Carbonate stringer	0.80	7.99	62	1.88	0.82	15.6	12.7	0.82
RF-1	3547	A2C*	n.d.	Carbonate stringer- saline*	0.62	4.68	68	2.87	0.84	8.4	5.0	0.59
SJT-1	5033	A2C	0.86	Carbonate, pustular laminite	0.93	9.80	52	3.16	0.64	5.2	0.3	0.06
SJT-1	5053	A2C	1.39	Carbonate, thrombolite	1.04	10.1	55	3.64	1.10	5.6	2.1	0.37
DHS-3	2997	A1C	1.22	Carbonate stringer	0.77	6.42	69	2.88	0.96	18.6	9.4	0.51
MIN-1	3400	A1C*	n.d.	Carbonate stringer- saline facies*	0.58	3.98	70	2.15	1.35	11.6	4.9	0.42
SB-1	1569-1602	Buah	2.3	Marlstone?	0.89	12.9	63	1.34	0.53	4.4	5.4	1.24
AMSE-1	2345-2375	Buah	1.6	Carbonate	1.12	10.5	67	1.91	0.72	4.2	2.4	0.57
ZFR-1	1905-1940	Shuram	3.4	Mudstone/siltstone	0.99	12.9	60	2.71	0.66	14.1	17.2	1.22
SNK-1	930-990	Shuram	n.d.	Mudstone/siltstone, Lower Shuram	0.55	13.3	58	4.58	1.35	2.7	1.3	0.49
JF-1	2648-2676	Masirah B	n.d.	Mudstone/siltstone, Upper Masirah	0.73	14.2	55	5.60	1.35	3.8	2.6	0.69
HNR-1	2026-2060	Masirah B	n.d.	Mudstone/sitstone, Upper Masirah	1.21	12.0	54	3.43	1.52	2.4	1.7	0.70
GM-1	2420-2446	Ghad. Manquil	0.59	Laminated lime mudstone	0.68	9.70	66	3.04	1.31	6.2	3.5	0.56
Athel Group												
AM-9	1731	Thuleilat	2.2	Black shale	0.97	9.89	57	2.46	1.24	12.0	10.1	0.84
MAR-248	2068-2084	Thuleilat	10.4	Mudstone/silicylite transitional	2.49	15.8	65	2.00	0.74	16.3	16.5	1.01
MAR-248	2104-2120	Silicylite	3.4	Upper silicylite	2.10	12.4	69	2.25	0.69	11.2	11.0	0.99
MAR-248	2240-2352	Silicylite	2.3	Lower silicylite	1.46	6.73	75	2.08	1.05	34.3	26.5	0.77
MAR-248	2420-2460	U shale	6.4	Black shale	1.19	13.2	53	2.71	1.66	9.5	6.4	0.67

a: ratio of (C_{27}-C_{29} steranes)/(C_{27}+C_{29-35} hopanes)
b: ratio of (21-nor- +27-norcholestanes)/Σ(C_{26}-C_{29} steranes), for C_{26} desmethylsteranes (C_{27}-C_{29} 21-norsteranes peak areas were not included)
c: ratio of C_{29} steranes to the total sum of C_{27}-C_{29} steranes
d: ratio of (24-*n*-propylcholestanes+24-isopropylcholestanes)/Σ(C_{27}-C_{30} steranes) for C_{30} desmethylsteranes
e: ratios and compound yields were calculated from summing peak areas of all 4 regular isomers of each compound (αααS, αββR, αββS, αααR)
f: ratios and compound yields for 26-methylstigamstane (26-mes) were calculated from the peak area of the αααR isomer
n.d.: not determined
*: elevated salinity and marine facies
Analytical errors with 27-norcholestane and 24-isopropylcholestane absolute yields are estimated at ± 30%. Average uncertainties in hopane and sterane biomarker ratios are ± 8% as calculated from multiple analyses of a saturated hydrocarbon fraction prepared from an AGSO standard oil (n = 30 MRM analyses).
Note: All products from HyPy were monitored to ensure that the bulk of the biomarkers generated were released by cleavage of covalent bonds and were not simply residual bitumen components. This was achieved by observing only very low or nil amounts of certain rearranged steranes and hopanes found exclusively as free hydrocarbons. For example, for all HyPy analyses here (Ts/Tm) <0.15, (diasteranes/regular steranes) <0.1 with much reduced levels of 28,30-bisnorhopanes relative to total hopanes compared with the corresponding free extracts.

Table 3: C_{30} sterane abundances and distributions in a selection of rocks and oils through geologic time

Age	SampleID	Location	Type	TOC (wt.%)	Lithology/ Facies	Basin/Fm./Gp./Well	Major Sterane[a]	$\%C_{30}$[b]	ipc/ npc[c]	26-mes/ ipc[c]	26-mes/ npc[c]
Ediacaran	OMO005[#]	Oman	oil	N/A		A1C	stigmastane	2.6%	1.35	0.45	0.61
	OMO003[#]	Oman	oil	N/A		PS Huqf	stigmastane	3.9%	1.44	0.50	0.72
	OMO014[#]	Oman	oil	N/A		PS Huqf	stigmastane	3.7%	0.64	0.68	0.43
	ES0001[$]	E. Siberia	oil	N/A		Kamov Gp.	stigmastane	2.3%	1.03	0.35	0.36
	ES0053[$]	E. Siberia	oil	N/A		Byuk	stigmastane	2.3%	1.73	0.40	0.70
Cambrian	IA0016[*]	India	oil	N/A		Baghewala-1	stigmastane	2.0%	4.42	0.23	1.01
	OMO043[#]	Oman	oil	N/A		A5C	stigmastane	3.1%	1.73	0.36	0.62
	ES0083[$]	E. Siberia	oil	N/A		Usol'ye	stigmastane	2.4%	1.03	0.64	0.66
Ordovician	VA-23[%]	Nevada, USA	rock	18.4	Shale	Vinini	stigmastane	0.2%	n.d.	n.d.	n.d.
	SGH-43.0[%]	Indiana, USA	rock	0.2	Arg. Carb.	Liberty/Whitewater	stigmastane	0.1%	n.d.	n.d.	n.d.
Silurian	901-16.0[%]	Anticosti, Canada	rock	0.2	Carbonate	Becscie	stigmastane	0.1%	n.d.	n.d.	n.d.
	G1+2.0[%]	Gotland, Sweden	rock	0.2	Marlstone	Visby	stigmastane	0.6%	n.d.	n.d.	n.d.
Devonian	Pando1[^]	Bolivia	rock	5.6	Shale	Madre de Dios	stigmastane	1.5%	0.16	0.98	0.16
	Pando4[^]	Bolivia	rock	9.5	Shale	Madre de Dios	stigmastane	3.0%	0.16	1.00	0.17
	Pando12[^]	Bolivia	rock	11.8	Shale	Madre de Dios	stigmastane	2.7%	0.25	0.57	0.14
	Pando18[^]	Bolivia	rock	18.8	Shale	Madre de Dios	stigmastane	4.1%	0.27	0.52	0.14
	OK0620[*]	Oklahoma, USA	oil	N/A		Arnold 2-17H	stigmastane	3.6%	0.16	0.64	0.11
	OK0621[*]	Oklahoma, USA	oil	N/A		Sabre 1-7H	stigmastane	2.7%	0.10	1.15	0.12
Permian	M22[*]	China	rock	n.d.	Micrite	Maokou Fm.	stigmastane	3.4%	0.78	0.68	0.26
	W13[*]	China	rock	n.d.	Micrite	Wujchaping Fm.	stigmastane	2.5%	0.58	0.46	0.23
Jurassic	JR13[*]	United Kingdom	rock	8.9	Shale	Jet Rock	cholestane	4.9%	0.11	0.00	0.00
	8022[*]	North Sea	oil	N/A		Clair	cholestane	7.3%	0.13	0.00	0.00
Cretaceous	207-1258A[+]	Suriname	rock	10.8	Shale	Demerara Rise	cholestane	6.3%	0.12	0.00	0.00
	207-1258B[+]	Suriname	rock	14.7	Shale	Demerara Rise	cholestane	4.4%	0.13	0.00	0.00
	207-1258C[+]	Suriname	rock	1.8	Shale	Demerara Rise	cholestane	7.1%	0.11	0.00	0.00
Phanerozoic Avg.	GeoMark	-	oil	N/A		Mixed oil	stigmastane	1.5%	0.00	n.d.	0.00
(oil standards)	AGSO	-	oil	N/A		Mixed oil	stigmastane	3.3%	0.00	n.d.	0.00
Procedural Blank	Blank sats1	-	-			-	-	0.0%	-	-	-
	Blank sats2	-	-			-	-	0.0%	-	-	-

a: cholestane/ergostane/stigmastane ($C_{27}/C_{28}/C_{29}$) predominance using all the major diastereoisomer forms present

b: Expressed as a % total of C_{27}-C_{30} steranes calculated from summing peak areas of all 4 regular isomers of each C_{30} sterane compound (αααS, αββR, αββS, αααR)

c: C_{30} sterane ratio for αααR isomer from MRM-GCMS; ipc, 24-isopropylcholestane; npc, 24-n-propylcholestane; 26-mes, 26-methylcholestane || n.d.: proportions were not detected as overall C_{30} sterane abundances are very low in some early Paleozoic rocks (Rohrssen et al., 2015) with 24-ipc and 26-mes absent

#Grosjean et al., 2009; $Kelly et al., 2011; %Rohrssen et al., 2015; ^Haddad et al., 2016; +Owens et al., 2016; *Love Lab sample (UCR)

Permian rocks M22 & W13 have appreciable amounts of siliceous sponge spicules (unpublished data) with high amount of 24-ipc & 26-mes biomarkers

Table 4: Taxonomic assignments for the sponges used in this study

Class	Order	Family	*Genus species*	locality	depth (m)	Collection ID/ Museum accession#
Demospongiae	Tetractinellida	Geodiidae	*Geodia phlegraei*	Svalbard	215	PC511/ ZMBN 89719
			Geodia parva	Flemish Cap, off Newfoundland	1180	PC535/ UPSZMC 78274
			Geodia parva	Mohns Ridge, Greenland Sea	1834-1863	GpII
			Geodia hentscheli	Kolbeinsey Ridge, Greenland Sea	145-215	GhII
			Rhabdastrella distincta	North Sulawesi, Indonesia	27	PC1127
			Rhabdastrella wondoensis	Yeoseo Island, South Korea	shallow	PC866
			Rhabdastrella wondoensis	Yeoseo Island, South Korea	shallow	PC865
			Rhabdastrella globostellata	Penghu Archipelago, Taiwan	shallow	PC922
			Rhabdastrella globostellata	Manus Island, Papua New Guinea	shallow	PC140/ UCMPWC1072
			Rhabdastrella globostellata	Guam Island	shallow	PC492
			Stelletta tuberosa	Flemish Cap, off Newfoundland	1339	PC675
		Tetillidae	*Cinachyrella kuekenthali*	Broward county, Florida	shallow	PC941
			Craniella zetlandica	Korsfjord, Norway	310	PC667
	Haplosclerida	Petrosiidae	*Petrosia (St.)* cf. *vansoesti*	off Lagos, SW Portugal	60	PC982
			Petrosia (St.) durissima	North Sulawesi, Indonesia	20	PC1068
			Petrosia (St.) durissima	Sri Lanka	n/a	NHMUK 1907.2.1.37
	Suberitida	Halichondriidae	*Ciocalypta carballoi*	Rhodes, Greece	15	PC1064
			Halichondria sp.[a]	Marine Biological Laboratory, MA	shallow	sponge 1
		Suberitidae	*Suberites* sp.[a]	Marine Biological Laboratory, MA	shallow	sponge 2
	Bubarida	Bubaridae	*Phakellia ventilabrum*	Tjärnö, Sweden	n/a	FKOG-POR2
	Chondrillida	Chondrillidae	*Thymosiopsis conglomerans*	Tremies cave, Marseille, France	12	Tremies
			Thymosiopsis cf. *cuticulatus*	Endoume cave, Marseille, France	7	Endoume
	Verongiida	Aplysinidae	*Aplysina aerophoba*			TLE430
			Aplysina fulva	Bocas del Toro, Panama	3	A. fulva
			Verongula rigida	Bocas del Toro, Panama	3	sponge 8
			Verongula reiswigi	Bocas del Toro, Panama	3	BT13
	Agelasida	Agelasidae	*Cymbaxinella corrugata*[a]			1153725
	Dictyoceratida	Dysideidae	*Dysidea fragilis*[a]			D. fragilis
	Clionaida	Clionaidae	*Cliona* sp.[a]			sponge 3
	Poecilosclerida	Microcionidae	*Microciona* sp.[a]	Marine Biological Laboratory, MA	shallow	sponge 4
Homoscleromorpha	Homosclerophorida	Plakinidae	*Plakinastrella onkodes*[b]	off Panama, Caribbean Sea	shallow	1133732
			Plakortis halichondrioides[b]	off Panama, Caribbean Sea	shallow	1133720
Hexactinellida	Lyssacinosida	Rossellidae	*Vazella pourtalesii*	Emerald Basin, off Nova Scotia	183-212	HUD16-019-B0362
Calcarea	Leucosolenida	Leucosoleniidae	*Leucosolenia* sp.[a]	Marine Biological Laboratory, MA	shallow	sponge 5

a: from Love et al., 2009
b: courtesy of Allen G. Collins, Smithsonian National Museum of Natural History
UCMPWC: University of California Museum of Paleontology, Berkeley, CA; UPSZMC: Zoological Museum of Uppsala, Sweden
ZMBN: Bergen Museum, Norway; NHMUK: The Natural History Museum, London, UK

Table 5: C_{30} regular (4-desmethyl) sterane patterns from catalytic hydropyrolysis (HyPy) of the sponges used in this study

Genus species	Major HyPy C_{27}-C_{30} sterane	Major HyPy C_{30} sterane	24-npc	24-ipc	26-mes	%26-mes[a]	%C_{30} steranes[a]	%Conventional[e]	%Unconventional[b]	TAR[c]
Geodia phlegraei	aplysterane	26-mes	✓	✓	✓	4.0%	5.1%	25.6%	74.4%	2.9
Geodia parva (PC535)	aplysterane	26-mes	✓	✓	✓	4.5%	6.8%	30.9%	69.1%	2.2
Geodia parva (GpII)	aplysterane	26-mes	✓	✓	✓	3.6%	5.4%	32.7%	67.3%	2.1
Geodia hentscheli	ergostane	24-npc	✓	x	x	0.0%	0.9%	100.0%	0.0%	0.0
Rhabdastrella distincta	aplysterane	26-mes	✓	✓	✓	3.8%	4.4%	22.5%	77.5%	3.5
Rhabdastrella wondoensis (PC866)	aplysterane	26-mes	✓	✓	✓	4.1%	5.2%	43.7%	56.3%	1.3
Rhabdastrella wondoensis (PC865)	aplysterane	26-mes	✓	✓	✓	4.4%	5.0%	51.0%	49.0%	1.0
Rhabdastrella globostellata (PC922)	aplysterane	26-mes	✓	✓	✓	9.3%	10.6%	47.8%	52.2%	1.1
Rhabdastrella globostellata (PC140)	stigmastane	26-mes	✓	✓	✓	2.9%	3.9%	69.5%	30.5%	0.5
Rhabdastrella globostellata (PC492)	stigmastane	26-mes	✓	✓	✓	0.5%	0.6%	95.7%	4.3%	0.1
Stelletta tuberosa	ergostane	24-npc	✓	✓	x	0.0%	0.6%	99.6%	0.4%	<0.01
Cinachyrella kuekenthali	stigmastane	24-npc	✓	✓	x	0.0%	0.3%	99.6%	0.4%	<0.01
Craniella zetlandica	stigmastane	24-npc	✓	✓	x	0.0%	0.6%	100.0%	0.0%	0.0
Petrosia (St.) cf. *vansoesti*	stigmastane	24-npc	✓	x	x	0.0%	1.2%	72.8%	27.2%	0.4
Petrosia (St.) durissima (PC1068)	stigmastane	24-ipc	✓	✓	x	0.0%	0.7%	100.0%	0.0%	0.0
Petrosia (St.) durissima (1907.2.1.37)	stigmastane	24-npc	✓	✓	x	0.0%	0.5%	100.0%	0.0%	0.0
Ciocalypta carballoi	24-ipc	24-ipc	✓	✓	x	0.0%	41.6%	99.8%	0.2%	<0.01
Halichondria sp.[d]	cholestane	24-npc	✓	x	x	0.0%	0.2%	100.0%	0.0%	0.0
Suberites sp.[d]	cholestane	24-npc	✓	x	x	0.0%	0.4%	100.0%	0.0%	0.0
Phakellia ventilabrum	cholestane	24-npc	✓	x	x	0.0%	0.8%	100.0%	0.0%	0.0
Thymosiopsis conglomerans	thymosiosterane	thymosiosterane	x	x	x	0.0%	53.5%	43.4%	56.6%	1.3
Thymosiopsis cf. *cuticulatus*	cholestane	24-ipc	✓	✓	x	0.0%	0.7%	99.9%	0.1%	<0.01
Aplysina aerophoba	aplysterane	verongulasterane	✓	✓	✓	0.06%	1.8%	27.9%	72.1%	2.6
Aplysina fulva	aplysterane	verongulasterane	✓	✓	✓	0.03%	1.3%	35.8%	64.2%	1.8
Verongula rigida	cholestane	verongulasterane	✓	✓	✓	0.15%	4.4%	66.6%	33.4%	0.5
Verongula reiswigi	aplysterane	verongulasterane	✓	✓	✓	0.10%	2.9%	62.6%	37.4%	0.6
Cymbaxinella corrugata[d]	cholestane	24-npc	✓	✓	✓	0.12%	1.6%	97.1%	2.9%	0.1
Dysidea fragilis[d]	cholestane	24-npc	✓	✓	x	0.0%	0.4%	98.9%	1.1%	<0.01
Cliona sp.[d]	cholestane	24-npc	✓	x	x	0.0%	0.3%	100.0%	0.0%	0.0
Microciona sp.[d]	cholestane	none	x	x	x	0.0%	0.0%	100.0%	0.0%	0.0
Plakinastrella onkodes	cholestane	none	x	x	x	0.0%	0.0%	100.0%	0.0%	0.0
Plakortis halichondrioides	stigmastane	none	x	x	x	0.0%	0.0%	100.0%	0.0%	0.0
Vazella pourtalesii	cholestane	24-npc	✓	x	x	0.0%	0.2%	100.0%	0.0%	0.0
Leucosolenia sp.[d]	cholestane	none	x	x	x	0.0%	0.0%	100.0%	0.0%	0.0

a: Expressed as a % total of C_{27}-C_{30} steranes for ααα*R* isomer from MRM-GCMS
b: Unconventional = alkylation at [terminal] position C-26 or C-27 in the sterane side-chain (e.g. 26-mes, aplysterane, verongulasterane, thymosiosterane, cryostane)
c: TAR = Terminal Alkylation Ratio = Σ(terminally alkylated steranes)/Σ(C-24 alkylated steranes)
e: Conventional = cholestane, ergostane, stigmastane, 24-npc and 24-ipc
✓: compound present on MRM-GCMS trace after HyPy
x: compound absent on MRM-GCMS trace after HyPy
See Chart I for sterane structures, sponges are listed in the same order as in Table 4 for specimens of the same species

Table 6: GC retention time offsets for various αααR steranes using MRM-GCMS with our standard GC conditions[5]

#C[1]	Sterane[2]	RRT[3]	Alkylation at[4]:
27	cholestane	0.00	-
28	ergostane	2.39	C-24
	cryostane[+]	2.77	C-26
29	stigmastane	4.33	C-24
	aplysterane[#]	4.77	C-24,26
30	24-npc	5.92	C-24
	24-ipc	6.13	C-24
	26-mes	6.43	C-24,26
	verongulasterane[^,#]	6.68	C-24,26,27
	thymosiosterane[^,%]	6.71	C-24,26,26'

1: total number of carbons in each compound
2: for αααR isomer of each sterane; 24-npc = 24-n-propylcholestane; 24-ipc = 24-isopropylcholestane; 26-mes = 26-methylstigmastane; aplysterane = 24,26-dimethylcholestane
3: RRT = GC Relative Retention Time (min) offset to cholestane (αααR); standard deviation +/- 0.02 min
4: site of alkylation on the sterane side-chain
5: The GC temperature program consisted of an initial hold at 60 °C for 2 min, heating to 150 °C at 10 °C/min followed by heating to 320 °C at 3 °C/min and a final hold for 22 min using a DB-1MS capillary column (60 m x 0.25 mm, 0.25 µm film) with He as carrier gas (see **Materials and Methods**)
^co-elution of αααR peaks for verongulasterane (24,26,27-trimethylcholestane) and thymosiosterane (24,26,26'-trimethylcholestane) within RRT standard deviation
[+]Brocks et al., 2017; [#]Kokke et al., 1978; [%]Vacelet et al., 2000

CHAPTER 2: FREE AND KEROGEN-BOUND BIOMARKERS FROM TONIAN SEDIMENTARY ROCKS RECORD ABUNDANT EUKARYOTES IN EARLY NEOPROTEROZOIC MARINE COMMUNITIES

Abstract

Lipid biomarker assemblages generated from the bitumen and kerogen phases of sedimentary rocks from the ca. 780-729 Ma Chuar and Visingsö Groups facilitate paleoenvironmental reconstructions and reveal fundamental aspects of early Neoproterozoic marine community structures. The Chuar and Visingsö Groups were deposited offshore two distinct paleocontinents (Laurentia and Baltica, respectively) during the Tonian period (1000-720 Ma) and unlike many successions of this age, samples used in this study had not undergone excessive metamorphism. The major polycyclic biomarkers detected in the rock bitumens and kerogen hydropyrolysates consisted of tricyclic terpanes, hopanes, methylhopanes and steranes. Substantial values for the sterane/hopane (S/H) ratio (between 0.09 and 0.38) were found for both the *free* and *kerogen-bound* biomarker pools for the organic-rich Chuar Group samples and were typically similar in magnitude in comparison with the more organic-lean Visingsö Group samples (S/H between 0.03 and 0.37). The overall biomarker distributions and stereochemical configurations were consistent with the thermal maturity gradient evident within the sample set, as recognized independently from Rock-Eval pyrolysis parameters. Major features of the biomarker assemblages include the first robust occurrences of *kerogen-bound* steranes from Tonian rocks; including 21-norcholestane, 27-norcholestane,

cholestane, ergostane and cryostane, along with an unidentified C_{30} sterane series from our least thermally mature Chuar Group samples. A C_{27} sterane (cholestane) predominance amongst total steranes was a common feature found for all samples investigated, with C_{26} steranes (norcholestanes) more prominent in the more mature rocks due to side-chain cracking during catagenesis. Apart from one late eluting C_{30} sterane series with an unknown side-chain chemistry, no traces of common ancient C_{30} sterane compounds, including 24-isopropylcholestanes, 24-*n*-propylcholestanes or 26-methylstigmastanes, were detected in any of these pre-Sturtian rocks. Our biomarker results support the view that the Tonian Period was a key interval in the history of life on our planet since it marked the transition from a bacterially dominated marine biosphere to an ocean system which became progressively enriched with eukaryotes, likely encompassing both autotrophic and heterotrophic organisms.

Introduction

Lipid biomarker (molecular fossil) assemblages recovered from thermally well-preserved sedimentary rocks can help unravel the temporal dynamics tied to the emergence, diversification and ecological expansion of Eukarya across the Proterozoic Eon (2500-541 Ma) and may be used to assess the quantitative impact of early eukaryotes within ancient marine communities (Dutkiewicz et al., 2003; Brocks et al., 2005, 2015, 2017; Luo et al., 2016; Gallagher et al., 2017; Isson et al., 2018). The mid-Proterozoic (1800-1000 Ma) interval was characterized by a remarkably long period of geochemical and climatic stability resulting from redox-dependent feedbacks within the coupled nutrient-carbon

cycles imposed on primary production in the surface ocean during this time (Holland et al., 2006; Lyons et al., 2014; Planavsky et al., 2014; Lee et al., 2015; Cole et al., 2016; Hardisty et al., 2017). Evidence from a wide array of geochemical proxy records, used in tandem with the microfossil record, shows a dramatic transition from the persistently reducing and stable mid-Proterozoic marine realm to a world of dramatic change and instability in climatic and tectonic conditions, ocean-atmosphere redox, the carbon cycle and biological innovation sometime later during the Neoproterozoic era (1000-541 Ma). Consistent with this body of work constraining ocean and atmospheric chemistry, recent evidence from lipid biomarker assemblages suggest that primary productivity in Mesoproterozoic (~1640-1000 Ma) oceans was dominated by communities rich in bacteria as revealed by a dearth of sterane (eukaryotic) biomarkers below detection limits of the most sensitive instrumentation (Fig. 10; Brocks et al., 2005, 2015, 2017; Blumenberg et al., 2012; Gueneli et al., 2012; Flannery & George, 2014; Luo et al., 2015; Suslova et al., 2017, Isson et al. 2018; Nguyen et al., 2019).

The emergence and subsequent ecological expansion of unicellular eukaryotes (e.g. planktonic algae) in ancient marine environments was a momentous evolutionary step that signified the divergence from a predominantly bacterial world and would later pave the way for the evolution of more complex multicellular organisms. However, our understanding of Proterozoic temporal dynamics and environmental changes that sparked the expansion of eukaryotes in the marine realm is quite sparse due to a patchy record of microfossil and biomarker data; particularly during the early stages of the Neoproterozoic

Era (1000-720 Ma). The resulting ‘temporal gap’ of biomarker data during this time is partly due to a scarcity of thermally well-preserved strata suitable for molecular biomarker analyses. Conversely, abundant steroidal lipid biomarker assemblages have been detected in younger rocks and oils from various Cryogenian-Cambrian paleoenvironments (~660-540 Ma) that have undergone a mild thermal history and reveal the widespread expansion of eukaryotic phytoplankton, convincing evidence for primitive sponges (Metazoa) and a marine trophic structure with diverse and complex communities by this time (Fig. 10; Grosjean et al., 2009; Love et al., 2009; Kelley et al., 2011; Dutta et al., 2013; Hoshino et al., 2017; Brocks et al., 2017; Zumberge et al., 2018).

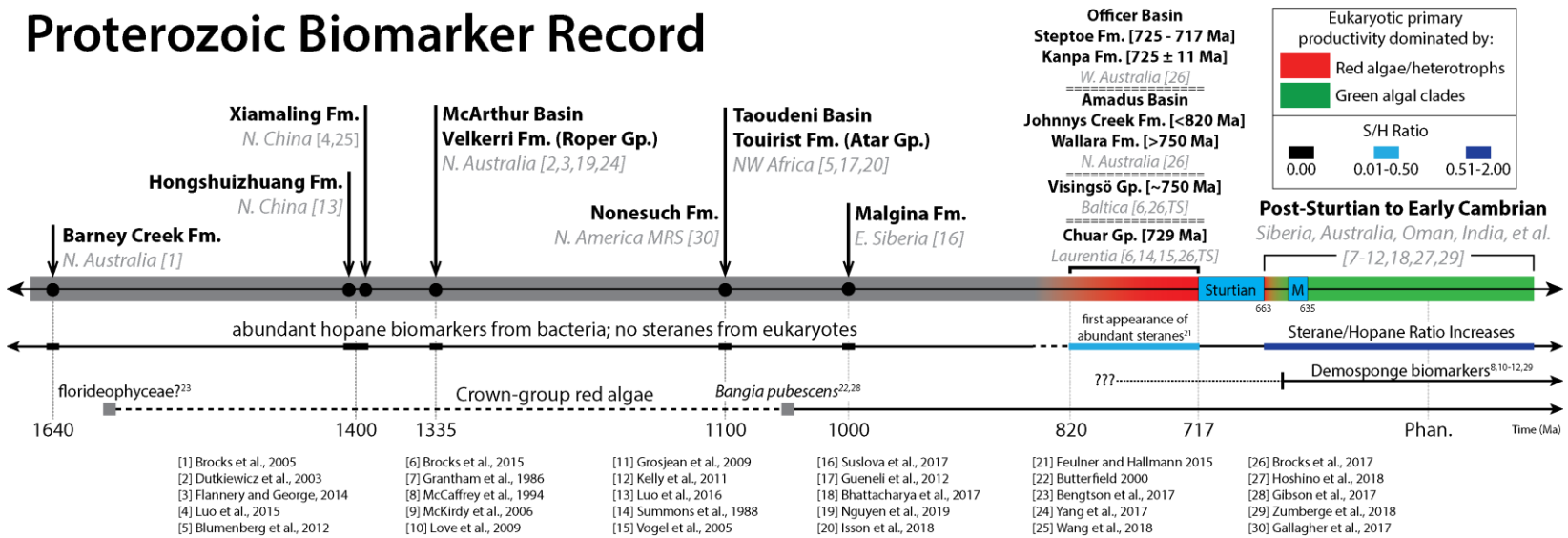

Figure 10. Biomarker record from numerous organic-rich sedimentary rock packages deposited throughout the Mesoproterozoic and into the Early Cambrian depicting the ecological expansion of steroid-producing eukaryotes as they became more abundant relative to bacteria, which dominated the biomarker record from ca. 1640-800 Ma. Steranes first appear in the rock record between ca. 820-717 Ma causing a stepwise increase in the S/H ratio here and once more during the Cryogenian-Early Cambrian before reaching average Phanerozoic S/H values of ~0.5-2.0. A shift in the dominating eukaryotic primary productivity biomarkers, from a C_{27} (red shaded area) to a C_{29} (green shaded area) sterane dominance, differentiates pre- and post-Sturtian marine paleoenvironments, respectively. It isn't until the interglacial period starting ca. 650 Ma that we see convincing evidence for complex eukaryotic organisms from demosponge-derived C_{30} steranes as well as the first appearance of macroscopic body fossils from the Ediacara biota.

Time resolved biomarker stratigraphic records compiled from successions of Proterozoic and Phanerozoic sedimentary rocks often target and compare hopane and sterane distributions and abundances as an insightful proxy for tracking the ecological input from the domains Bacteria and Eukarya, respectively (Grantham and Wakefield, 1988; Summons and Walter, 1990; Schwark and Empt, 2006). The basis of this application comes from the knowledge garnered from decades of microbial lipid surveys coupled with extensive genomic data which have shown that hopanoid and steroid lipids are synthesized in abundance by a broad range of bacteria and eukaryotes, respectively (Brocks and Pearson, 2005; Kodner et al., 2008; Gold et al., 2016). Authentic and verified biomarker records for the early Neoproterozoic (1000-720 Ma) can offer important ecological insights into Earth's evolving biosphere, such as the relative contributions of bacteria versus algae as major primary producers (Brocks et al., 2005; Love et al., 2009; Kelly et al., 2011; Blumenberg et al., 2012) as well as providing insights regarding the taxonomic affinities of the major eukaryotic organismal inputs (for example, the balance of source inputs from red versus green algal clades).

In this study, we investigated the composition of the diverse biomarker assemblages preserved in Tonian rocks sampled from two different paleocontinents, Baltica and Laurentia (Fig. 11). The sedimentary strata analyzed was deposited between ca. 780-729 Ma during a crucial interval of time which straddles the first appearance of genuine ancient steroidal biomarkers in the rock record derived from emerging unicellular eukaryotes prior to the Sturtian glaciation and the imminent appearance of Earth's earliest animals during

the Cryogenian Period (Love et al., 2009; Brocks et al., 2015; Zumberge et al., 2018). Outcrops from the Chuar Group (Grand Canyon, Arizona, USA) and the Visingsö Group (Sweden) were assessed via parallel analyses of the *free* and *bound* lipid biomarker assemblages recovered from the bitumen and kerogen phases of organic matter, respectively (Love et al., 1995, 2009; French et al., 2015). Parallel analyses of both the *free* (solvent-extractable) and the *kerogen-bound* biomarker pools offer the considerable advantages of ground-truthing free hydrocarbon biomarker data and identification of contaminants, as well as accessing a far higher proportion of the biomarker record since kerogen is quantitatively the most abundant organic matter pool in the geosphere (Love et al., 1995). This comprehensive analytical approach arguably renders a more accurate assessment of key ecological interpretations including the balance of source organismal inputs and information concerning the prevailing paleoenvironmental conditions at the time of deposition. Successful recovery and analysis of the *kerogen-bound* biomarkers via fixed-bed hydrogen pyrolysis (HyPy) confirms the syngenetic nature of the reported compounds since prevailing molecules in these paleoenvironments were readily incorporated during proto-kerogen formation; before burial and deposition of the host sediment (Love et al., 1995, 1997, 2009; Bishop et al., 1998; Meredith et al., 2014). Alternative methods that scrutinize the syngeneity of target compounds, including the comparison of exterior vs. interior rock portions (E/I), have also been successfully employed on rocks of this age (Brocks et al., 2015, 2017). The HyPy approach, however, offers the advantage of accessing a separate *bound* pool of biomarkers covalently linked within the kerogen, which is immobile by definition, and is the organic phase which is least

susceptible to biomarker contamination from drilling fluids and/or migrated petroleum products (Love et al., 2009; French et al., 2015). As such, HyPy is a valuable approach for testing the syngenicity of biomarker compounds in ancient rocks (Love et al., 1995, 2009; Meredith et al., 2014; Zumberge et al., 2018) and it was a key analytical strategy that verified that polycyclic biomarker alkanes reported from over mature Archean and Proterozoic rocks were in fact exogenous trace contaminants (French et al., 2015). Here we present and discuss the first combined *free* and *kerogen-bound* records obtained from early-Neoproterozoic biomarker assemblages from two different pre-Sturtian marine paleoenvironments. A quantitatively significant component of the biomarker assemblages detected are composed of steranes, and our results suggest that marine phytoplankton communities rich in algae emerged significantly prior to the onset of the Sturtian glaciation. This purported Tonian marine algal rise is in agreement with prior evidence proposed from zinc isotope records (Isson et al., 2018) and biogeochemical models (Feulner et al., 2015).

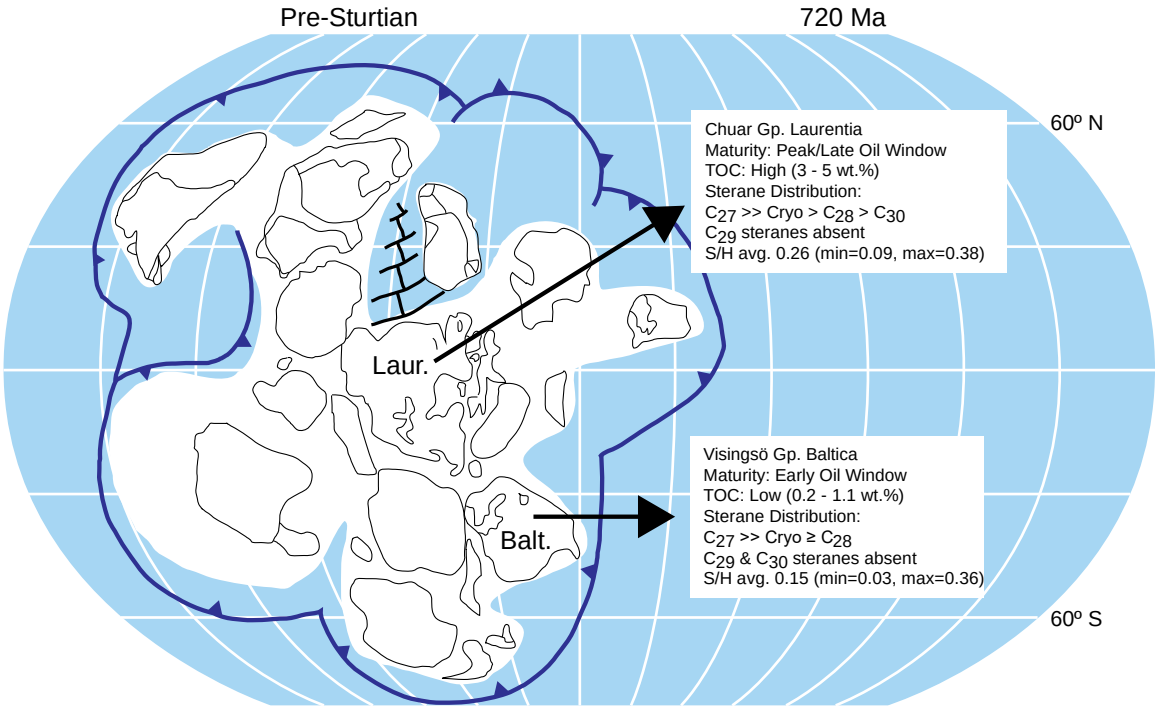

Figure 11. Tonian paleography highlighting the locations of two paleocontinents, Laurentia (Laur.) and Baltica (Balt.), where the sedimentary rocks in this study were originally deposited. Differences in thermal maturity and TOC content help make this an insightful dataset. Map adapted and modified from Hoffman et al., 2017.

Materials and Methods

Samples

Rock powders from the Chuar Group were obtained from GeoMark Research (Houston, TX) and have been described in detail elsewhere (Cook, 1991). Briefly, all Chuar samples were taken from one of two outcrop locations, Nankoweap Butte and Sixtymile Canyon, and are strata from within the Upper Walcott Member of the Kwagunt Formation, Chuar Group, Grand Canyon, Arizona. The Chuar Group mainly consists of marine mudstone deposited in an intracratonic extensional basin with evidence of ferruginous bottom waters with a later development of possibly euxinic conditions as revealed by carbon, sulfur and

iron chemostratigraphy (Johnston et al., 2010; Lillis 2016). Our results show that there is an obvious thermal maturity gradient of considerable magnitude between the two sampled outcrop locations. In particular, rocks from the Sixtymile Canyon section are less thermally mature (around *peak* oil window maturity) than rocks from the Nankoweap Butte section, which are designated as *late* oil window maturity. Recently, the age of the Upper Walcott Member was reassessed using coupled radioisotopic Re-Os and U-Pb geochronology to yield a date of 729 ± 0.9 Ma (Rooney et al., 2018) which is notably younger than the previous assigned date of 742 ± 6 Ma (Karlstrom et al., 2000).

Outcrops from the Visingsö Group were sampled within the Upper Member from previously described sections/localities including Uppgranna, Girabäcken and Boeryd (Vidal 1976; Samuelsson and Strauss 1999) along the southeastern shoreline of Lake Vättern in south-central Sweden. Additionally, a new outcrop section was found and sampled, dubbed *Broken Nodule*, and we report the biomarker results from strata in this location for the first time in this study. Thermal maturity parameters for our Visingsö Group outcrops reveal that all sampled sections/localities are *early-middle* oil window maturity and therefore suitable for biomarker analysis. The Visingsö Group has been interpreted as a shallow marine intertidal and subtidal environment that experienced intermittent upwelling of nutrient rich waters with organic rich shales and carbonates in the upper member (Vidal, 1976; Knoll and Vidal 1980; Samuelsson and Strauss, 1999). The maximum depositional age of the Visingsö Group has been reported as 919 ± 25 Ma, constrained by detrital zircon U-Pb (Pulsipher and Dehler, 2019), while the minimum

depositional age heavily relies on the biostratigraphic similarities of other temporally equivalent locations including the Chuar Group and the lower Mount Harper Group (Yukon, Canada) which were both deposited during the Tonian (Moczydlowska et al., 2018). The appearance and widespread distribution of organic walled vase-shaped microfossils (VSMs) within the Visingsö Group support a Tonian age of approx. 780-730 Ma (Martí Mus and Moczydlowska 2000; Porter and Knoll 2000; Moczydlowska et al., 2018; Riedman et al., 2018; Pulsipher and Dehler 2019).

Extraction and separation

Rock outcrop samples were carefully trimmed with a clean rock saw to remove the outer portion of the rock (typically 1-3 cm thickness) to isolate the inner rock portion for biomarker analyses and to minimize potential sources of contamination. The saw blade was extensively cleaned with a stepwise solvent wash of hexane, dichloromethane (DCM) and methanol (MeOH) between samples. Inner portions were then sonicated in sequence with the same solvent series. A SPEX 8515 shatterbox with a zirconian ceramic puck mill was used to powder the inner portion rock cuttings. Between each powdering step, the ceramic puck mill was extensively cleaned with the above solvent rinse cycle and pre-combusted sand (850 °C overnight) was powdered between samples to eliminate cross contamination. Rock samples from the Chuar Group were previously crushed and arrived at UCR as powders.

Lipid biomarkers were extracted in 9:1 v:v DCM:MeOH from the rock powders (~1-5 g depending on TOC wt.%.) using a Microwave Accelerated Reaction System (MARS; CEM Corp.) at 100 °C for 15 min with constant stirring (stirbar). Laboratory procedural blanks using combusted sand were extracted alongside each batch of rock powders to ensure that any background signals were negligible relative to the biomarker analytes recovered from these pre-Sturtian (pre-717 Ma) rocks. The extracts cooled to room temperature and were vacuum filtered. Excess solvent from the filtered total lipid extract (TLE) was evaporated from pre-weighed vials. After filtration, the extracted kerogen powder was collected and saved for fixed-bed hydrogen pyrolysis (HyPy) treatment. The extracted bitumen was separated into saturate, aromatic and polar fractions by silica gel column chromatography (36-70 mesh, activated at 450 °C overnight). The aliphatic (saturate) fraction was eluted with *n*-hexane, the aromatic fraction was eluted with 1:1 v:v *n*-hexane:DCM and the polar fraction was eluted with 3:1 v:v DCM:MeOH. Excess solvent from each fraction was evaporated and fractions were transferred to pre-weighed vials.

Hydropyrolysis (HyPy) of extracted rocks

As well as a detailed investigation of the *free* (extractable) biomarker hydrocarbons, the parallel analysis of the *kerogen-bound* pool of a subset of samples was performed for comparison. The technique of hydropyrolysis (HyPy) involves heating samples in a stream of high pressure H_2 gas in a continuous-flow reactor configuration. HyPy has been used previously to solubilize a significant fraction of sedimentary kerogen and other geomacromolecules, principally by cleavage of covalent cross-linkages (C-S, C-O, and C-

C) connecting the structural moieties together in the polymeric matrix. This fragmentation generates large quantities of aliphatic hydrocarbon products and fosters the release of the covalently bound lipid biomarkers from the macromolecular matrix of kerogen with minimal alteration to their stereochemistry (Love et al., 1995; Meredith et al., 2014).

The HyPy procedure for pre-extracted rocks and kerogen concentrates has been described in detail previously (Love et al., 1995, 2009; French et al., 2015; Zumberge et al., 2018). Briefly, pre-extracted sample powders (~0.5-1.0 g) were secured in the HyPy reactor tube atop a steel wool ball which was Soxhlet extracted (DCM, 48 h) and baked (450 ºC, 2 h) prior to use to ensure that no contaminants were introduced to the sample. Full procedural HyPy blanks were conducted using pre-fired silica gel as a substrate. Blank HyPy runs with the steel wool ball loaded in the reactor tube were run to verify that the batch of steel wool was clean and free of contamination, as described in French *et al*. (2015). HyPy is a temperature programmed pyrolysis technique using two temperature ramps: ambient to 250 °C at 100 °C/min immediately followed by 250 °C to 520 °C at 8 °C/min while maintaining constant hydrogen pressure of ~150 bar with a flow rate of 6 L/min. The pyrolysate product for each sample was collected onto silica gel (36-70 mesh, activated at 450 °C overnight) contained within a dry ice-cooled trap. After each HyPy run, the silica gel with the adsorbed pyrolysate product was separated using the same silica gel column chromatography method as described above for the extracted rock bitumens.

Instrumental Analysis

Multiple Reaction Monitoring-Gas Chromatography-Mass Spectrometry (MRM-GC-MS) of the saturate hydrocarbon fractions

Saturate fractions isolated from the extracted bitumen and kerogen HyPy pyrolysates were analyzed by MRM-GC-MS conducted at UCR on a Waters Autospec Premier mass spectrometer equipped with an Agilent 7890A gas chromatograph and DB-1MS coated capillary column (60 m x 0.25 mm i.d., 0.25 μm film thickness) using He for carrier gas. Typically, one microliter of a hydrocarbon fraction dissolved in *n*-hexane was injected onto the GC column in splitless injection mode. The GC temperature program consisted of an initial hold at 60 °C for 2 min, heating to 150 °C at 10 °C/min followed by heating to 320 °C at 3 °C/min and a final hold for 22 min. Analyses were performed in electron impact (EI) mode, with an ionization energy of 70 eV and an accelerating voltage of 8 kV. MRM transitions for C_{27}–C_{35} hopanes, C_{31}–C_{36} methylhopanes, C_{21}–C_{22} and C_{26}–C_{30} steranes, C_{30} methylsteranes and C_{19}–C_{26} tricyclic terpanes were monitored in the method used.

Procedural blanks with pre-combusted sand typically yielded less than 0.1 ng of individual hopane and sterane isomers per gram of combusted sand (Haddad et al., 2016). Polycyclic biomarker alkanes (tricyclic terpanes, hopanes, steranes, etc.) were quantified by addition of a deuterated C_{29} sterane standard [d_4-ααα-24-ethylcholestane (20R)] to saturated hydrocarbon fractions and comparison of relative peak areas. In MRM analyses, this standard compound was detected using 404→221 Da ion transition. Cross-talk of non-sterane signal in 414→217 Da ion chromatograms from C_{30} and C_{31} hopanes was < 0.2%

of 412→191 Da hopane signal [mainly 17α,21β(H)-hopane, which is resolvable from C_{30} steranes] and <1% of the 426→191 Da signal, respectively (Rohrssen et al., 2015).

Polycyclic biomarkers were quantified assuming equal mass spectral response factors between analytes and the d_4-C_{29}-ααα-24-ethylcholestane (20R) internal standard. Analytical errors for absolute yields of individual hopanes and steranes are estimated at ± 30%. Average uncertainties in hopane and sterane biomarker ratios are ± 8% as calculated from multiple analyses of a saturated hydrocarbon fraction prepared from AGSO and GeoMark Research standard oils (n = 30 MRM analyses).

Full scan GC-MS of the saturate and aromatic hydrocarbon fractions

Total Ion Chromatograms (TICs) for the saturate and aromatic fractions were generated by GC-MS in full scan mode over a mass range of 50 to 600 Da using an Agilent 7890A gas chromatograph coupled to an Agilent 5975C inert Mass Selective Detector (MSD). Samples were injected as hexane solutions in splitless injection mode using He as the carrier gas. The GC was equipped with a DB-1MS capillary column (60 m x 0.32 mm i.d., 0.25 µm film thickness). The GC oven was programmed from 60 ºC (2 min), ramped to 150 ºC at 20 ºC/min, then to 325 ºC at 2 ºC/min, and held at 325 ºC for 20 min.

GC-MS/MS (QQQ) of the saturate and aromatic hydrocarbons

GC-MS/MS was performed on an Agilent 7000A Triple Quad (QQQ) interfaced with an Agilent 7890A gas chromatograph equipped with a J&W Scientific DB-5MS+DG capillary

column (60 m x 0.25 mm i.d., 0.25 µm film thickness, 10 m guard). Using He as carrier gas, the flow was programmed from 1.2 mL/min to 3.2 mL/min. The GC oven was programmed from 40 °C (2 min) to 325 °C (25.75 min) at 4 °C/min. Samples were spiked with a mixture of 7 internal standards (Chiron Routine Biomarker Internal Standard Cocktail 1) and injected in cold splitless mode at 45 °C with the injector temperature ramped at 700 °C/min to 300 °C. The MS source was operated in EI-mode at 300 °C with ionization energy at -70 eV. The number of molecular ion to fragment transitions varied throughout the run; dwell time was adjusted as needed to produce 3.5 cycles/second.

Results and Discussion

Total organic carbon (TOC) and thermal maturity

TOC values for our Chuar rock samples are among some of the highest reported in the literature to date (Brocks et al., 2015, 2017) for Tonian sedimentary rocks (min=3.54, max=5.61, mean=4.36 wt.%; Table 7). Rock Eval pyrolysis parameters reveal that within the Chuar Group, outcrops from the Nankoweap Butte section are *late* oil window thermal maturity while outcrops from the Sixtymile Canyon section are noticeably less mature and fall near *peak* oil window. Rock Eval S2 values reflect the high amounts of organic carbon covalently bound within the kerogen (min=4.13, max=7.39, mean=4.51 mg HC/g rock) while decreasing HI values show the effects of elevated thermal maturity (min=64, max=132, mean=101 mg/g TOC; Table 7). Additional evidence for this interpretation is supported by several thermally sensitive biomarker proxies that confirm the elevated maturity in both the *free* and *bound* biomarker pools for Nankoweap Butte section in

particular. Therefore, thermal maturity differences between the four Chuar Group samples plays a significant role in modifying the hopane and sterane biomarker patterns, as reflected by diastereoisomer ratios that are sensitive to elevated levels of thermal stress (Table 8, Fig. 12; e.g. tricyclics/$C_{30}\alpha\beta H$, C_{27} Ts/Tm, C_{29} Ts/Tm, loss of $C_{31\text{-}35}$ homohopanes) (Seifert and Moldowan, 1978; Zumberge 1987; Moldowan et. al., 1991; Peters et al., 2005).

The extract and HyPy pyrolysate products from the Nankoweap Butte locality are more mature than the stratigraphically equivalent Sixtymile Canyon samples and as a result the structural and stereochemical features of the polycyclic biomarker alkane signals from this section are not as well preserved (Fig. 12). The apparent thermal maturity gradient between the two sections is an important factor to consider when using biomarkers as a tool in the interpretation of past paleoenvironmental conditions and in the inferred reconstruction of the Chuar Group's depositional environment. Thus, the two samples from Sixtymile Canyon (SWE2 & SW4) host the most thermally well-preserved biomarker assemblages and are ideal candidates for source organismal and paleoenvironmental reconstruction because of the lower thermal maturity assessment and better preservation of a wider range of linear, branched and polycyclic hydrocarbon biomarker structures.

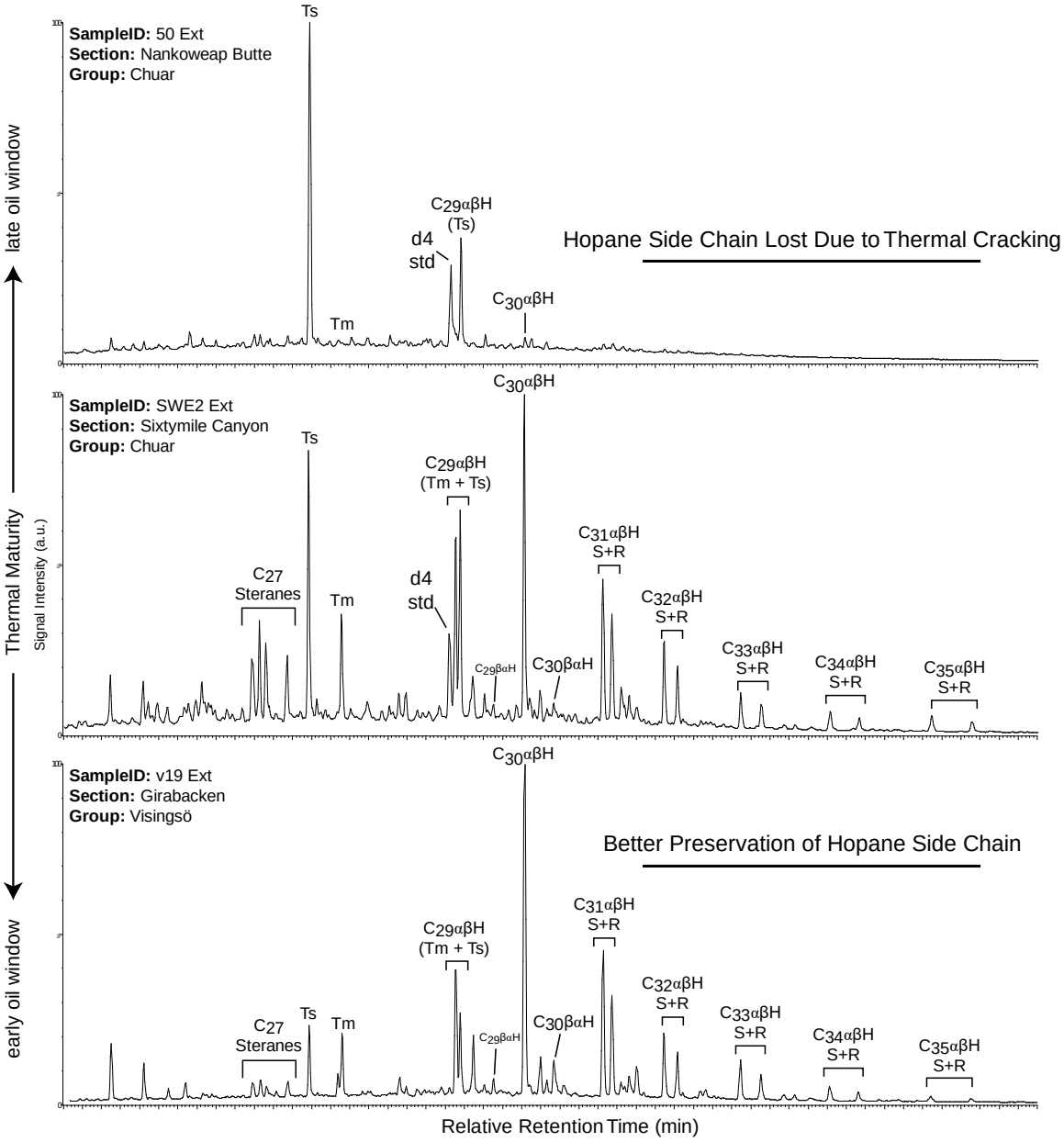

Figure 12. C_{26}-C_{30} sterane and C_{27}-C_{35} hopane distributions from composite chromatograms (MRM-GC-MS transitions $M^{+}\rightarrow217+191$) of the free (extractable) organic matter shows thermal maturity differences between samples in this study. Rocks from the Walcott Member of the Chuar Group are either (top) *late* oil window maturity, characteristic of the Nankoweap Butte Section or (middle) *peak* oil window maturity, characteristic of the Sixtymile Canyon Section. Conversely, rocks recovered from all sections in the Visingsö Group are (bottom) *early-middle* oil window maturity, consistent with stereoisomer distributions. See Table 8 for peak identifications.

Compared to the Chuar Group, the Visingsö Group samples in this study had lower TOC (min=0.26, max=1.13, mean=0.52 wt.%; Table 7) contents but were better thermally preserved. The sample maturity sits within the *early* to *middle* oil window resulting in better preservation of the polycyclic hydrocarbon biomarkers including steranes, hopanes and their methylated homologues (Fig. 12). Rock Eval parameters for eight Visingsö Group outcrops from four distinct sections report low S2 values (min=0.22, max=2.54, mean=0.79 mg HC/g rock) and a range of HI values (min=60, max=225, mean=130 mg/g TOC; Table 7) mostly related to organic matter source inputs under low productivity environmental conditions that were not strongly reducing. The *early-middle* oil window maturity assignment reported from the Rock Eval data is in agreement with thermally sensitive biomarker ratios, including C_{27} hopane isomers Ts and Tm (C_{27} Ts/Tm; min=0.44, max=1.46, mean=0.92) and the total amount of tricyclic terpanes relative to C_{30} hopane (tricyclics/$C_{30}\alpha\beta H$; min=0.61, max=2.69, mean=1.51). The combined sampling of Chuar and Visingsö Groups allows for a more complete picture of Tonian marine biomarker assemblage variations.

Table 7. TOC (total organic carbon, wt.%) and Rock-Eval pyrolysis data for the samples in this study. S2 (mg HC/g) captured at a high ramp temperature [~430-460 °C] = volume of hydrocarbons (HC) that are measured during thermal pyrolysis of the sample; HI (Hydrogen Index, mg/g TOC) = S2*100/TOC

Section/Locality	SampleID	TOC (wt.%)	S2 (mg HC/g)	HI (mg/g TOC)
Chuar Gp., Kwagunt Fm., Walcott Mbr. (Grand Canyon, AZ, USA)				
Nankoweap Butte	36	4.70	4.13	88
	50	3.54	2.27	64
Sixtymile Canyon	SW4	3.57	4.25	119
	SWE2	5.61	7.39	132
Visingsö Gp., Upper Fm. (Lake Vättern, South Central Sweden)				
Uppgranna	v1	0.37	0.22	60
Broken Nodule	v10	0.82	1.44	176
	v12	1.13	2.54	225
	v24	0.57	0.75	132
	v31	0.31	0.37	120
	v37	0.26	0.28	107
Girabacken	v19	0.35	0.43	124
Boeyrd	v21	0.31	0.30	97

Total aliphatic hydrocarbon distributions

Trends within the total aliphatic hydrocarbon distributions (e.g. tricyclic terpanes, hopanes and steranes) are evident when comparing samples from the Chuar and Visingsö Groups (Fig. 13). Typically, a snapshot of all aliphatic hydrocarbons permits rapid assessment of major source biota inputs, environmental conditions at the time of deposition and thermal maturity. For example, samples from the Chuar Group typically have higher abundances of tricyclic terpanes relative to hopanes whereas the opposite is true for the thermally immature Visingsö Group. This is due, in part, to the release of more tricyclic terpanes relative to hopanes from the kerogen at high levels of thermal maturity (Aquino Neto et al., 1983).

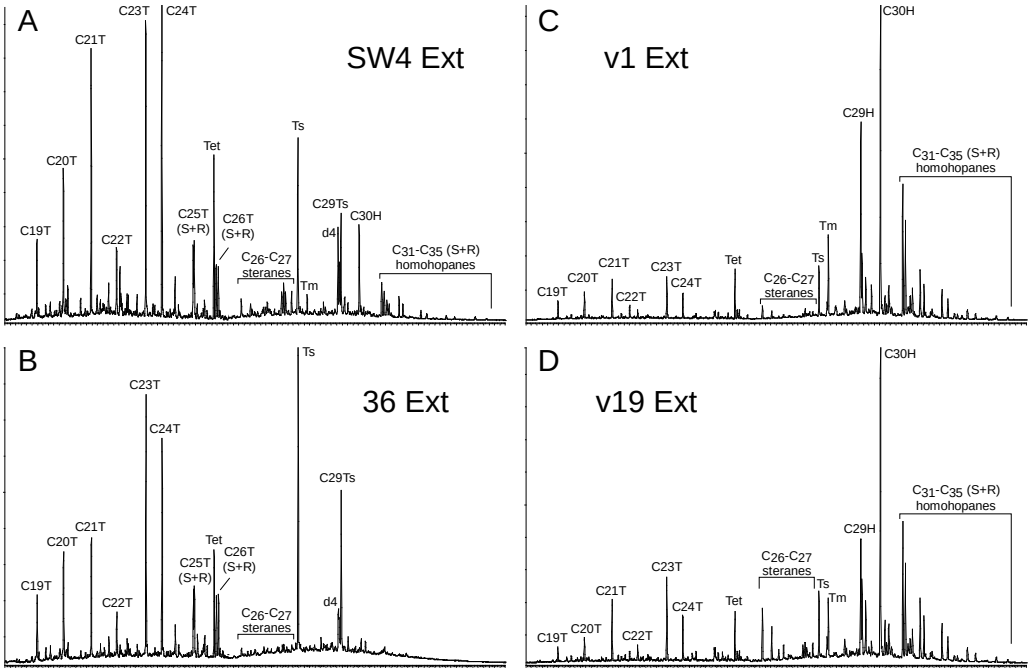

Figure 13. MRM-GC-MS traces of the total ion chromatograms (TIC) for representative samples from the (A-B) Chuar and (C-D) Visingsö Groups. Aliphatic hydrocarbon distributions (e.g. tricyclic terpanes, hopanes and steranes) are influenced by source biota, depositional environment and the thermal maturity of the host rock. See Table 8 for detailed peak identification.

Sterane assemblages in the Chuar Group

Saturated sterane biomarkers recovered from the *free* and *bound* phases of organic matter (Fig. 14) via solvent extraction and HyPy treatment, respectively, reveal that C_{26} and C_{27} dia- and regular steranes collectively account for the majority of detectable steranes with a combined average of 94% of the total C_{26}-C_{30} steranes. Cryostane (26-methylcholestane), a terminally methylated late-eluting and age diagnostic C_{28} sterane biomarker unique to pre-Sturtian paleoenvironments (Vogel et al., 2005; Brocks et al., 2015, 2017; Adam et al., 2018), was recovered in all Chuar outcrops in this study and constituted an average of 4% of the total C_{26}-C_{30} steranes detected.

Contrary to recent studies of Chuar Group sedimentary extracts (Brocks et al., 2015), we were able to detect appreciable amounts of ergostane (24-methylcholestane) in the free extract phase from all samples with an average abundance of 4% of the total steranes (Table 8). Ergostane was readily detected in the lipid biomarker assemblages generated from fragmentation of kerogen from the two most thermally well-preserved samples, SWE2 and SW4 (Fig. 15), which helps confirm the syngenicity with the host rocks. Due to the elevated thermal maturity of the two outcrops from Nankoweap Butte, samples 36 and 50, any ergostane and cryostane from the HyPy products were below detection limits and instead only C_{26} and C_{27} regular steranes were detected. It's worth noting that for the high maturity samples from Nankoweap Butte, 96% of the total steranes resided in the *free* extract phase while only 4% were from the *kerogen-bound* component. The majority of the bound sterane pool would have been released by covalent bond cleavage into the free hydrocarbon phase during catagenesis at this late stage of the oil window. This explains why only the most abundant steranes (nor-cholestanes and cholestanes) were detected in the two over-mature Nankoweap Butte HyPy products.

Stigmastane was seemingly absent in both the *free* and *bound* phases of all outcrops from the Chuar Group. This parallels previous work on samples from the Kwagunt Formation and the absence of any known C_{29} sterane series seems to be an attribute common to pre-Sturtian sedimentary srata, which have been selected for their appropriate thermal maturity and possess no significant contributions of organic contamination from younger/exogenous hydrocarbons (Summons et al., 1988; Vogel et al., 2005; Brocks et al., 2015, 2017).

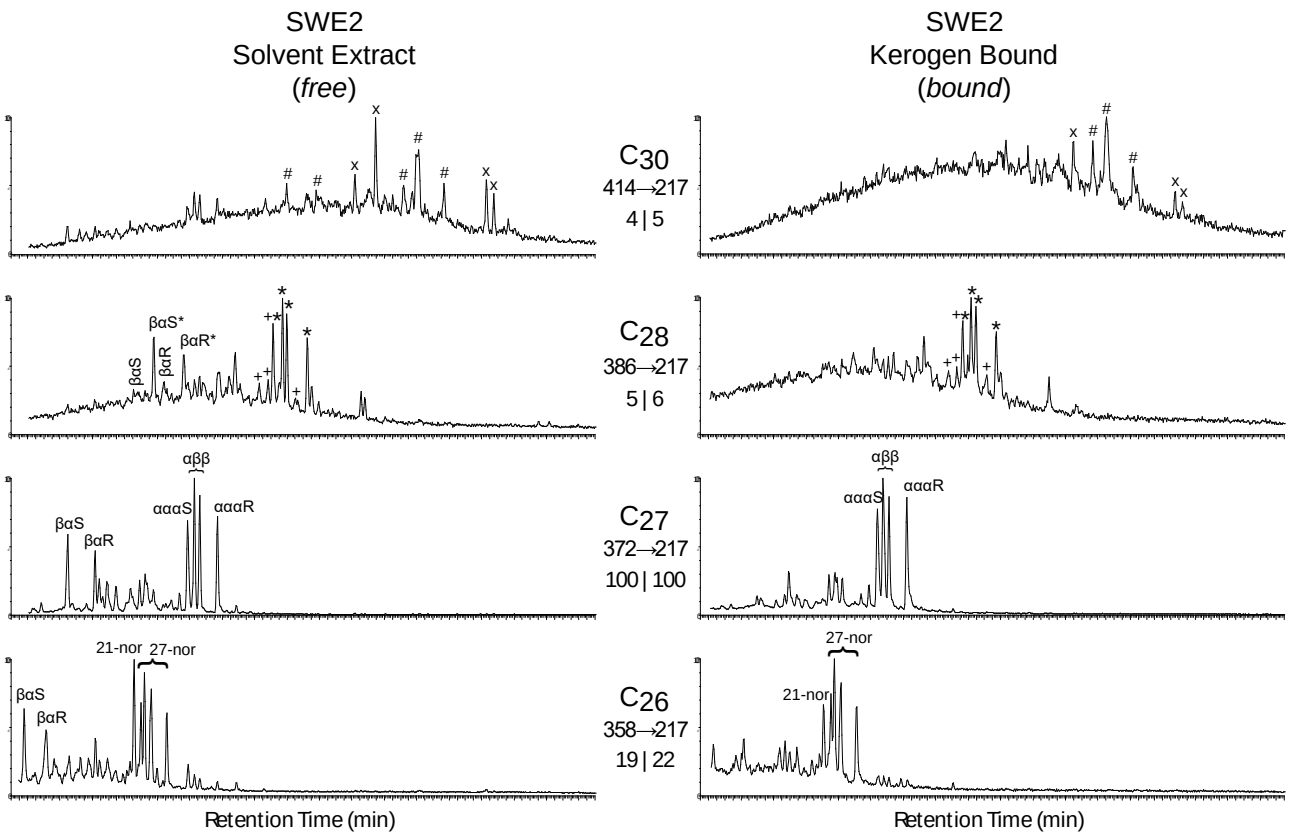

Figure 14. MRM-GC-MS ($M^+ \rightarrow 217$ Da) chromatograms of the *free* (left) and *kerogen-bound* (right) C_{26}-C_{30} steranes from sample SWE2 (Chuar Group, Sixtymile Canyon Section). Sterane distributions and relative abundance comparisons between the bitumen and kerogen phases of organic matter show that the biomarkers are syngenetic with the host sedimentary rocks and exhibit no discernible signs of contamination from younger/exogenous hydrocarbons are present. Compared to the *free* phase, the sterane distributions from the *bound* phase show a slightly less mature isomer distribution (21-nor < 27-nor, C_{27} αααR > αααS). There are at least five detectable 'regular' sterane series (each with αααR+S and αββR+S isomers). 21-nor = 21-norcholestane; 27-nor = 27-norcholestane; + = ergostane; * = cryostane; # = C_{30} series with unknown side-chain chemistry. Cross-talk (x) from the more abundant hopanes can interfere with the C_{30} (414→217 Da) trace.

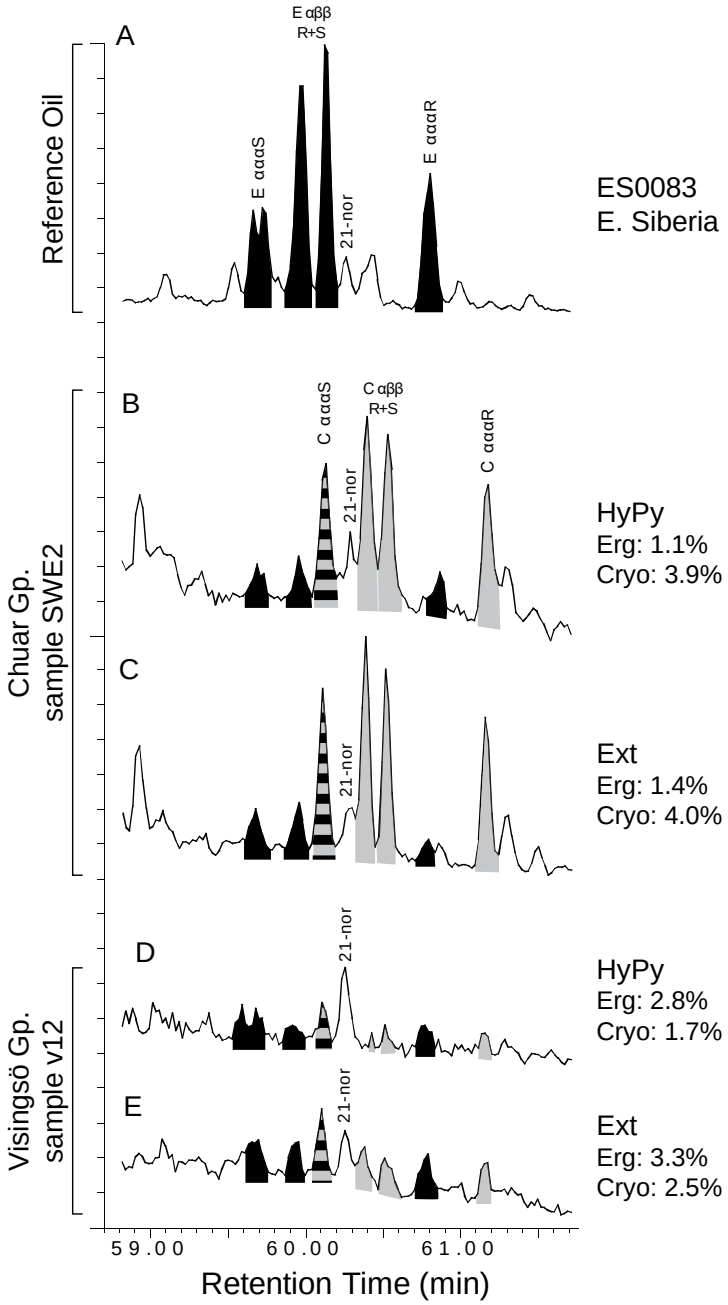

Figure 15. MRM-GC-MS (386→217 Da) chromatograms of the C_{28} steranes from the *kerogen-bound* (HyPy) and *solvent extractable* (Ext) biomarker pools from representative samples from the Chuar Group (B-C) and Visingsö Group (D-E). Percent ergostane (Erg) and cryostane (Cryo), relative to the total detectable C_{26}-C_{30} steranes, are shown on the right and the absence of cryostane in (A) a Lower Cambrian Reference Oil from Eastern Siberia (Kelly et al., 2011; ES0083) is noted. Black shaded peaks = ergostane (αααR+S and αββR+S isomers) = E; Gray shaded peaks = cryostane (αααR+S and αββR+S isomers) = C; Stripped peak = co-elution of αββ 20(S) ergostane and ααα 20(S) cryostane; 21-nor = 21-norstigmastane.

Interestingly, and reported here for the first time, we discovered a low abundance but robust signal of a late eluting C_{30} sterane series (with all four geologic isomers; αααS+R and αββS+R) in both samples from the Sixtymile Canyon locality (SWE2 & SW4). In the *free* hydrocarbon phase in the rock bitumen, this unknown C_{30} sterane series comprised 1% of the total C_{26}-C_{30} sterane signal for both outcrops and its presence was confirmed as a syngenetic compound via recovery from the kerogen-bound HyPy component in which it constituted ca. 2% of the total detectable steranes for both samples (Fig. 16; Table 8). Relative to the elution patterns of other C_{30} steranes with known structures; including 24-*n*-propylcholestane (24-npc), 24-isopropylcholestane (24-ipc) and 26-methylstigamstane (26-mes) (Moldowan et al., 1984; McCafferty et al., 1994; Love et al., 2009; Zumberge et al., 2018), this series has a markedly higher retention time and has been confirmed on two separate mass spectrometers that employ columns with different stationary phases (DB-1MS and DB-5MS). These features suggest a sterane core hydrocarbon structure with extensive alkylation on the side chain, most likely with all three additional carbon atoms (relative to the basic cholestane skeleton) restricted to the terminal C-26 and/or C-27 positions making it a possible C_{30} analogue of cryostane (26-methylcholestane). No 24-npc, 24-ipc or 26-mes steranes were detectable in any of our Tonian rock extracts or kerogen hydropyrolysates products, consistent with previous work that these steranes are only found in Cryogenian and younger rocks and oils (Zumberge et al., 2018).

Our current understanding of eukaryotic steroid biosynthetic pathways that modify and extend the steroid side chain point to Porifera, specifically the demosponge group, as

plausible candidate parent organisms for such a derived C_{30} steroid structure. As is the case with cryostane, this hypothesis needs further investigation since the appropriate sterol precursor compound, possessing the specific structural features in the hydrocarbon core, has not yet been recovered from any modern taxa. Parallel analysis of intact sterol precursors with their sterane derivatives produced directly from hydrogenation of biomass from extant taxa has proved to be a reliable method for the elucidation of C_{30} sterane compounds detected commonly and in abundance in Neoproterozoic-Cambrian rocks and oils (Zumberge et al., 2018). The absence of any corresponding sterol precursor match reported to date for the late-eluting C_{30} sterane series may alternatively suggest this was the product of an extinct enzymatic pathway that isn't utilized by any modern demosponge or other eukaryotic group. It is possible that it may even constitute an ancient metazoan biomarker compound given that terminally methylated steroids have a deep origin within the demosponge clade (Zumberge et al., 2018).

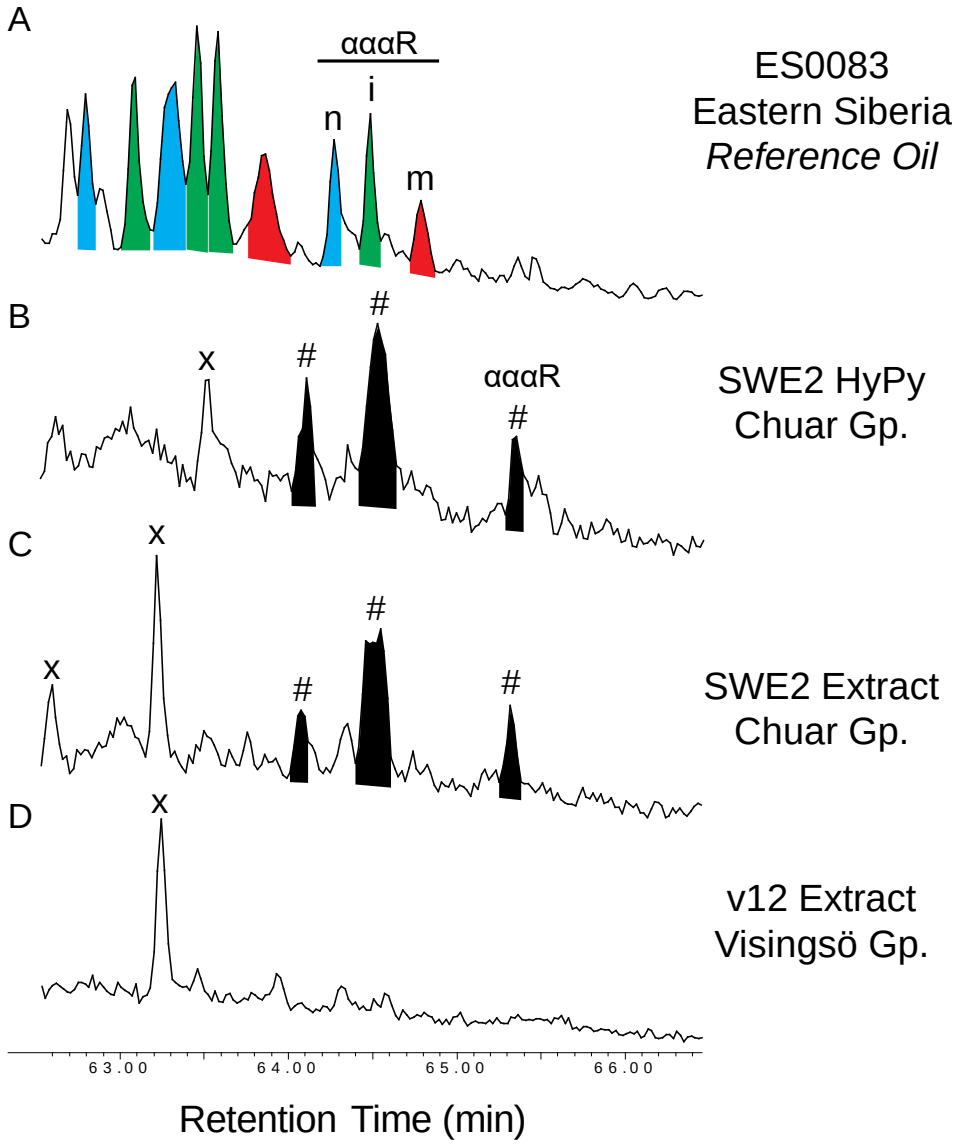

Figure 16. MRM-GC-MS (414→217 Da) chromatograms showing the C_{30} sterane distributions in representative Tonian sedimentary rocks (this study) compared with a (A) Lower Cambrian Reference Oil from Eastern Siberia (Kelly et al., 2011). ES0083 has a typical post-Sturtian C_{30} sterane distribution with three resolvable compounds: 24-*n*-propylcholestane (n/blue peaks), 24-isopropylcholestane (i/green peaks) and 26-methylstigmastane (m/red peaks) (Love et al., 2009; Zumberge et al., 2018). One novel C_{30} sterane series (#/black peaks), with a conventional mature stereoisomer distribution (αααS, αββ(R+S), αααR) and unknown side-chain chemistry was recognized from the most thermally well-preserved section of the Chuar Group; Sixtymile Canyon. The unknown C_{30} sterane series was first found in the (C) solvent extract (*free*) phase of sample SWE2 and was later confirmed to be a genuine signal after it was identified in the (B) kerogen (*bound*) phase. Sample (D) v12 conveys the absence of *any* C_{30} steranes within the Visingsö Group outcrops. Peaks labeled 'X' represent crosstalk. The αααR isomer is emphasized to show the difference in compound elution time between all four C_{30} steranes, with the new C_{30} sterane compound eluting last.

Based on the elution patterns of all known geologic regular (4-desmethyl) C_{30} steranes (Zumberge et al., 2018), we predict the unknown C_{30} sterane series detected in our Chuar outcrops is biogenic and likely contains an extended side chain through successive methylation exclusively at terminal positions with no carbon substituents at the C-24 position as typically found for conventional steroids. It is less likely that this unknown C_{30} sterane series is the product of secondary diagenetic alteration of C_{29} and other steranes. A biological rather than diagenetic origin for this C_{30} sterane compound can be supported by a number of lines of evidence including: i) we would expect to see multiple (not just one) series/peaks if three extra carbon atoms were randomly added to the steryl side chain at different positions, ii) this sterane compound is not ubiquitous in the ancient rock record as it has been shown from immature Ediacaran rocks from Baltica, for which C_{29} steranes dominate, that any C_{30} steranes are either only found at vanishingly trace levels or mainly below detection limits (Pehr et al., 2018) suggesting that any diagenetic source contribution to C_{30} steranes are negligible, and iii) this specific unknown C_{30} sterane compound seems thus far to be age-diagnostic for the Tonian Period since it has not been detected in sedimentary strata from any other age.

Sterane assemblages in the Visingsö Group

Some of the main features of the sterane distribution patterns from our eight Visingsö Group samples are strikingly similar to what was reported in our Chuar Group samples even though both locations were subject to different thermal histories and are interpreted as being deposited in different depositional marine paleoenvironmental settings. Outcrops

from all four sections show cholestanes dominating over other steranes with appreciable amounts of nor-cholestanes, ergostanes and cryostanes detected while no stigmastanes, 24-npc, 24-ipc or 26-mes series were reported (Fig. 17).

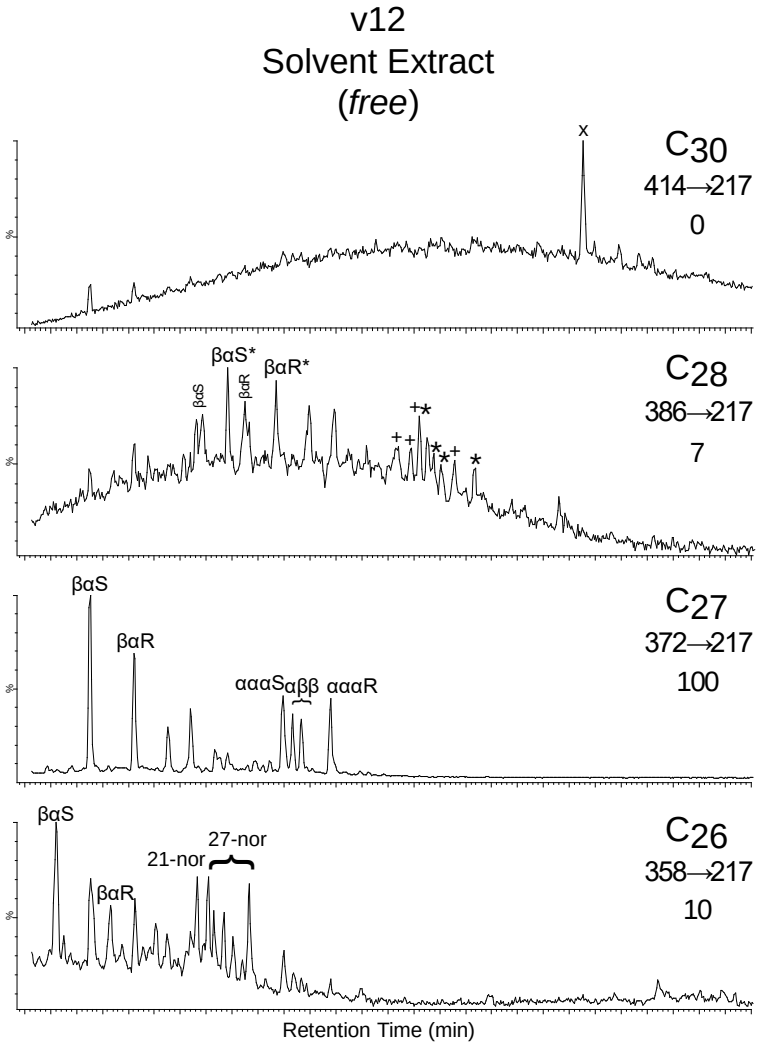

Figure 17. MRM-GC-MS ($M^+ \rightarrow 217$ Da) chromatograms of the solvent extract (*free*) C_{26}-C_{30} steranes from sample v12 (Visingsö Group, Broken Nodule). There are at least four detectable 'regular' sterane series (each with αααR+S and αββR+S isomers). 21-nor = 21-norcholestane; 27-nor = 27-norcholestane; + = ergostane; * = cryostane. Cross-talk (x) from the more abundant hopanes can interfere with the C_{30} (414→217 Da) trace.

The confirmed presence of ergostane (24-methylcholestane) in Tonian sedimentary rock samples from both Chuar and Visingsö Groups is an important finding since 24-alkylated steranes are only known from eukaryotes and cannot apparently be produced by bacteria (Wei et al., 2016). There are select bacteria capable of making cholestane, as well as cholestane precursors, but not apparently steroids with additional side chain alkylation at C-24 or other side chain sites (Summons et al., 2006; Wei et al., 2016). Additionally, the detection of ergostane and steranes other than cholestane also argues against eukaryotic source organismal inputs exclusively comprised of heterotrophic protists (Brocks et al., 2017) and suggests that eukaryotic phytoplankton and other primary producers made a significant source contribution to the total sterane biomarker pool during this time.

Unlike the Chuar Group, however, we did not detect the late eluting unknown C_{30} sterane series that was found in the most thermally well preserved Chuar outcrops from Sixtymile Canyon (Fig. 16). This is potentially due to i) the stark contrast in TOC contents between the two locations where average TOC content for samples from the Visingsö Group were 0.52 wt.% while those from the Chuar Group were 4.36 wt.%, ii) primary differences in the bacterial communities and ecologies between the two locations or iii) local environmental conditions and nutrient budgets that would not be favorable for the host organism(s) responsible for biosynthesizing the necessary sterol precursor that would be deposited and preserved as the unknown C_{30} sterane biomarker. Since the unknown C_{30} sterane series detected in our Chuar Group samples, which have TOC values that are up to an order of magnitude higher than the Visingsö Group, constitutes only ~1-2% of the *total*

C_{26}-C_{30} steranes we suspect the low organic carbon content of the Visingsö Group might mask the presence of this compound due to a reduction in total sterane signal below the detection limits of even our most sensitive MRM-GC-MS instrument. To test this theory, the search for this unknown C_{30} sterane series should continue in other thermally well-preserved pre-Sturtian rocks with similar or higher TOC contents.

Hopane assemblages in the Chuar and Visingsö Groups

The distribution of tricyclic, tetracyclic and pentacyclic terpanes (particularly hopanes) in our suite of Chuar and Visingsö Group outcrops reflects source organismal inputs as well as preservational controls from thermal maturity trends that were independently observed from Rock Eval pyrolysis parameters reported in Table 7. For example, the maturity gradient between the Nankoweap Butte and Sixtymile Canyon section of our Chuar Group outcrops is clearly illustrated by numerous maturity-sensitive hopane and other terpane stereoisomer ratios including the overall abundance of tricyclic terpanes to C_{30} αβ-hopane (tricyclics/C_{30}αβH), Ts/Tm isomer ratios from both C_{27} and C_{29} hopanes (C_{27} Ts/Tm, C_{29} Ts/Tm) and the relative abundance of C_{30} βα-hopane (moretane) to C_{30} αβ-hopane (C_{30}βαH/C_{30}αβH) (Fig. 18, Table 8). Conversely, the hopane biomarker distribution from our Visingsö Group rocks resembles a typical *early* oil window maturity assessment with low (ca. <1.5) Ts/Tm isomer ratios in both C_{27} and C_{29} hopanes (C_{27} Ts/Tm, C_{29} Ts/Tm) and full preservation of the C_{31}-C_{35} homohopane series in all samples (Fig. 18, Table 8) since thermal cracking of the hopane side chain was not as pronounced as it was for the Chuar Group samples.

In addition to the obvious contrast of thermal maturity levels from each location, our collection of Chuar and Visingsö Group rocks also show stark variances in certain source specific triterpane biomarker ratios, particularly the relative abundance of gammacerane to C_{30} hopane ($G/C_{30}\alpha\beta H$; Table 8). More specifically, the Chuar Group $G/C_{30}\alpha\beta H$ ratio ranges from 0.11 – 0.45 (mean=0.24) while the Visingsö Group values range from 0.01 – 0.07 (mean=0.03); approximately an order of magnitude difference between the two locations. Gammacerane is the diagenetic product of the lipid tetrahymanol, found in abundance in ciliates, and is most often associated with water column stratification and/or hypersaline marine depositional environments (Sinninghe Damste et al., 1995). Ciliates are a class of heterotrophic protists that are analogous to the abundant testate amoeba (vase shaped microfossils; VSMs) found widespread throughout the Chuar Group and other Tonian paleoenvironments (Porter and Knoll 2000; Porter et al., 2003). It should be noted that in relation to the diverse distribution of VSM species recovered from the Chuar Group (which is the only Tonian environment where all known VSM species (n=8) have been recovered), the Visingsö Group hosts approximately half as much VSMs (Riedman et al., 2018), perhaps explaining the stark difference in the $G/C_{30}\alpha\beta H$ ratio between these two locations. These heterotrophic protists prey on bacterial and/or algal biomass and considering both of these organisms had a pronounced presence in the Chuar Group, ciliates in this environment may have thrived.

Biomarker evidence for abundant Neoproterozoic ciliates, and by inference a rise in bacterivorous herbivory, was previously proposed from the detection of elevated

abundances of gammacerane (Summons et al., 1988). The earliest spike in gammacerane abundance relative to hopanes above a low Mesoproterozoic background value is first observed in sedimentary strata from the Chuar Group (ca. 780-729 Ma), deposited prior to the Sturtian glaciation (Summons et al., 1988; van Maldegem et al., 2019; this study) and we confirm the elevated gammacerane/hopane ratio here for the first time for the *kerogen-bound* biomarker pool from Walcott Member of the Chuar Group after HyPy treatment. Alternatively, bacteria are a plausible source of gammacerane (and methyl-gammacerane) which could explain the trace amounts of gammacerane detected in Mesoproterozoic rocks from the Roper Group (Takashita et al, 2017; Nguyen et al., 2019), although in much lower abundances relative to hopanes than as found for Chuar Group rocks. Together, these biomarker assemblages are likely indicative of a marine environment and trophic structure rich in eukaryotic organisms during the Tonian Period which was substantially different to the communities supported by bacterially dominated Mesoproterozoic ocean systems.

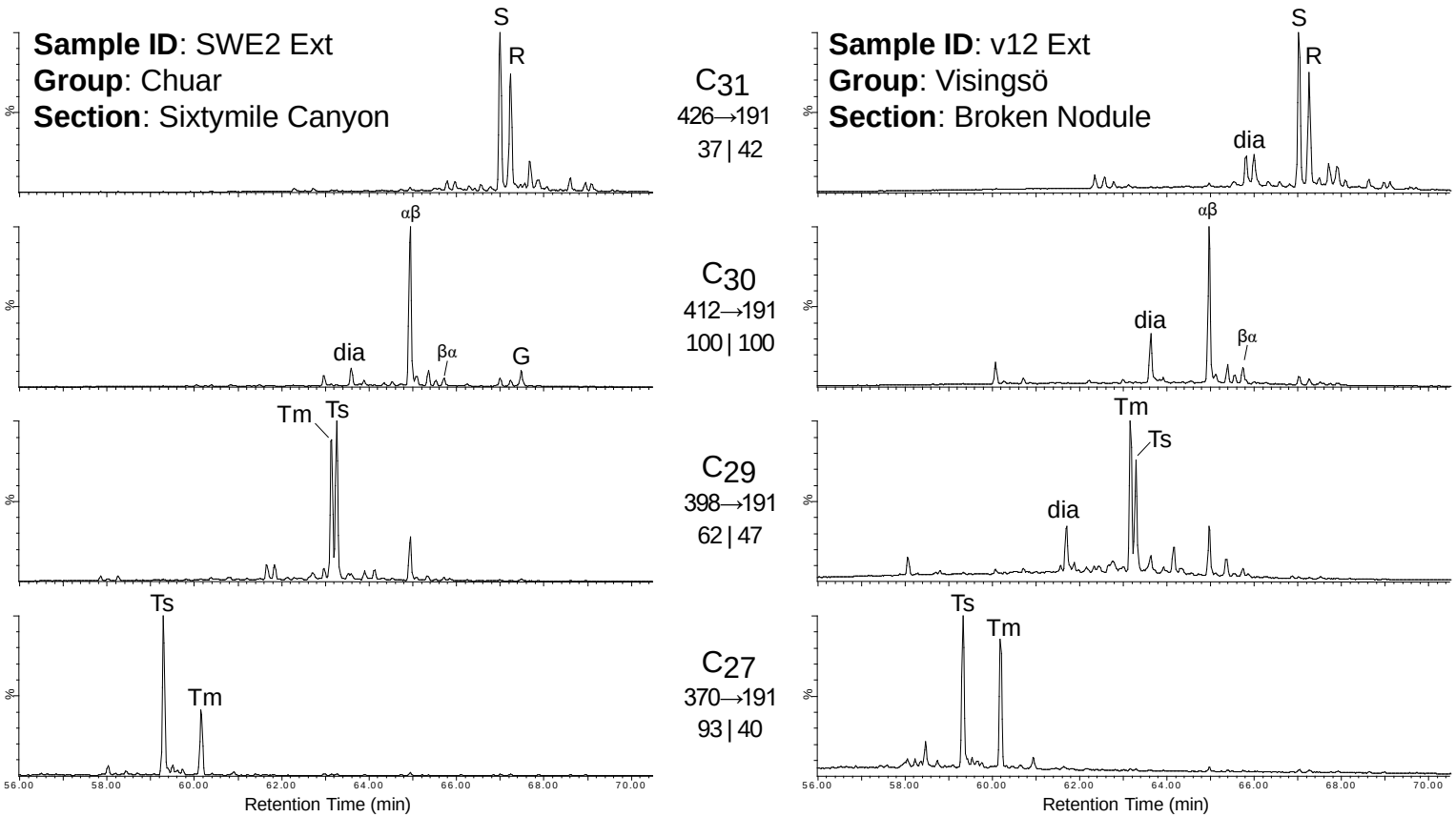

Figure 18. MRM-GC-MS ($M^+ \rightarrow 191$ Da) chromatograms of the C_{27}-C_{31} hopanes for samples (left) SWE2 from the Walcott Member of the Chuar Group and (right) v12 from the Visingsö Group. Differences in the thermal history or each sample is reflected by key hopane compound ratios: C_{27} Ts/Tm; C_{29} Ts/Tm; C_{30} βαH/αβH. Additionally, there are diagnostic biomarker characteristics unique to each location: the Chuar Group has high amounts of gammacerane (G) while the Visingsö Group has elevated diahopanes (dia) reflecting different ecologies and depositional environmental conditions. Relative abundances for each trace are shown beneath the MRM transition. See Table 8 for detailed peak identification.

Table 8. Maturity and source sensitive biomarker ratios from the solvent extract (SE) and kerogen-bound (KB) phases of organic matter for the samples in this study. Upg: Uppgranna; Byd: Boeyrd; Tricyclics: C_{19}-C_{26} tricyclic terpanes; C_{30}αβH: 17α(H),21β(H)-hopane; C_{27}Ts: 18α(H)-trisnorneohopane; C_{27}Tm: 17α(H)-trisnorhopane; C_{29}Ts: 18α-30-norneohopane; C_{29}Tm (C_{29}αβH): 17α(H),21β(H)-30-norhopane; 30-norH: 17α(H),21β(H)-30-norhomohopane; C_{30}βαH: 17β(H),21α(H)-hopane (moretane); C_{31}αβH: 17α(H),21β(H)-homohopane (S & R denote stereochemistry at the C-22 position); Tet: C_{24} tetracyclic terpane; C_{23}T: C_{23} tricyclic terpane; C_{26}T: C_{26} tricyclic terpane; C_{25}T: C_{25} tricyclic terpane; G: gammacerane; 2αMeH: 2α-methylhopane; 3βMeH: 3β-methylhopane; S: steranes; H: hopanes; S/H (1) as defined in this study: Σ(dia- + regular C_{26}-C_{30} steranes [includes cryostanes and the unknown C_{30} series])/Σ(C_{27}-C_{35} hopanes); S/H (2) from Brocks *et al*., 2017: Σ(dia- + regular C_{27}-C_{29} steranes [excludes C_{26}-norcholestanes, cryostanes and the unknown C_{30} series])/Σ(C_{27}-C_{35} hopanes); S/H (3) from Brocks *et al*., 2015: Σ(dia- + regular cholestanes and cryostanes [excludes C_{26}-norcholestanes, ergostanes and the unknown C_{30} series]/Σ(C_{27}-C_{35} hopanes); %C_{26}-C_{30} St: Relative abundances (%) of C_{26}-C_{30} steranes (including cryostanes and the unknown C_{30} series]; Cryo (cryostane): 26-methylcholestane; Chol: cholestane; Dia/Reg C_{27}: βα-20(S+R)-diacholestanes/ααα- and αββ-20(S+R)-regular cholestanes; n.d.: not determined due to low signal intensity; n.a.: not applicable (divides by 0 or peaks are not present in kerogen bound pyrolysates).

Location	Chuar Group								Visingsö Group									
Section	Nankoweap Butte				Sixtymile Canyon				Broken Nodule						Upg	Girabacken		Byd
SampleID	36		50		SW4		SWE2		v10	v12		v24	v31	v37	v1	v19		v21
Free(SE)/Bound(KB)	SE	KB	SE	KB	SE	KB	SE	KB	SE	SE	KB	SE	SE	SE	SE	SE	KB	SE
Hopane Distributions																		
Maturity Sensitive																		
Tricyclics/C_{30}αβH	191	77	170	239	14	96	5.8	8.7	2.7	2.6	48	2.2	1.5	1.0	0.6	0.8	7.1	0.7
C_{27} Ts/Tm	214	2.68	111	1.71	8.99	0.15	2.39	0.07	1.30	1.17	0.04	1.46	0.86	0.44	0.58	1.07	0.04	0.46
C_{29} Ts/Tm	7.10	0.66	7.13	0.49	1.86	0.07	1.09	0.09	0.80	0.76	0.02	1.08	0.56	0.34	0.31	0.63	0.03	0.24
30-norH/C_{30}αβH	2.52	0.25	0.98	0.24	0.11	0.13	0.08	0.14	0.06	0.06	0.10	0.05	0.04	0.06	0.04	0.03	0.04	0.05
C_{30}βαH/C_{30}αβH	0.00	0.25	0.00	0.08	0.05	0.09	0.05	0.06	0.12	0.13	0.34	0.10	0.12	0.14	0.10	0.09	0.32	0.12
C_{31}αβH 22S/(S+R)	0.51	0.47	0.54	0.50	0.56	0.57	0.57	0.59	0.57	0.56	0.54	0.56	0.58	0.57	0.57	0.58	0.60	0.58
Source Sensitive																		
Tet/C_{23}T	0.30	0.35	0.24	0.24	0.42	0.14	0.43	0.20	0.27	0.29	0.32	0.24	0.24	0.70	0.84	0.42	0.48	1.38
C_{26}T/C_{25}T	1.02	1.04	1.05	0.87	0.77	0.85	0.74	1.00	1.09	0.99	0.95	1.29	0.73	1.21	1.36	0.78	1.07	0.97
C_{29}αβH/C_{30}αβH	4.05	1.58	1.43	1.82	0.55	2.60	0.54	1.89	0.49	0.43	4.43	0.41	0.41	0.55	0.64	0.38	3.00	0.65
G/C_{30}αβH	0.30	0.21	0.27	0.22	0.19	0.45	0.11	0.15	0.03	0.03	n.d.	0.04	0.07	0.01	0.02	0.03	0.02	0.01
2αMeH/3βMeH	n.d.	n.d.	1.13	n.d.	0.24	0.50	0.13	0.38	0.40	0.39	3.65	0.36	0.43	0.52	0.67	0.34	1.33	0.36
Sterane/Hopane Ratios																		
S/H (1)	0.09	0.56	0.19	1.01	0.38	1.26	0.37	0.36	0.23	0.36	0.37	0.15	0.18	0.07	0.04	0.16	0.16	0.03
S/H (2)	0.05	0.38	0.11	0.69	0.27	0.81	0.28	0.28	0.20	0.32	0.30	0.13	0.17	0.06	0.04	0.15	0.15	0.03
S/H (3)	0.04	0.27	0.10	0.41	0.22	0.46	0.23	0.23	0.16	0.24	0.23	0.12	0.14	0.06	0.04	0.13	0.13	0.03
Sterane Distributions																		
%C_{26}	40	32	38	32	23	30	17	17	12	8	16	9	4	6	3	4	7	2
%C_{27}	50	68	53	68	70	63	76	76	80	86	80	81	89	82	86	91	88	98
%C_{28}	6.8	n.d.	4.9	n.d.	2.0	1.6	1.4	1.1	4.8	3.3	2.8	6.0	4.3	7.8	7.8	3.0	2.9	n.d.
%Cryostane	3.8	n.d.	3.5	n.d.	4.0	4.4	4.0	3.9	3.5	2.5	1.7	4.5	2.6	4.3	3.2	1.9	2.0	n.d.
%C_{30} (unknown)	n.d.	n.d.	n.d.	n.d.	1.1	1.7	1.1	1.8	n.d.	n.d.	n.d.	n.d.	n.d.	n.d.	n.d.	n.d.	n.d.	n.d.
Cryo/Chol	0.08	n.d.	0.07	n.d.	0.06	0.07	0.05	0.05	0.04	0.03	0.02	0.06	0.03	0.05	0.04	0.02	0.02	n.d.
Dia/Reg C_{27}	1.43	n.a.	0.79	n.a.	0.31	n.a.	0.31	n.a.	1.64	1.02	n.a.	1.42	1.45	1.11	1.40	1.57	n.a.	1.14

Sterane/Hopane relationships

The ratio of the major (C_{27}-C_{35}) hopanes to (C_{27}-C_{29}) regular steranes provides a broad but direct and informative measure of the relative contributions of bacteria and eukaryotes to sedimentary organic matter, which has proved useful to track the evolving Proterozoic surface ocean ecology. A temporal step change occurs as sterane/hopane (S/H) ratios shift from values of approximately zero (0) throughout the Paleoproterozoic and Mesoproterozoic as revealed by a dearth of sterane hydrocarbons (e.g. Brocks et al., 2005, 2015, 2017; Blumenberg et al., 2012; Gueneli et al., 2012; Flannery & George, 2014; Luo et al., 2015; Suslova et al., 2017, Isson et al., 2018; Nguyen et al., 2019) before increasing significantly during the Ediacaran Period (Grosjean et al., 2009; Love et al., 2009; Brocks et al., 2017; Stolper et al., 2017) attaining Phanerozoic average S/H values of ~0.5–2.0 for sedimentary rocks and oils in many cases. Eukaryotic sterane biomarkers first become ubiquitous in the ancient rock record and found in significant abundance relative to bacterial hopanes in thermally well preserved marine sedimentary rocks deposited between 800 to 635 Ma (Brocks et al., 2017; Isson et al., 2018). However, due to a deficiency of thermally well-preserved strata, little is known about the evolution and range of S/H and other lipid biomarker ratios across the Tonian Period (1000-717 Ma), making the Chuar and Visingsö Group samples described here attractive candidates for addressing this issue and filling this void. Assessing the range of S/H ratios for suitable early Neoproterozoic rock targets, encompassing a range of TOC contents, will help us better understand when the mode of marine primary productivity and ecology shifted from bacterially dominated populations to communities rich in eukaryotic phytoplankton and heterotrophs.

We generally attribute the scarcity of sterane biomarkers in strata older than ca. 800 Ma to a low overall ecological abundance of eukaryotes but not due to the complete absence of eukaryotes in these environments. It is also possible, but less likely, that low-oxygen-adapted eukaryotes which did not possess sterols may have been part of the community structure, since a few anaerobic protists have recently been shown to lack sterols in their cell membranes (Takashita et al., 2017). Although microfossil (Javaux et al., 2001, 2004; Lamb et al., 2009) and molecular clock evidence suggest the eukaryotic domain of life had diverged by at least 2100-1600 Ma (King 2004; Parfrey et al., 2011), the relative abundance of algal contributions to marine planktonic communities seems to have been suppressed with respect to bacteria in most mid-Proterozoic marine settings and therefore difficult to discern and quantify with most approaches. In contrast, evidence for diverse and abundant eukaryotic microfossil assemblages and heterotrophic protists is not found until much later in the Neoproterozoic from about 800 Ma and younger (Butterfield et al., 1994; Porter & Knoll, 2000; Knoll et al., 2006; Knoll 2014; Strauss et al., 2014; Morais et al., 2017). The acritarch microfossil record, however, can only provide a qualitative assessment of eukaryotic protist abundance relative to total organic matter so we look to the lipid biomarker record to gauge the relative [quantitative] abundance of eukaryotes versus bacteria and to constrain the timing when eukaryotes first noticeably became widespread and abundant in different Proterozoic marine settings.

Unlike other studies, which exclude certain regular or rearranged sterane compounds in the S/H calculations, our approach was to use the most abundant compounds that accounted

for a significant amount of the total detectable steranes in each of our sample locations thus minimizing biases from our dataset. These include all quantifiable isomers (dia- and regular steranes) of C_{26}-C_{28} steranes (norcholestanes, cholestanes, ergostanes, cryostanes), as well as the newly detected but unknown C_{30} sterane series that has, as of now, only been reported in the Sixtymile Canyon section of the Chuar Group. As previously described, regular C_{29} steranes (stigmastanes) and most of the C_{30} sterane compounds (24-npc/24-ipc/26-mes) were not detected in any of our Tonian samples so these were not used in our S/H ratio calculations. For the denominator 'H' parameter, we used the mature and most stable 17α,21β(H)-hopane series across the whole C_{27}-C_{35} carbon number range as described in detail in the footnote of Table 8.

S/H values for our two most thermally mature Chuar Group outcrops from the Nankoweap Butte section (outcrops 36 & 50) were 0.09 and 0.19, respectively, while those from the more thermally well preserved Sixtymile Canyon section (outcrops SW4 & SWE2) were 0.38 and 0.37, respectively (Fig. 19; Table 8). All eight of the outcrops from the upper member of the Visingsö Group, sampled from four different sections with and *early* to *middle* oil window maturity, produced S/H values ranging from 0.03 – 0.36 (mean=0.15) (Fig. 19; Table 8). Thus, the highest ratios of S/H found for these Tonian rocks are lower than but moving close to values associated with the typical range for organic-rich Phanerozoic rocks and oils (typically in the 0.5-2.0 range), suggesting abundant eukaryotic source contributions.

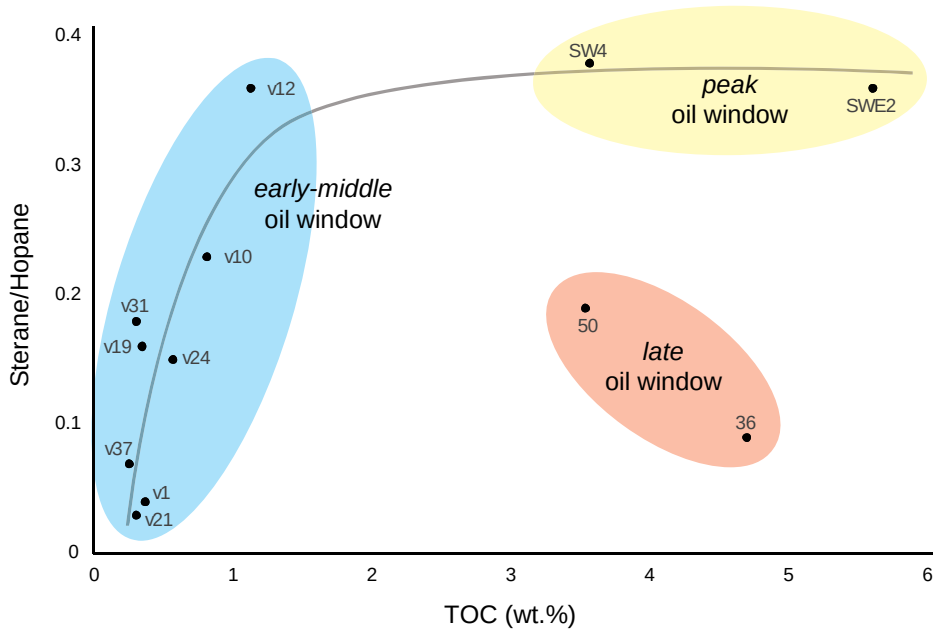

Figure 19. TOC (wt.%) vs S/H for all samples in this study, measured from the solvent extractable (*free*) phase. Samples from the Visingsö Group fall within the *early-middle* oil window (blue shaded area) with TOC values between (1.13-0.26 wt.%). A maturity gradient in the organic-rich Chuar Group samples (5.61-3.54 wt.% TOC) affects the observed S/H ratios, with the *late* oil window samples (orange shaded area) having lower S/H values compared to the *peak* oil window (yellow shaded area) samples.

To obtain a more accurate measure of eukaryotic to bacterial source contributions to sedimentary organic matter, the omission of abundant sterane or hopane compounds should be avoided when calculating the S/H ratio. Recent work has illustrated that pre-Sturtian age (pre-717 Ma) sterane distributions are vastly different than what is recovered from a typical Phanerozoic rock extract or crude oil (i.e. Brocks et al., 2015, 2017; Hoshino et al., 2018), but certain precautions must be considered when utilizing S/H ratios in rocks/oils of this age. For example, Brocks et al. (2017) only include the main C_{27}-C_{29} sterane (regular and diasterane) isomers but not certain specific C_{26} and C_{28} sterane compounds. They used βα-20(S+R)-diasteranes and ααα- and αββ-20(S+R)-regular C_{27}-C_{29} sterane isomers (cholestanes/ergostanes/stigmastanes) in their S/H calculations of a suite of Chuar Group

(Walcott Member) rocks while omitting norcholestanes and cryostanes. When combined, these two compounds can account for a significant portion of the total detectable steranes (ca. 5-40% in our sample set; Table 8). As a result, Brocks et al. (2017) concludes that low S/H values (0.003-0.42) in conjunction with a predominance of C_{27} steranes within the total sterane assemblage from several pre-Sturtian locations reflects the source contributions of unicellular heterotrophic protists but not from algae. If norcholestanes and cryostanes were included in those calculations, the range of S/H values would be significantly higher and their conclusions regarding the source biota input for these pre-Sturtian steranes could be different since numerous studies have shown that certain red algal clades biosynthesize predominantly C_{27} sterols but with lower/finite amounts of C_{28} sterols (Patterson 1971; Kodner et al., 2008). It should be noted that Brocks et al. (2015) detected ergostane within the interior portion of one sample from the Girabäcken locality of the Visingsö Group (equivalent to sample v19 in this study) however this result was discounted since the same compound couldn't be reliably recovered from a collection of outcrops from the Chuar Group (n=9). Ironically, and in agreement with the dataset in this study, the absence of ergostane from those nine Chuar Group outcrops was most likely a consequence of high maturity; equivalent to samples 36 & 50 (this study) where ergostane couldn't be recovered from the HyPy products due to enhanced thermal alteration but it was readily observed in the less mature samples, SW4 & SWE2.

If there were indeed a significant proportion of red algae in these Tonian marine settings, the resulting biomarker assemblage would reflect a dominance of C_{27} cholestanes, exactly

what is observed. We also point out that eukaryotic heterotrophic protists primary consumers and an absence of eukaryotic primary producers (e.g. red algae) would imply that these protists would have accounted for a high proportion of the total biomass according to the range of S/H values that have been reported (Brocks et al., 2017; Hoshino et al., 2018). This scenario is difficult to imagine in any paleoenvironment setting through time, given that the base of the food web which supports higher trophic levels is supplied mainly by primary producers. If primary producers make recalcitrant lipids, such as the case with steroids in eukaryotic phytoplankton, then these autotrophic sources will dominate the overall signal abundance for the particular biomarker class in comparison with heterotrophs. So, we argue that a significant contribution of photosynthetic eukaryotic primary producers, specifically red algal clades, is the most parsimonious explanation for the absolute values and range of S/H values we observe in our Chuar and Visingsö Group sedimentary strata.

Conclusions

Lipid biomarker assemblages recovered from the *free* and *kerogen-bound* phases of sedimentary organic matter from the 780-729 Ma Chuar and Visingsö Groups, two Tonian successions from Laurentia and Baltica, respectively, reveal convincing evidence for the proliferation of pre-Sturtian-age eukaryotic organisms. The sterane carbon number patterns detected, with C_{27} steranes dominant in most samples (in some cases up to 98% of total steranes) but with discernible amounts of C_{28} regular steranes (ergostane) also present, suggests that red algae may have been significant photosynthetic primary producers during

this interval. The main characteristic features of the biomarker assemblages obtained from the solvent extract (*free*) phase, verified by parallel analysis of the *kerogen-bound* pool generated from HyPy, provides an important validation of the biomarker data and confirms the syngeneity of these ancient biomarker compounds.

We have generated the oldest known occurrence of *kerogen-bound* regular sterane biomarkers in Precambrian sedimentary rocks. The C_{27} sterane (cholestane) dominance shows obvious similarities to the free sterane patterns reported previously for Tonian rocks but very different to the C_{29} (stigmastane) dominance found in Cryogenian and younger samples deposited after the Sturtian glaciation. Along with cholestane, appreciable amounts of norcholestanes, ergostanes and cryostanes were also found in most of our Tonian samples collected from both the Chuar and Visingsö Groups. The presence of ergostanes implies the enzymatic capacity for alkylation at position C-24 on the steroid side-chain was possible in the Tonian Period, although the absence of any stigmastanes and conventional C_{30} steranes (24-npc and 24-ipc) suggests a more limited array of steroids in eukaryotic cell membranes prior to the Sturtian glaciation. We also found a novel, late-eluting C_{30} sterane series from Chuar Group samples, which is likely biogenic and contains an extended side chain although the precise side chain chemistry could not be elucidated. This new unknown C_{30} sterane series may be a structural analog of cryostane, and therefore a possible demosponge or stem metazoan biomarker, although this source assignment is tentative at this stage.

Sterane/hopane (S/H) ratios shift from below a zero baseline [0] for Mesoproterozoic rocks to finite values [0.03 – 0.38] for rock bitumens from the Chuar and Visingsö Groups, as found from this study. Such a significant temporal change in biomarker patterns is consistent with the concept of a fundamental global marine ecological upheaval as Proterozoic oceans transitioned from a bacterially dominated ecosystems to communities rich in eukaryotic primary producers and heterotrophic protists. The values for our S/H ratios were generally higher in the more organic-rich Tonian rocks than the organic-lean samples, suggesting a possible nutrient throttle control on marine eukaryotic proliferation. The apparent discrepancy between the first appearance of eukaryotic acritarchs in the microfossil record (ca. 1800-1600 Ma) and the first detection of appreciable eukaryotic sterane biomarker signals, approximately one billion years later in Earth history, suggests a very protracted rise of eukaryotes perhaps throttled by environmental and ecological factors. This prolonged and suppressed rise of microbial eukaryotes in marine environments may also have delayed the evolution of complex multicellular organisms, as the natural selection pressures within the marine biosphere would have changed as eukaryotic cells, and heterotrophs capable of ingesting those cells, became more widespread and abundant in the ocean.

CHAPTER 3: PATTERNS OF STEROID SYNTHESIS IN MODERN DEMOSPONGES AND THE IDENTIFICATION OF NOVEL FOSSIL STERANE BIOMARKER TARGETS

Abstract

Comprising more than 75% of the 8,800+ known extant sponge species, demosponges (Demospongiae) are the most diverse class within the phylum Porifera. Demosponges have been shown to biosynthesize a diverse array of conventional and unconventional sterols, usually within their cell membranes. Unconventional sponge steroids have long been of interest to natural product chemists and to pharmacologists as targets for new medicines, particularly as some compounds show antimicrobial and anticancer properties. Additionally, demosponge steroids containing unusually alkylated side chains are an attractive choice for serving as ancient animal biomarkers, especially since demosponges are a derived class of Porifera. Prerequisite properties are that the core hydrocarbon (sterane) skeletons are stable over long burial times in the geologic record and that they are analytically resolvable from other sterane compounds, as well as other polycyclic biomarker alkanes. Through the parallel analysis of intact functionalized sterol precursors and individual geologically stable sterane derivatives, generated in the laboratory via mild reduction from continuous-flow catalytic hydropyrolysis (HyPy), we have a powerful analytical approach for identifying promising fossil sterane biomarker targets. Through this approach, applied to extant demosponges, we have identified a suite of novel C_{29} to C_{31} steranes as major steroids (1-99%) in certain species that have not yet been reported in the

organic geochemical literature. These constitute already, at least, six novel and analytically resolvable steranes from lipid analysis of over 90 different species of extant sponges which may be preserved in ancient sedimentary rocks and oils that have undergone a mild thermal history. In this way, we can considerably expand the existing lipid biomarker repertoire to be able to track the emergence and environmental expansion of the earliest animal life on Earth.

Introduction

Sponges (Porifera) are sessile, filter-feeding benthic organisms found predominantly in marine environments although freshwater species are also known (Ruppert et al., 2004). There are four major classes of the phylum Porifera: Calcarea, Hexactinellida, Demospongiae and Homoscleromorpha (Gazave et al., 2012; Morrow and Cárdenas 2015) and from recent phylogenomic studies, it is commonly accepted that sponges are the sister group of all other animals (Feuda et al., 2017; Simion et al., 2017). Research involving the chemistry of Porifera natural products began in the 1940s and has since been an alluring topic across numerous fields given the diversity of metabolites found. Over the past five decades, extensive investigations from researchers interested in natural product chemistry (encompassing medicinal chemistry, chemical oceanography, pharmacology, etc.) have used state-of-the-art analytical methods to elucidate the precise structures and stereochemistries of sponge steroids, along with assessing the absolute abundances and compound distributions of sterols in different species. These compounds include a variety of conventional and unconventional steroids, some of which possess complex side chain

structures and varying degrees of unsaturation. This has led to the discovery of at least 250 different polar steroid structures (as of 2002; Sarma et al., 2005) as well as revealing some robust phylogenetic patterns within the observed steroid distributions via chemotaxonomic investigations (e.g., Djerassi and Silva, 1991; Giner et al., 1993; Gold et al., 2016).

Perhaps surprisingly for an animal with a relatively simple body plan, demosponges produce the most diverse collection of individual sterols amongst extant taxa (Bergquist et al., 1980, 1986, 1991; Kerr and Baker 1991; Giner 1993). The assemblages of demosponge sterols appear to be distinct from their Calcarea and Hexactinellida relatives, which typically acquire their largely conventional steroids via dietary uptake (Blumenberg et al., 2002; Hagernann et al., 2008, Love et al., 2009; Zumberge et al., 2018, this study). Goad (1981) hypothesized four possible pathways for sponges to obtain their sterols: i) *de novo* biosynthesis exclusively performed by the host sponge, ii) dietary uptake from marine organic detritus, iii) via modification of dietary sterols and iv) through *de novo* biosynthesis but with at least a partial role for symbiotic microorganisms. Additionally, and possibly the most unique feature of sponge sterol biosynthesis which sets them apart from other eukaryotes, is their ability to alkylate *and* dealkylate the sterol side chain at multiple positions (Djerassi and Silva 1991).

The biosynthetic pathways involved in the production of sponge metabolites can be complex and many demosponges synthesize highly derived sterols, with structural variations occurring in/around the steroid nucleus and/or side chain, including: i) the

number and position of extra carbons via alkylation, typically added as alkyl substituents to the side chain, ii) the number and position of unsaturated double bonds via dehydrogenation, common to both the steroid nucleus and side chain and iii) the number and position of hydroxyl (-OH), ketogenic (=O) or sulphatic (-OSO_2OH) polar groups, usually as part of the tetracyclic steroid nucleus. In a geologic context, however, only some of these unusual structural features actually influence the number of fossil molecular derivatives that will ultimately be preserved from each steroid precursor, particularly since reactive oxygen-containing functional moieties and double bonds are reduced and lost through sedimentary diagenesis. Since it is principally the core hydrocarbon features of the steroid precursor, based on the stable carbon-carbon bonding within the sterane skeleton, which dictates which sterane derivative survives in the rock record then there are far fewer distinct ancient steranes found in comparison with possible steroid precursors. For example, a variety of naturally occurring sterols with 27 carbons (e.g. cholesterol (structure **B1** in Charts II-III), desmosterol (**B2**), 22-dehydrocholesterol (**B3**), etc.) would all be converted to cholestane in the rock record after burial and diagenesis, regardless of the position and number of double bonds in the precursor biomolecule in the source organism (Fig. 20).

Assessing the exact functional roles of unconventional steroids in sponges has been the subject of much interest and debate for decades but this aspect lies outside the scope of this study. Our major focus was to explore the variety of analytically resolvable and stable sterane targets that could be generated from chemical conversion of unconventional sponge

steroids and that could survive in adequate amounts to be detectable in the geologic record, possibly extending back to the Neoproterozoic Era. Additionally, we sought to gain new insights into the phylogenetic patterns of occurrence of these steroids within Porifera in order to better constrain the taxonomic affinity of the groups of modern sponges capable of synthesizing the appropriate sterol precursors.

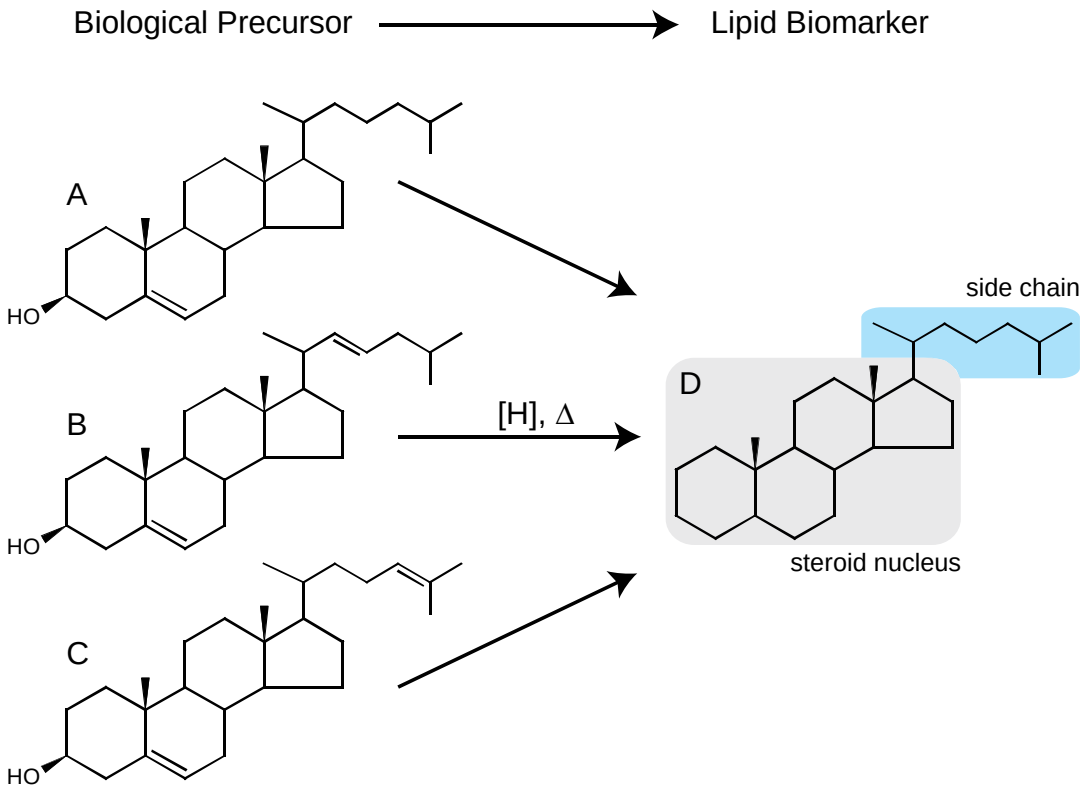

Figure 20. Schematic representation of the biomarker principle, using steroids as the example. After burial and diagenesis of cellular organic matter, functionalized groups within the steroid nucleus and/or side chain are lost and sterol precursors are converted to a recalcitrant core hydrocarbon skeleton (sterane lipid biomarker), which is stable on geologic timescales in rocks and oils that have undergone a mild thermal history. Naturally occurring sterols, for example, containing 27 carbons including (**A**) cholesterol, (**B**) 22-dehydrocholesterol and (**C**) desmosterol would all be preserved in the rock record as (**D**) cholestane, with two major stereoisomers (5β,14α,17α(H),20R; βααR and 5α,14α,17α(H),20R; αααR). Only the αααR form survives late diagenesis and catagenesis in the ancient rock record as one of four stable diastereoisomers (αααS, αββR, αββS, αααR), but this allows direct correlation with αααR steranes generated from mild thermal reduction of extant biomass.

The earliest reported animal biomarkers are proposed to be derived from demosponges and are recorded in a ca. 100-Myr-long sequence of Neoproterozoic-Cambrian marine sedimentary strata from the Huqf Supergroup (South Oman Salt Basin) commencing in the Cryogenian Period (Love et al., 2009; Zumberge et al., 2018). Three different structural series of ancient C_{30} regular (4-desmethyl) steranes (McCaffrey et al., 1994; Love et al., 2009; Zumberge et al., 2018) are known which occur together in some Cryogenian and Ediacaran (ca. 660-542 Ma) rocks and oils, but which are absent in older Neoproterozoic biomarker assemblages (see Chapter 2). In order of chromatographic elution times these are: 24-*n*-propylcholestane (24-npc (**A13**)), 24-isopropylcholestane (24-ipc (**A16**)) and, the newly reported, 26-methylstigmastane (26-mes (**A27**)). These steranes correspond with three of the most commonly occurring sterane skeletons in C_{30} sterols found in extant demosponges. The 24-npc steranes found in the Neoproterozoic rock record could possibly be sourced from foraminifera (Grabenstatter et al., 2013), as well as from demosponges (Love et al., 2009). However, the only eukaryotic organisms that are predicted to have the genetic capacity to biosynthesize 24-ipc steranes as major steroids during the Neoproterozoic era are demosponges, as determined from *sterol methyltransferase* (SMT) gene sequence analysis combined with molecular clocks (Gold et al., 2016). Given these findings, the co-occurrence of 24-ipc and 26-mes (Zumberge et al., 2018) in the geologic record, particularly when 24-ipc/24-npc abundance ratios exceed 0.50 (Love et al., 2009), have been used as strong molecular fossil evidence for ancient demosponge inputs and allows us to track the radiation of the earliest animal life. While future assays of other eukaryotic groups may reveal other biological affinities for these molecules, currently

demosponges appear to be the most likely Neoproterozoic-Cambrian source of these steranes, and they are the only extant taxa known to make *both* 24-ipc and 26-mes structures amongst their major steroids (see **Background**).

Other than the 24-ipc and 26-mes steranes, no other diagnostic animal molecular biomarkers have been routinely applied to the geologic record that are resolvable from the conventional steroids found as abundant membrane lipids of extant microbial eukaryotes. This is perhaps surprising but reflects only an emerging body of knowledge concerning the variety, abundance and taxonomic distributions of unconventional steroids made predominantly or exclusively by animals that can be preserved as detectable and resolvable ancient sterane markers. Other recalcitrant lipids could expand the molecular biomarker repertoire significantly in the search for early animal fossil evidence.

In this study, we screened the sterol content of over 50 poriferan species and our observations reveal that there is an apparent host control that regulates the 'downstream' sterols (with 29-31 carbons) produced by the appropriate corresponding 'upstream' sterol precursors (with 27-28 carbons). Our dataset of extant sponge sterol assemblages revealed two distinct biosynthetic pathways that explain some of the major features of sponge steroid systematics, with little/no crossover between the two. Dubbed 'conventional' and 'unconventional' pathways, we report systematic patterns within demosponge steroid assemblages observed in multiple species from different clades of demosponges. The sterol patterns were compared to the corresponding sterane product distributions after successful

conversion of functionalized lipid precursors to stable sterane derivatives via mild laboratory chemical reduction using HyPy treatment of biomass, which helped reveal these precursor-product synthesis relationships. Additionally, the identification of novel unconventional steroid structures with elongated side chains (side chain alkylation at terminal C-26 and/or C-27 positions) from different clades of extant demosponges provide new biomarker targets to search for in the geologic record and allows us to assess their potential as chemotaxonomic markers for identifying different species that are phylogenetically related.

Material and Methods

Sponges (Porifera)

Sponge specimens were supplied by Paco Cárdenas (Uppsala University) and Erik Sperling (Stanford University) and their colleagues; including Jean Vacelet, Ute Hentschel, Kevin Peterson, Ted Molinski, Thierry Pérez, Hans Tore Rapp, Alexander Plotkin, Jae-Sang Hong, Yusheng M. Huang, Sven Rohde, Scott Nichols, Barbara Calcinai, Jose V. Lopez, Gulia Gatti, Bartek Ciperling, João-Pedro Fonseca, Luís Magro, Francesca Azzini, Allen G. Collins, Shirley Pomponi, Lakmini Kosgahakumbuta and the Bedford Institute of Oceanography (Dartmouth, Canada).

The sponge specimens used in this study were retrieved from marine habitats all over the world but with an emphasis on specimens collected from the Arctic Circle, the Mediterranean Sea, the East China Sea, the Philippine Sea and the Great Barrier Reef. Most

sponges were collected in shallow waters (<25 m) as these are easily accessible via SCUBA diving although our collection also includes deep water marine species, collected to 2 km water depth.

Extraction and analysis of sterols in modern sponge cells

Modern sponge samples were subjected to extraction with organic solvents to assess their free sterol contents as trimethylsilyl (TMS) ethers. Sponge biomass either arrived immersed in ethanol or as freeze-dried cells. Combined ethanol washings for each sample were filtered to remove suspended particulates, concentrated into a small volume and then transferred to a pre-weighed glass vial and blown down carefully under dry N_2 gas. Freeze-dried sponge biomass was extracted via exhaustive ultrasonication for 30 minutes in DCM:methanol (3:1 v/v) to recover the total lipid extract. Multiple rounds of solvent extractions were performed, typically until no more color was observed in the solution.

Total lipid extracts (TLEs) were separated into 3 fractions, based on compound polarity, using silica gel adsorption chromatography. Approximately, 1-5 mg of TLE was adsorbed on the top of a 10 cm silica gel (35-70 mesh fired at 450 °C overnight) pipette column and then sequentially eluted with ~1.5 column volumes of *n*-hexane (Fraction 1), ~2 column volumes of DCM (Fraction 2) and ~3 column volumes of DCM:methanol (7:3 v/v) (Fraction 3). Aliphatic hydrocarbons eluted in Fraction 1 and the most polar compounds eluted in Fraction 3. The alcohol products, including 3β-hydroxysteroids, typically eluted in Fraction 2 and approximately 20-50 µg of this fraction was derivatized with 10-20 µl of

bis(trimethylsilyl)trifluoroacetamide (BSTFA) in 10-20 µl of pyridine and heated at 70 ^{o}C for 30 minutes. The resulting TMS ethers were diluted with DCM:*n*-hexane (3:1 v/v) before GC-MS analysis.

Catalytic hydropyrolysis of sponge biomass

Continuous-flow hydropyrolysis (HyPy) experiments were performed on ca. 50-300 mg of catalyst-loaded sponge biomass (either as solvent extracted biomass or whole cells, depending on the initial amount received for each specimen) at UC-Riverside as described previously (Love et al., 2005, 2009; Zumberge et al., 2018). Freeze-dried sponge biomass was initially impregnated with an aqueous methanol (deionized water:methanol 4:1 v/v) solution of ammonium dioxydithiomolybdate [$(NH_4)_2MoO_2S_2$] to give a give a nominal loading of ~3-10 wt.% catalyst. Ammonium dioxydithiomolybdate reductively decomposes *in situ* under HyPy conditions above 250 ^{o}C to form a catalytically active molybdenum sulfide (MoS_2) phase.

The catalyst-loaded samples were heated in a stainless steel (316 grade) reactor tube from ambient temperature to 250 ^{o}C at 100 ^{o}C/min immediately followed by 250 ^{o}C to 460 ^{o}C at 8 ^{o}C/min while maintaining constant hydrogen pressure of ~150 bar. A hydrogen sweep gas flow rate of 6 L/min, measured at ambient temperature and pressure, through the reactor bed ensured that the residence times of volatiles generated was the order of only a few seconds. Products were collected on a silica gel trap cooled with dry ice and recovered for subsequent fractionation using silica gel adsorption chromatography.

HyPy products (hydropyrolysates) of sponge biomass were separated by silica gel adsorption chromatography into aliphatic (alkane + alkene), aromatic and polar (N, S, O containing) compounds by elution with *n*-hexane, *n*-hexane:DCM (1:1 v/v) and DCM:methanol (3:1 v/v), respectively. For hydropyrolysates, solvent-extracted activated copper turnings were added to concentrated solutions of aliphatic hydrocarbon fractions to remove all traces of elemental sulfur, which is formed from disproportionation of the catalyst during HyPy. Aliphatic fractions were further purified to a saturated hydrocarbon fraction (alkanes) by the removal of any unsaturated products (alkenes) via silver nitrate impregnated silica gel ($AgNO_3$ ~10 wt.% loading on +230 mesh; Sigma Aldrich) adsorption chromatography and elution with *n*-hexane. We found this last step to be crucial in the analytical workflow with respect to sterol → sterane conversion via HyPy. Without the separation of alkenes from the aliphatic hydrocarbon HyPy product, the potential for false positives in the $M^+ \rightarrow 217$ Da transition from MRM-GC-MS greatly increases, allowing for the likely mis-identification of genuine sterane (alkane) peaks (Fig. 21).

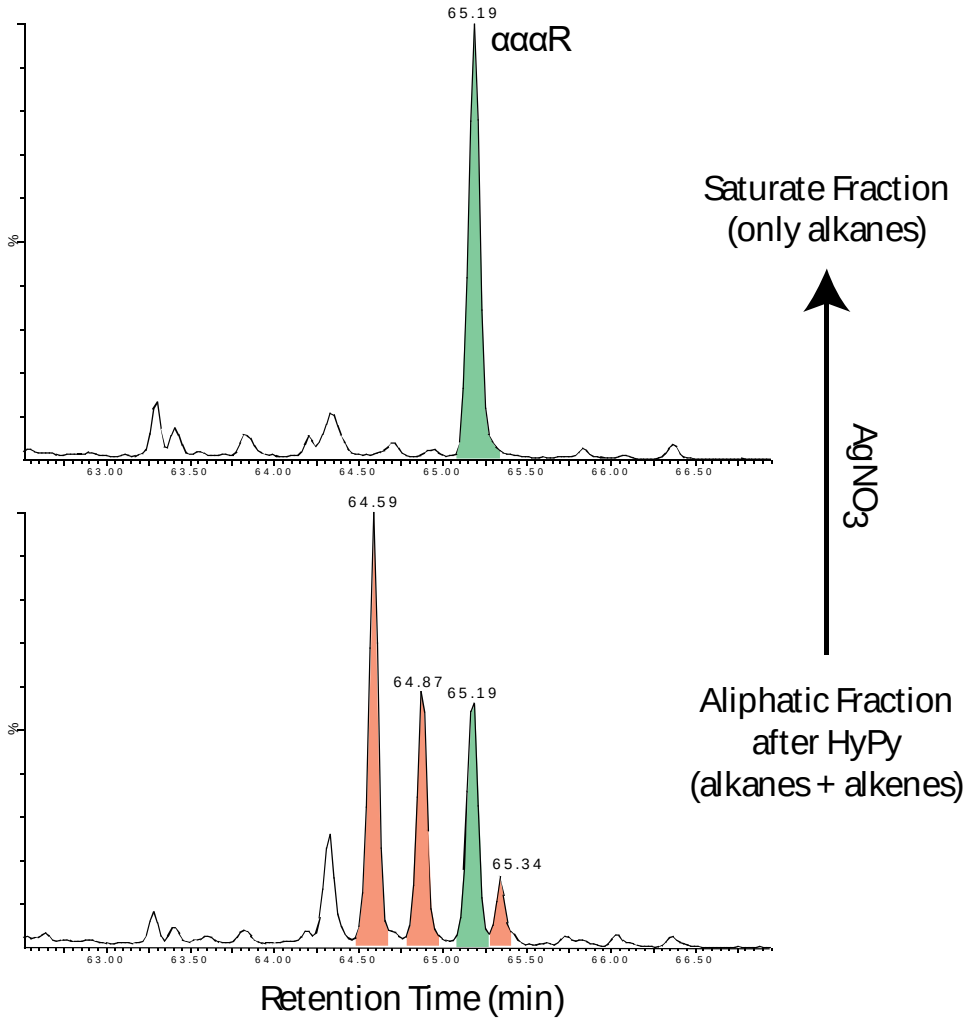

Figure 21. MRM-GC-MS chromatograms for C_{30} sterane and sterene distributions (414→217 Da) from the sponge *Thymosiopsis conglomerans* (Tremies). The (*bottom*) aliphatic fraction recovered after HyPy treatment contains a sterene overprint (red peaks) that could lead to 'false positive' peaks and overestimate the number of true C_{30} sterane compounds. This is because some sterols are prone to dehydrate on heating and form sterenes. To avoid this complication, aliphatic fractions were separated into alkanes and alkenes on a silver nitrate ($AgNO_3$) impregnated silica column. The resulting (*top*) saturate hydrocarbon fraction only includes alkanes (green peak) and not alkenes. Retention times (in minutes) are shown above each peak. The only major C_{30} sterane (αααR isomer) in the saturate fraction is thymosiosterane which is consistent with the sterol analysis for this species (Vacelet et al., 2000; this study).

Instrumental Analysis

Extracted sterol analysis by Gas Chromatography-Mass Spectrometry (GC-MS)

Alcohol fractions after solvent extraction of the original sponge biomass were analyzed by GC-MS as trimethylsilyl (TMS) ethers within 36 hours of derivatization in full scan mode on an Agilent 7890A GC system coupled to an Agilent 5975C inert mass selective detector (MSD) mass spectrometer. Sample solutions were volatilized via programmed-temperature vaporization (PTV) injection onto a DB1-MS capillary column (60 m × 0.32 mm, 0.25 μm film thickness) and helium was used as the carrier gas. The oven temperature program used for GC for the derivatized alcohol fractions consisted of an initial temperature hold at 60 °C for 2 min, followed by an increase to 150 °C at 20 °C/min, and then a subsequent increase to 325 °C at 2 °C/min and held for 20 min. Data was analyzed using ChemStation G10701CA (Version C) software, Agilent Technologies.

Synthetic 3β-hydroxysteroid standards, including desmosterol (cholesta-5,24-dien-3β-ol; ≥84%; Sigma-Aldrich), campesterol (24R-ergosta-5-en-3β-ol; ~65%; Sigma-Aldrich), stigmasterol (stigmasta-5,22-dien-3β-ol; ~95%; Sigma-Aldrich) and fucosterol (stigmasta-5,24(28)-dien-3β-ol; ≥93%; Sigma-Aldrich), were converted to TMS ethers using the same BSTFA/pyridine derivatization method as previously described for the naturally occurring sponge sterols. These were used as references for relative retention times and fragmentation patterns, as previously described (Goad and Akihisa 1997). Additionally, sterol identification was aided by widely available mass fragmentation patterns from previously published research.

Sterane analysis using Multiple Reaction Monitoring-GC-MS (MRM-GC-MS)

Saturated hydrocarbon fractions from modern sponge HyPy pyrolysates were analyzed by Multiple Reaction Monitoring-Gas Chromatography-Mass Spectrometry (MRM-GC-MS) on a Waters Autospec Premier mass spectrometer equipped with an Agilent 7890A gas chromatograph and DB-1MS coated capillary column (60 m x 0.25 mm, 0.25 μm film) using He for carrier gas (Fig. 22). Typically, one microliter of a hydrocarbon fraction dissolved in hexane was injected onto the GC column in splitless injection mode. The GC temperature program consisted of an initial hold at 60 °C for 2 min, heating to 150 °C at 10 °C/min followed by heating to 320 °C at 3 °C/min and a final hold for 22 min. Analyses were performed via splitless injection in electron impact mode, with an ionization energy of 70 eV and an accelerating voltage of 8 kV. MRM transitions for C_{27}–C_{35} hopanes, C_{31}–C_{36} methylhopanes, C_{21}–C_{22} and C_{26}–C_{30} steranes, C_{30} methylsteranes and C_{19}–C_{26} tricyclic terpanes were monitored in the method used. Procedural blanks with pre-combusted sand yielded less than 0.1 ng of individual hopane and sterane isomers per gram of combusted sand (Haddad et al., 2016).

Peak identifications of sponge steranes were confirmed by comparison of retention times with an AGSO oil saturated hydrocarbon standard and with Neoproterozoic oils from Eastern Siberia (McCaffrey et al., 1994; Kelly et al., 2011) and India (Peters et al., 1995) which were reported previously to contain significant quantities of 24-ipc (**A16**) and which we have now demonstrated contain significant quantities of 26-mes (**A27**) (Zumberge et al., 2018).

Sterane analysis by GC-triple quadrupole-MS (GC-QQQ-MS)

To confirm and investigate the retention times of the analyte peaks compared with other C_{26}-C_{30} steranes, the saturated hydrocarbon (alkane) fractions from sponge HyPy products and oils from Eastern Siberia and India were run on a different instrument employing a different GC column to that used in the MRM-GC-MS instrument at UCR. GC-QQQ-MS was performed at GeoMark Research (Houston, TX) on an Agilent 7000A Triple Quad interfaced with an Agilent 7890A gas chromatograph and DB-5MS+DG capillary column (60 m x 0.25 mm i.d., 0.25 μm film thickness, 10 m guard column) (Fig. 22). Using helium as carrier gas, the flow was programmed from 1.2 mL/min to 3.2 mL/min. The GC oven was programmed from 40 °C (2 min) to 325 °C (25.75 min) at 4 °C/min. Saturated hydrocarbon fractions were spiked with a mixture of 7 internal standards (Chiron Routine Biomarker Internal Standard Cocktail 1). Samples were concentrated without being taken to dryness and were injected in cold splitless mode at 45 °C with the injector temperature ramped at 700 °C/min to 300 °C. The MS source was operated in EI-mode at 300 °C with ionization energy at -70 eV. Several molecular ion-to-fragment transitions were monitored throughout the run and dwell time was adjusted as needed to produce 3.5 cycles/second.

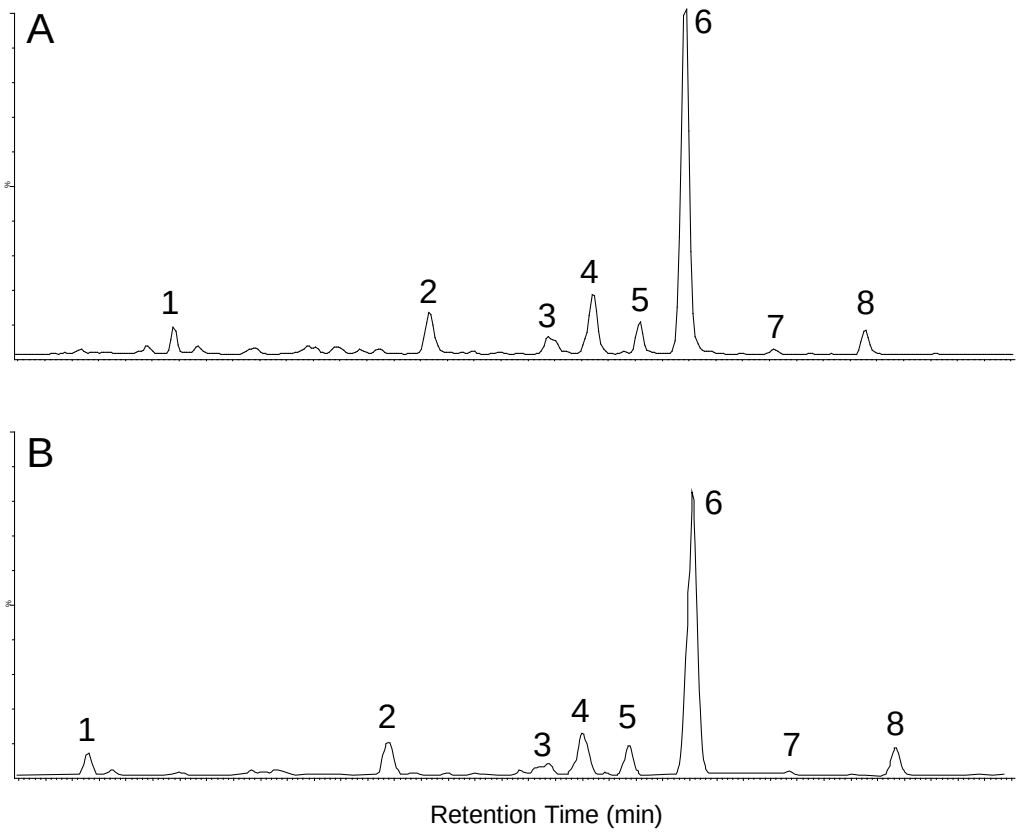

Figure 22. Total C_{27}-C_{30} sterane distributions ($M^+ \rightarrow 217$ Da chromatogram) for the demosponge *Rhabdastrella distincta* (PC1127) using (**A**) MRM-GC-MS (60 m DB-1MS) and (**B**) GC-QQQ-MS (60 m DB-5MS) analysis. Analysis on two different GC column stationary phases is crucial in the identification of genuine sterane products and aides in the elucidation of potential false positive peaks (e.g. cross talk from hopanoids and/or sterenes). Peak IDs: 1 = C_{27} cholestane (**A1**; αααR); 2 = C_{28} ergostane (**A4**; αααR); 3 = C_{29} stigmastane (**A8**; βααR); 4 = C_{29} aplysterane (**A22**; βααR); 5 = C_{29} stigmastane (**A8;** αααR); 6 = C_{29} aplysterane (**A22;** αααR); 7 = C_{30} 26-methylstigmastane (**A27;** βααR); 8 = C_{30} 26-methylstigmastane (**A27;** αααR).

Background

Sterol biosynthesis in eukaryotes

Almost all known eukaryotes, regardless of taxonomic affinity, contain at least some quantity of sterols within their cells, produced either by *de novo* biosynthesis or by uptake and modification of dietary sterols (Wei et al., 2016). Eukaryotes utilize these compounds for several vital cellular functions including membrane fluidity/rigidity, membrane trafficking and cell signaling (Nes 1974; Bloch 1991; Xu et al., 2005; Hannich et al., 2011). Molecular clock analyses using genes required for sterol biosynthesis, which is an aerobic metabolic process that requires many oxygen-intensive intermediate steps (Summons et al., 2006), reveal that the biosynthetic capacity for the production of simple sterols likely dates as far back as the Great Oxidation Event ca. 2310 Ma (Gold et al., 2017), perhaps prior to the emergence of eukaryotic crown groups. Other molecular clock studies estimate that extant eukaryotes evolved later in Earth history from a last eukaryotic common ancestor (LECA; O'Malley et al., 2019), sometime between 1800-1500 Ma (Parfrey et al., 2011; Eme et al., 2014; Betts et al., 2018) but substantially prior to the Neoproterozoic Era (1000-720 Ma). Consistent with the knowledge that eukaryote cell membranes are heavily dependent on the biochemical properties of sterols and their derivatives as primary metabolites, there are commonalities in the sterol biosynthetic pathway between phylogenetically unrelated eukaryotes, including: i) the initial steps of oxidation of squalene to oxidosqualene, ii) the subsequent cyclization of oxidosqualene to either lanosterol (animals and fungi) or cycloartenol (plants and most algae) and iii) numerous

enzymes (e.g. *isomerases*, *methyltransferases*, *reductases*, *desaturases*, etc.) involved in the intermediate steps towards the final sterol product(s) (Scheme I).

Within a generalized sterol biosynthetic pathway, however, the three major multicellular groups of the domain Eukaryota (Animalia, Fungi and Plantae) selectively employ different enzymes primarily during the initial steps of sterol biosynthesis; proceeding through two upstream C_{30} intermediates, cycloartenol (plants and algae) and lanosterol (animals and fungi)(Scheme I), but are limited in the array of potential downstream sterols that they produce (Hannich et al., 2011). Recent advances in the field of phylogenomics reveal that Porifera are most commonly recognized as the sister group of all animals (Feuda et al., 2017; Simion et al., 2017) and radiolabeling experiments with labelled molecular precursor feedstocks (Kerr et al., 1989; Djerassi and Silva 1991) have shown that certain sponges can isomerize cycloartenol to lanosterol as well as alkylate the side chain at different carbon positions. Such versatility in their biosynthetic toolkit allows some sponge groups to routinely synthesize a diverse array of conventional and unconventional sterol and other steroid (e.g. steroid sulfate) products; a trait that sets certain sponges apart from other eukaryotes that are limited in this regard.

It should be noted that there are a few known bacteria with the biosynthetic capabilities required for sterol production (Wei et al., 2016), however it is thought that these organisms are not likely important parent source organisms for the array of regular (4-desmethyl) sterane biomarkers detected in the Neoproterozoic and younger geologic rock record. Gene

sequencing and sterol analysis from *Methylococcus capsulatus* and *Gammata obscuriglobus* reveal that these bacteria have the ability to produce trace amounts of certain sterols (Bouvier et al., 1976; Pearson et al., 2003), but largely with a methyl group still present at the C-4 position on the steroid nucleus. This research concluded, however, that these particular bacteria only produced upstream precursor sterols, principally as lanosterol or cycloartenol, in trace amounts and there is as yet no report of any bacterium producing sterols that are alkylated at the C-24 position that would produce the downstream C_{28}-C_{30} sterol precursors of ergostane, stigmastane and propylsteranes despite an intensive search in a recent investigation (Wei et al., 2016). The latter point is significant since the C-24 position is a common site for alkylation of the sterol side chain within the eukaryote domain of life (Giner 1993) and it appears that 24-alkylated steroids are uniquely produced by the eukaryotic domain of life. Additionally, recent studies reveal that eukaryotes and sterol-producing bacteria may use separate and distinct pathways during the intermediate steps of sterol synthesis. Lee et al (2018) confirmed that bacteria with the ability to biosynthesize simple sterols utilize proteins unique to their domain of life while eukaryotes employ their own enzymes/proteins at various intermediate steps during sterol biosynthesis. The recognition that bacteria and eukaryotes have two separate pathways for the production of sterols suggests that this innovation and biosynthetic capacity evolved at least twice; once in bacteria and once in eukaryotes. Molecular clock approached have not been able to resolve the lineage that the innovation of sterol synthesis first evolved in (Gold et al., 2017).

Other putative sources of Neoproterozoic-Cambrian C_{30} steranes

Nettersheim et al. (2019) claimed to have identified 24-ipc in different groups of extant unicellular Rhizaria as well as trace quantities of putative 26-mes in the phylum Cercozoa. They concluded that Rhizaria are the most probable source for Neoproterozoic 24-ipc and 26-mes, and not demosponges. However, due to the very small amounts of 24-ipc and 26-mes reported (all <<1% of total C_{27}-C_{30} steranes from hydrogenation of sterols), the impossibility to reproduce their results (using their own extracts in two independent laboratories) and the analytical shortcomings of their study, we are currently not convinced by their data (Love et al., 2019, reply submitted). Fundamental problems beset this new steroid biomarker dataset and interpretations.

The vanishingly low C_{30} steroid contents reported for the majority of Rhizaria exposes an intractable sterane mass balance problem that cannot be reconciled with the %C_{30} sterane abundances and compound ratios found in the Neoproterozoic-Cambrian record (Love et al., 2009; Zumberge et al., 2018). Failing to account for dietary steroids, the lack of comprehensive blank controls and reproducibility problems for C_{30} sterane data for Cercozoa render the findings and conclusions of Nettersheim et al., (2019) dubious. There is currently no convincing evidence that Rhizaria can produce abundant 24-ipc and/or 26-mes. Demosponges are currently the only known source of 24-ipc and 26-mes sterol precursors that account for the patterns of C_{30} steranes typically observed in the Neoproterozoic-Cambrian rock record. Demosponges are the most plausible Neoproterozoic-Cambrian source of 24-npc as well as 24-ipc because both are produced

by extant demosponges (Love et al., 2009). Foraminifera are another possible source of 24-npc (Grabenstatter et al., 2013). Pelagophyte algae likely account for the 24-npc steranes that are found in Devonian and younger marine sediments and their derived oils (Gold et al., 2016).

Sponge sterol naming conventions

For the purpose of this study, it is best to classify all possible variations of novel sponge sterols relative to their common HyPy sterane products which effectively produces the fossil alkane form which is the major class of ancient steroids preserved in the rock record (the natural degradation and conversion of functionalized sterols to steranes via burial and diagenesis). We routinely denote cholestane, ergostane, stigmastane and 24-npc as 'common/conventional' steranes with 27, 28, 29 and 30 carbons, respectively (Chart IV). These conventional steranes are all alkylated at position C-24 in the sterane side chain, an important distinction that will be discussed further. With regards to this proposed framework, which outlines sterols that are known to be only synthesized by demosponges, 24-ipc (**A16**) is also considered a conventional C_{30} sterane since it is alkylated at position C-24 and certain eukaryotes outside phylum Porifera (e.g. some pelagophyte algae and foraminifera) can make 24-isopropylcholesterols in trace amounts, most likely as a by-product during 24-npc sterol biosynthesis (Love et al., 2009). It should be noted, however, that extant demosponges within a newly defined clade including species of *Cymbastella* (order Axinellida), *Ciocalypta*, *Topsentia*, *Halichondria* (order Suberitida) and *Petromica* (order Bubarida) have been shown to make 24-isopropylcholesterols (**B16**/**B17**/**B18**) as

major lipid components, between 1-99 wt.% of their total C_{27}-C_{30} sterols (Hofheinz and Oesterhelt 1979; Ishibashi et al., 1997; Barnathan et al., 2004; Calderón et al., 2004; Love and Summons 2015; Morrow and Cárdenas 2015, Zumberge et al., 2018; this study). This is in stark contrast to the levels of 24-ipc found in other eukaryotes (typically <<1% of total C_{27}-C_{30} sterols), so, very high abundances of 24-ipc in the rock record (defined relative to 24-npc with a minimum threshold ratio of 0.5) are most likely sourced from ancient demosponges since other eukaryotes aren't known to make these as major sterol constituents (Love et al., 2009; Zumberge et al., 2018).

A universal definition of what we call conventional steranes aids in the classification and/or reconstruction of marine paleoenvironments based on their sterane assemblages and permits the search for novel sterane compounds that would require unique biological precursors. These sterane structures, with distinct variations in the core hydrocarbon skeleton and separate from what is already known in the molecular fossil (biomarker) literature, would in turn enhance paleoenvironmental interpretations and become viable targets for novel fossil sterane biomarkers.

Sterol identification and elucidation from the solvent extracts of extant sponges

After extraction of modern sponge biomass with organic solvent and isolation of the subsequent lipid fraction (see **Materials and Methods**), sponge sterols were analyzed as trimethylsilyl (TMS) ethers via GC-MS. This method offers a well-established approach that prolongs the life of the GC stationary phase and provides characteristic fragment

patterns that aid in sterol identification (Brooks et al., 1968; Goad and Akihisa 1997). Mass spectra from GC-MS analysis were an integral component of compound identification, especially when multiple TMS ethers elute close to or on top of each other. For example, the ion with a mass to charge ratio of 129 (denoted as m/z 129) is representative of the common Δ^5-3β-OTMS unsaturated sterol regardless if there are other [additional] unsaturation sites in the steroid side chain. Additionally, a hypothetical mass spectrum with a dominant fragment ion of m/z 386 is the result of a McLafferty rearrangement after fragmentation and rearrangement in the sterol side chain and is indicative of a $\Delta^{5,24(28)}$ unsaturated TMS ether (Djerassi 1978). Apart from signature fragment ions from the mass spectra of TMS ethers, there are prominent molecular peaks (denoted as M^+) that describe i) the total number of carbons in the parent compound and ii) the total number of unsaturation sites, if any, within the parent sterol since two less hydrogens are required in a C=C double bond compared to a saturated C-C single bond. Building from these established patterns, the identification of co-eluting compounds like β-sitosterol and fucosterol, for example, which are two C_{29} sterols with identical core hydrocarbon skeletons but vary with respect to the number of unsaturation sites can be elucidated by their differences in M^+ and major fragment ions: β-sitosterol is a mono-unsaturated Δ^5 sterol with M^+ 486 while fucosterol is a di-unsaturated $\Delta^{5,24(28)}$ sterol with M^+ 484 and large m/z 386 fragment (because of the double bond at position C-24(28)).

CHART II

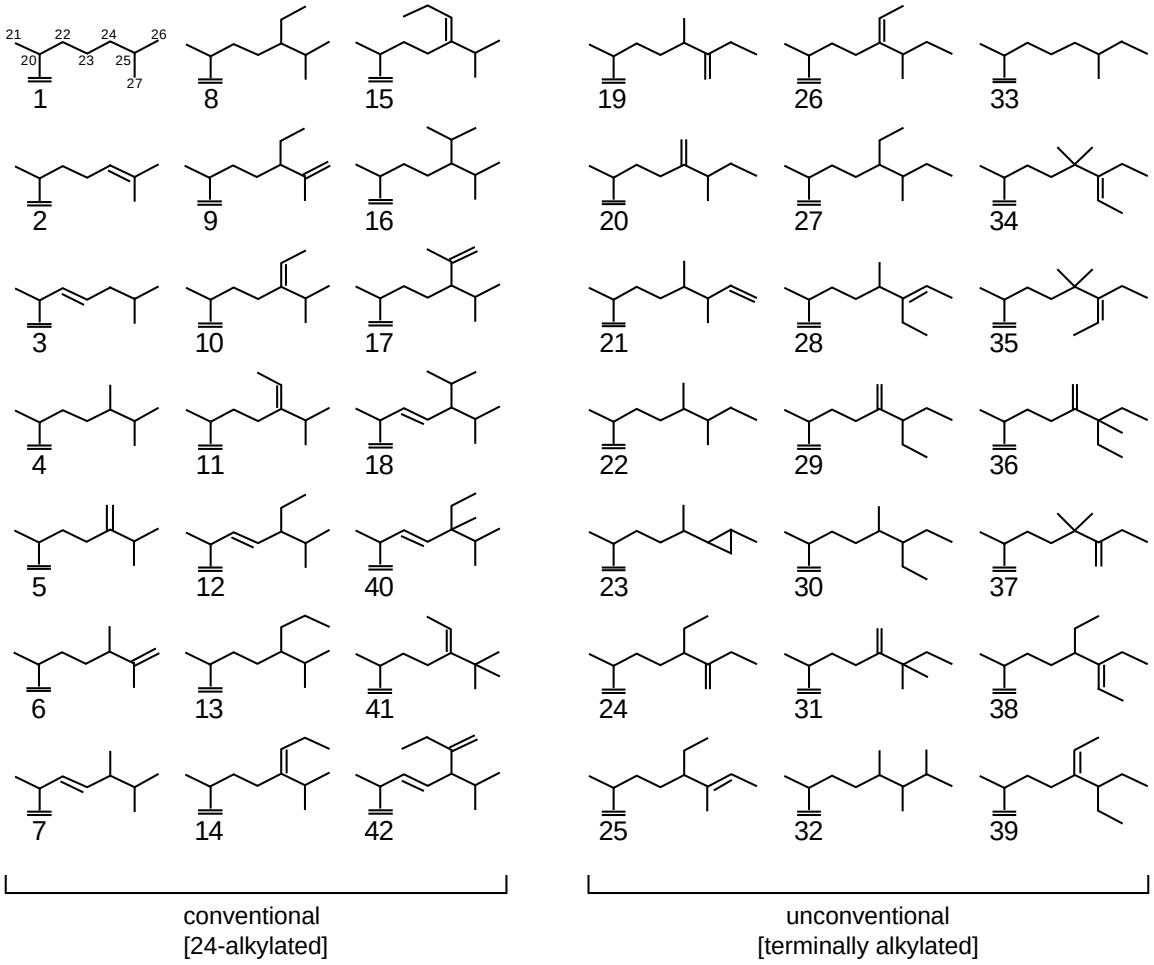

CHART III

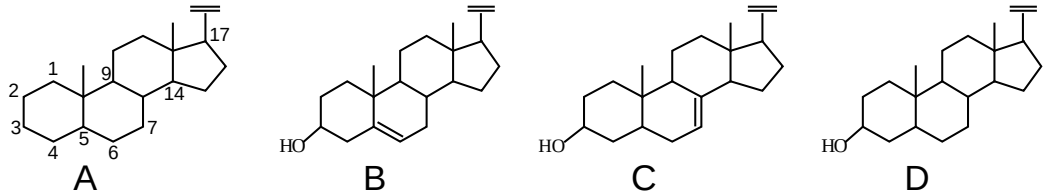

CHART IV

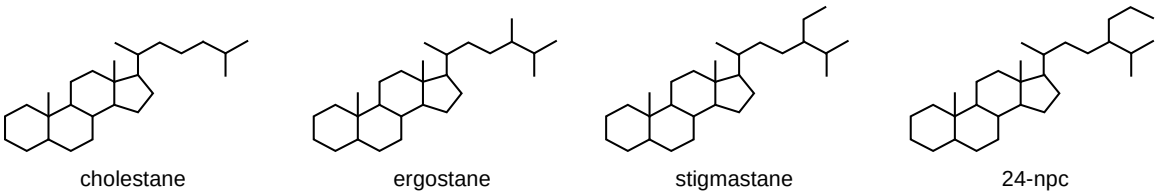

Results and discussion

Our collection of extant sponges encompasses a variety of specimens from all around the world, recovered from a wide range of marine environments. Table 9 lists the taxonomic coverage of the sponge specimens used in this study. We purposely targeted mainly Demospongiae, since this class of sponge is known to produce the most diverse array of steroids, often with distinctive structural features. Demosponges thus offer the highest potential for generating unique/unconventional sterane biomarker targets that could expand the current repertoire of animal biomarkers for interrogating the ancient rock record.

Table 9. Taxonomic affinities of Porifera used in this biomarker study. The numbers shown in each column represent the taxonomic coverage of the 114 total specimens analyzed.

Class	#Families	#Genera	#Species	#Specimens
Demospongiae	23	36	77	107
Hexactinellida	3	3	4	4
Homoscleromorpha	1	2	2	2
Calcarea	1	1	1	1

Sterol distributions from the solvent extracts of extant sponges

The majority of sterols recovered from our collection of marine sponges had the common Δ^5-3β-hydroxysteroid nucleus however we did encounter a few species with Δ^7 unsaturation patterns as well as a variety of stanols (no unsaturation). Stanols are commonly associated with hexactinellid sponges, which lack the ability to biosynthesize Δ^5 sterols *de novo* but instead modify and reduce steroids acquired from dietary uptake (Blumenberg et al., 2002; Chart III). Average unsaturation patterns across the total sterol assemblages screened in this study (n= ~40) were distributed between fully saturated

(14%), mono-unsaturated (26%) and di-unsaturated (59%) sterols. In almost every case, the reported mono-unsaturated sterols were primarily Δ^5-unsaturated while our observed di-unsaturated sterols were $\Delta^{5,SC}$ (where 'SC' denotes that the 2nd double bond was located somewhere in the side chain of the sterol, such as at C-22, as opposed to within the steroid nucleus). Additionally, the average number of carbons detected in these sponge sterol assemblages typically varied between 27 and 30 total carbons. Sterols with 29 carbons were the most common (47%) while those with 27 (22%), 28 (23%) and 30 (8%) carbons were less prevalent. This is somewhat surprising given that cholesterol (a C_{27} sterol; **C1**) is commonly associated with being the major animal steroid in eumetazoans. It should be noted that in certain instances, trace amounts of C_{26} and C_{31} sterols were tentatively identified however their overall abundance relative to the more common C_{27}-C_{29} sterols were generally low (<1%) for species screened thus far.

Conventional sterol biosynthesis patterns in Porifera

Sponges in this study that produced mainly cholesterol/cholestanol (**B1**/**D1**) and 24-alkylated C_{28}-C_{30} sterols were classified as utilizing a common sterol biosynthetic pathway that numerous other eukaryotic organisms are known to follow in the production of similar sterol products; hence the term 'conventional'. This pattern included the incorporation of fully saturated stanols as well as mono- and di-unsaturated sterols. The position and relative abundance of unsaturation sites in the side chain of upstream sterols proved to be an integral part in understanding the biosynthetic pathways towards downstream (e.g. higher carbon number) sterol products.

For example, Table 10 displays several sponge specimens (n=8) of different taxonomic affinities that all possessed a ubiquitous upstream and conventional compound, 24-methylenecholesterol (**B5**; a $C_{28}\Delta^{5,24(28)}$ sterol), as the primary sterol constituent (≥25% of the total C_{27}-C_{30} sterols). In every sponge we surveyed, when $C_{28}\Delta^{5,24(28)}$ was the major sterol, two patterns emerged: i) the C_{29} downstream products typically consisted of conventional sterols including (but not limited to) fucosterol (**B11**) and isofucosterol (**B10**) and ii) the *E*- and/or *Z*-isomers of 24-*n*-propylidenecholesterol (**B14**/**B15**) was the *only* C_{30} sterol product, if detected at all. Note that the $\Delta^{5,24(28)}$ unsaturation pattern, the same as in (**B5**), was typically carried on to the remaining abundant downstream sterols (Table 10). As expected, this pattern had no effect on the upstream C_{26} and/or C_{27} sterols which were free to exist with a Δ^{5}- and/or $\Delta^{5,22}$-unsaturation. Additionally, our own investigations revealed that no sponge specimen from our collection that produced unconventional downstream sterols, alkylated at C-26 and/or C-27, contained (**B5**) as a dominant sterol.

Table 10. Amongst sponges from our collection that follow the conventional sterol biosynthetic pathway, and when 24-methylenecholesterol (**B5**; $C_{28}\Delta^{5,24(28)}$) was the primary sterol constituent (≥25% of the total C_{27}-C_{30} sterols), downstream C_{29} and C_{30} sterols typically had the same $\Delta^{5,24(28)}$ unsaturation pattern. 24-*n*-propylidenecholesterol (**B14**/**B15**) was the *only* C_{30} sterol product, if detected at all. "-" = not detected.

Family	*Genus species* (sponge ID)	$C_{28}\Delta^{5,24(28)}$ (%)	2nd - 4th most abundant sterols	24-npc (%)
Geodiidae	*Caminella intuta* (PC1162)	77	$C_{27}\Delta^{5}$, $C_{29}\Delta^{5}$, $C_{29}\Delta^{5,24(28)}$	-
	Geodia barretti (PC529)	79	$C_{29}\Delta^{5,24(28)}$, $C_{27}\Delta^{5}$, $C_{28}\Delta^{5,22}$	0.4
	Geodia barretti (PC617)	58	$C_{29}\Delta^{5,24(28)}$, $C_{27}\Delta^{5}$, $C_{28}\Delta^{5,22}$	-
	Geodia hentscheli (GhII)	76	$C_{29}\Delta^{5,24(28)}$, $C_{28}\Delta^{5,22}$, $C_{27}\Delta^{5}$	-
	Geodia pachydermata (PC681)	64	$C_{29}\Delta^{5,24(28)}$, $C_{27}\Delta^{5}$, $C_{28}\Delta^{5,22}$	-
	Pachymatisma johnstonia (Roscoff #4)	42	$C_{29}\Delta^{5,24(28)}$, $C_{27}\Delta^{5}$, $C_{28}\Delta^{5,22}$	-
	Pachymatisma normani (PC952)	43	$C_{29}\Delta^{5,24(28)}$, $C_{27}\Delta^{5}$, $C_{28}\Delta^{5,22}$	0.7
Ancorinidae	*Rhabdastrella intermedia* (PC399)	25	$C_{29}\Delta^{5,24(28)}$, $C_{27}\Delta^{5}$, $C_{29}\Delta^{5}$	1.1
Tethyidae	*Tethya aurantium* (Roscoff #2)	69	$C_{27}\Delta^{5}$, $C_{28}\Delta^{5,22}$, $C_{29}\Delta^{5,24(28)}$	-

This pattern, illustrated in Scheme II, must employ an enzymatic pathway that is widely distributed within Eukaryota since it is observed in the sterol assemblages of other phylogenetically distinct organisms (e.g. phytosterols in plants, sterols in algae/fungi/animals; Porter and Spurgeon 1981; Zimmerman and Djerassi 1991; Volkman 2003). For instance, the same conventional pathway was reported for other eukaryotes, including the pelagophyte algae *Aureococcus anophagefferens* which has (**B5**) as 48% of its total sterols and both structural isomers (*E* and *Z*) of 24-*n*-propylidenecholesterol (**B14**/**B15**) as 44% of the total sterols (Giner and Boyer 1998). Therefore, it seems that the production of downstream conventional sterols, including fucosterol (**B11**), isofucosterol (**B10**) and 24-*n*-propylidenecholesterol (**B14**/**B15**), relies on (**B5**) as a precursor since the double bond exposed at C-24(28) provides an optimal site for conventional alkylation at the C-24 position. Importantly, after at least one carbon (methyl group) is added to the C-24 position, terminal alkylation seems to be *extremely* restricted or more likely completely unachievable due to enhanced steric hindrance from the 24-alkylated moiety (Stoilov et al., 1986; Djerassi and Silva 1991).

As another example from a specimen in our collection, a typical 'conventional' sponge might produce cholesterol (**B1**), campesterol (**B4**) and sitosterol (**B8**) as the prominent C_{27}, C_{28} and C_{29} sterols, respectively (e.g. *Cinachyrella kuekenthali* PC941). All three of these are mono-unsaturated Δ^5-3β-hydroxysteroids and are common throughout all eukaryotes; though perhaps not common as a trifecta from the same species, as is the case here, but nonetheless these are distributed amongst phylogenetically diverse eukaryotes. This sterol

assemblage may be useful in a chemotaxonomic study that relies on matching the sterol profile of an unknown extant sponge specimen, and utilizes the number and position of double bonds as key characteristics, however this particular sterol pattern loses diagnostic information when transformed into ancient steroids as double bonds are reduced during sedimentary diagenesis. Because this sponge only makes conventional 24-alklyated sterols, burial and diagenesis of the host biomass would convert these compounds into cholestane, ergostane and stigmastane (Chart IV), respectively, which are the most commonly occurring sterane biomarkers and sterol precursor compounds with similar core hydrocarbon structures to these three are widespread throughout all eukaryotes. The same hypothetical marine paleoenvironment would have hosted a plethora of other eukaryotes including a variety of primary producers that also readily synthesize the same 24-alkylated (conventional) sterols but in much greater abundances compared to any second level trophic organism (i.e. sponges). The same diagenetic processes would in turn produce the same collection of conventional C_{27}-C_{29} steranes, rendering the sponge's impact to the overall sterane distribution of this proposed paleoenvironment miniscule.

While sponges containing conventional sterol patterns are not the best targets for distinguishing ancient sponge source inputs in the rock record as they generally do not produce unusual sterane skeletons, we found that investigating the overall systematics and noting commonalities in steroid assemblages was still a productive endeavor which yielded valuable biochemical insights regarding steroid synthesis. Our predictive capacity for assessing which sponge specimens may produce good candidate unconventional steroids

has significantly improved as a result of gaining a better understanding of the overall sequential sterol biosynthetic transformations, particularly the control of unsaturation sties in the side chain. Upon receipt of new specimens, intact sponge sterol analyses can be used to predict and filter the best sponge candidates for biosynthesizing unconventional sterols in significant amounts (>1% of total sterols) that may yield distinctive sterane biomarker targets in the rock record.

Scheme I

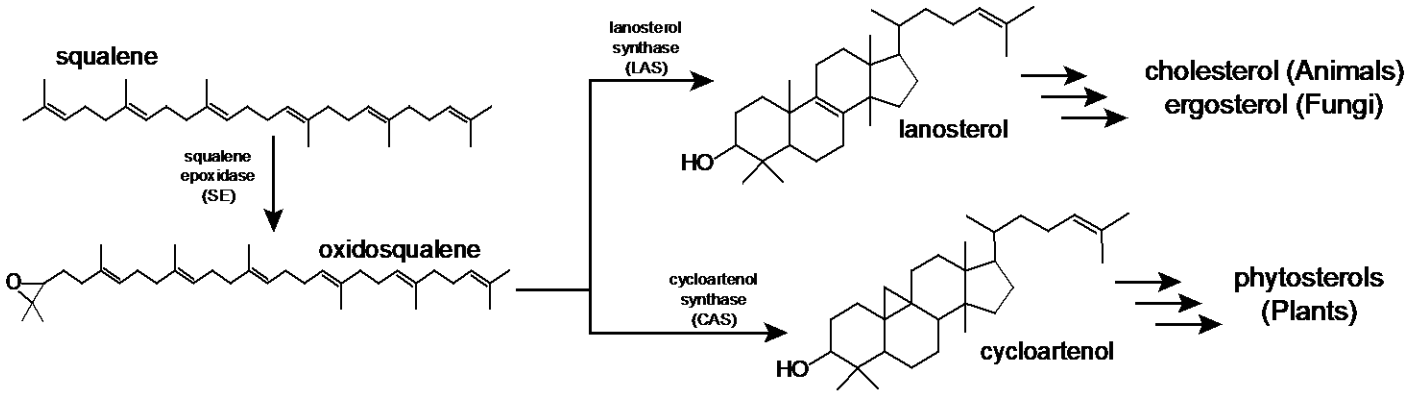

Scheme II
[conventional]

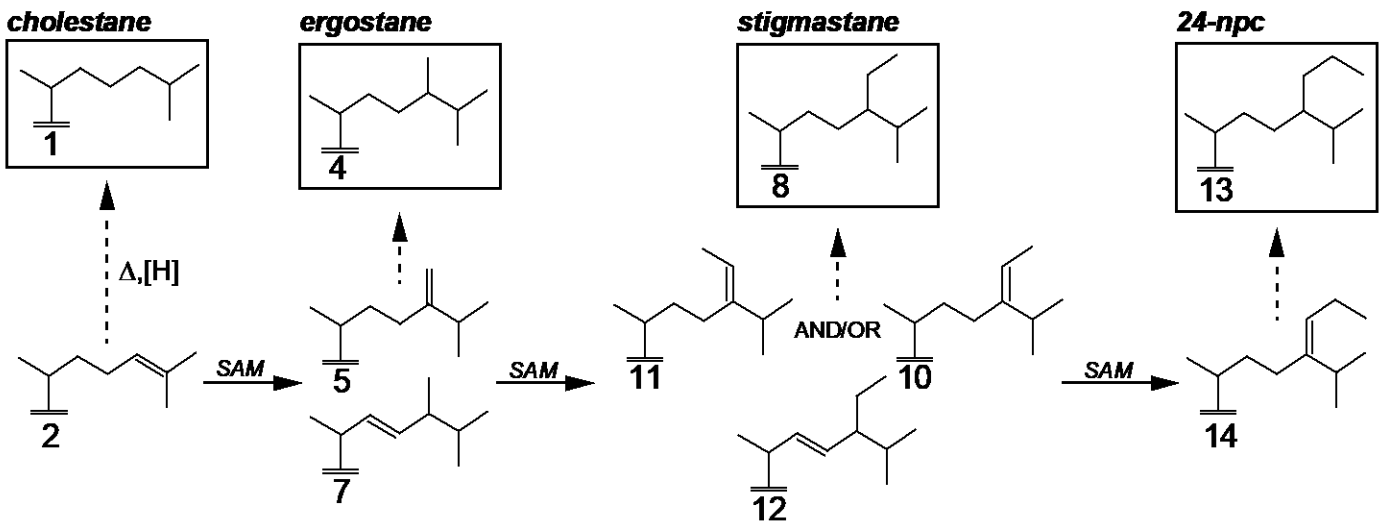

Unconventional sterol biosynthesis patterns in Porifera

Conventional C_{27}-C_{30} sterol synthesis generally follows a highly conserved biosynthetic pathway in eukaryotic crown groups, involving a similar subset of upstream molecular intermediates and enzymatic transformations, yielding structural variations in downstream sterol products dependent on the number of side chain methylations and/or the number and positions of unsaturation. This general mechanistic pathway also seems to apply to demosponges that contain conventional sterols and most demosponges appear to have the genetic capacity to synthesize their sterols *de novo* (Silva et al., 1991; Silva and Djerassi 1992; Gold et al., 2016), unlike hexactinellid sponges which acquire their sterols primarily from dietary uptake (Blumenberg et al., 2002). However, we have also recognized systematic patterns within the overall C_{27}-C_{30} sterol distributions of certain demosponges that contained abundant [major] unconventional sterol products. To reiterate, our definition of 'unconventional' here implies carbon addition at the terminus of the steroid side chain, specifically at positions C-26 and/or C-27 (Scheme III) by selective enzymatic methylation. Recognition of clear sterol distribution patterns adds to a growing body of evidence that the host demosponge can strongly control the overall major sterol distributions in demosponge cells through coordination of *desaturase* and *sterol methyltransferase* enzymatic activity in order to closely regulate the positions of side chain unsaturation and alkylation. Unconventional steroid patterns offer promise as the basis of chemotaxonomy for helping to better resolve demosponge phylogeny; to complement and scrutinize related groupings obtained from molecular sequencing and morphological (spicule) analysis (Morrow and Cárdenas, 2015).

Consistent with proposed biosynthetic pathways (Bortolotto et al., 1978; Theobald and Djerassi 1978; Theobald et al., 1978; Stoilov et al., 1986; Cho et al., 1988), all terminally alkylated sterols that we identified had either one (methyl-) or two (ethyl- or dimethyl-) carbon constituent(s) at position C-24 (Fig. 23). It is generally recognized from the conventional pathway (Scheme II) that three carbon additions can be achieved at this site via addition of a propyl- substituent (e.g. 24-npc/24-ipc) however we have yet to encounter a terminally alkylated sterol containing any propyl- substituent added to the C-24 position. Interestingly, there are reports of 24-ethyl-24-methylcholesterols from the literature, including 24-ethyl-24-methyl-22-dehydrocholesterol (**B40**), which was isolated as the most abundant sterol (38% of the total C_{27}-C_{30} sterols) from the sponge *Topsentia ophiraphidites* (Calderón et al., 2004; Echigo et al., 2011). For (**B40**), there are three carbon atoms bound to the C-24 position, as methyl- and ethyl- substituents, subsequently producing a quaternary carbon at this site (Li and Djerassi 1981; Li and Djerassi 1983; Tam et al., 1985). It is important to note that, under the terms defined in this study, (**B40**) is classified as a conventional sterol since it is void of any terminal alkylation. So, the pattern described above for unconventional sterols still holds true; there have been no reports, as far as we know, of unconventional sterols with three carbon atoms at position C-24. Even amongst the rare C_{31} sterols that are found in certain demosponges, including one/two tentative structures observed in trace amounts from a few specimens in our sample set, it is often the case that this extra carbon atom is added to the C-24 or C-25 position to produce a quaternary carbon (opposed to it being added to the already extended side chain again) (Fig. 23).

Along these lines, it seems that side chain extension through terminal alkylation is restricted to exclusively methyl groups and not larger substituents. We have observed up to two methyl additions to the C-26 position (i.e. thymosiosterol (**C32**)) but from our own sterol assays and from scanning the available literature, we have yet to encounter an extended steroid side chain with an ethyl group at the terminal C-26 or C-27 position. These apparent patterns and systematic trends imply a strong host control on the biosynthetic pathways leading to unconventional alkylation and elongation of the steroid side chain and reinforce demosponges as good source candidates for distinctive sterane biomarker targets for exploring the ancient rock record.

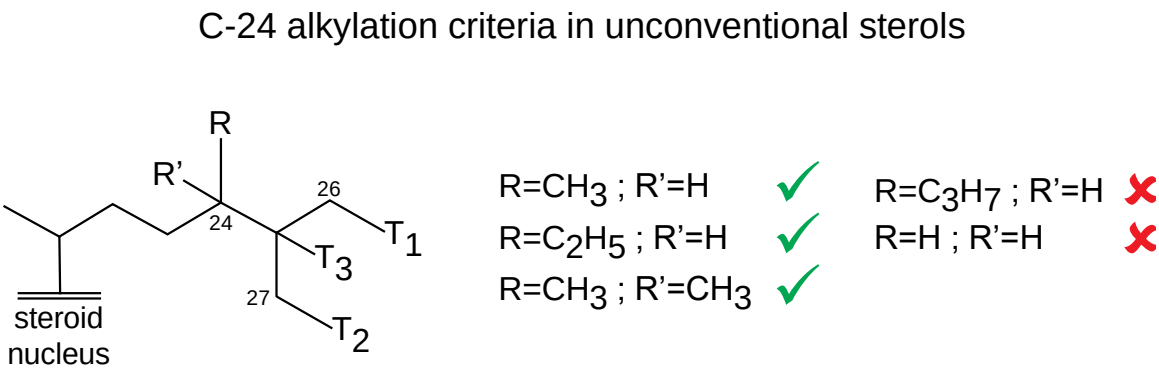

Figure 23. Observations of alkylation patterns from numerous unconventional sterols reveal systematic patterns and regulation of the possible substituent groups (R, R') that could be bound to position C-24 in the steroid side chain. T_1-T_3 implies the presence of a methyl (-CH_3) group, at a minimum. A green checkmark denotes the possible/known substituents found at C-24. A red 'x' infers incompatible substituents at C-24 since these structural combinations have not yet been encountered in unconventional sponge sterols.

After screening more than 95 specimens, with successful elucidation of the resulting sterol assays from over half of these, we have identified five demosponge clades in which certain species produce unconventional sterols:

- The *Rhabdastrella/Geodia* phlegraei clade (order Tetractinellida, family Geodiidae):
  - Moderate amounts of 26-mes precursors (**B24**/**B25**/**B26**) (3-12% of total sterols)
  - High amounts of aplysterols (**B20**) (up to 92%)
- The *Xestospongia* clade (order Haplosclerida, family Petrosiidae):
  - High amounts of 26-mes precursors (**B24**/**B25**/**B26**) (>95%)
  - High amounts of cyclopropyl-containing side chains (**B23**) (>95%)
  - Moderate amounts of verongulasterane (**A30**) precursors (1-10%)
  - Possibly two different clades in this family
- The Aplysinidae family (order Verongiida):
  - Low amounts of 26-mes precursors (**B24**/**B25**/**B26**) (0.03-0.15%)
  - High amounts of aplysterols (**B19**/**B22**) (up to 75%)
  - Moderate amounts of verongulasterane (**A30**) precursors (1-8%)
- The *Cymbaxinella* clade (order Agelasida, family Hymerhabdidae):
  - Low amounts of 26-mes. Only one species tested so far: *C. corrugata* (0.12%)
- The "Topsentia" clade (new order):
  - Hight amounts of 24-ipc precursors (**B16**/**B17**/**B18**) (41 to >99%)
  - This is an entirely new demosponge clade with currently no name or definition

Other putative occurrences of unconventional sterols in Eukaryota

There are a small number of examples of unconventional sterols found in eukaryotes other than demosponges; however it is important to bear in mind that: i) these are often trace constituents (<<0.5% of total sterols) or are too scare to be quantified, ii) structures based on relative GC/HPLC elution times are often just inferred rather than robustly tested since often the analyte mass is insufficient to garner a mass spectrum, iii) these are often restricted to a certain single species but not commonly found in other species of the same genus or within phylogenetically related taxa and iv) these may be trace metastable transformation products of conventional sterols, such as minor by-products from the synthesis of 24-propylidenecholesterol (**B14**/**B15**) that proceeds through a cyclopropyl-containing transition state, as a consequence of imperfect enzymatic machinery operating within the host organism (Kokke et al., 1984; Ito et al., 1994; Giner et al., 2009). Even with these caveats, most currently available evidence suggests that Demospongiae are unique in their capacity to make a wide array of unconventional compounds as major sterol constituents within their cell membranes and robust phylogenetic patterns are starting to become increasingly evident.

Inferred unconventional sterols in the geologic rock record

Another common pattern amongst the distribution of unconventional sterols reported here is that we have yet to identify a terminally alkylated sterol where alkylation at C-24 is absent. This has important implications for fossil sterane biomarkers in the geologic record since cryostane, with the confirmed structural assignment of 26-methylcholestane (**A33**)

(Adam et al., 2018), is anomalously prominent as a biomarker constituent of mid-Tonian (ca. 800-717 Ma) sedimentary rocks that have undergone a mild thermal history (Brocks et al., 2015, 2017; see Chapters 1-2). The discovery and identification of 'cryosterol' (i.e. **B33**), the implied name of the cryostane precursor compound, as a major sterol constituent from an extant demosponge would significantly extend convincing evidence for Porifera (Metazoa) into the Tonian Period (1000-720 Ma). However, plausible precursor sterols for cryostane have not yet been found in any extant organisms. Thus, cryostane (**A33**) cannot currently be applied as a robust animal biomarker until more is known about its biological origins. Currently, the oldest *reliable* evidence for early metazoans dates back to at least 650 Ma, supported by the abundant demosponge-derived 24-ipc and 26-mes sterane biomarkers in Cryogenian and Ediacaran rocks and oils from Oman, India and Eastern Siberia (Love et al., 2009; Zumberge et al., 2018).

Relative abundances of unconventional sterols in Porifera

With no evidence as yet for cryosterol (a hypothetical C_{28} compound containing a terminal methyl-substituent at C-26) in any extant taxa, the unconventional sterol catalogue described herein mainly encompasses steroid structures containing primarily 29 and 30 total carbons, with a few occurrences of minor C_{31} sterols. One particularly interesting feature of unconventional sterol production, as seen in our sponge sample set, is that the C_{29} and/or C_{30} products reported here are, in every case, the major sterol constituents of their respective total 3β-hydroxysteroid assays. This is in stark contrast to what we found from sponges that followed the conventional pathway since those specimens did not yield

a predictable carbon number distribution of their major sterols (i.e. we have examples of sponges with conventional sterol/stanol distributions with either 27, 28 or 29 carbons as their major constituents with no clear pattern amongst the dominant unsaturation sites either).

Consistency within the sterol assays of the same species across multiple localities

If the guiding principles that drive unconventional sterol production (Scheme III) are applicable across multiple clades of Demospongiae, then the sterol assemblages of various specimens of the *same* species that are collected from *different* geographic localities should be generally consistent, within analytical error and assuming taxonomic assignments are correct (e.g. Fromont et al., 1994; Hagernann et al., 2008). Fromont et al. (1994) tested this hypothesis by surveying the sterol assays of seven specimens of the barrel sponge *Xestospongia testudinaria* (order Haplosclerida, family Petrosiidae) and found that each specimen, which was collected at various geographic localities across the Australian Great Barrier Reef, showed similar sterol distributions. From our own dataset, the sterol distributions of six different specimens of *Rhabdastrella globostellata* (order Tetractinellida, family Ancorinidae) are strikingly similar, further validating this hypothesis (Fig 5). In all six instances, C_{29} 24(28)-dehydroaplysterol (**B20**) was by far the dominant sterol (on average, accounted for 78% of the total C_{27}-C_{30} sterols), with appreciable amounts of the di-unsaturated unconventional C_{30} sterol, stelliferasterol (**B25**) and its mono-unsaturated structural isomer (**B27**).

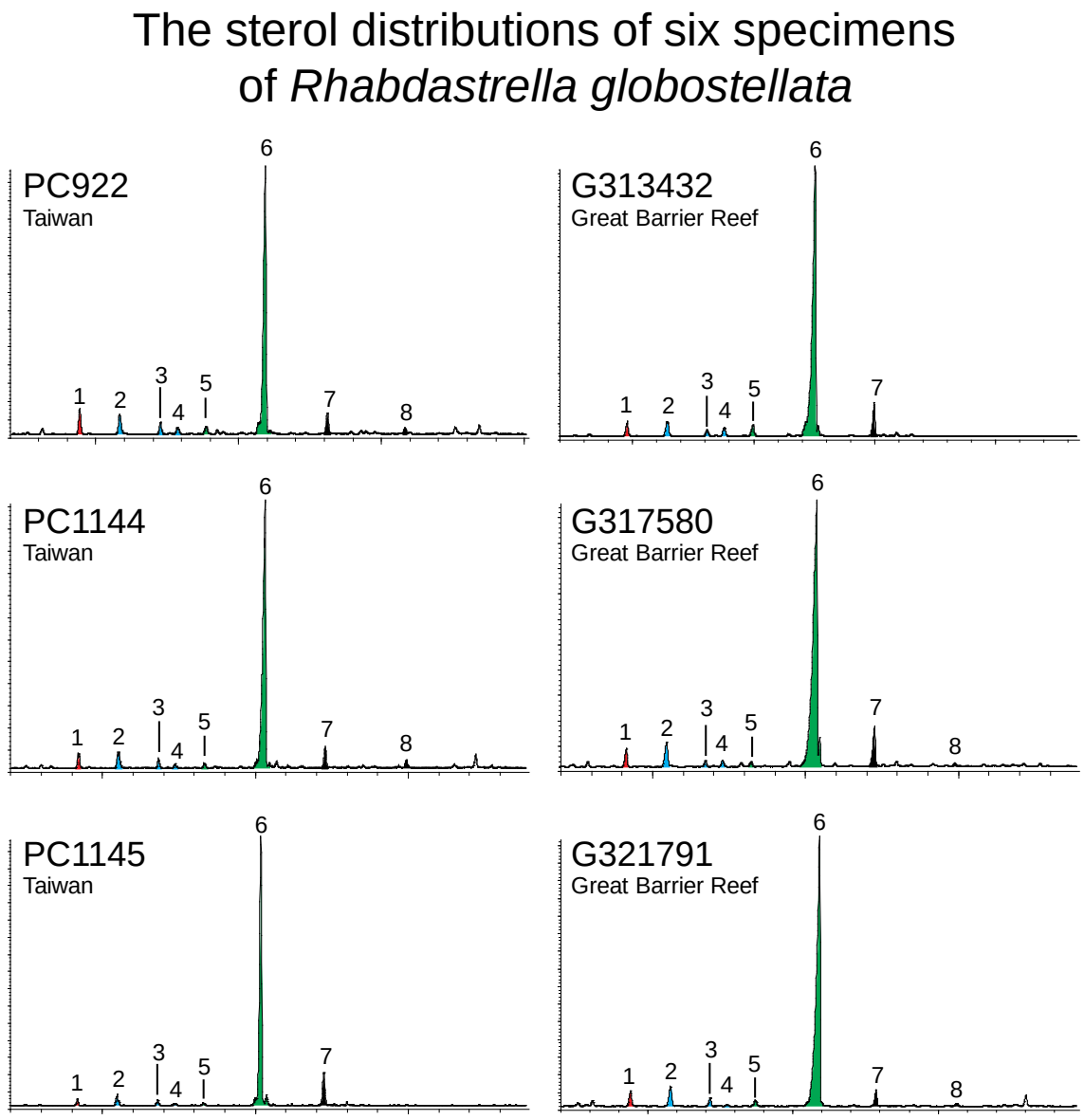

Figure 24. C_{27}-C_{30} sterol distributions from GC-MS (m/z 129) for six different specimens of *Rhabdastrella globostellata* collected from Taiwan and Australia. Note the similarity in the sterol abundance patterns and in the major sterol constituents (each chromatogram has the sponge ID in the upper left; see Table 11 for taxonomic information). Unconventional sterols with extended side chains (e.g. peaks 6-8) are the dominant sterol constituents in all specimens. Two general localities are represented: (*left*) the Penghu Archipelago off the coast of Taiwan and (*right*) three different reefs within the Great Barrier Reef off the coast of Eastern Australia. Peak IDs: 1 = cholesterol (**B1**); 2 = brassicasterol (**B7**); 3 = codisterol (**B6**); 4 = campesterol (**B4**); 5 = stigmasterol (**B12**); 6 = 24(28)-dehydroaplysterol (**B20**); 7 = stelliferasterol (**B25**); 8 = stelliferastanol (**B27**).

Sequence-selective bioalkylation patterns in Porifera

24(28)-dehydroaplysterol (**B20**) can be used as a model compound for understanding the specificity and sequential patterns of side chain elongation and mid-chain alkylation within the unconventional sterol biosynthetic pathway. As portrayed in Scheme III, the path to (**B20**) proceeds exclusively via codisterol (**B6**). Unlike 24-methylenecholesterol (**B5**), which is a common precursor for downstream C_{29}-C_{30} sterol production in the conventional pathway, codisterol (**B6**) has an exposed double bond in an unusual position at the C-25(26) terminus of the steroid side chain. A critical step towards downstream C_{29}-C_{30} unconventional sterol production begins here, with terminal methylation proceeding prior to subsequent methylation at position C-24 (Theobald and Djerassi 1978; Theobald et al., 1978; Stoilov et al., 1986; Cho et al., 1988; Djerassi 1981; Li et al., 1981). There is no published evidence that the reverse sequence, with C-24 alkylation occurring before terminal alkylation, occurs at all. The biosynthetic pathway to (**B20**) was thoroughly described by Stoilov et al. (1986) using radiolabeling experiments with sponge specimens to elucidate the most likely sequence of molecular transformation (see **Chapter 1**). After surveying a wide array of phylogenetically distinct demosponges, we've found that the same underlying concept probably applies to other unconventional C_{29} and C_{30} sterols including (but probably not limited to) 25-dehydroaplysterol (**B19**), aplysterol (**B22**), strongylosterol (**B24**), stelliferasterol (**B25**), isostelliferasterol (**B26**), verongulasterol (**B28**), xestosterol (**B29**) and mutasterol (**B31**).

From Scheme III, it may seem that clerosterol (**B9**) would be an ideal candidate for terminal alkylation towards the production of **B24**/**B25**/**B26** since this sterol already contains prerequisite moieties including the 24-ethyl constituent *and* the exposed double bond at the C-25(26) position. During testing of this hypothesis, however, when radiolabeled (epi)clerosterol (**B9**) was incorporated as a feedstock of the demosponge "*Strongylophora durissima*" [recently acknowledged by us as being originally mis-identified but with *Petrosia (Strongylophora) corticata* as the true source] which produces strongylosterol (**B24**) as its single major sterol constituent, researchers found that the labeled (**B9**) was <u>not</u> incorporated into the unconventional sterol product (Theobald and Djerassi 1978; Theobald et al., 1978; Stoilov et al., 1986). The systematic steps underlining this failed incorporation experiment exceptionally highlight the fundamental differences between the conventional and unconventional pathways towards sterol biosynthesis. To expand further, (**B9**) has been routinely reported as an abundant sterol in some unicellular algae, including the green alga *Codium fragile* (Rubinstein and Goad 1974; Wilkomirski and Goad 1983), however these eukaryotes lack the basic biosynthetic toolkit (enzymes, protein packages, etc.) needed for the production of unconventional sterols and are consequently restricted within the more common conventional pathway. This illustrates, once again, more direct evidence for a strong host control on the production of downstream unconventional C_{29} and C_{30} sterols; a trait that is likely deeply rooted within Demospongiae since different structural varieties of unconventional steroids are found in multiple clades.

Scheme III
[unconventional]

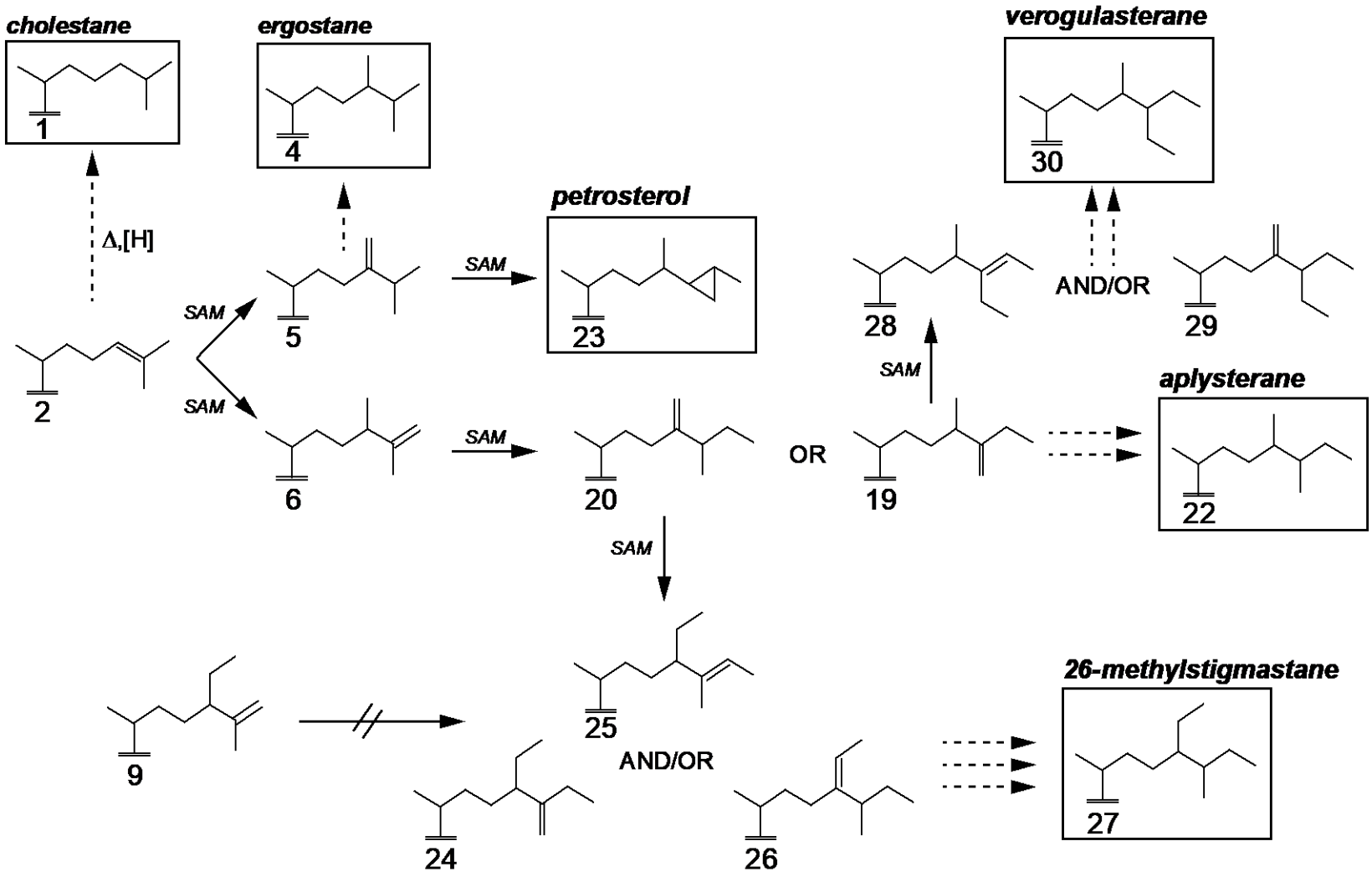

Sterane distributions from the HyPy pyrolysates of extant sponges

Catalytic hydropyrolysis (HyPy) treatment of biomass facilitates the reductive conversion of sterols to steranes in the laboratory with excellent preservation of structural and stereochemical features (see **Materials and Methods**). The sterane products from HyPy from our collection of modern sponge taxa specimens were analyzed in detail using full scan GC-MS and MRM-GC-MS to investigate the sterane carbon number distributions and assess any taxonomic patterns, including the presence or absence of known unconventional steranes. Steranes detected from MRM-GC-MS were integrated to quantify the percent sterane relative to all steranes detected (reported as percent C_{27}-C_{30} steranes). For all our sponge hydropyrolysates from widely different species (n=42), the sterane carbon number distributions found for the major C_{27}-C_{30} steranes (n=10) were as follows (see Table 11):

- C_{27} (**A1**): [min=0.4%, max=97%, mean=33%]
- C_{28} (**A4**): [min=0.8%, max=79%, mean=16%]
- C_{29} (**A8**/**A22**/**A23**): [min=1.7%, max=84%, mean=43%]
- C_{30} (**A13**/**A16**/**A27**/**A30**/**A32**): [min=0.0%, max=94%, mean=8%]

Table 11. Sterane distributions generated from reductive conversion of biomass for various sponge species using catalytic hydropyrolysis (HyPy) treatment as determined from MRM-GC-MS analysis. The relative abundance of C_{27}-C_{30} steranes (as % of total) are shown to highlight the sterane carbon number patterns found for each species, with conventional and unconventional sterane contributions summed together (e.g. Total C_{29} includes stigmastane and/or aplysterane). TAR = terminal alkylation ratio = Σ(terminally alkylated steranes)/Σ(C-24 alkylated steranes).

Family	Specimen *(Genus species)*	Sponge ID	Total C_{27}	Total C_{28}	Total C_{29}	Total C_{30}	%Conventional	%Unconventional	TAR
Ancorinidae	*Rhabdastrella distincta*	PC1127	4%	7%	84%	4%	22%	78%	3.4
	Rhabdastrella globostellata	G317580	16%	17%	60%	8%	49%	51%	1.0
	Rhabdastrella globostellata	PC140	20%	17%	60%	4%	69%	31%	0.4
	Rhabdastrella globostellata	PC492	5%	32%	62%	1%	96%	4%	<0.1
	Rhabdastrella globostellata	PC922	16%	16%	57%	11%	48%	52%	1.1
	Rhabdastrella wondoensis	PC865	21%	17%	57%	5%	51%	49%	1.0
	Rhabdastrella wondoensis	PC866	11%	19%	65%	5%	44%	56%	1.3
	Stelletta tuberosa	PC675	9%	72%	18%	1%	100%	0%	0.0
Aplysinidae	*Aplysina aerophoba*	TLE430	11%	7%	80%	2%	28%	72%	2.6
	Aplysina fulva	A. fulva	19%	7%	72%	1%	36%	64%	1.8
	Verongula reiswigi	BT-13	43%	8%	46%	3%	63%	37%	0.6
	Verongula rigida	Sponge 8	45%	9%	42%	4%	67%	33%	0.5
Bubaridae	*Phakellia ventilabrum*	FKOG-POR2	67%	22%	11%	1%	100%	0%	0.0
Calthropellidae	*Pachataxa enigmatica*	MNHN-IP-2015-1781	17%	16%	37%	30%	71%	29%	0.4
Chondrillidae	*Thymosiopsis* cf. *cuticulatus*	Endoume	73%	4%	22%	1%	100%	0%	0.0
	Thymosiopsis conglomerans	Tremies	22%	10%	14%	53%	43%	57%	1.3
Clionaidae	*Cliona* sp.	Sponge 3	62%	31%	7%	0.3%	100%	0%	0.0
Dysideidae	*Dysidea fragilis*	D. fragilis	68%	21%	11%	0.4%	99%	1%	<0.01
Geodiidae	*Geodia hentscheli*	GhII	9%	79%	12%	1%	100%	0%	0.0
	Geodia parva	GpII	13%	8%	73%	5%	33%	67%	2.1
	Geodia parva	PC535	9%	9%	75%	7%	31%	69%	2.2
	Geodia phlegraei	PC511	11%	6%	78%	5%	26%	74%	2.9
	Geodia cf. *phlegraei*	PC567	12%	15%	65%	7%	38%	62%	1.7
Halichondriidae	*Ciocalypta carballoi*	PC1064	14%	9%	36%	42%	100%	0%	0.0
	Ciocalypta penicillus	Roscoff #1	86%	6%	8%	<0.1%	100%	0%	0.0
	Halichondria sp.	Sponge 1	89%	8%	3%	0.2%	100%	0%	0.0
	Topsentia sp.	PC1213	6%	3%	74%	17%	28%	72%	2.6
Hymerhabdiidae	*Cymbaxinella corrugata*	1153725	60%	17%	22%	2%	97%	3%	<0.1
Leucosoleniidae	*Leucosolenia* sp.	Sponge 5	75%	15%	10%	0%	100%	0%	0.0
Microcionidae	*Microciona* sp.	Sponge 4	97%	1%	2%	0%	100%	0%	0.0
Petrosiidae	*Petrosia (Strongylophora)* cf. *vansoesti*	PC982	10%	11%	78%	1%	73%	27%	0.4
	Petrosia (Strongylophora) corticata	PC1211	0.4%	1%	4%	94%	10%	90%	9.3
	Petrosia (Strongylophora) durissima	1907.2.1.37	21%	14%	65%	1%	100%	0%	0.0

	Petrosia (Strongylophora) durissima	PC1068	15%	9%	76%	1%	100%	0%	0.0
	Petrosia crassa	#11	5%	9%	80%	6%	64%	36%	0.6
	Xestospongia sp.	#070818 #04-1	47%	9%	40%	4%	88%	12%	0.1
Plakinidae	*Plakinastrella onkodes*	1133732	56%	20%	24%	0%	100%	0%	0.0
	Plakortis halichondrioides	1133720	42%	16%	42%	0%	100%	0%	0.0
Rossellidae	*Vazella pourtalesii*	HUD16-019-B0362	70%	20%	10%	0.2%	100%	0%	0.0
Suberitidae	*Suberites* sp.	Sponge 2	68%	19%	13%	0.4%	100%	0%	0.0
Tetillidae	*Cinachyrella kuekenthali*	PC941	34%	20%	46%	0.3%	100%	0%	0.0
	Craniella zetlandica	PC667	24%	26%	50%	1%	100%	0%	0.0

Table 11 compares sterane product abundances and reveals that different species within the same genus can have distinct sterane distributions (e.g. *Geodia parva* vs *Geodia hentscheli*). This same comparison for *Geodia* additionally demonstrates that certain species yield predominantly conventional C_{27}-C_{30} steranes while others may contain a high proportion of unconventional steroids. Importantly though, specimens of the same species collected from different sampling locations yield a similar steroid distribution (Fromont et al., 1994; this study), as discussed previously. We indeed found this to be true for our sterol assay comparisons for *Rhabdastrella globostellata* specimens collected from Taiwan and Australia (Fig. 24). Likewise, we observed similarities in the sterane distributions generated from HyPy, down to the species level, for specimens collected from various geographic localities, including (Table 11):

i) *Rhabdastrella globostellata* (G317580 and PC922)

ii) *Geodia parva* (GpII and PC535)

iii) *Geodia phlegraei* (PC511 and PC567)

iv) *Petrosia (Strongylophora) durissima* (1907.2.1.37 and PC1068)

This illustrates the effective conversion of the biological precursor sterol to the saturated sterane 'core skeleton' after HyPy treatment and provides the basis for comparisons between modern and ancient sponge-derived biomarkers since both contain the αααR diastereoisomer peak.

Our compiled modern sponge sterane database revealed that the combined HyPy and MRM-GC-MS analytical approach is sensitive at detecting trace sterane constituents (down to 0.1% of total C_{27}-C_{30} steranes with robust assignments). While most sponges exhibited at least detectable traces of C30 steroids (Table 11), not all species contained unique C_{30} sterol compounds. We find that 24-npc and 24-ipc are generally the most common constituents, with 24-npc the dominant form for sponges that contain common and conventional C_{27}-C_{29} sterols as their major steroid compounds. This is not surprising since both compounds are made from similar biosynthetic pathways (methylation at position C-24 in the sterol side chain) which might require a similar 'promiscuous' *methylase* gene (Gold et al., 2016), and 24-ipc can be a minor by-product of 24-npc synthesis (Love et al., 2009). Sterol side chain modification involving elongation through methylation at the terminal C-26 and/or C-27 positions, yielded unconventional C_{30} sterols in certain species within our collection. Terminal methylation of the sterol side chain presumably uses a different biosynthetic route to that required for alkylation at the C-24 position, likely requiring a host coordination of *desaturase* and *methylase* enzymes to control the position of unsaturation and SAM methylation on the end of the side chain. The specific enzymes and their associated genes involved in terminal methylation, analogous to *24-sterolmethyltransferase* (Gold et al., 2016), for unconventional sterol synthesis have not yet been identified but this is the subject of an ongoing investigation with our project collaborators involving the mining of available genomes and transcriptomes for steroid-synthesis genes for sponge species which make specific unconventional steroids in high amounts. Our biomarker results show that numerous groups of extant demosponges can

produce terminally methylated C_{29} and C_{30} steroids amongst their major steroids and suggests that this biosynthetic capacity has a deep origin within the demosponge clade. Indeed, one unconventional C_{30} sterane compound, 26-methylstigmastane (**A27**), is found as the core skeleton in some of the major sterols of *Petrosia*, *Rhabdastrella* and *Geodia* demosponges as well as being detectable as an ancient fossil sterane found in the Neoproterozoic-Cambrian rock record (Zumberge et al., 2018).

Novel C_{29}-C_{31} steranes found from this study

Our modern sponge-derived sterane patterns via HyPy analysis reveal at least seven distinct C_{29}-C_{30} sterane structural isomers from specimens in our sponge collection: stigmastane (**A8**), aplysterane (24,26-dimethylcholestane; **A22**), 24-npc (**A13)**, 24-ipc (**A16**), 26-mes (**A27**), verongulasterane (24,26,27-trimethylcholetane; **A30**) and thymosiosterane (24,26,26-trimethylcholestane; **A32**) (listed in relative elution order; Figs. 25 and 26). Four of these are novel sterane compounds not reported before in the geochemical literature. The chromatographic elution order of the different C_{30} sterane compounds is consistent with chromatographic first principles: compounds with all three additional carbon atoms positioned in the interior of the sterane side-chain at position C-24 (i.e. (**A13**) and (**A16**)) will elute *before* compounds with extra carbons in terminal sites (i.e. (**A27**), (**A30**) and (**A32**)). Since (**A27**) contains two side chain carbons through an ethyl-substituent at C-24 and a terminal methyl-substituent at C-26, the predicted elution time is between (**A16**) (no extra terminal carbon) and (**A32**) (two terminal methyl groups both attached at C-26), as is observed (Fig. 26).

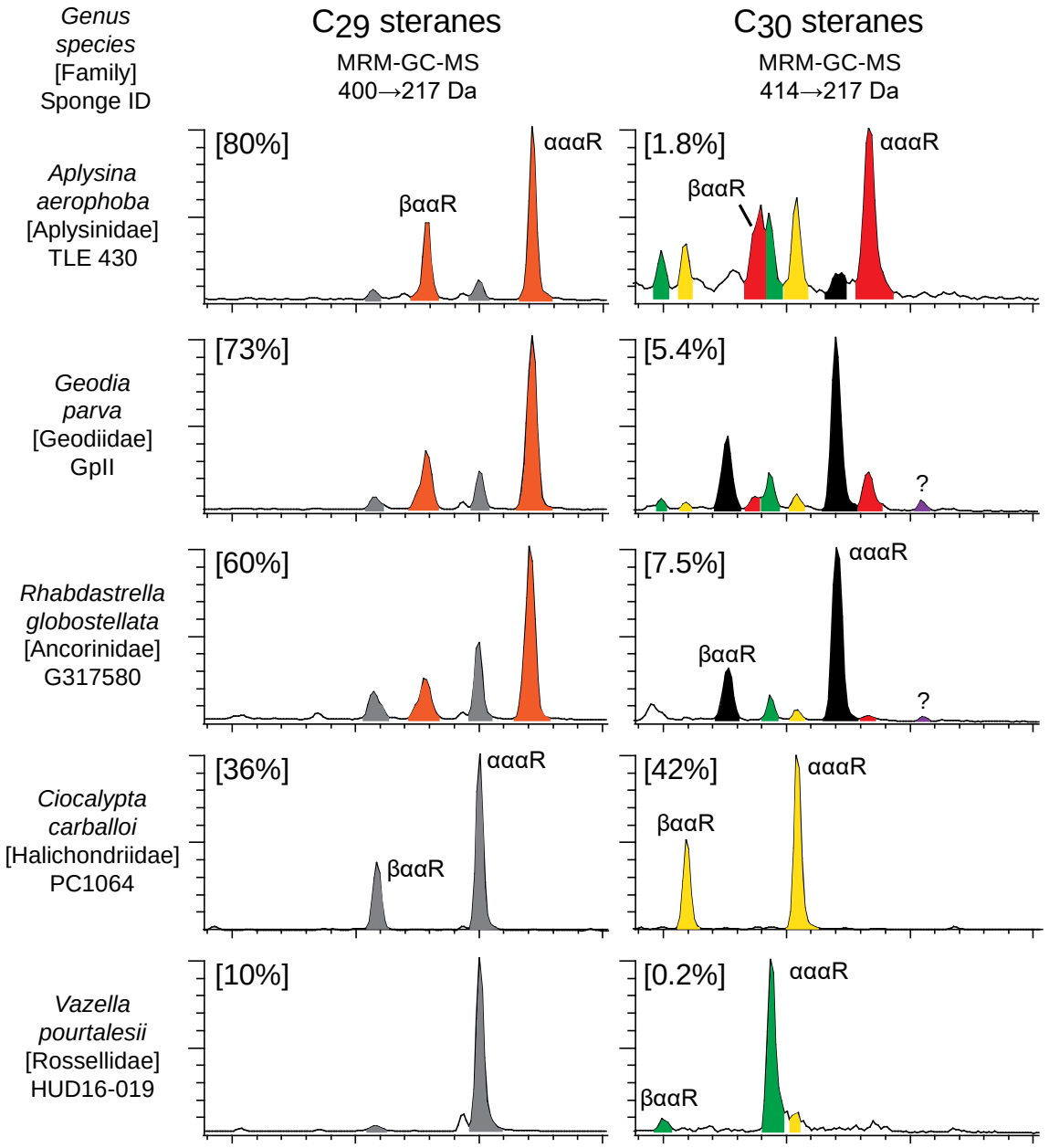

Figure 25. Conventional and unconventional C_{29} (*left column*) and C_{30} (*right column*) sterane distributions generated from representative sponge hydropyrolysates, as detected by selective MRM-GC-MS analysis using the appropriate molecular ion to fragment ion transitions. Each colored peak is a separate compound with both expected, and resolvable, βααR and αααR stereoisomers from hydrogenation of Δ^5-unsaturated sterols. $\%C_{29}$ and $\%C_{30}$ are shown in brackets for each sample (relative to total C_{27}-C_{30} steranes). Peak IDs (See Charts II-III): stigmastane (**A8**/gray); aplysterane (**A22**/orange); 24-npc (**A13**/green); 24-ipc (**A16**/yellow); 26-mes (**A27**/black); verongulasterane (**A30**/red) and an unidentified C_{30} sterane (purple) compound that occasionally occurs as a minor constituent in our *Geodia* and *Rhabdastrella* species. All species shown here are demosponges except for the hexactinellid *Vazella pourtalesii*.

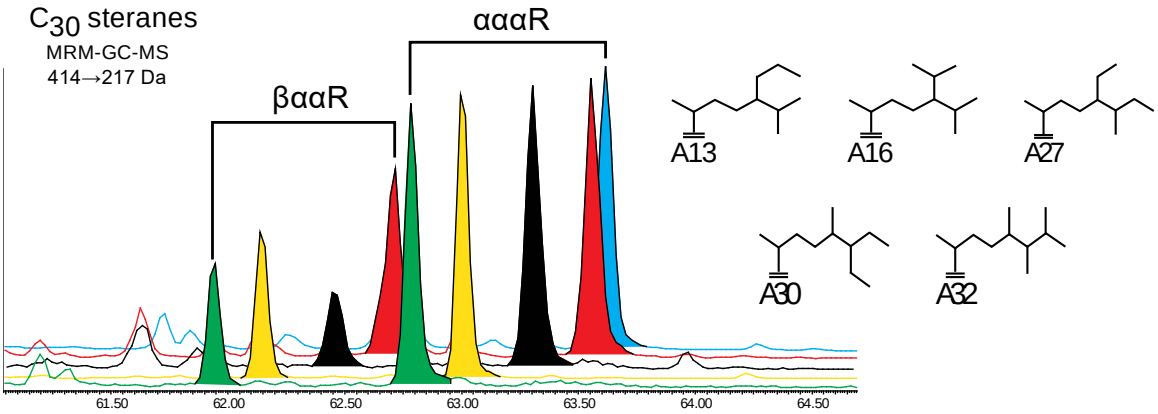

Figure 26. Stacked chromatograms showing five different and resolvable C_{30} sterane compounds, each with a βααR and αααR stereoisomer, generated from representative sponge hydropyrolysates and detected by selective MRM-GC-MS analysis. Peak IDs (see Charts II-III): 24-npc (**A13**/green); 24-ipc (**A16**/yellow); 26-mes (**A27**/black); verongulasterane (**A30**/red) and thymosiosterane (**A32**/blue).

Compounds (**A8**) and (**A13**) are well established sterane biomarker targets and are routinely applied to studies that characterize organic matter in the geologic record, either extracted from candidate reservoir and/or source rocks or from produced oil (Moldowan 1984; Peters et al., 2005). As described in the previous sections, 24-ipc (**A16**) and 26-mes (**A27**) are two distinct C_{30} sterane compounds that provide compelling evidence for the presence of Neoproterozoic animals significantly prior to the Cambrian Explosion of more complex animal body plans (Love et al., 2009; Zumberge et al., 2018) since the corresponding sterol precursors can be made by certain demosponges as major sterol constituents within their cell membranes. Compounds (**A22**), (**A30**) and (**A32**) are novel sterane structures that have not yet been reported in the biomarker literature while 26-mes (**A27**) was also recently identified and reported (Zumberge et al., 2018) but as an integral part of this thesis investigation (Chapter 1). In this regard, the repertoire of sterane biomarkers, which have traditionally revolved around a small range of structures and

carbon number patterns applicable across the Eucarya domain, can be greatly expanded when our analytical approach is applied to demosponge clades that have the capacity to make abundant unconventional steroids.

The diagenetic conversion of the sterol precursor compound to steranes in thermally well-preserved strata in the geologic record is systematically consistent with no apparent preservation bias and regardless of the number of carbons in the original biological marker (Killops and Killops 2005; Love and Summons 2015). Less stable structural features like the degree of unsaturation and/or the presence of biologically important functional groups are lost during diagenesis leaving the core sterane skeleton to provide the basis for comparisons between modern and ancient organisms (Fig. 20). Long term sedimentary diagenesis of deposited eukaryote biomass initiates the conversion of two sterol stereoisomers (the 'biologic forms'; βααR + αααR) to four, more thermodynamically stable, sterane stereoisomers (the 'geologic forms'; αααS, αββR, αββS, αααR). The kinetics of this transformation from the biological form to the geological form is consistent regardless of the number of carbons on the 'parent' sterol compound and does not alter the preserved sterane carbon number patterns or discriminate against particular structures. Both the biologic and geologic forms of these steroid biomarkers contain the αααR diastereoisomer. This αααR isomeric configuration, therefore, is used as the target compound peak to match modern versus ancient sterane signals in MRM-GC-MS analysis. If the ancient and modern sterane signals are the same sterane compound then perfect co-elution of the αααR peaks must be observed in the different samples (as measured by

retention time), even when different GC temperature programs and GC column stationary phases are used. Robust compound verifications should only be attempted when sterane signal peaks are demonstrably reproducible and consistent from repeat runs, and for strong mass spectral responses such that signal abundance is high and significantly above noise levels.

We seem to just be scratching the surface with respect to the potential for new discoveries of distinctive ancient sterane compounds that can be classified as sponge-selective biomarkers. Our current knowledge of demosponge-derived C_{31} steroids is improving but is still at an early stage, however, these steroid compounds have the potential to augment the existing C_{29} and C_{30} sponge sterane targets and are amendable to selective and sensitive biomarker detection methods including MRM-GC-MS. Outside of the relatively simple 3β-hydroxysteroids and their related sterane biomarkers, reported here, additional research efforts should be directed toward the elucidation of other lipid compound classes that may contain structural varieties that are unique to or selectively made by demosponges and which possess stable core structures that can be preserved in the geologic record.

Conclusions

Through the parallel analyses of intact sterols and their sterane derivatives generated from HyPy of biomass from over 90 sponge specimens, we were able to scrutinize the demosponge sterol distribution patterns to an unprecedented level in order to better understand the likely biosynthetic pathways and precursor-product relationships,

particularly with respect to sponges capable of making 24-ipc and 26-mes steroids. This emerging knowledge in turn helped us target species for steroid investigation which offer a high potential of identifying novel fossil sterane biomarkers. Recognition of systematic patterns in steroid distributions, encompassing sites of unsaturation in the tetracyclic nucleus and in side chain chemistry that are applicable to both conventional and unconventional sterol synthesis, adds to a growing body of evidence that the host demosponge plays a major role in *de novo* synthesis of the major sterol constituents within the cell membranes. The synthesis of elongated steroid side chains with terminal methyl groups attached must require the concerted participation of regioselective steroid enzymes, possibly through coordination of *desaturase* and *sterol methyltransferase* enzymatic activity to control double bond sites that can be reactive centers for methylation. As a result, certain demosponges can closely regulate the positions of side chain unsaturation and alkylation, which are guiding principles behind the production of unique sterol precursors that might be preserved in the rock record as novel sterane biomarkers.

We generated a suite of novel and analytically resolvable C_{29} and C_{30} steranes from HyPy hydrogenation treatment of sponge biomass which have not been reported before in the organic geochemical literature. These new sterane structures expand the biomarker geochemistry toolbox and will prove useful for searching for early animal fossil evidence in ancient sedimentary rocks and oils. The new sterane compounds that we could confidently identify through ties to known sterol precursors comprised the C_{29} compound name aplysterane (24,26-dimethylcholestane; **A22**), as well as three new C_{30} steranes

named 26-methylstigmastane (26-mes; **A27**), verongulasterane (24,26,27-trimethylcholestane; **A30**) and thymosiosterane (24,26,26-trimethylcholestane; **A32**) in terms of elution order observed in gas chromatography separation. These four compounds are all geologically stable and when present will be preserved in sedimentary rocks and oils that have undergone a mild thermal history. Additionally, we have tentatively identified at least three resolvable C_{31} sterane products generated from sponges for which the exact structures require further verification.

Our results show that numerous groups of extant demosponges can produce terminally methylated C_{29} and C_{30} steroids amongst their major steroids and suggests that this biosynthetic capacity has a deep origin within the demosponge clade. Indeed, one unconventional C_{30} sterane compound, 26-methylstigmastane (26-mes; **A27**), is found as the core skeleton in some of the major sterols of *Petrosia*, *Rhabdastrella* and *Geodia* demosponges as well as being detectable as an ancient fossil sterane found in the Neoproterozoic-Cambrian rock record.

The discovery of novel fossil steranes is a challenging endeavor but Porifera offer attractive potential amongst eukaryotic source organisms in this regard to provide new targets for tracking the ecological expansion of early animals and to greatly enhance our understanding of the ancient paleoenvironments in which these organisms flourished.

REFERENCES

Adam, P., Schaeffer, P., Brocks, J.J., 2018. Synthesis of 26-methyl cholestane and identification of cryostanes in mid-Neoproterozoic sediments. Organic Geochemistry 115, 246-249.

Antcliffe, J.B., 2013. Questioning the Evidence of Organic Compounds Called Sponge Biomarkers. Palaeontology 56, 917-925.

Aquino Neto, F.R., Restle, A., Trendel, J.M., Connan, J., Albrecht, P., 1983. Occurrence and formation of tricyclic and tetracyclic terpanes in sediments and petroleum. In Bjorøy, M, ed. *Advances in Organic Geochemistry 1983*. Wiley, Chichester, England, pp. 659-667.

Barnathan, G., Velosaotsy, N., Al-Lihaibi, S., Njinkoue, J.-M., Kornprobst, J.-M., Vacelet, J., Boury-Esnault, N., 2004. Unusual sterol compositions and classification of three marine sponge families. Moscow University Biological Sciences Bulletin 68, 201-208.

Bengtson, S., Sallstedt, T., Belivanova, V., Whitehouse, M., 2017. Three-dimensional preservation of cellular and subcellular structures suggests 1.6 billion-year-old crown-group red algae. Plos Biology 15, 1-38.

Berelson, W.M., Prokopenko, M., Sansone, F.J., Graham, A.W., McManus, J., Bernhard, J.M., 2005. Anaerobic diagenesis of silica and carbon in continental margin sediments: Discrete zones of TCO2 production. Geochimica Et Cosmochimica Acta 69, 4611-4629.

Bergquist, P.R., Hofheinz, W., Oesterhelt, G., 1980. Sterol Composition and the Classification of the Demospongiae. Biochemical Systematics and Ecology 8, 423-435.

Bergquist, P.R., Lavis, A., Cambie, R.C., 1986. Sterol Composition and Classification of the Porifera: Part 2. Biochemical Systematics and Ecology 14, 105-112.

Bergquist, P.R., Karuso, P., Cambie, R.C., Smith, D.J., 1991. Sterol Composition and Classification of the Porifera: Part 3. Biochemical Systematics and Ecology 19, 17-24.

Betts, H.C., Puttick, M.N., Clark, J.W., Williams, T.A., Donoghue, P.C.J., Pisani, D., 2018. Integrated genomic and fossil evidence illuminates life's early evolution and eukaryote origin. Nature Ecology and Evolution 2, 1556-1562.

Bhattacharya, S., Dutta, S., Summons, R.E., 2017. A distinctive biomarker assemblage in an Infracambrian oil and source rock from western India: Molecular signatures of eukaryotic sterols and prokaryotic carotenoids. Precambrian Research 290, 101-112.

Bishop, A.N., Love, G.D., McAulay, A.D., Snape, C.E., Farrimond, P., 1998. Release of kerogen-bound hopanoids by hydropyrolysis. Organic Geochemistry 29, 989-1001.

Bloch, K., 1991. Cholesterol: evolution of structure and function. In Vance, D.E., Vance, J., eds. *Biochemistry of Lipids, Lipoproteins, and Membranes*. Elsevier, Amsterdam, pp. 363-381.

Blumenberg, M., Thiel, V., Pape, T., Michaelis, W., 2002. The steroids of hexactinellid sponges. Naturwissenschaften 89, 415-419.

Blumenberg, M., Thiel, V., Riegel, W., Kah, L.C., Reitner, J., 2012. Biomarkers of black shales formed by microbial mats, Late Mesoproterozoic (1.1 Ga) Taoudeni Basin, Mauritania. Precambrian Research 196, 113-127.

Bortolotto, M., Braekman, J.C., Daloze, D., Tursch, B., 1978. Chemical Studies of Marine-Invertebrates 36: Strongylosterol, a Novel C-30 Sterol from Sponge Strongylophora-Durissima Dendy. Bulletin Des Societes Chimiques Belges 87, 539-543.

Botting, J.P., Muir, L.A., 2018. Early sponge evolution: A review and phylogenetic framework. Palaeoworld 27, 1-29.

Bouvier, P., Rohmer, M., Benveniste, P., Ourisson, G., 1976. Delta8(14)-steroids in bacterium *Methylococcus capsulatus*. Biochemical Journal 159, 267-271.

Brocks, J.J., Pearson, A., 2005. Building the biomarker tree of life. Molecular Geomicrobiology 59, 233-258.

Brocks, J.J., Love, G.D., Summons, R.E., Knoll, A.H., Logan, G.A., Bowden, S.A., 2005. Biomarker evidence for green and purple sulphur bacteria in a stratified Palaeoproterozoic sea. Nature 437, 866-870.

Brocks, J.J., Jarrett, A.J.M., Sirantoine, E., Kenig, F., Moczydlowska, M., Porter, S., Hope, J., 2015. Early sponges and toxic protists: possible sources of cryostane, an age diagnostic biomarker antedating Sturtian Snowball Earth. Geobiology 14, 129-149.

Brocks, J.J., Jarrett, A.J.M., Sirantoine, E., Hallmann, C., Hoshino, Y., Liyanage, T., 2017. The rise of algae in Cryogenian oceans and the emergence of animals. Nature 548, 578-581.

Brooks, C.J., Horning, E.C., Young, J.S., 1968. Characterization of sterols by gas chromatography-mass spectrometry of the trimethylsilyl ethers. Lipids 3, 391-402.

Butterfield, N.J., Knoll, A.H., Swett, K., 1994. Paleobiology of the Upper Proterozoic Svanbergfjellet Formation, Spitsbergen. Fossils and Strata 34, 1-84.

Butterfield, N.J., 2000. *Bangiomorpha pubescens* n. gen., n. sp.: implications for the evolution of sex, multicellularity and the Mesoproterozoic/Neoproterozoic radiation of eukaryotes. Paleobiology 26, 386-404.

Calderón, G.J., Castellanos, L., Duque, C., Echigo, S., Hara, N., Fujimoto, Y., 2004. Ophirasterol, a new C_{31} sterol from the marine sponge *Topsentia ophiraphidites*. Steroids 69, 93-100.

Cárdenas, P., Xavier, J.R., Reveillaud, J., Schander, C., Rapp, H.T., 2011. Molecular phylogeny of the Astrophorida (Porifera, Demospongiae(p)) reveals an unexpected high level of spicule homoplasy. PloS one, 6(4), e18318.

Cho, J.H., Thompson, J.E., Stoilov, I.L., Djerassi, C., 1988. Biosynthetic-Studies of Marine Lipids .14. 24(28)-Dehydroaplysterol and Other Sponge Sterols from Jaspis-Stellifera. Journal of Organic Chemistry 53, 3466-3469.

Cole, D.B., Reinhard, C.T., Wang, X.L., Gueguen, B., Halverson, G.P., Gibson, T., Hodgskiss, M.S.W., McKenzie, N.R., Lyons, T.W., Planavsky, N.J., 2016. A shale-hosted Cr isotope record of low atmospheric oxygen during the Proterozoic. Geology 44, 555-558.

Cook, D.A., 1991. Sedimentology and shale petrology of the Upper Proterozoic Walcott Member, Kwagunt Formation, Chuar Group, Grand Canyon, Arizona [M.S. thesis]: Flagstaff, Northern Arizona University, 128p.

Djerassi, C., 1978. Recent advances in the mass spectrometry of steroids. Pure and Applied Chemistry 50, 171-184.

Djerassi, C., Silva, C.J., 1991. Sponge Sterols: Origin and Biosynthesis. Accounts of Chemical Research 24, 371-378.

Dohrmann, M., Wörheide, G., 2017. Dating early animal evolution using phylogenomic data. Scientific Reports 7: 3599.

dos Reis, M., Thawornwattana, Y., Angelis, K., Telford, M.J., Donoghue, P.C.J., Yang, Z.H., 2015. Uncertainty in the Timing of Origin of Animals and the Limits of Precision in Molecular Timescales. Current Biology 25, 2939-2950.

Dutkiewicz, A., Volk, H., Ridley, J., George, S., 2003. Biomarkers, brines, and oil in the Mesoproterozoic, Roper Superbasin, Australia. Geology 31, 981-984.

Dutta, S., Bhattacharya, S., Raju, S.V., 2013. Biomarker signatures from Neoproterozoic-Early Cambrian oil, western India. Organic Geochemistry 56, 68-80.

Echigo, S., Castellanos, L., Duque, C., Uekusa, H., Hara, N., Fujimoto, Y., 2011. C-24 Sterochemistry of Marine Sterols: (22*E*)-24-ethyl-24-methylcholesta-5,22-dien-3β-ol and 24-ethyl-24-methylcholest-5-en-3β-ol. Journal of the Brazilian Chemical Society 22, 997-1004.

Eme, L., Sharpe, S.C., Brown, M.W., Roger, A.J., 2014. On the Age of Eukaryotes: Evaluating Evidence from Fossils and Molecular Clocks. Cold Spring Harbor Perspectives in Biology 4:a016139.

Erwin, D.H., Laflamme, M., Tweedt, S.M., Sperling, E.A., Pisani, D., Peterson, K.J., 2011. The Cambrian Conundrum: Early Divergence and Later Ecological Success in the Early History of Animals. Science 334, 1091-1097.

Feuda, R., Dohrmann, M., Pett, W., Philippe, H., Rota-Stabelli, O., Lartillot, N., Wörheide, G., Pisani, D., 2017. Improved Modeling of Compositional Heterogeneity Supports Sponges as Sister to All Other Animals. Current Biology 27, 3864-3870.

Feulner, G., Hallmann, C., Kienert, H., 2015. Snowball cooling after algal rise. Nature Geoscience 8, 659-662.

Flannery, E.N., George, S.C., 2014. Assessing the syngeneity and indigeneity of hydrocarbons in the similar to 1.4 Ga Velkerri Formation, McArthur Basin, using slice experiments. Organic Geochemistry 77, 115-125.

French, K.L., Hallmann, C., Hope, J.M., Schoon, P.L., Zumberge, J.A., Hoshino, Y., Peters, C.A., George, S.C., Love, G.D., Brocks, J.J., Buick, R., Summons, R.E., 2015. Reappraisal of hydrocarbon biomarkers in Archean rocks. Proceedings of the National Academy of Sciences 112, 5915-5920.

Fromont, J., Kerr, S., Kerr, R., Riddle, M., Murphy, P., 1994. Chemotaxonomic Relationships Within, and Comparisons Between, the Orders Haplosclerida and Petrosida (Porifera: Demospongiae) Using Sterol Complements. Biochemical Systematics and Ecology 22, 735-752.

Gallagher, T.M., Sheldon, N.D., Mauk, J.L., Petersen, S.V., Gueneli, N., Brocks, J.J., 2017. Constraining the thermal history of the North American Midcontinent Rift System using carbonate clumped isotopes and organic thermal maturity indices. Precambrian Research, 294, 53-66.

Gazave, E., Lapébie, P., Ereskovsky, A.V., Vacelet, J., Renard, E., Cárdenas, P., Borchiellini, C., 2012. No longer Demospongiae: Homoscleromorpha formal nomination as a fourth class of Porifera. Hydrobiologia 687, 3-10.

Gibson, T.M., Shih, P.M., Cumming, V.M., Fischer, W.W., Crockford, P.W., Hodgskiss, M.S.W., Wörndle, S., Creaser, R.A., Rainbird, R.H., Skulski, T.M., Halverson, G.P., 2018. Precise age of *Bangiomorpha pubescens* dates the origin of eukaryotic photosynthesis. Geology 46, 135-138.

Giner, J.-L., 1993. Biosynthesis of marine sterol side chains. Chemical Reviews 93, 1735-1752.

Giner, J.-L., Boyer, G.L., 1998. Sterols of the brown tide alga *Aureococcus anophagefferens*. Phytochemistry 48, 475-477.

Giner, J.-L., Zhao, H., Boyer, G.L., Satchwell, M.F., Andersen, R.A., 2009. Sterol Chemotaxonomy of Marine Pelagophyte Algae. Chemistry & Biodiversity 6, 1111-1130.

Goad, L.J., Akihisa, T., 1997. *Analysis of Sterols*. Blackie Academic, London.

Gold, D.A., Grabenstatter, J., de Mendoza, A., Riesgo, A., Ruiz-Trillo, I., Summons, R.E., 2016. Sterol and genomic analyses validate the sponge biomarker hypothesis. Proceedings of the National Academy of Sciences of the United States of America 113, 2684-2689.

Grabenstatter, J., Mehay, S., McIntyre-Wressnig, A., Giner, J.L., Edgcomb, V.P., Beaudoin, D.J., Bernhard, J.M., Summons, R.E., 2013. Identification of 24-n-propylidenecholesterol in a member of the Foraminifera. Organic Geochemistry 63, 145-151.

Grantham, P.J., Lijmbach, G.W.M., Posthuma, J., Hughes Clarke, M.W., Willink, R.J., 1987. Origin of crude oils in Oman. Journal of Petroleum Geology 11, 61-80.

Grantham, P.J., Wakefield, L.L., 1988. Variations in the Sterane Carbon Number Distributions of Marine Source Rock Derived Crude Oils through Geological Time. Organic Geochemistry 12, 61-73.

Grosjean, E., Love, G.D., Stalvies, C., Fike, D.A., Summons, R.E., 2009. Origin of petroleum in the Neoproterozoic-Cambrian South Oman Salt Basin. Organic Geochemistry 40, 87-110.

Gueneli, N., Legendre, E., Brocks, J.J., 2012. 1.1 Billion-years-old biomarkers from a microbial mat. Goldschmidt 2012, Montréal Canada.

Haddad, E.E., Tuite, M.L., Martinez, A.M., Williford, K., Boyer, D.L., Droser, M.L., Love, G.D., 2016. Lipid biomarker stratigraphic records through the Late Devonian Frasnian/Famennian boundary: Comparison of high-and low-latitude epicontinental marine settings. Organic Geochemistry 98, 38-53.

Hardisty, D.S., Lu, Z., Bekker, A., Diamond, C.W., Gill, B.C., Jiang, G., Kah, L.C., Knoll, A.H., Loyd, S.J., Osburn, M.R., Planavsky, N.J., Wang, C., Zhou, X., Lyons, T.W., 2017. Perspectives on Proterozoic surface ocean redox from iodine contents in ancient and recent carbonate. Earth and Planetary Science Letters 463, 159-170.

Hagernann, A., Voigt, O., Worheide, G., Thiel, V., 2008. The sterols of calcareous sponges (Calcarea, Porifera). Chemistry and Physics of Lipids 156, 26-32.

Hannich, J.T., Umebayashi, K., Riezman, H., 2011. Distribution and Function of Sterols and Sphingolipids. Cold Spring Harbor Perspectives in Biology 3:a004762.

Hoffman, P.F., Abbot, D.S., Ashkenazy, Y., Benn, D.I., Brocks, J.J., Cohen, P.A., Cox, G.M., Creveling, J.R., Donnadieu, Y., Erwin, D.H., Fairchild, I.J., Ferreira, D., Goodman, J.C., Halverson, G.P., Jansen, M.F., Le Hir, G., Love, G.D., Macdonald, F.A., Maloof, A.C., Partin, C.A., Ramstein, G., Rose, B.E.J., Rose, C.V., Sadler, P.M., Tziperman, E., Voigt, A., Warren, S.G., 2017. Snowball Earth climate dynamics and Cryogenian geology-geobiology. Science Advances 3, e1600983.

Hofheinz, W., Oesterhelt, G., 1979. 24-Isopropylcholesterol and "22-Dehydro-24-Isopropylcholesterol, Novel Sterols from a Sponge. Helvetica Chimica Acta 62, 1307-1309.

Holland, H.D., 2006. The oxygenation of the atmosphere and oceans. Philosophical Transactions of the Royal Society B 361, 903-915.

Hoshino, Y., Poshibaeva, A., Meredith, W., Snape, C., Poshibaev, V., Versteegh, G.J.M., Kuznetsov, N., Leider, A., van Maldegem, L., Neumann, M., Naeher, S., Moczydlowska, M., Brocks, J.J., Jarrett, A.J.M., Tang, Q., Xiao, S., McKirdy, D., Das, S.K., Alvaro, J.J., Sansjofre, P., Hallmann, C., 2017. Cryogenian evolution of stigmasteroid biosynthesis. Science Advances 3, e1700887.

Ishibashi, M., Yamagishi, E., Kobayashi, J., 1997. Topsentinols A-J, New Sterols with Highly Branched Side Chains from Marine Sponge Topsentia sp. Chemical and Pharmaceutical Bulletin 45, 1435-1438.

Isson, T.T., Love, G.D., Dupont, C.L., Reinhard, C.T., Zumberge, A.J., Asael, D., Gueguen, B., McCrow, J., Gill, B.C., Owens, J., Rainbird, R.H., Rooney, A.D., Zhao, M.Y., Stueeken, E.E., Konhauser, K.O., John, S.G., Lyons, T.W., Planavsky, N.J., 2018. Tracking the rise of eukaryotes to ecological dominance with zinc isotopes. Geobiology 16, 341-352.

Ito, A., Yasumoto, R.K., Yamasaki, K., 1994. A sterol with an unusual side chain from *Anoectochilus koshunensis*. Phytochemistry 36, 1465-1467.

Itoh, T., Sica, D., Djerassi, C., 1983. Minor and Trace Sterols in Marine-Invertebrates 35: Isolation and Structure Elucidation of 74 Sterols from the Sponge Axinella-Cannabina. Journal of the Chemical Society, Perkin Transactions 1, 147-153.

Javaux, E.J., Knoll, A.H., Walter, M.R., 2001. Morphological and ecological complexity in early eukaryotic ecosystems. Nature 412, 66-69.

Javaux, E.J., Knoll, A.H., Walter, M.R., 2004. TEM evidence for eukaryotic diversity in mid-Proterozoic oceans. Geobiology 2, 121-132.

Johnston, D.T., Poulton, S.W., Dehler, C., Porter, S., Husson, J., Canfield, D.E., Knoll, A.H., 2010. An emerging picture of Neoproterozoic ocean chemistry: Insights from the Chuar Group, Grand Canyon, USA. Earth and Planetary Science Letters 290, 64-73.

Karlstrom, K.E., Bowring, S.A., Dehler, C.M., Knoll, A.H., Porter, S.M., Des Marais, D.J., Weil, A.B., Sharp, Z.D., Geissman, J.W., Elrick, M.B., Timmons, J.M., Crossey, L.J., Davidek, K.L., 2000. Chuar Group of the Grand Canyon: Record of breakup of Rodinia, associated change in the global carbon cycle, and ecosystem expansion by 740 Ma. Geology 28, 619-622.

Kelly, A.E., Love, G.D., Zumberge, J.E., Summons, R.E., 2011. Hydrocarbon biomarkers of Neoproterozoic to Lower Cambrian oils from eastern Siberia. Organic Geochemistry 42, 640-654.

Kennedy, J.A., 2000. Resolving the ‘Jaspis stellifera’ complex. Memoirs of the Queensland Museum 45, 453-476.

Kerr, R.G., Stoilov, I.L., Thompson, J.E., Djerassi, C., 1989. Biosynthetic Studies of Marine Lipids 16: *De Novo* Sterol Biosynthesis in Sponges. Incorporation and Transformation of Cycloartenol and Lanosterol into Unconventional Sterols of Marine and Freshwater Sponges. Tetrahedron 45, 1893-1904.

Kerr, R.G., Baker, B.J., 1991. Marine Sterols. Nature Product Reports 8, 465-497.

King, N., 2004. The Unicellular Ancestry of Animal Development. Developmental Cell 7, 313-325.

Knoll, A.H., Vidal, G., 1980. Late Proterozoic vase-shaped microfossils from the Visingsö Beds, Sweden. Geologiska Föreningens i Stockholm Förhandlingar 102 (3), 207-211.

Knoll, A.H., Javaux, E.J., Hewitt, D., Cohen, P., 2006. Eukaryotic organisms in Proterozoic oceans. Philosophical Transactions of the Royal Society of London. Series B, Biological Sciences 361, 1023-1038.

Knoll, A.H., 2014. Paleobiological Perspectives on Early Eukaryotic Evolution. Cold Spring Harbor Perspectives in Biology 6.

Kodner, R.B., Pearson, A., Summons, R.E., Knoll, A.H., 2008. Sterols in red and green algae: quantification, phylogeny, and relevance for the interpretation of geologic steranes. Geobiology 6, 411-420.

Kokke, W.C.M.C., Fenical, W.H., Pak, C.S., Djerassi, C., 1978. Minor and trace sterols in marine invertebrates IX. Verongulasterol – A marine sterol with a novel side chain alkylation pattern. Tetrahedron Letters 45, 4373-4376.

Kokke, W.C.M.C., Shoolery, J.N., Fenical, W., Djerassi, C., 1984. Biosynthetic Studies of Marine Lipids 4: Mechanism of Side Chain Alkylation in (*E*)-24-Propylidenecholesterol by a Chrysophyte Alga. Journal of Organic Chemistry 49, 3742-3752.

Lamb, D.M., Awramik, S.M., Chapman, D.J., Zhu, S., 2009. Evidence for eukaryotic diversification in the similar to 1800 million-year-old Changzhougou Formation, North China. Precambrian Research 173, 93-104.

Lawson, M.P., Thompson, J.E., Djerassi, C., 1988. Phospholipid Studies of Marine Organisms 19: Localization of Long-Chain Fatty-Acids and Unconventional Sterols in Spherulous Cells of a Marine Sponge. Lipids 23, 1037-1048.

Lee, C., Love, G.D., Fischer, W.W., Grotzinger, J.P., Halverson, G.P., 2015. Marine organic matter cycling during the Ediacaran Shuram excursion. Geology 43, 1103-1106.

Lee, A.K., Banta, A.B., Wei, J.H., Kiemle, D.J., Feng, J., Giner, J-L., Welander, P.V., 2018. C-4 sterol demethylation enzymes distinguish bacterial and eukaryotic sterol synthesis. Proceedings of the National Academy of Sciences May 2018, 201802930; DOI: 10.1073/pnas.1802930115

Li, L.N., Djerassi, C., 1981. Minor and Trace Sterols in Marine Invertebrates 23: Xestospongesterol and Isoxestospongesterol – First Examples of Quadruple Biomethylation of the Sterol Side Chain. Journal of the American Chemical Society 103, 3606-3608.

Li, L.N., Sjöstrand, U., Djerassi, C., 1981. Minor and Trace Sterols in Marine Invertebrates 27: Isolation, Structure Elucidation, and Partial Synthesis of 25-methylxestosterol, a New Sterol Arising from Quadruple Biomethylation in the Side Chain. Journal of Organic Chemistry 46, 3867-3870.

Li, X., Djerassi, C., 1983. Minor and Trace Sterols in Marine Invertebrates 40: Structure and Synthesis of Axinyssasterol, 25-methylfucosterol and 24-ethyl-24-methylcholesterol – Novel Sponge Sterols with Highly Branched Side Chains. Tetrahedron Letters 24, 665-668.

Lillis, P.G., 2016. The Chuar Petroleum System, Arizona and Utah. In Dolan, M.P., Higley, D.K., Lillis, P.G., eds. *Hydrocarbon Source Rocks in Unconventional Plays, Rocky Mountain Region*. The Rocky Mountain Association of Geologists.

Love, G.D., Snape, C.E., Carr, A.D., Houghton, R.C., 1995. Release of covalently-bound alkane biomarkers in high yields from kerogen via catalytic hydropyrolysis. Organic Geochemistry 23, 981-986.

Love, G.D., McAulay, A., Snape, C.E., 1997. Effect of Process Variables in Catalytic Hydropyrolysis on the Release of Covalently Bound Aliphatic Hydrocarbons from Sedimentary Organic Matter. Energy & Fuels 11, 522-531.

Love, G.D., Bowden, S.A., Jahnke, L.L., Snape, C.E., Campbell, C.N., Day, J.G., Summons, R.E., 2005. A catalytic hydropyrolysis method for the rapid screening of microbial cultures for lipid biomarkers. Organic Geochemistry 36, 63-82.

Love, G.D., Grosjean, E., Stalvies, C., Fike, D.A., Grotzinger, J.P., Bradley, A.S., Kelly, A.E., Bhatia, M., Meredith, W., Snape, C.E., Bowring, S.A., Condon, D.J., Summons, R.E., 2009. Fossil steroids record the appearance of Demospongiae during the Cryogenian period. Nature 457, 718-721.

Love, G.D., Summons, R.E., 2015. The molecular record of Cryogenian sponges - a response to Antcliffe (2013). Palaeontology 58, 1131-1136.

Luo, G., Hallman, C., Shucheng, X., Xiaoyan, R., Summons, R.E., 2015. Comparative microbial diversity and redox environments of black shale and stromatolite facies in the Mesoproterozoic Xiamaling Formation. Geochimica et Cosmochimica Acta 151, 150-167.

Luo, Q.Y., George, S.C., Xu, Y.H., Zhong, N.N., 2016. Organic geochemical characteristics of the Mesoproterozoic Hongshuizhuang Formation from northern China: Implications for thermal maturity and biological sources. Organic Geochemistry 99, 23-37.

Lyons, T.W., Reinhard, C.T., Planavsky, N., 2014. The rise of oxygen in Earth's early ocean and atmosphere. Nature 506, 307-315.

McCaffrey, M.A., Moldowan, J.M., Lipton, P.A., Summons, R.E., Peters, K.E., Jeganathan, A., Watt, D.S., 1994. Paleoenvironmental Implications of Novel C-30 Steranes in Precambrian to Cenozoic Age Petroleum and Bitumen. Geochimica Et Cosmochimica Acta 58, 529-532.

McKirdy, D.M., Webster, L.J., Arouri, K.R., Grey, K., Gostin, V.A., 2006. Contrasting sterane signatures in Neoproterozoic marine rocks of Australia before and after the Acraman asteroid impact. Organic Geochemistry 37, 189-207.

Meredith, W., Sun, C.G., Snape, C.E., Sephton, M.A., Love, G.D., 2006. The use of model compounds to investigate the release of covalently bound biomarkers via hydropyrolysis. Organic Geochemistry 37, 1705-1714.

Meredith, W., Snape, C.E., Love, G.D., 2014. Development and Use of Catalytic Hydropyrolysis (HyPy) as an Analytical Tool for Organic Geochemical Applications. In Grice, K., ed. Principles and Practice of Analytical Techniques in Geosciences. The Royal Society of Chemistry.

Moczydlowska, M., Pease, V., Willman, S., Wickstrom, L., Agic, H., 2018. A Tonian age for the Visingsö Group in Sweden constrained by detrital zircon dating and biochronology: implications for evolutionary events. Geological Magazine 155, 1175-1189.

Moldowan, J.M., 1984. C-30-Steranes, Novel Markers for Marine Petroleums and Sedimentary-Rocks. Geochimica Et Cosmochimica Acta 48, 2767-2768.

Moldowan, J.M., Lee, C.Y., Watt, D.S., Jeganathan, A., Slougui, N.E., Gallegos, E.J., 1991. Analysis and occurrence of C26-steranes in petroleum and source rocks. Geochimica et Cosmochimica Acta 55, 1065-1081.

Moldowan, J.M., 1984. C-30-Steranes, Novel Markers for Marine Petroleums and Sedimentary-Rocks. Geochimica Et Cosmochimica Acta 48, 2767-2768.

Morais, L., Fairchild, T.R., Lahr, D.J.G., Rudnitzki, I.D., Schopf, J.W., Garcia, A.K., Kudryavtsev, A.B., Romero, G.R., 2017. Carbonaceous and siliceous Neoproterozoic vase-shaped microfossils (Urucum Formation, Brazil) and the question of early protistan biomineralization. Journal of Paleontology 91, 393-406.

Morrow, C., Cárdenas, P., 2015. Proposal for a revised classification of the Demospongiae (Porifera). Frontiers in Zoology 12:7.

Murray, I.P., Love, G.D., Snape, C.E., Bailey, N.J.L., 1998. Comparison of covalently-bound aliphatic biomarkers released via hydropyrolysis with their solvent-extractable counterparts for a suite of Kimmeridge clays. Organic Geochemistry 29, 1487-1505.

Mus, M.M., Moczydlowska, M., 2000. Internal morphology and taphonomic history of the Neoproterozoic vase-shaped microfossils from the Visingsö Group, Sweden. Norsk Geologisk Tidsskrift 80, 213-228.

Muscente, A.D., Michel, F.M., Dale, J.G., Xiao, S.H., 2015. Assessing the veracity of Precambrian 'sponge' fossils using in situ nanoscale analytical techniques. Precambrian Research 263, 142-156.

Nes, W.R., 1974. Role of sterols in membranes. Lipids 9, 596-612.

Nettersheim, B.J., Brocks, J.J., Schwelm, A., Hope, J.M., Not, F., Lomas, M., Schmidt, C., Schiebel, R., Nowack, E.C.M., De Deckker, P., Pawlowski, J., Bowser, S.S., Bobrovskiy, I., Zonneveld, K., Kucera, M., Stuhr, M., Hallmann, C., 2019. Putative sponge biomarkers in unicellular Rhizaria question an early rise of animals. Nature Ecology and Evolution 3, 577-581.

Nguyen, K., Love, G.D., Zumberge, J.A., Kelly, A.E., Owens, J.D., Rohrssen, M.K., Bates, S.M., Cai, C., Lyons, T.W., 2019. Absence of biomarker evidence for early eukaryotic life from the Mesoproterozoic Roper Group: Searching across a marine redox gradient in mid-Proterozoic habitability. Geobiology doi.org/10.1111/gbi.12329

O'Malley, M.A., Leger, M.M., Wideman, J.G., Ruiz-Trillo, I., 2019. Concepts of the last eukaryotic common ancestor. Nature Ecology and Evolution 3, 338-344.

Parfrey, L.W., Lahr, D.J.G., Knoll, A.H., Katz, L.A., 2011. Estimating the timing of early eukaryotic diversification with multigene molecular clocks. PNAS 108, 13624-13629.

Patterson, G.W., 1971. Distribution of Sterols in Algae. Lipids 6, 120-127.

Pearson, A., Budin, M., Brocks, J.J., 2003. Phylogenetic and biochemical evidence for sterol synthesis in the bacterium *Gemmata obscuriglobus*. Proceedings of the National Academy of Sciences 100, 15352-15357.

Pehr, K., Love, G.D., Kuznetsov, A., Podkovyrov, V., Junium, C.K., Shumlyanskyy, L., Sokur, T., Bekker, A., 2018. Ediacara biota flourished in oligotrophic and bacterially dominated marine environments across Baltica. Nature Communications 9.

Peters, K.E., Moldowan, J.M., 1991. Effects of source, thermal maturity, and biodegradation on the distribution and isomerization of homohopanes in petroleum. Organic Geochemistry 17, 47-61.

Peters, K.E., Clark, M.E., Dasgupta, U., Mccaffrey, M.A., Lee, C.Y., 1995. Recognition of an Infracambrian Source-Rock Based on Biomarkers in the Bahewala-1 Oil, India. AAPG Bulletin-American Association of Petroleum Geologists 79, 1481-1494.

Peters, K.E., Walters, C.C., Moldowan, J.M., eds. 2005. The Biomarker Guide, second edition. Cambridge University Press.

Planavsky, N.J., Reinhard, C.T., Wang, X., Thomson, D., McGoldrick, P., Rainbird, R.H., Johnson, T., Fischer, W.W., Lyons, T.W., 2014. Low Mid-Proterozoic atmospheric oxygen levels and the delayed rise of animals. Science 346, 635-638.

Porter, J.W., Spurgeon, S.L., eds. 1981. *Biosynthesis of Isoprenoid Compounds*. John Wiley, New York.

Porter, S.M., Knoll, A.H., 2000. Testate amoebae in the Neoproterozoic Era: evidence from vase-shaped microfossils in the Chuar Group, Grand Canyon. Paleobiology 26, 360-385.

Porter, S.M., Meisterfeld, R., Knoll, A.H., 2003. Vase-shaped microfossils from the Neoproterozoic Chuar Group, Grand Canyon: a classification guided by modern testate amoebae. Journal of Paleontology 77, 409-429.

Pulsipher, M.A., Dehler, C.M., 2019. U-Pb detrital zircon geochronology, petrography, and synthesis of the middle Neoproterozoic Visingsö Group, Southern Sweden. Precambrian Research 320, 323-333.

Rambabu, M., Sarma, N.S., 1987. Chemistry of Herbacin and New Unusual Sterols from Marine Sponge Dysidea-Herbacea. Indian Journal of Chemistry B 26, 1156-1160.

Riedman, L.A., Porter, S.M., Calver, C.R., 2018. Vase-shaped microfossil biostratigraphy with new data from Tasmania, Svalbard, Greenland, Sweden and the Yukon. Precambrian Research 319, 19-36.

Rohrssen, M., Love, G.D., Fischer, W., Finnegan, S., Fike, D.A., 2013. Lipid biomarkers record fundamental changes in the microbial community structure of tropical seas during the Late Ordovician Hirnantian glaciation. Geology 41, 127-130.

Rohrssen, M., Gill, B.C., Love, G.D., 2015. Scarcity of the C-30 sterane biomarker, 24-n-propylcholestane, in Lower Paleozoic marine paleoenvironments. Organic Geochemistry 80, 1-7.

Rooney, A.D., Macdonald, F.A., Strauss, J.V., Dudas, F.O., Hallman, C., Selby, D., 2014. Re-Os geochronology and coupled Os-Sr isotope constraints on the Sturtian snowball Earth. Proceedings of the National Academy of Sciences 111, 51-56.

Rooney, A.D., Strauss, J.V., Brandon, A.D., Macdonald, F.A., 2015. A Cryogenian chronology: Two long-lasting synchronous Neoproterozoic glaciations. Geology 43, 459-462.

Rooney, A.D., Austermann, J., Smith, E.F., Li, Y., Selby, D., Dehler, C.M., Schmitz, M.D., Karlstrom, K.E., Macdonald, F.A., 2018. Coupled Re-Os and U-Pb geochronology of the Tonian Chuar Group, Grand Canyon. Geological Society of America Bulletin 130, 1085-1098.

Rubinstein, I., Goad, L.J., 1974. Sterols of the Siphonous marine alga *Codium fragile*. Phytochemistry 13, 481-484.

Ruppert, E.E., Fox, R.S., Barnes, R.D., 2004. Invertebrate Zoology: A Functional Evolutionary Approach. Brooks/Cole Thompson Learning, Belmont, California.

Samuelsson, J., Strauss, H., 1999. Stable carbon and oxygen isotope geochemistry of the upper Visingsö Group (early Neoproterozoic), southern Sweden. Geological Magazine 136, 63-73.

Sarma, N.S., Krishna, M.S.R., Rao, S.R., 2005. Sterol Ring System Oxidation Patterns in Marine Sponges. Marine Drugs 3, 84-111.

Schuster, A., Vargas, S., Knapp, I.S., Pomponi, S.A., Toonen, R.J., Erpenbeck, D., Worheide, G., 2018. Divergence times in demosponges (Porifera): first insights from new mitogenomes and the inclusion of fossils in a birth-death clock model. Bmc Evolutionary Biology 18.

Schwark, L., Empt, P., 2006. Sterane biomarkers as indicators of Palaeozoic algal evolution and extinction events. Palaeogeography Palaeoclimatology Palaeoecology 240, 225-236.

Seifert, W.K., Moldowan, J.M., 1978. Applications of Steranes, Terpanes and Mono-Aromatics to Maturation, Migration and Source of Crude Oils. Geochimica Et Cosmochimica Acta 42, 77-95.

Sephton, M.A., Meredith, W., Sun, C.G., Snape, C.E., 2005. Hydropyrolysis of steroids: a preparative step for compound-specific carbon isotope ratio analysis. Rapid Communications in Mass Spectrometry 19, 3339-3342.

Siegl, A., Kamke, J., Hochmuth, T., Piel, J., Richter, M., Liang, C.G., Dandekar, T., Hentschel, U., 2011. Single-cell genomics reveals the lifestyle of Poribacteria, a candidate phylum symbiotically associated with marine sponges. Isme Journal 5, 61-70.

Silva, C.J., Wünsche, L., Djerassi, C., 1991. Biosynthetic Studies of Marine Lipids 35: The Demonstration of *de novo* Sterol Biosynthesis in Sponges using Radiolabeled Isoprenoid Precursors. Comparative Biochemistry and Physiology – Part B: Biochemistry and Molecular Biology 99, 763-773.

Silva, C.J., Djerassi, C., 1992. Biosynthetic Studies of Marine Lipids 36: The Origin of Common Sterol Side Chains in Eleven Sponges using [3-^{3}H]-squalene. Comparative Biochemistry and Physiology – Part B: Biochemistry and Molecular Biology 101, 255-268.

Sim, C.-J., Kim, Y.-A., 1995. A systematic study on the marine sponges in Korea: 12. Tetractinomorpha (Porifera: Demospongiae). Korean Journal of Systematic Zoology 11, 147-158.

Simion, P., Philippe, H., Baurain, D., Jager, M., Richter, D.J., Di Franco, A., Roure, B., Satoh, N., Queinnec, E., Ereskovsky, A., Lapebie, P., Corre, E., Delsuc, F., King, N., Worheide, G., Manuel, M., 2017. A Large and Consistent Phylogenomic Dataset Supports Sponges as the Sister Group to All Other Animals. Current Biology 27, 958-967.

Sinninghe Damsté, J.S., Kenig, F., Koopmans, M.P., Köster, J., Schouten, S., Hayes, J.M., de Leeuw, J.W., 1995. Evidence for gammacerane as an indicator of water column stratification. Geochimica et Cosmochimica Acta 59, 1895-1900.

Stoilov, I.L., Thompson, J.E., Cho, J.H., Djerassi, C., 1986. Biosynthetic-Studies of Marine Lipids 9: Stereochemical Aspects and Hydrogen Migrations in the Biosynthesis of the Triply Alkylated Side-Chain of the Sponge Sterol Strongylosterol. Journal of the American Chemical Society 108, 8235-8241.

Stolper, D.A., Love, G.D., Bates, S., Lyons, T.W., Young, E., Sessions, A.L., Grotzinger, J.P., 2017. Paleoecology and paleoceanography of the Athel silicilyte, Ediacaran-Cambrian boundary, Sultanate of Oman. Geobiology 15, 401-426.

Strauss, J.V., Rooney, A.D., Macdonald, F.A., Brandon, A.D., Knoll, A.H., 2014. 740 Ma vase-shaped microfossils from Yukon, Canada: Implications for Neoproterozoic chronology and biostratigraphy. Geology 42, 659-662.

Summons, R.E., Brassell, S.C., Eglinton, G., Evans, E., Horodyski, R.J., Robinson, N., Ward, D.M., 1988. Distinctive Hydrocarbon Biomarkers from Fossiliferous Sediment of the Late Proterozoic Walcott Member, Chuar Group, Grand-Canyon, Arizona. Geochimica et Cosmochimica Acta 52, 2625-2637.

Summons, R.E., Walter, M.R., 1990. Molecular Fossils and Microfossils of Prokaryotes and Protists from Proterozoic Sediments. American Journal of Science 290A, 212-244.

Summons, R.E., Bradley, A.S., Jahnke, L.L., Waldbauer, J.R., 2006. Steroids, triterpenoids and molecular oxygen. Philosophical Transactions of the Royal Society B 361, 951-968.

Suslova, E.A., Parfenova, T.M., Saraev, S.V., Nagovitsyn, K.E., 2017. Organic geochemistry of rocks of the Mesoproterozoic Malgin Formation and their depositional environments (southeastern Siberian Platform). Russian Geology and Geophysics 58, 516-528.

Takashita, K., Chikarisa, Y., Tanifuji, G., Ohkouchi, N., Hashimoto, T., Fujikara, K., Roger, A.J., 2017 Microbial eukaryotes that lack sterols. Journal of Eukaryotic Microbiology 64, 897-900.

Tam, H.T.B., Kokke, W.C.M., Proudfoot, J.R., Djerassi, C., 1985. Minor and Trace Sterols in Marine Invertebrates 53: Further Novel Marine Sterols Resulting from Triple and Quadruple Biomethylation of the Cholesterol Side-Chain. Steroids 45, 263-276.

Theobald, N., Djerassi, C., 1978. Determination of Absolute-Configuration of Stelliferasterol and Strongylosterol - 2 Marine Sterols with Extended Side-Chains. Tetrahedron Letters, 4369-4372.

Theobald, N., Wells, R.J., Djerassi, C., 1978. Minor and Trace Sterols in Marine-Invertebrates .8. Isolation, Structure Elucidation, and Partial Synthesis of 2 Novel Sterols - Stelliferasterol and Isostelliferasterol. Journal of the American Chemical Society 100, 7677-7684.

Thomas, P.A., 1991. Sponges of Papua and New Guinea-Part order Haplosclerida Topsent. Journal of the Marine Biological Association of India 33, 308-316.

Vacelet, J., Borchiellini, C., Perez, T., Bultel-Ponce, V., Brouard, J-P., Guyot, M., 2000. Morphological, chemical and biochemical characterization of a new species of sponge without skeleton (Porifera, Demospongiae) from the Mediterranean Sea. Zoosytema 22, 313-326.

van Maldegem, L.M., Sansjofre, P., Weijers, J.W.H., Wolkenstein, K., Strother, P.K., Wörmer, L., Hefter, J., Nettersheim, B.J., Hoshino, Y., Schouten, S., Sinninghe Damsté, J.S., Nath, N., Griesinger, C., Kuznetsov, N.B., Elie, M., Elvert, M., Tegelaar, E., Gleixner, G., Hallmann, C., 2019. Bisnorgammacerane traces predatory pressure and the persistent rise of algal ecosystems after Snowball Earth. Nature Communications 10, 476.

Vidal, G., 1976. Late Precambrian microfossils from the Visingsö Beds in southern Sweden. Fossils and Strata 9, 1-57.

Vogel, M.B., Moldowan, J.M., Zinniker, D., 2005. Biomarkers from Units in the Uinta Mountain and Chuar Groups. Utah Geological Association Publication 33, 75-96.

Volkman, J.K., 1986. A Review of Sterol Markers for Marine and Terrigenous Organic-Matter. Organic Geochemistry 9, 83-99.

Volkman, J.K., Barrett, S.M., Dunstan, G.A., Jeffrey, S.W., 1994. Sterol Biomarkers for Microalgae from the Green Algal Class Prasinophyceae. Organic Geochemistry 21, 1211-1218.

Volkman, J.K., Barrett, S.M., Blackburn, S.I., Mansour, M.P., Sikes, E.L., Gelin, F., 1998. Microalgal biomarkers: A review of recent research developments. Organic Geochemistry 29, 1163-1179.

Volkman, J.K., 2003. Sterols in microorganisms. Applied Microbiology and Biotechnology 60, 495-506.

Wang, X., Zhao, W., Zhang, S., Wang, H., Su, J., Canfield, D.E., Hammarlund, E.U., 2018. The aerobic diagenesis of Mesoproterozoic organic matter. Scientific Reports 8:13324.

Wei, J.H., Yin, X., Welander, P.V., 2016. Sterol synthesis in diverse bacteria. Frontiers in Microbiology 7, 990.

Whelan, N.V., Kocot, K.M., Moroz, T.P., Mukherjee, K., Williams, P., Paulay, G., Moroz, L.L., Halanych, K.M., 2017. Ctenophore relationships and their placement as the sister group to all other animals. Nature Ecology & Evolution 1, 1737-1746.

Wilkomirski, B., Goad, L.J., 1983. The conversion of (24*S*)-24-ethylcholesta-5,22,25-trien,3β-ol into poriferasterol, both *in vivo* and with a cell-free homogenate of the alga *Trebouxia* sp. Phytochemistry 22, 929-932.

Xu, F., Rychnovsky, S.D., Belani, J.D., Hobbs, H.H., Cohen, J.C., Rawson, R.B., 2005. Dual roles for cholesterol in mammalian cells. Proceedings of the National Academy of Sciences 102, 14551-14556.

Yang, S., Kendall, B., Lu, X., Zhang, F., Zheng, W., 2017. Uranium isotope compositions of mid-Proterozoic black shales: Evidence for an episode of increased ocean oxygenation at 1.36 Ga and evaluation of the effect of post-depositional hydrothermal fluid flow. Precambrian Research 298, 187-201.

Zimmerman, M.P., Djerassi, C., 1991. Biosynthetic Studies in Marine Lipids 34: Stereochemical Features of the Enzymatic C-Methylation on the Path to Isofucosterol and Fucosterol. Journal of the American Chemical Society 113, 3530-3533.

Zumberge, J.E., 1987. Prediction of source rock characteristics based on terpane biomarkers in crude oils: A multivariate statistical approach. Geochimica Et Cosmochimica Acta 51, 1625-1637.

Zumberge, J.A., Love, G.D., Cardenas, P., Sperling, E.A., Gunasekera, S., Rohrssen, M., Grosjean, E., Grotzinger, J.P., Summons, R.E., 2018. Demosponge steroid biomarker 26-methylstigmastane provides evidence for Neoproterozoic animals. Nature Ecology & Evolution 2, 1709-1714.

Appendix A: Mass Spectral Library for Sterols Identified in this Study

# Carbons	Name	Alt. Name
27	22-dehydrocholesterol	Cholesta-5,22(E/Z)-dien-3β-ol

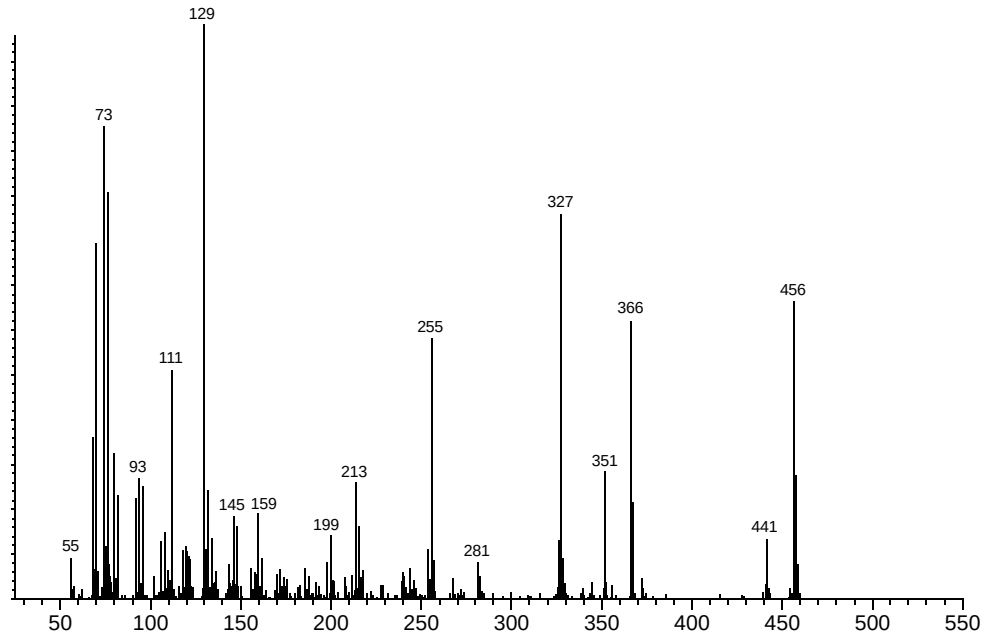

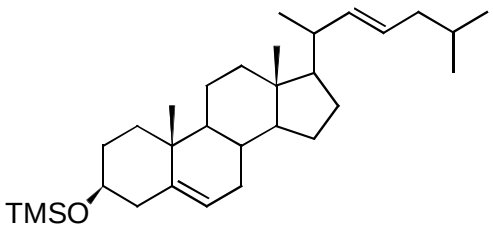

$C_{27}\Delta^{5,22}$

Mass Spectrum | *Structure*

Example: *Tethya aurantium* Roscoff #2

# Carbons	Name	Alt. Name
27	Cholestanol	5β-cholestan-3β-ol ; coprostanol

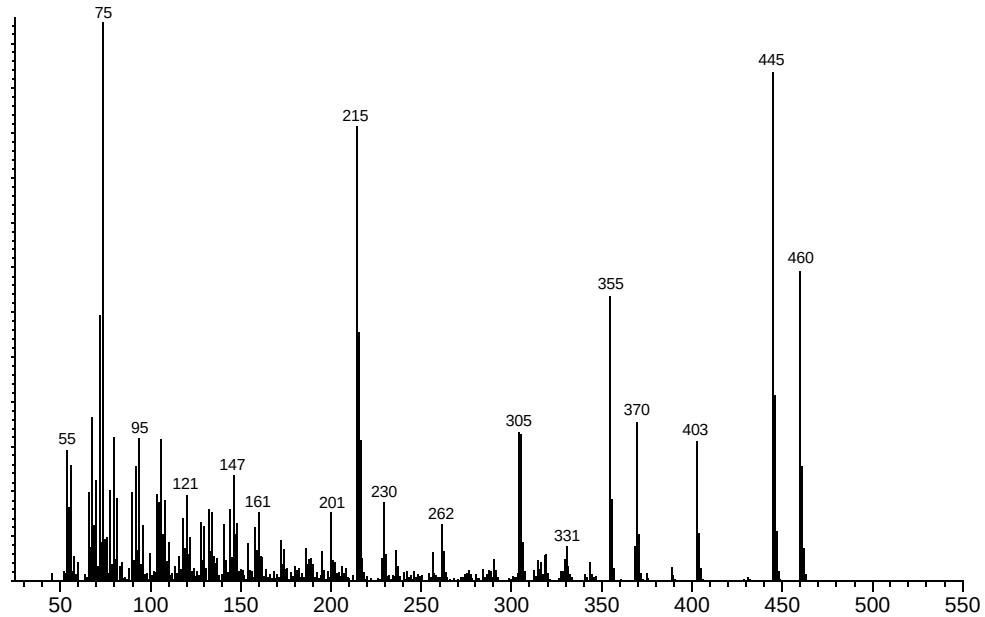

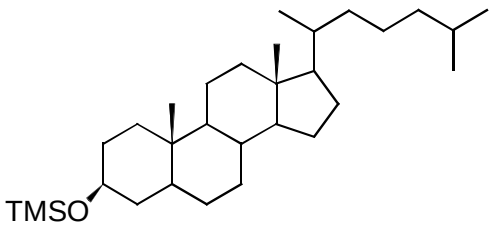

$C_{27}\Delta^0$

Mass Spectrum	Structure

Example: *Hymeniacidon perlevis* Roscoff #11

# Carbons	Name	Alt. Name
27	Cholesterol	Cholest-5-en-3β-ol

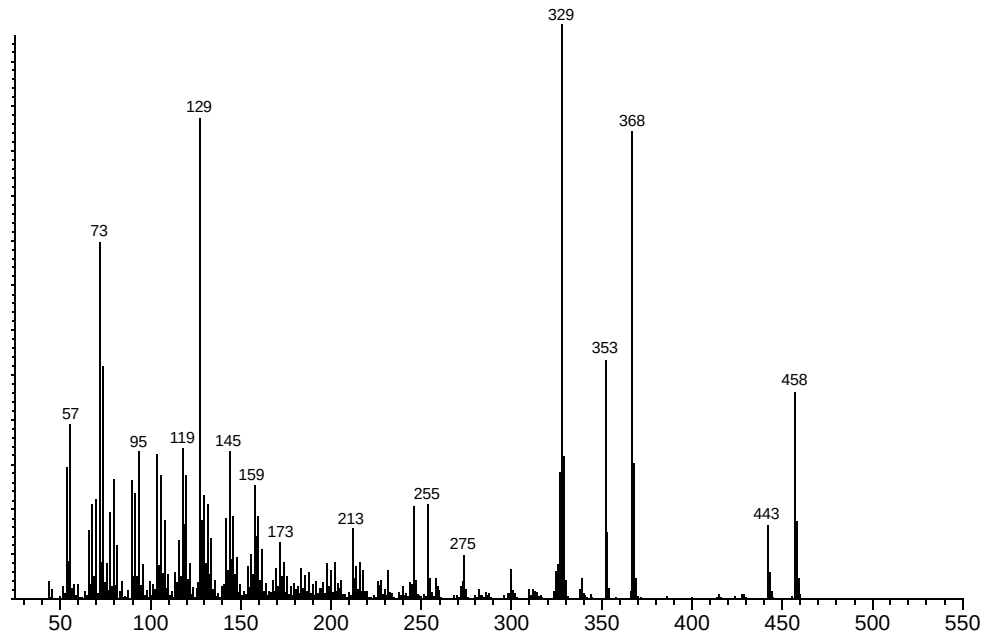

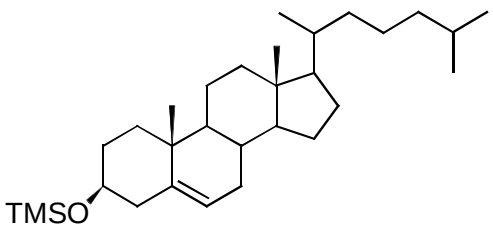

$C_{27}\Delta^5$

Mass Spectrum	Structure

Example: *Cliona celata* Roscoff #12

# Carbons	Name	Alt. Name
27	Desmosterol	cholesta-5,24-dien-3β-ol

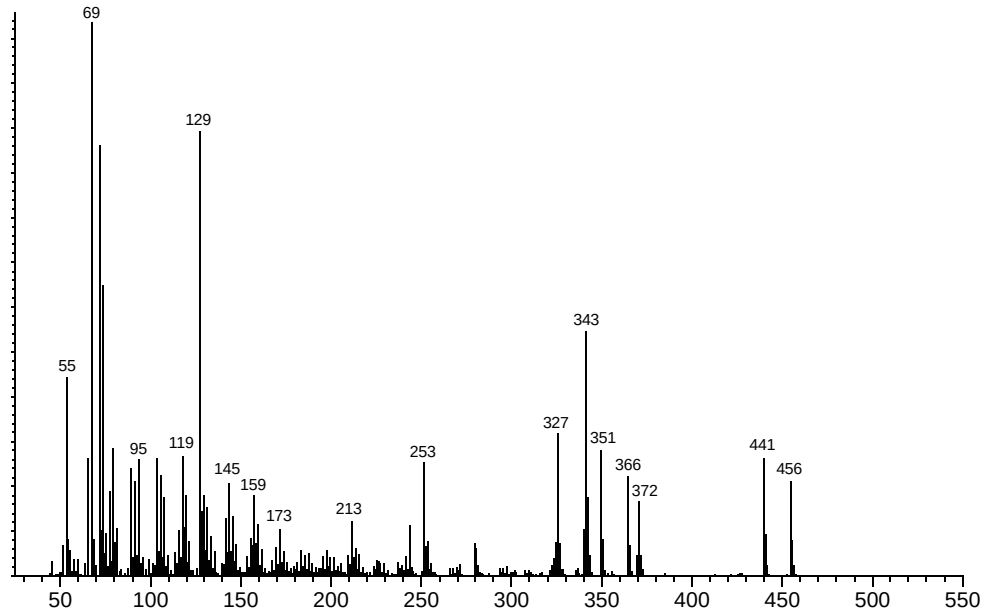

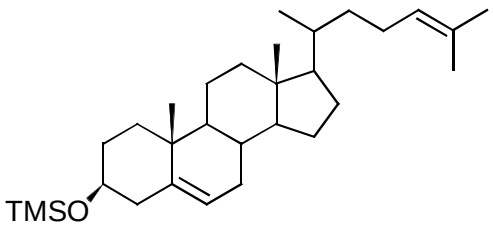

$C_{27}\Delta^{5,24}$

Mass Spectrum	Structure

Example: Desmosterol Sterol Standard [≥84% Sigma-Aldrich]

# Carbons	Name	Alt. Name
28	24-methylenecholesterol	24-methylcholesta-5,24(28)-dien-3β-ol

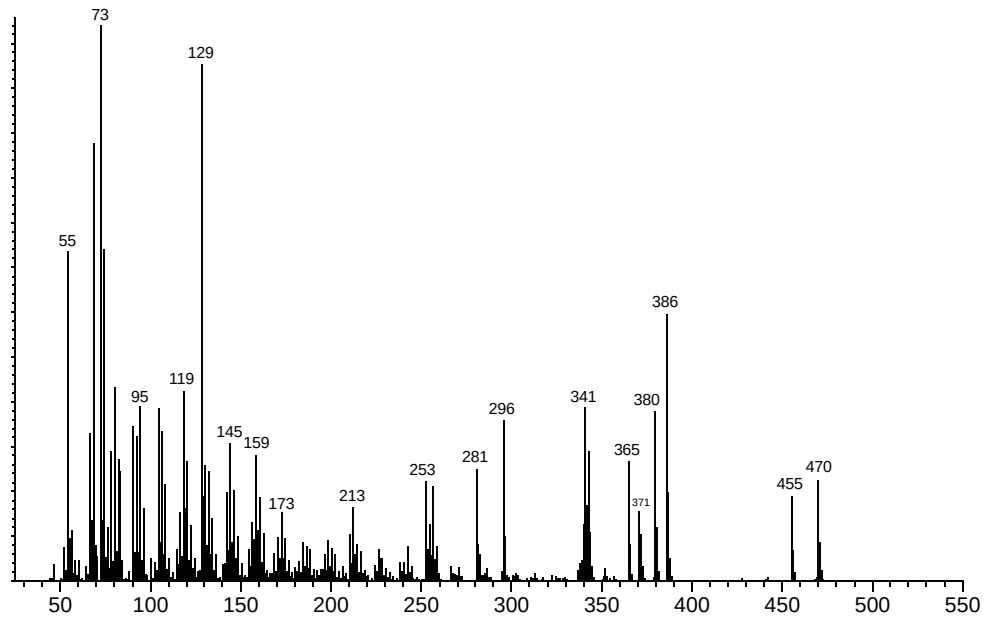

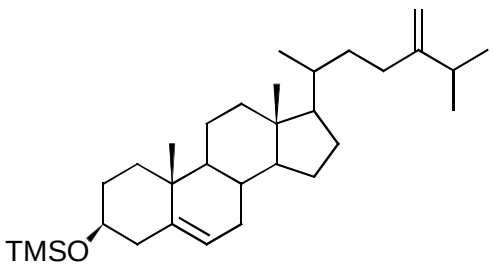

$C_{28}\Delta^{5,24(28)}$

Mass Spectrum	Structure

Example: *Caminella intuta* PC1162

# Carbons	Name	Alt. Name
28	Brassicasterol	24-methylcholesta-5,22E-dien-3β-ol

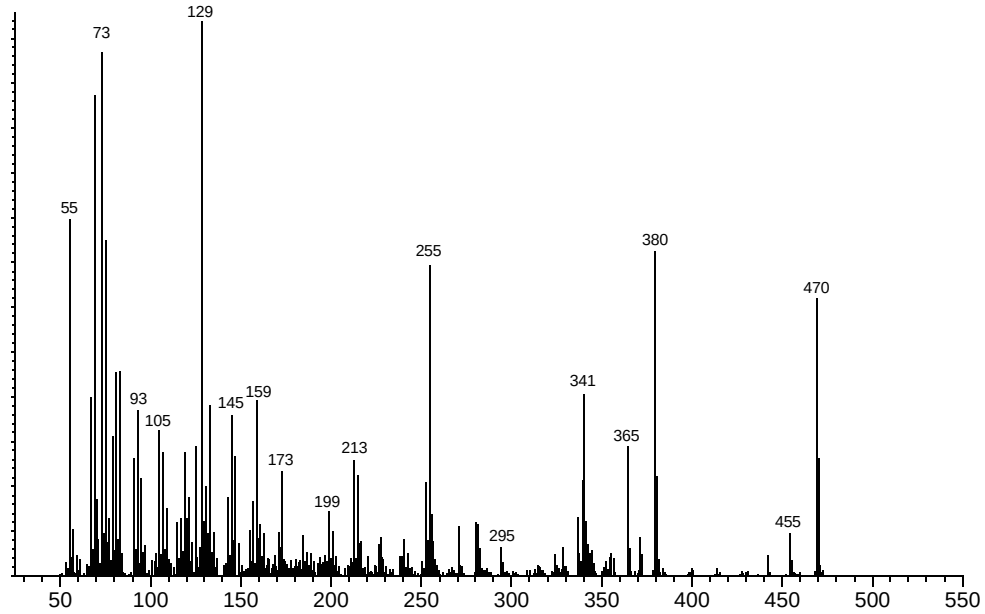

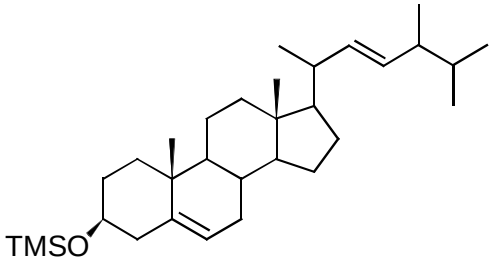

$C_{28}\Delta^{5,22}$

Mass Spectrum	Structure

Example: *Weberella bursa* PA2013-008

# Carbons	Name	Alt. Name
28	Campestanol	(24R)-methylcholestan-3β-ol

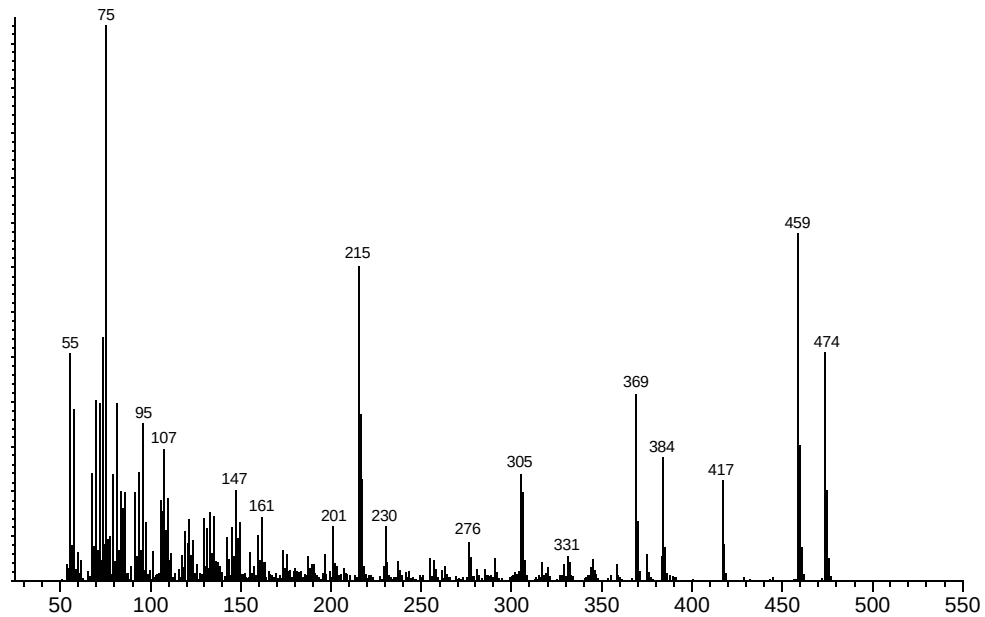

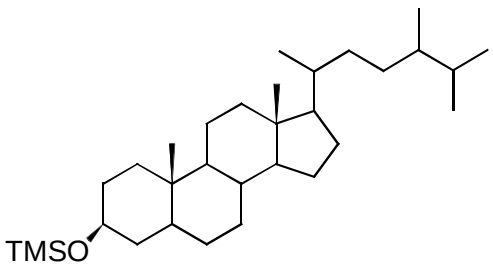

$C_{28}\Delta^0$

Mass Spectrum	Structure

Example: *Pheronema carpentei* BT12-809

# Carbons	Name	Alt. Name
28	Campesterol	(24R)-methylcholest-5-en-3β-ol

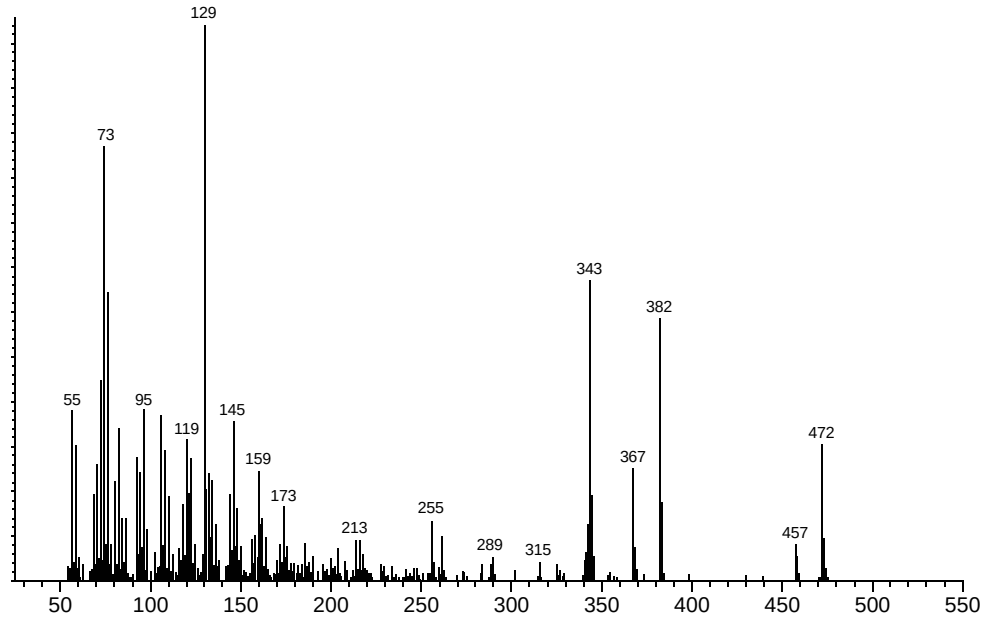

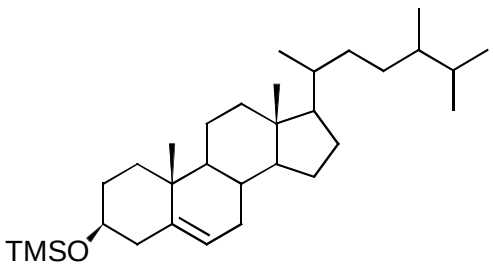

$C_{28}\Delta^5$

Mass Spectrum	Structure

Example: *Cinachyrella kuekenthali* PC941

# Carbons	Name	Alt. Name
28	Codisterol	(24S)-methylcholesta-5,25(26)-dien-3β-ol

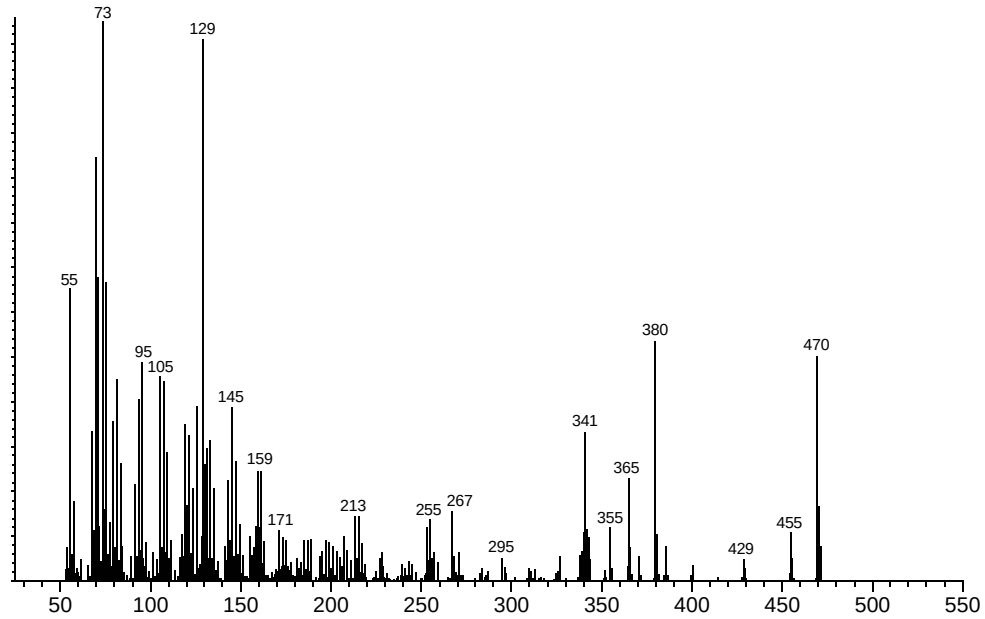

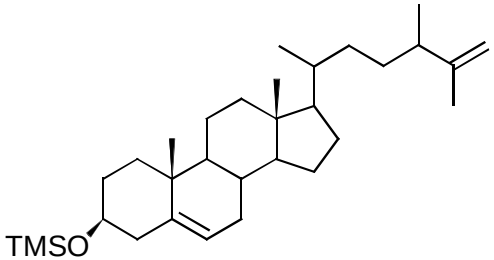

$C_{28}\Delta^{5,25(26)}$

Mass Spectrum	Structure

Example: *Rhabdastrella globostellata* PC922

# Carbons	Name	Alt. Name
29	24(28)-dehydroaplysterol	(25S)-24,26-dimethylcholesta-5,24(28)-dien-3 β-ol

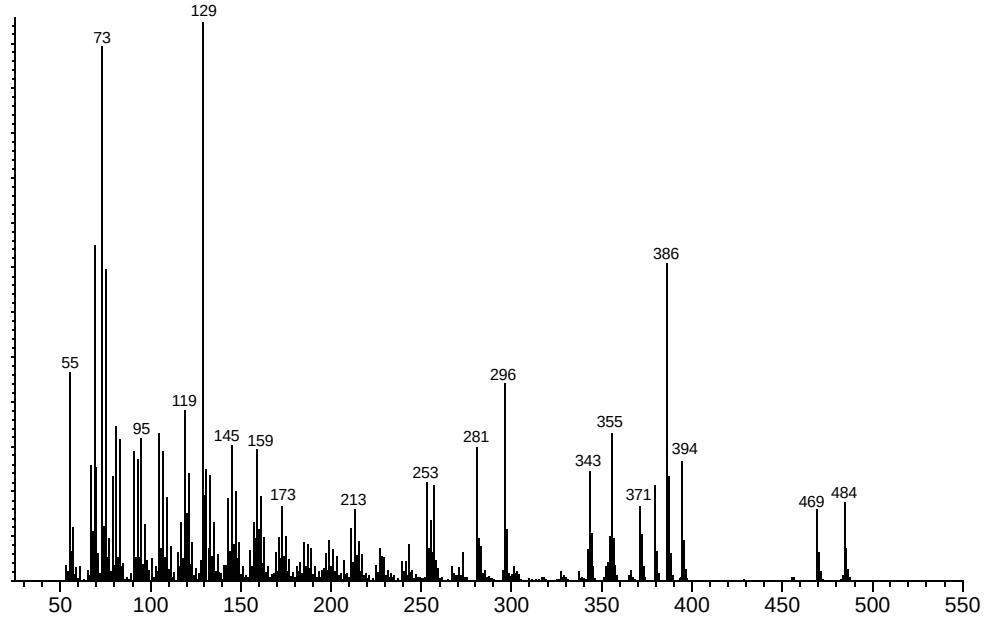

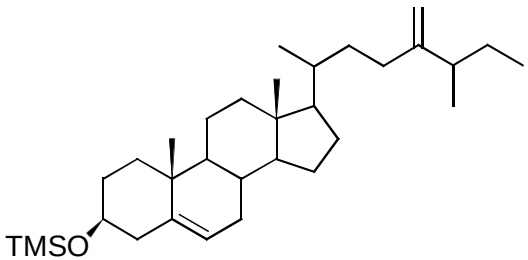

$C_{29}\Delta^{5,24(28)}$

Mass Spectrum	Structure

Example: *Geodia parva* PC994

# Carbons	Name	Alt. Name
29	25-dehydroaplysterol	(24R)-24,26-dimethylcholesta-5,25(27)-dien-3 β-ol

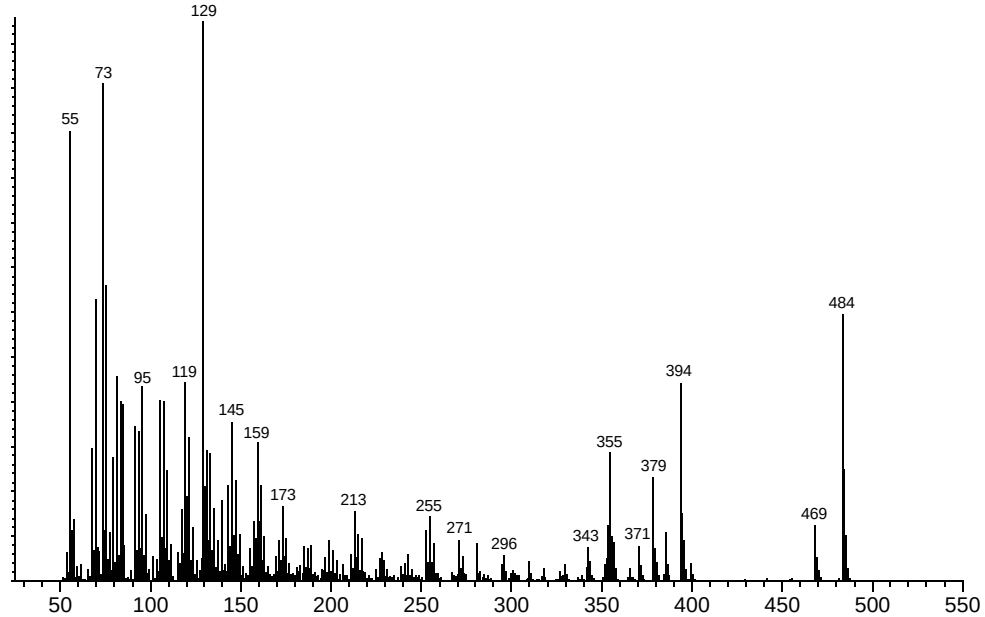

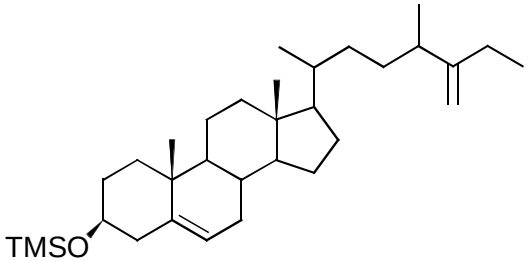

$C_{29}\Delta^{5,25(27)}$

Mass Spectrum	Structure

Example: *Aplysina aerophoba* TLE430

# Carbons	Name	Alt. Name
29	Aplysterol	(24R,25S)-24,26-dimethylcholest-5-en-3β-ol

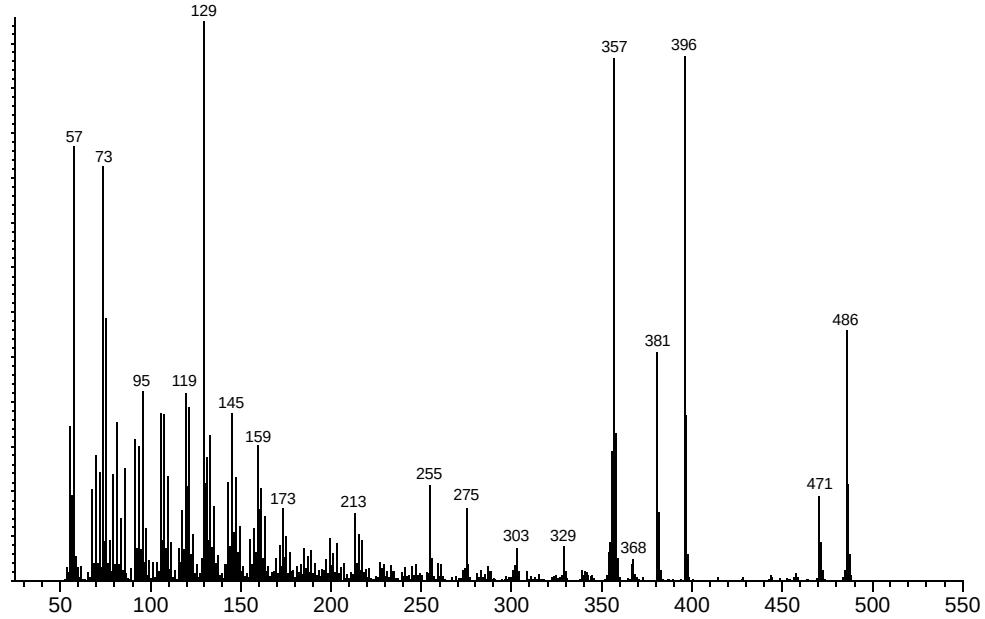

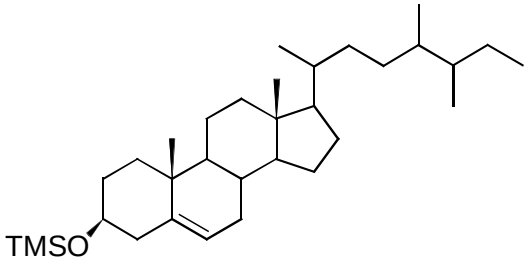

$C_{29}\Delta^5$

Mass Spectrum	Structure

Example: *Aplysina aerophoba* TLE430

# Carbons	Name	Alt. Name
29	Fucosterol	(24E)-ethylcholesta-5,24(28)-dien-3β-ol

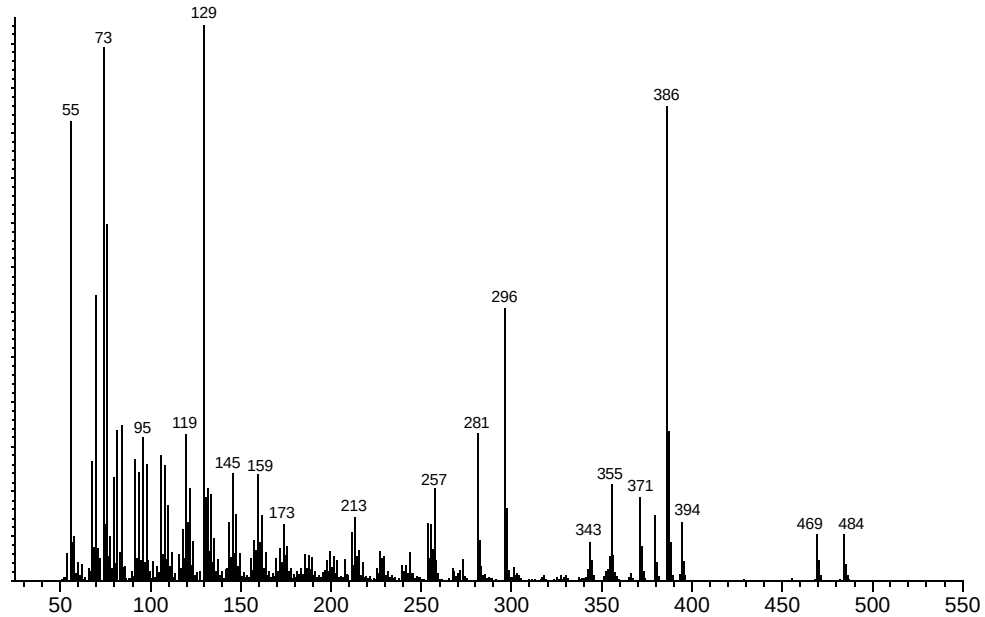

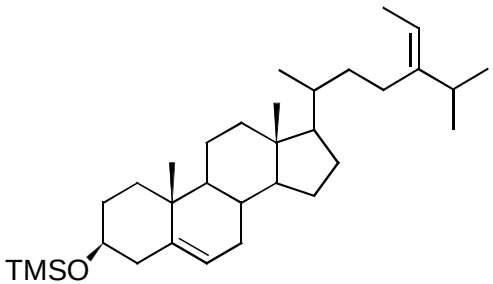

$C_{29}\Delta^{5,24(28)}$

Mass Spectrum	Structure

Example: Fucosterol Sterol Standard [≥93% Sigma-Aldrich]

# Carbons	Name	Alt. Name
29	Isofucosterol	(24Z)-ethylcholesta-5,24(28)-dien-3 β-ol

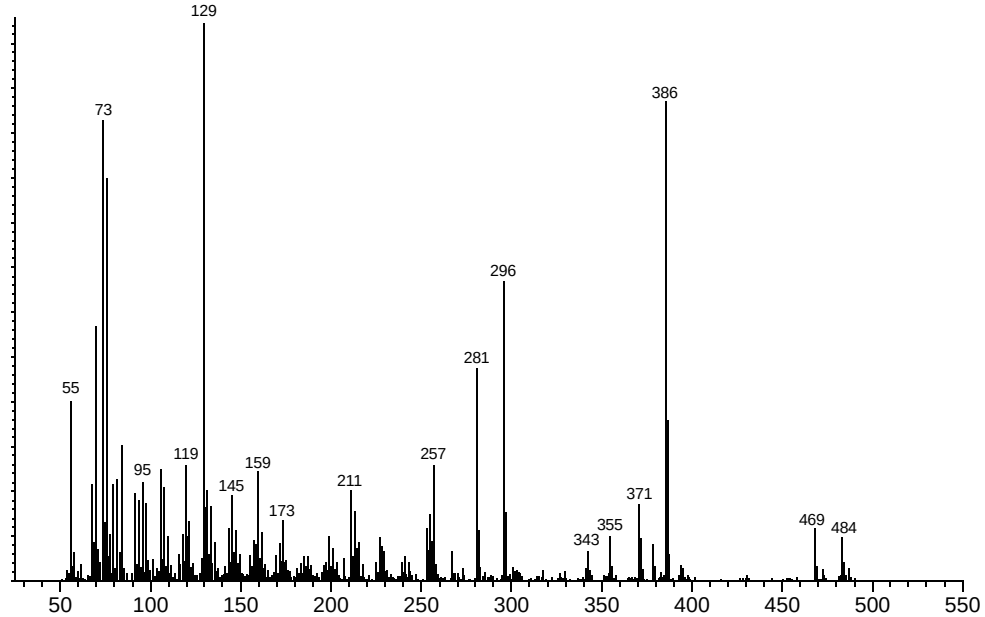

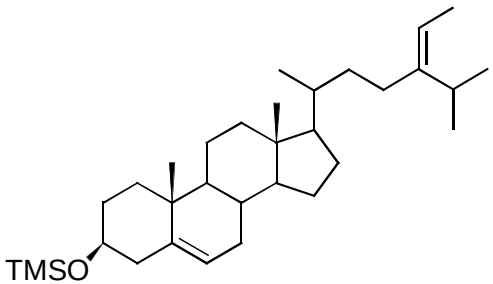

$C_{29}\Delta^{5,24(28)}$

Mass Spectrum	Structure

Example: *Polymastia boletiformis* Roscoff #9

# Carbons	Name	Alt. Name
29	Petrosterol	(25R)-24,26-dimethyl-26,27-cyclo-cholest-5-en-3 β-ol

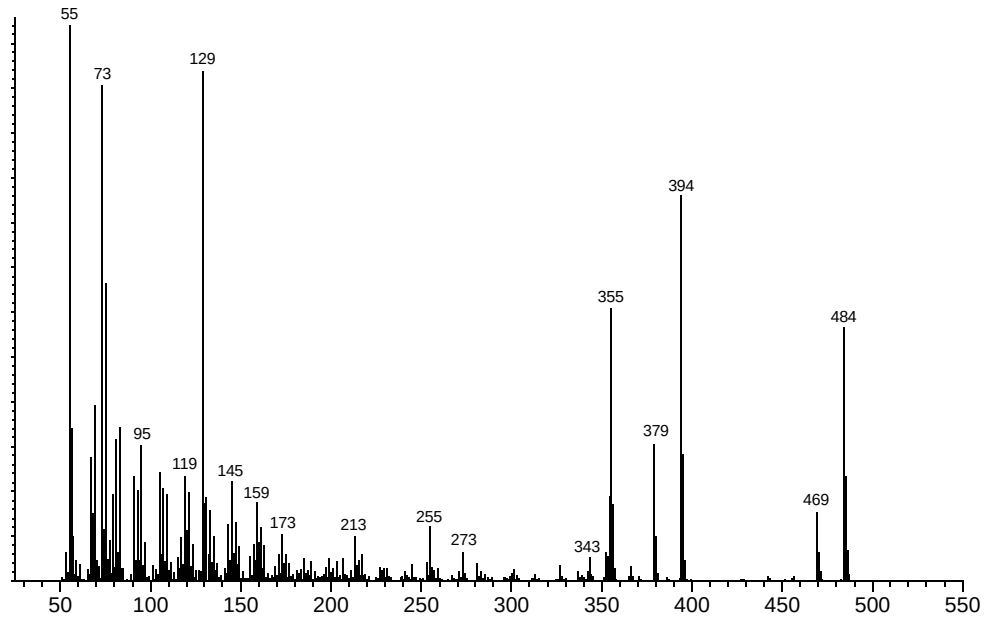

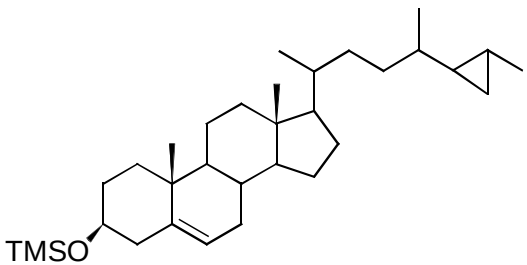

$C_{29}\Delta^5$

Mass Spectrum	Structure

Example: *Petrosia crassa* #11

# Carbons	Name	Alt. Name
29	Sitostanol	(24R)-ethylcholestan-3β-ol ; Stigmastanol ; Fucostanol

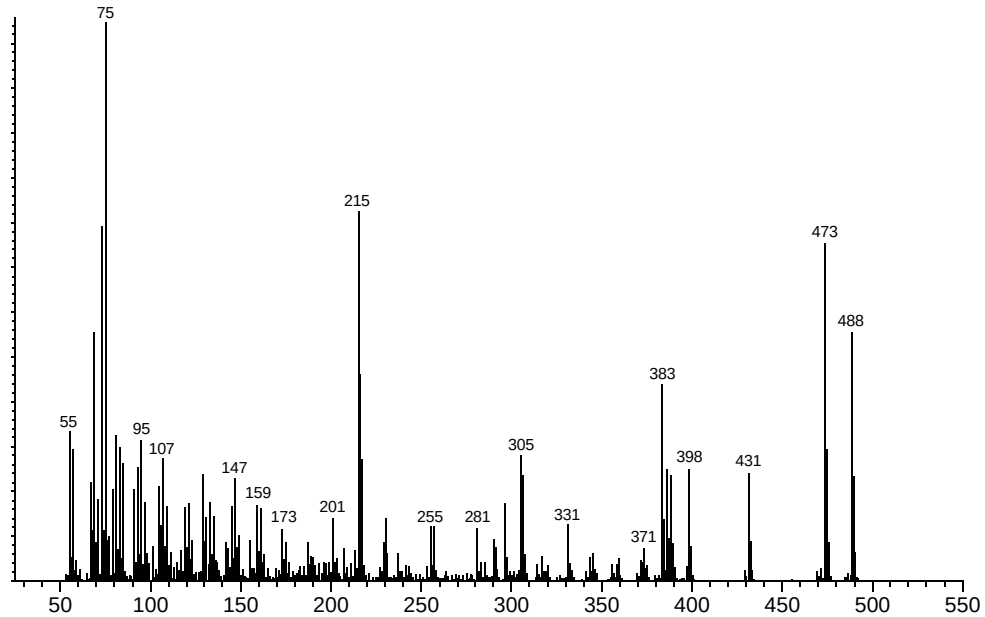

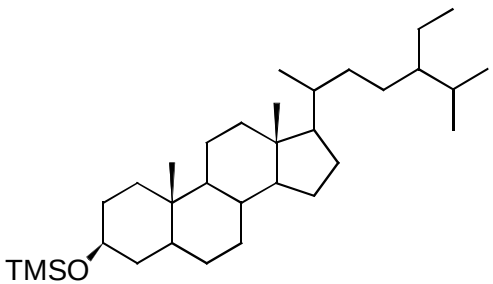

$C_{29}\Delta^0$

Mass Spectrum	Structure

Example: *Ciocalypta penicillus* Roscoff #1

# Carbons	Name	Alt. Name
29	Sitosterol	(24R)-ethylcholest-5-en-3β-ol ; 5β(H)-sitosterol

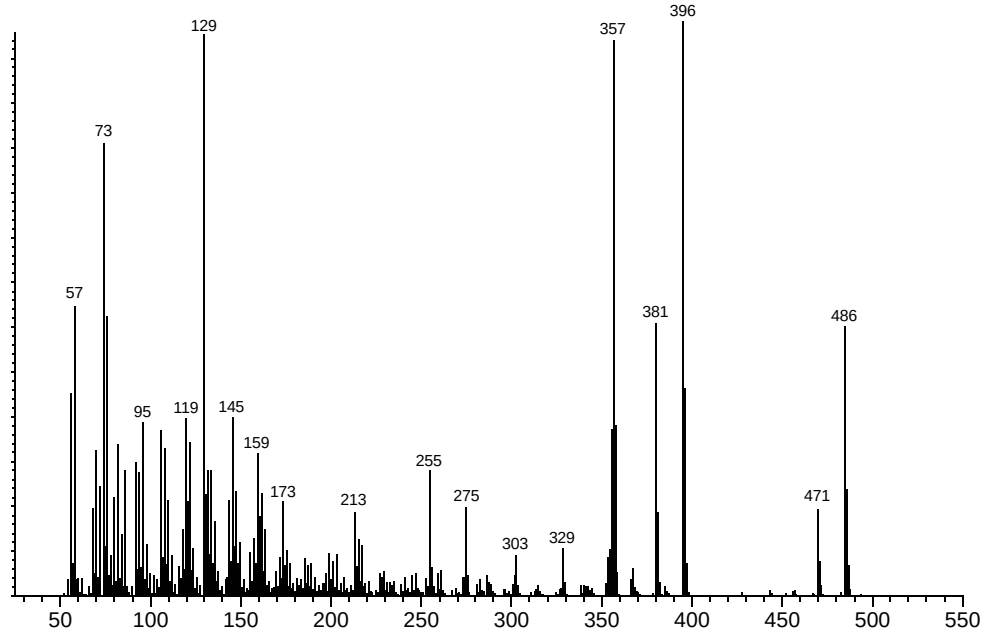

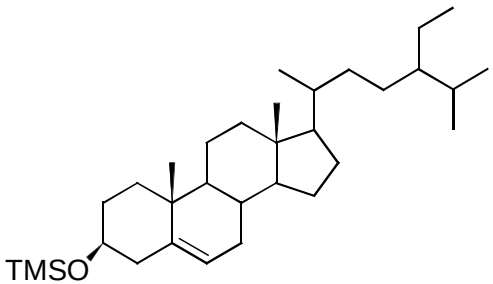

$C_{29}\Delta^5$

Mass Spectrum | *Structure*

Example: *Discodermia polymorpha* PC1156

# Carbons	Name	Alt. Name
29	Stigmasterol	24-ethylcholesta-5,22-dien-3β-ol

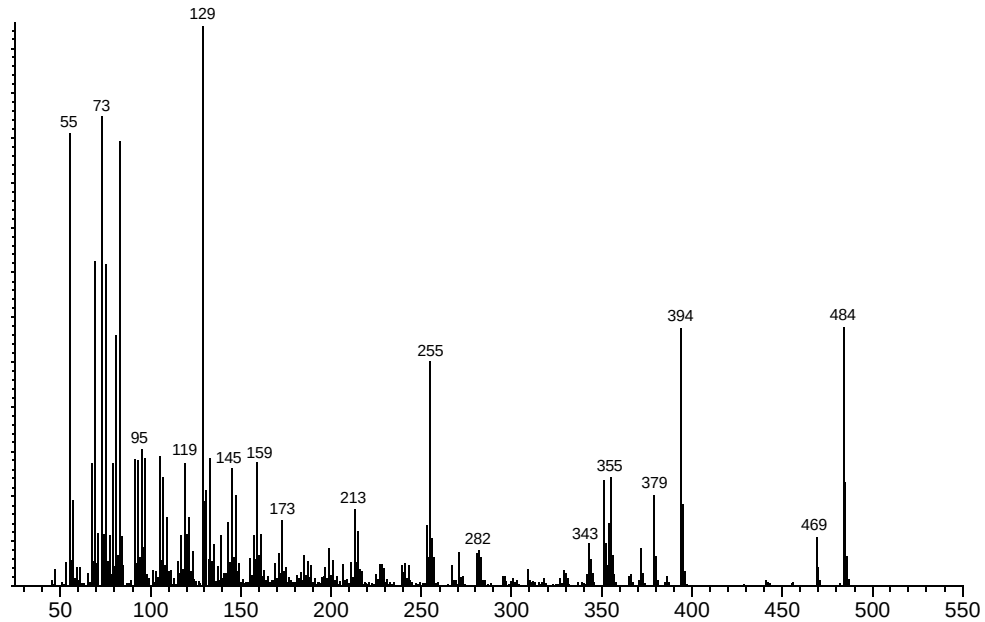

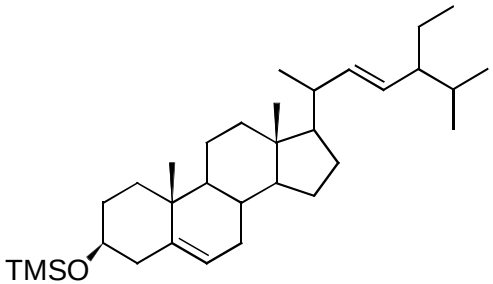

$C_{29}\Delta^{5,22}$

Mass Spectrum	Structure

Example: Stigmasterol Sterol Standard [~95% Sigma-Aldrich]

# Carbons	Name	Alt. Name
30	22-dehydro-24-IPC	(22E)-24-isopropylcholesta-5,22-dien-3β-ol

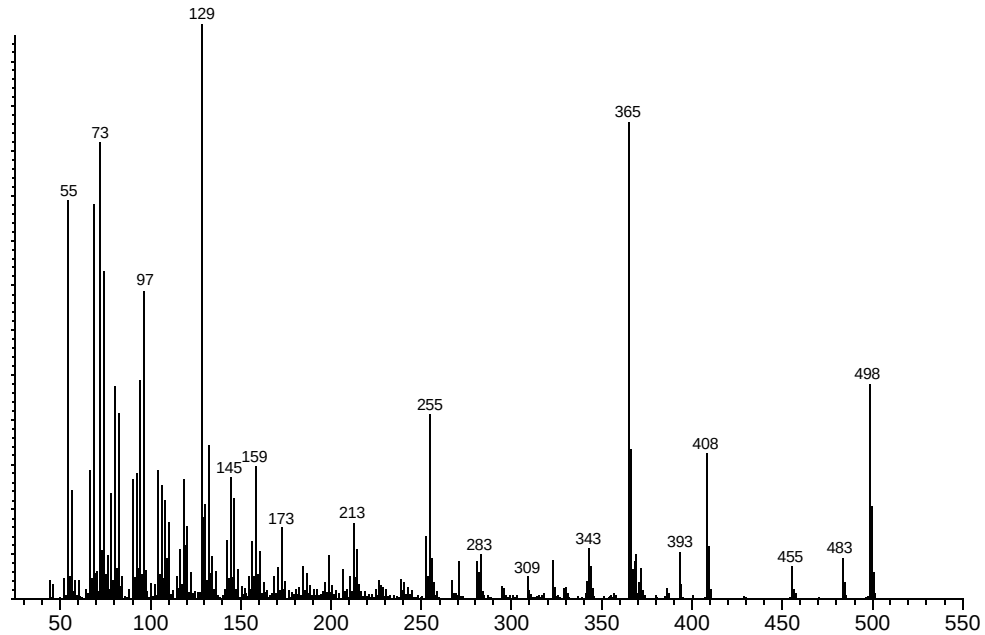

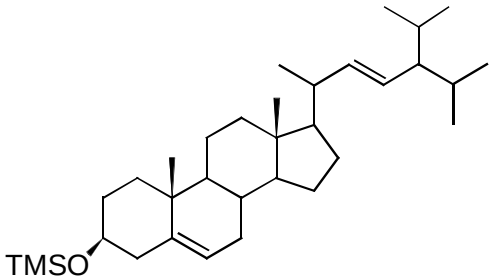

$C_{30}\Delta^{5,22}$

Mass Spectrum	Structure

Example: *Topsentia* sp PC1213

# Carbons	Name	Alt. Name
30	24-IPC	24-isopropylcholest-5-en-3β-ol

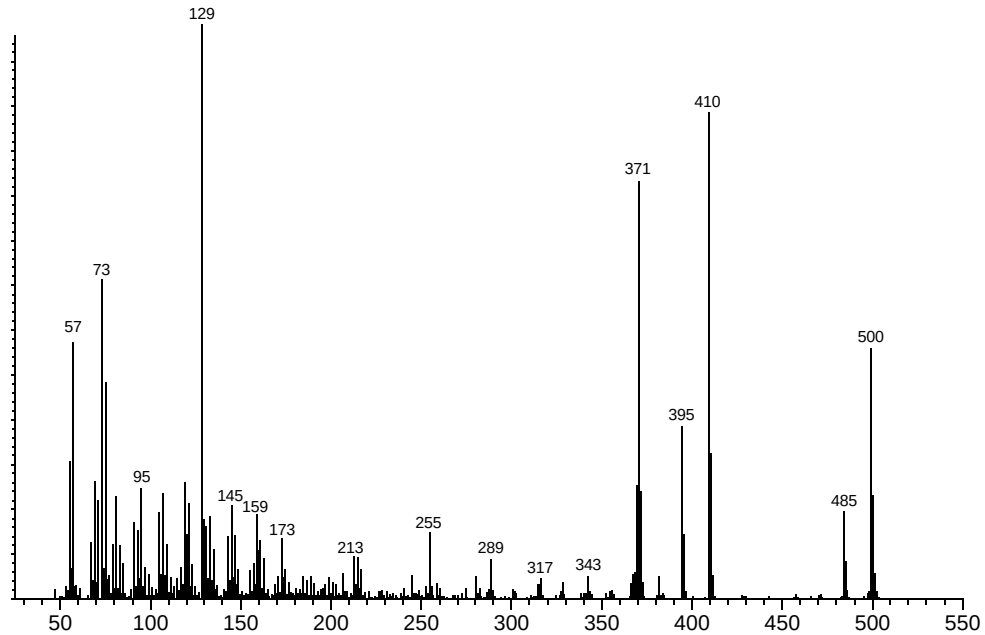

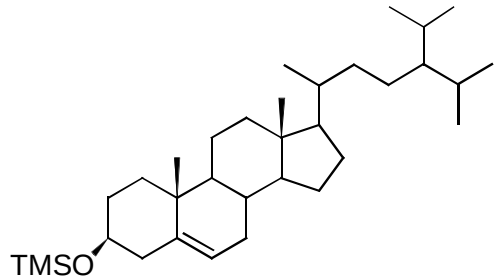

$C_{30}\Delta^5$

Mass Spectrum	Structure

Example: *Topsentia* sp PC1213

# Carbons	Name	Alt. Name
30	24-isopropenylcholesterol	24-isopropylcholesta-5,28(30)-dien-3β-ol

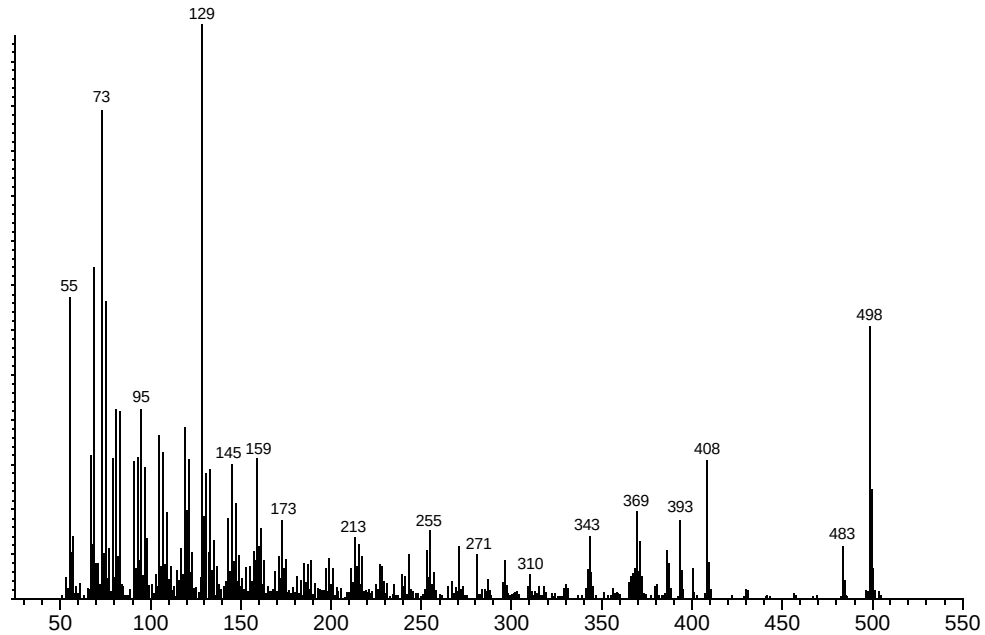

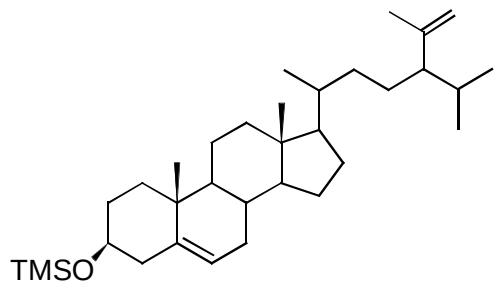

$C_{30}\Delta^{5,28(30)}$

Mass Spectrum	Structure

Example: *Ciocalpyta carballoi* PC1064

# Carbons	Name	Alt. Name
30	24-NPC	24(E/Z)-*n*-propylcholest-5,24(28)-dien-3 β-ol

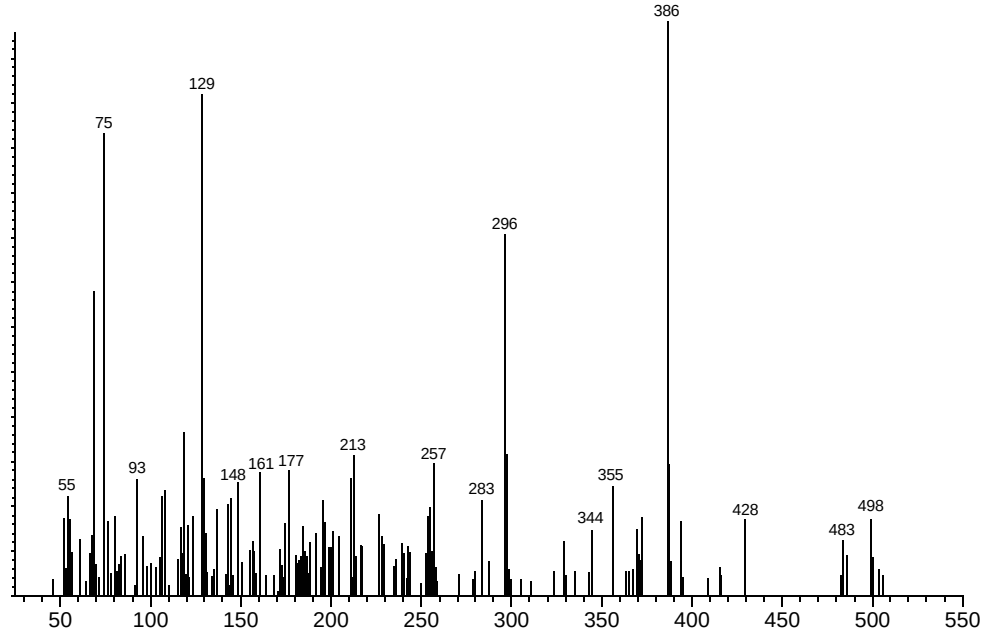

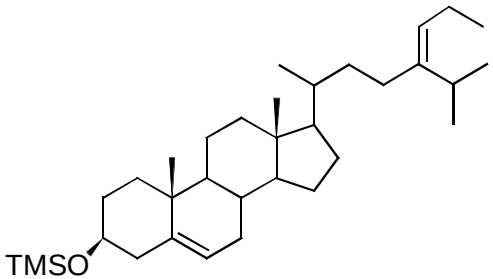

$C_{30}\Delta^{5,24(28)}$

Mass Spectrum | *Structure*

Example: *Rhabdastrella intermedia* PC399

# Carbons	Name	Alt. Name
30	25-dehydrothymosiosterol	(24,26,26')-trimethylcholesta-7,25(27)-dien-3 β-ol

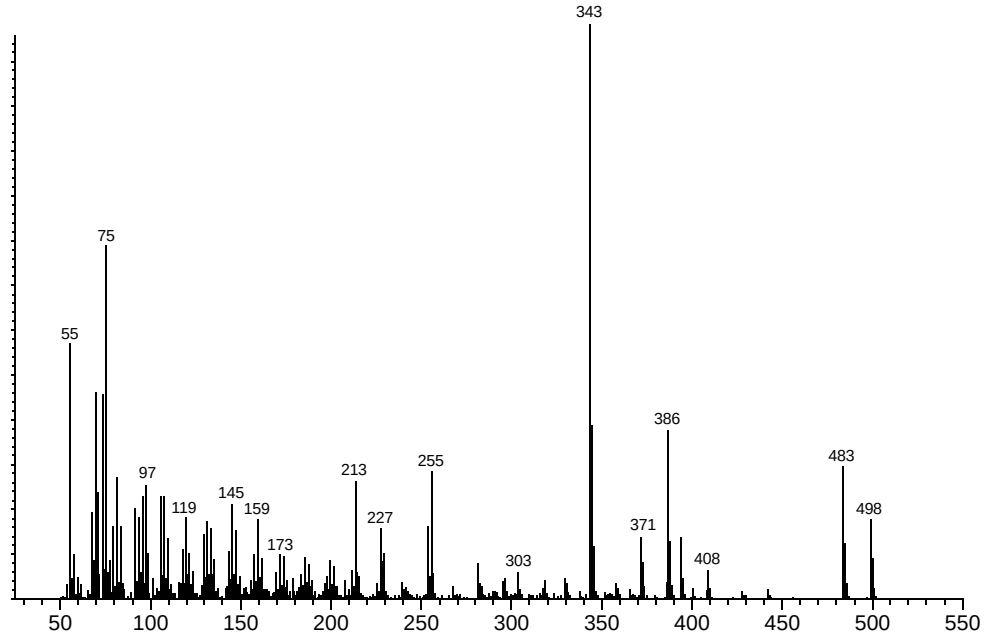

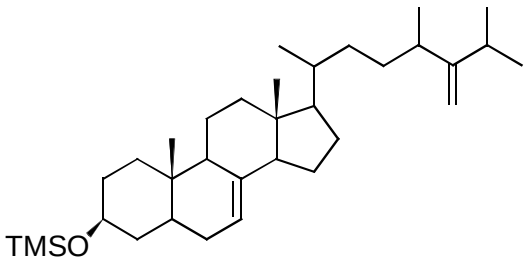

$C_{30}\Delta^{7,25(27)}$

Mass Spectrum | *Structure*

Example: *Thymosiopsis conglomerans* #25914

# Carbons	Name	Alt. Name
30	Stelliferasterol	(24R)-ethyl-26-methylcholesta-5,25(26)-dien-3 β-ol

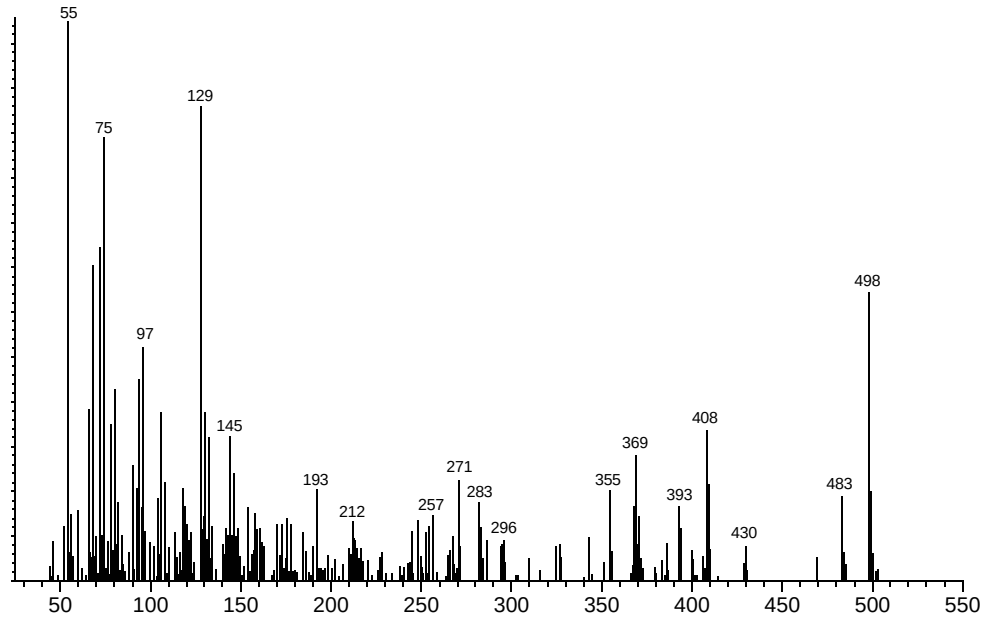

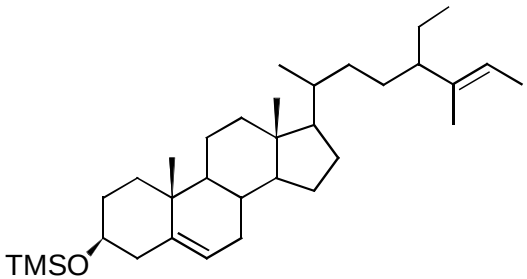

$C_{30}\Delta^{5,25(26)}$

Mass Spectrum	Structure

Example: *Rhabdastrella globostellata* PC1145

# Carbons	Name	Alt. Name
30	Strongylosterol	(24R)-ethyl-26-methylcholesta-5,25(27)-dien-3 β-ol

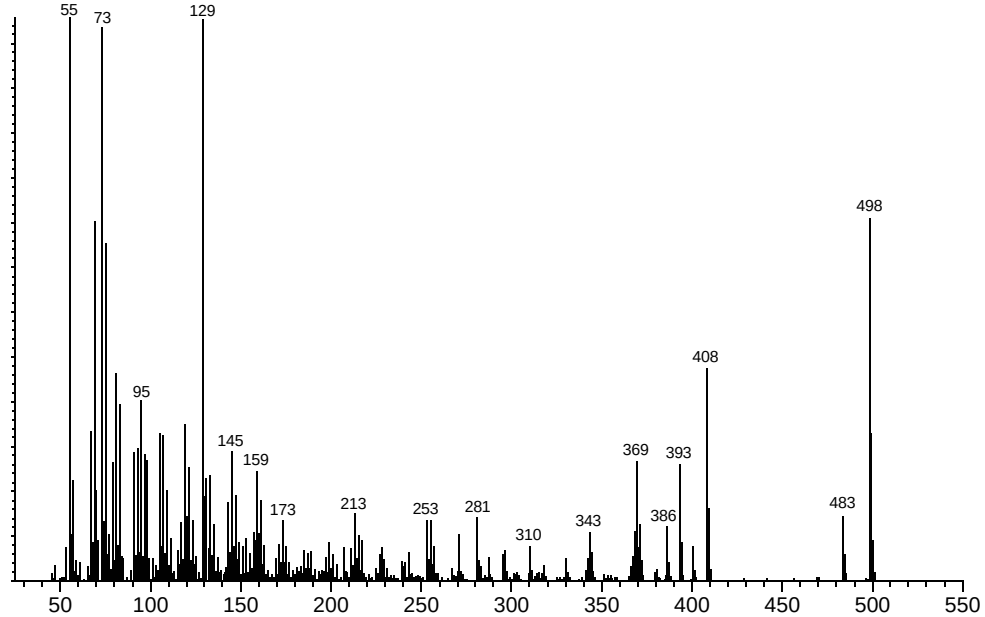

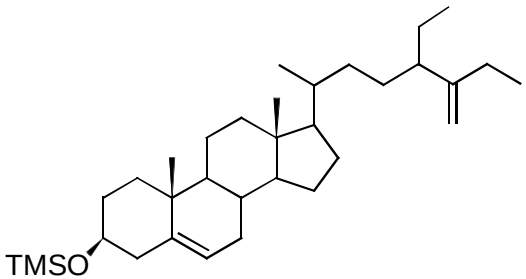

$C_{30}\Delta^{5,25(27)}$

Mass Spectrum	Structure

Example: *Petrosia (Strongylophora) corticata* PC1211

# Carbons	Name	Alt. Name
30	Thymosiosterol	(24,26,26')-trimethylcholest-7-en-3β-ol

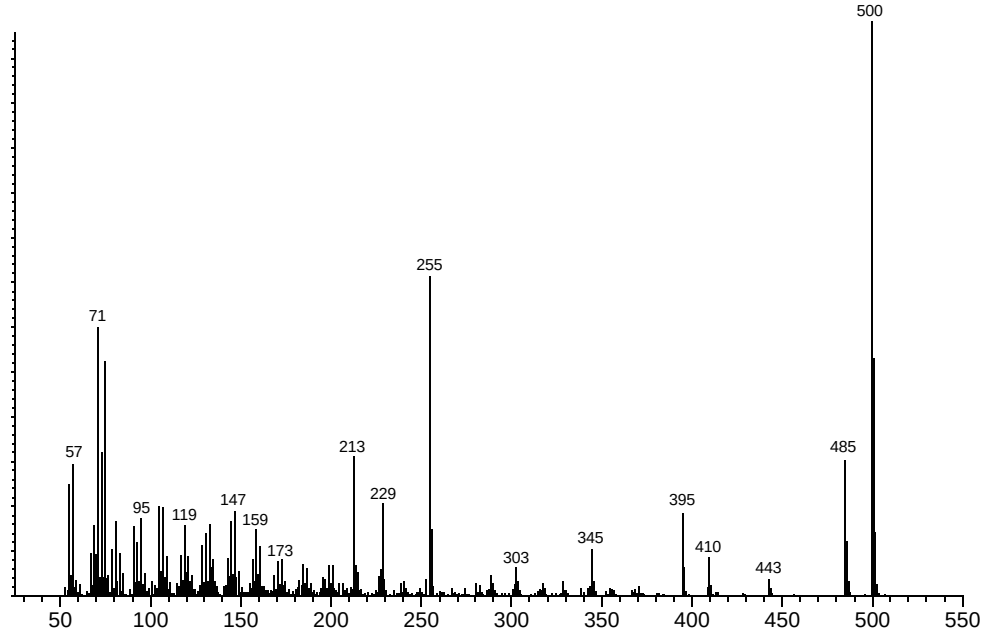

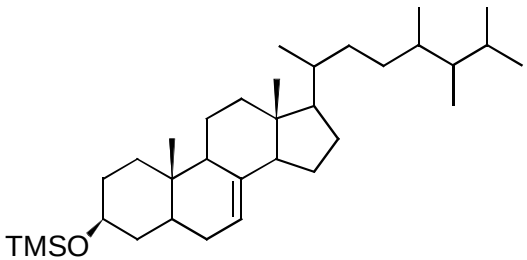

$C_{30}\Delta^7$

Mass Spectrum	Structure

Example: *Thymosiopsis conglomerans* #25914

# Carbons	Name	Alt. Name
30	Verongulasterol	(24R,26,27)-trimethylcholesta-5,25(27)-dien-3 β-ol

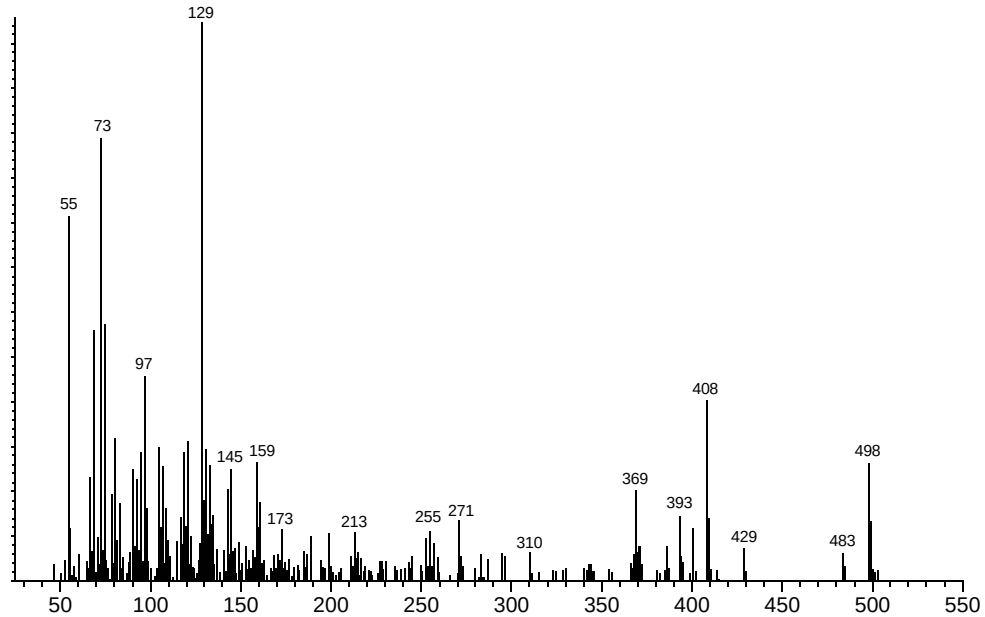

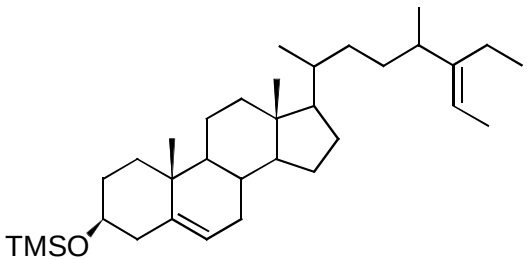

$C_{30}\Delta^{5,25(27)}$

Mass Spectrum	Structure

Example: *Verongula rigida* sponge 8

# Carbons	Name	Alt. Name
30	Xestosterol	24-methylene-26,27-dimethylcholest-5-en-3 β-ol

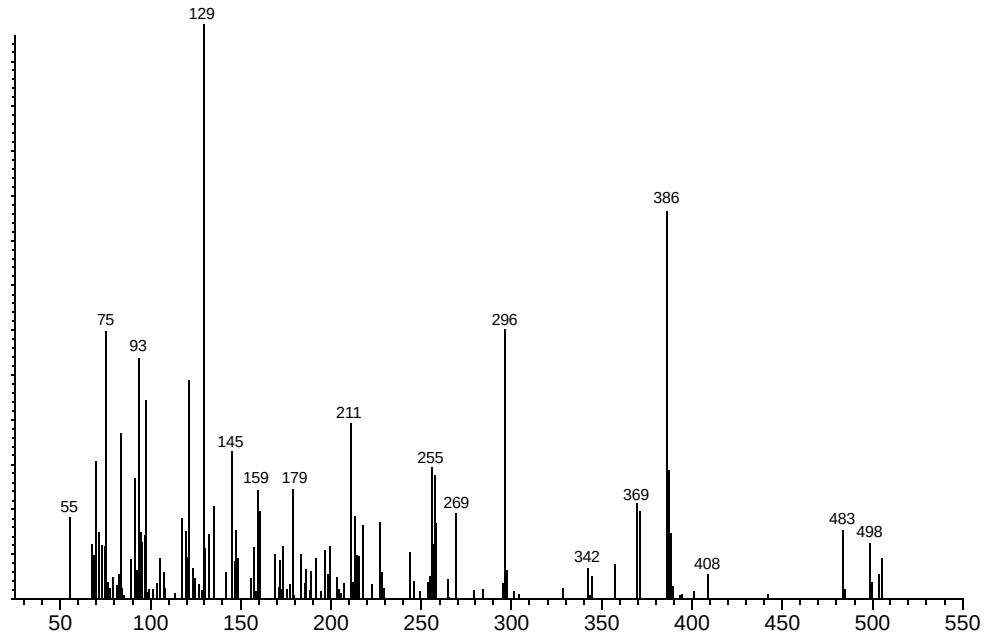

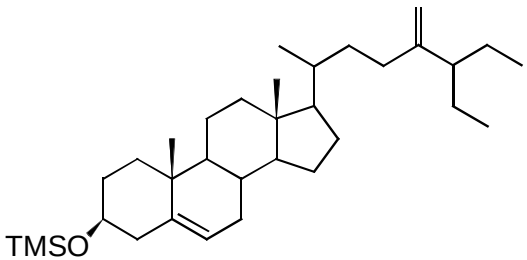

$C_{30}\Delta^{5,24(28)}$

Mass Spectrum	Structure

Example: *Xestospongia* sp #070818 #04-1

Appendix B: HyPy-generated Sterane Distributions of Sponge Biomass

Sponge: *Aplysina aerophoba*
Lab ID: TLE 430

Phylum: Porifera
Class: Demospongiae
Subclass: Verongimorpha
Order: Verongiida
Family: Aplysinidae
Genus: *Aplysina*
Species: *Aplysina aerophoba*

Locality: n/a
Depth: n/a

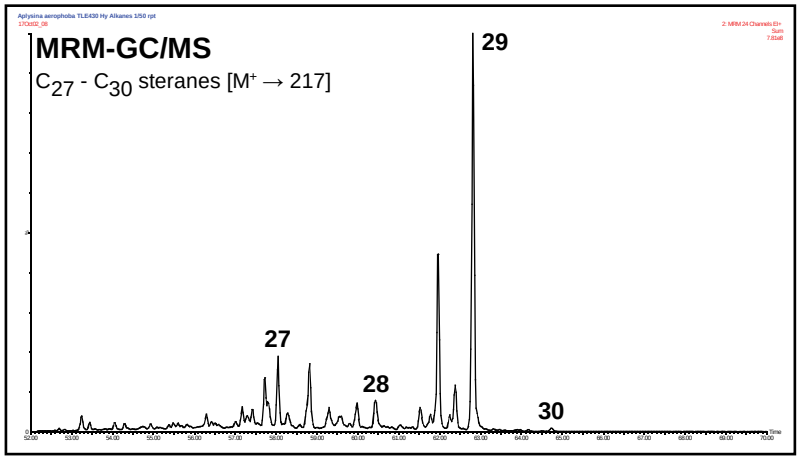

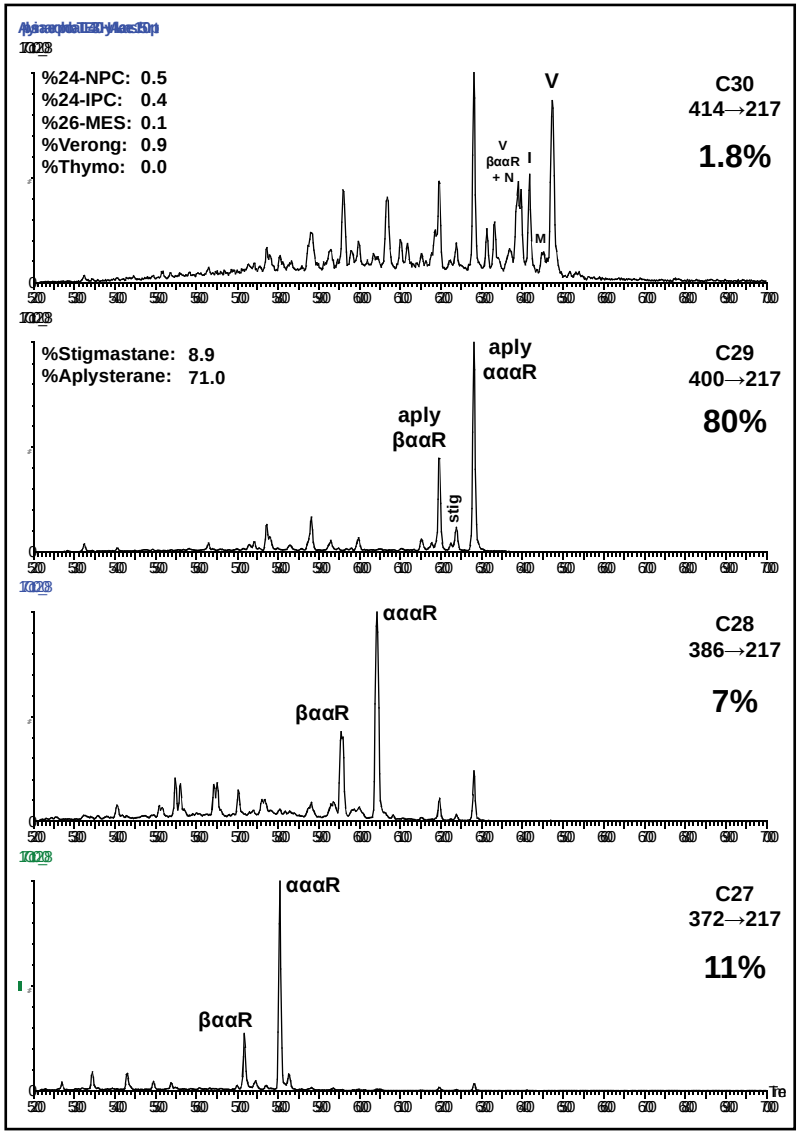

Sponge: *Aplysina fulva*
Lab ID: A. fulva

Phylum: Porifera
Class: Demospongiae
Subclass: Verongimorpha
Order: Verongiida
Family: Aplysinidae
Genus: *Aplysina*
Species: *Aplysina fulva*

Locality: Bocas del Toro, Panama
Depth: 3m

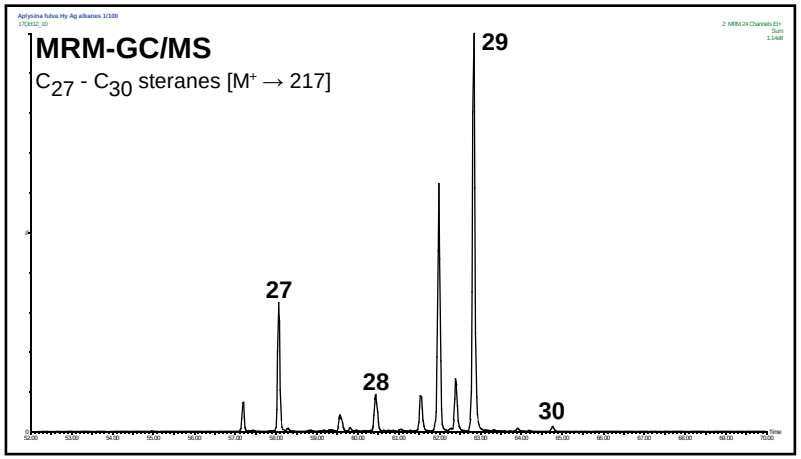

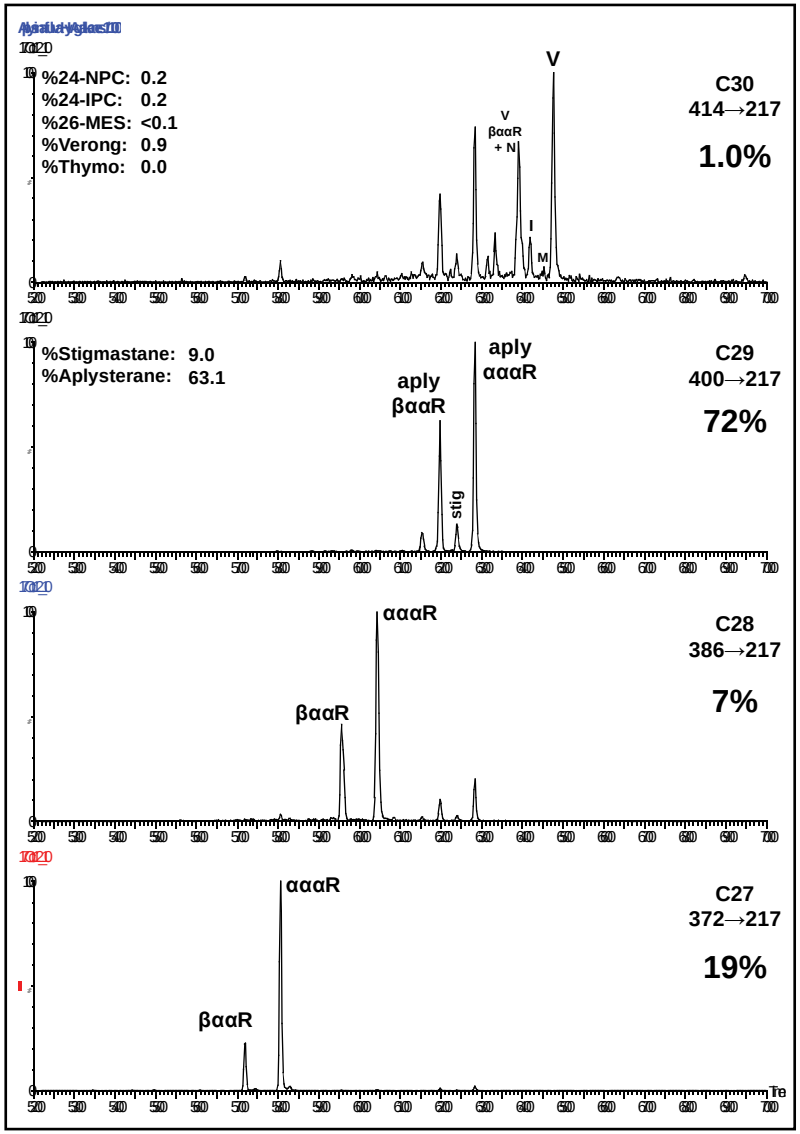

Sponge: *Cinachyrella kuekenthali*
Lab ID: PC941

Phylum: Porifera
Class: Demospongiae
Subclass: Heteroscleromorpha
Order: Tetractinellida
Family: Tetillidae
Genus: *Cinachyrella*
Species: *Cinachyrella kuekenthali*

Locality: Broward Co., Florida
Depth: shallow

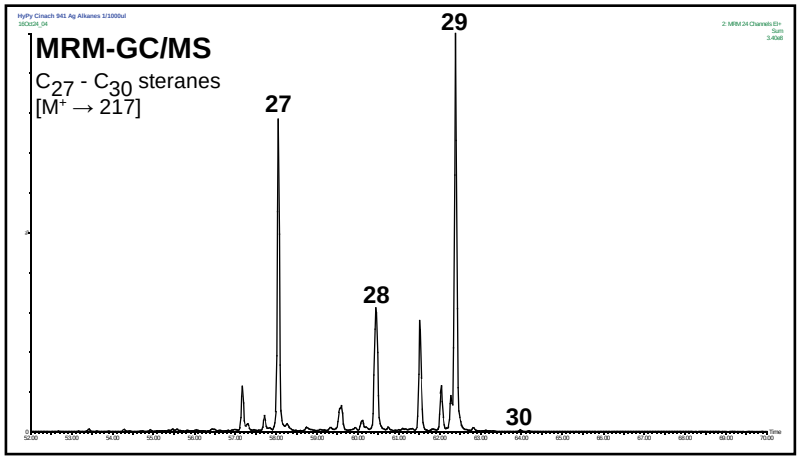

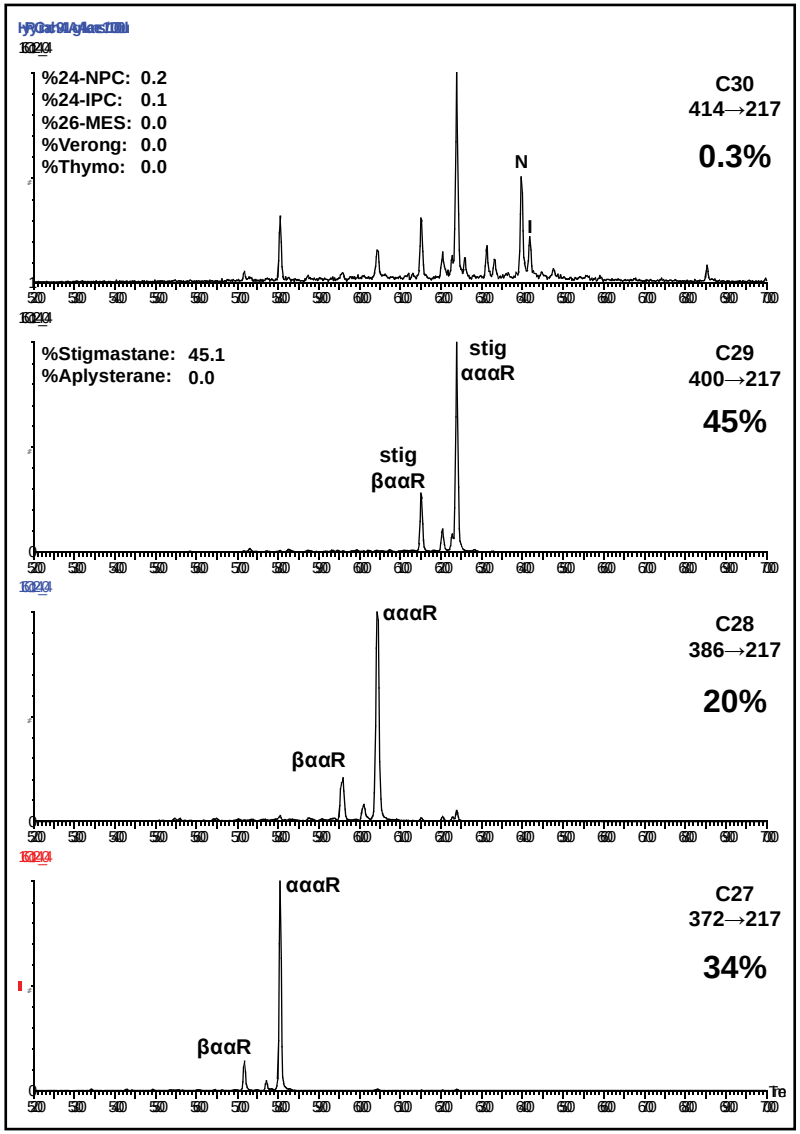

Sponge: *Ciocalypta carballoi*
Lab ID: PC1064

Phylum: Porifera
Class: Demospongiae
Subclass: Heteroscleromorpha
Order: Suberitida
Family: Suberitida
Genus: *Ciocalypta*
Species: *Ciocalypta carballoi*

Locality: Rhodes, Greece
Depth: 15m

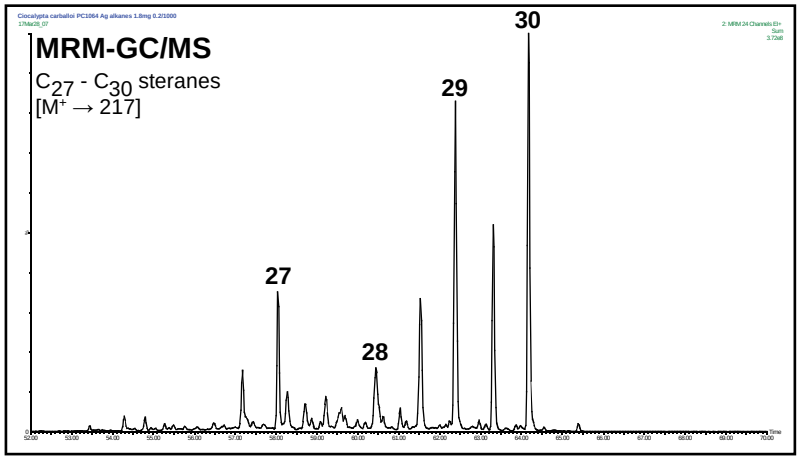

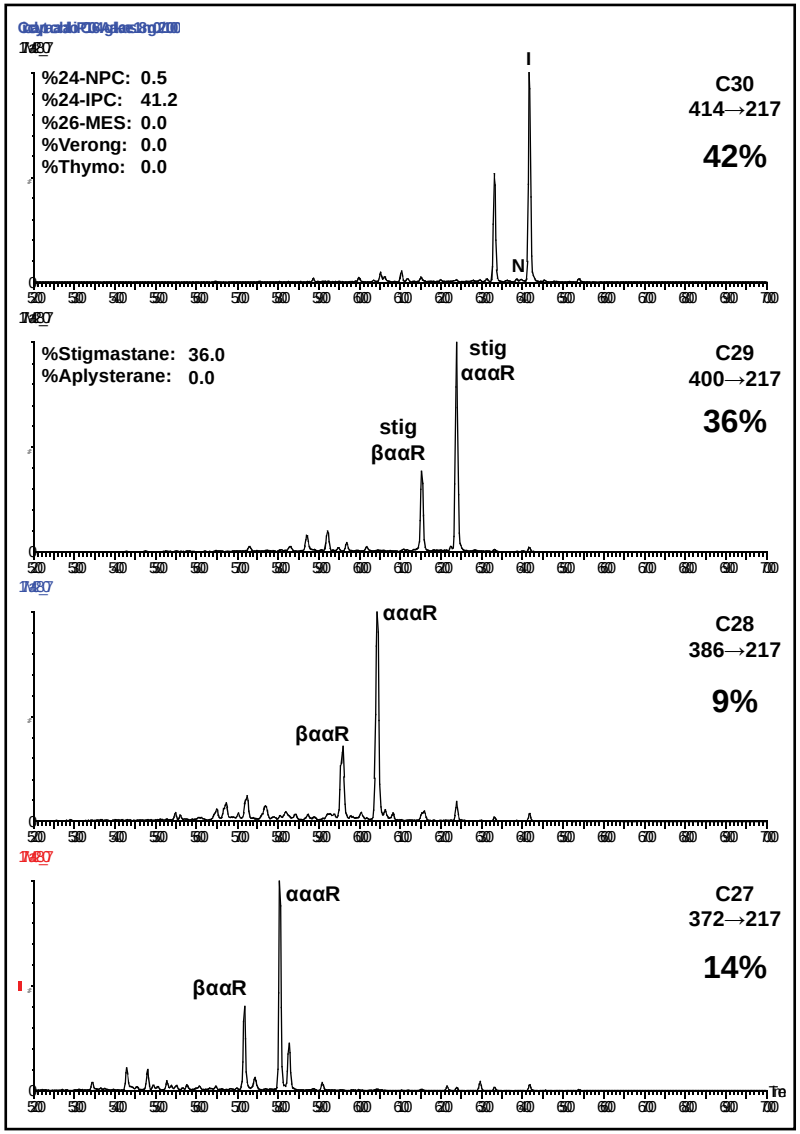

Sponge: *Craniella zetlandica*
Lab ID: PC667

Phylum: Porifera
Class: Demospongiae
Subclass: Heteroscleromorpha
Order: Tetractinellida
Family: Tetillidae
Genus: *Craniella*
Species: *Craniella zetlandica*

Locality: Korsfjord, Norway
Depth: 310m

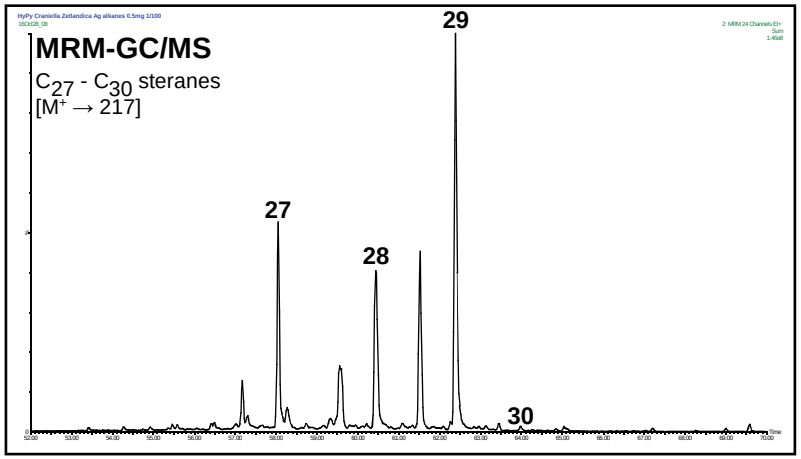

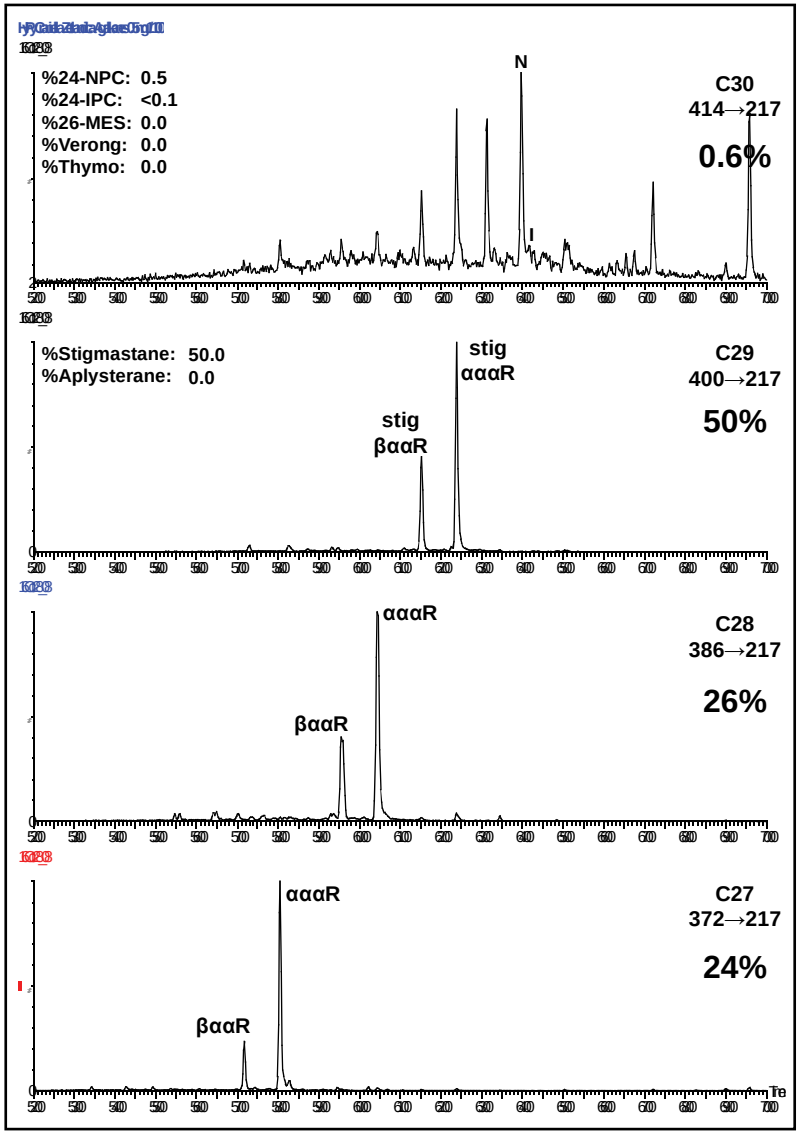

Sponge: *Cymbaxinella corrugata*
Lab ID: 1153725

Phylum: Porifera
Class: Demospongiae
Subclass: Heteroscleromorpha
Order: Agelasida
Family: Hymerhabdiidae
Genus: *Cymbaxinella*
Species: *Cymbaxinella corrugata*

Locality: n/a
Depth: n/a

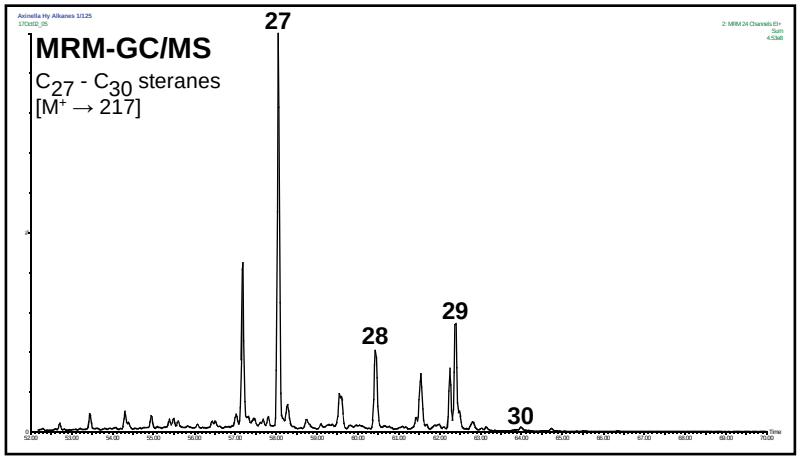

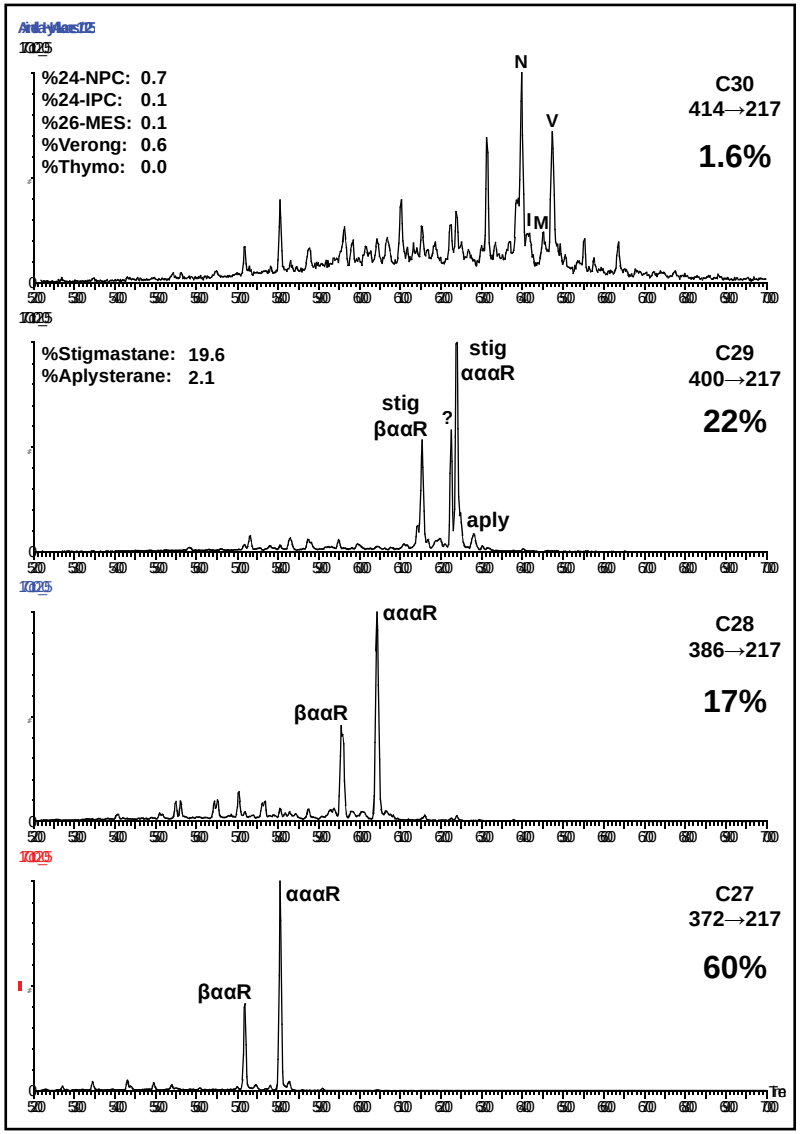

Sponge: *Dysidea fragilis*
Lab ID: D. fragilis

Phylum: Porifera
Class: Demospongiae
Subclass: Keratosa
Order: Dictyoceratida
Family: Dysideidae
Genus: *Dysidea*
Species: *Dysidea fragilis*

Locality: n/a
Depth: n/a

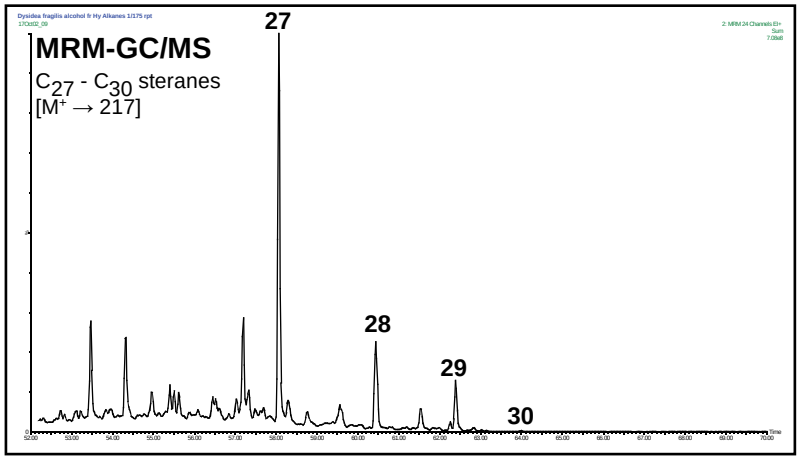

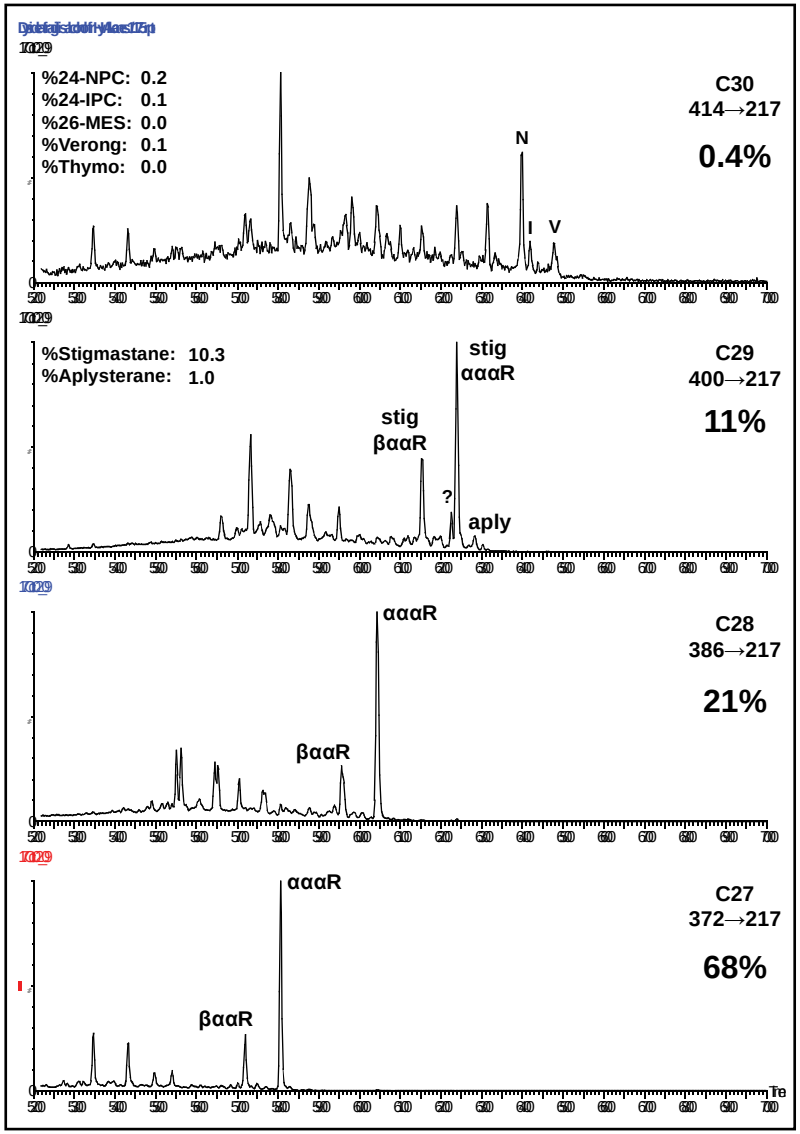

Sponge: *Geodia hentscheli*
Lab ID: GhII

Phylum: Porifera
Class: Demospongiae
Subclass: Heteroscleromorpha
Order: Tetractinellida
Family: Geodiidae
Genus: *Geodia*
Species: *Geodia hentscheli*

Locality: Kolbeinsey Ridge, Greenland Sea
Depth: 145-215m

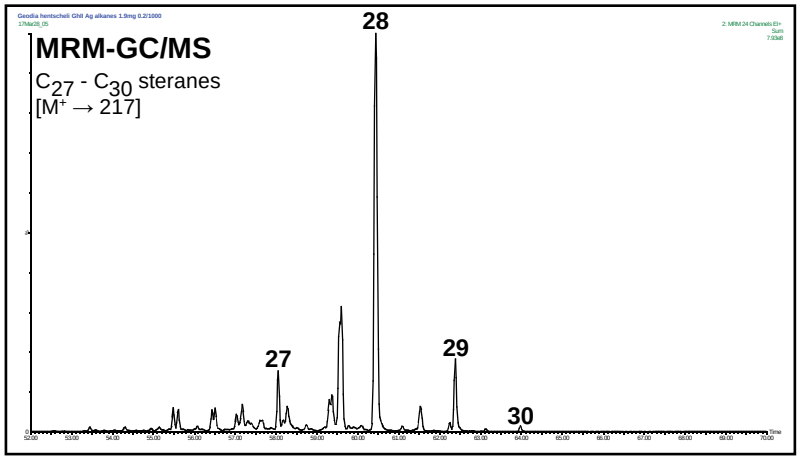

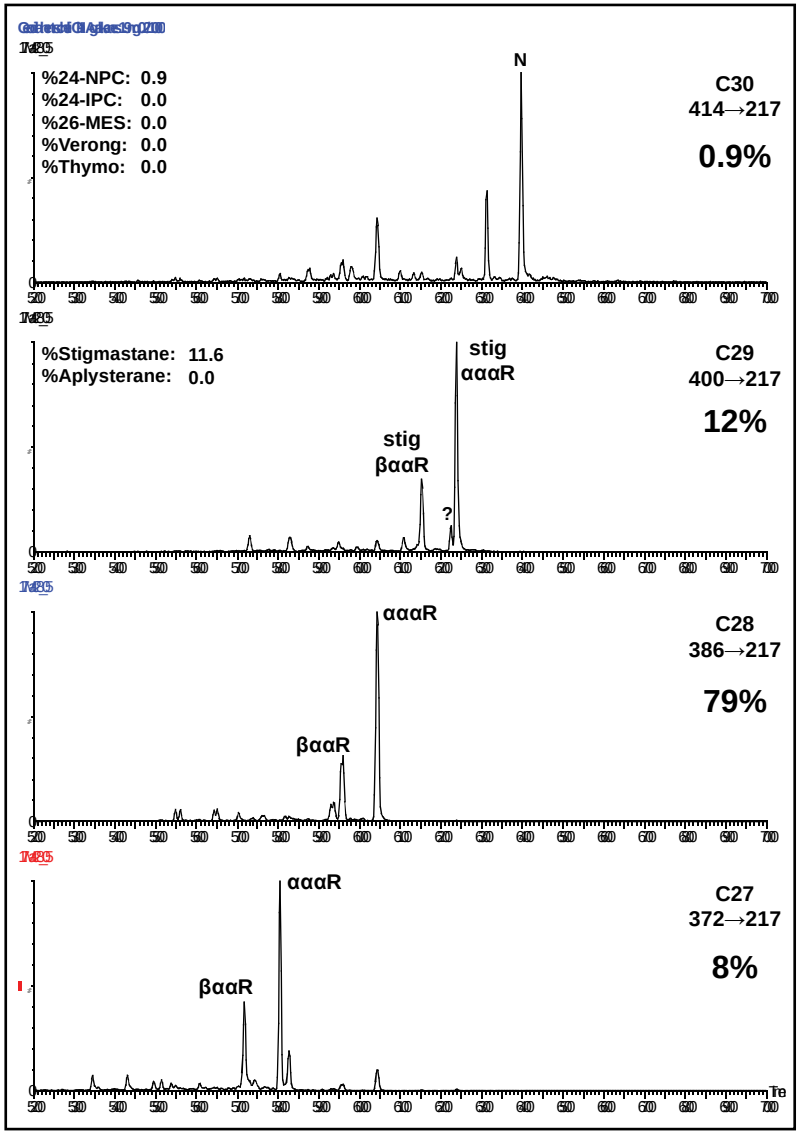

Sponge: *Geodia parva*
Lab ID: GpII

Phylum: Porifera
Class: Demospongiae
Subclass: Heteroscleromorpha
Order: Tetractinellida
Family: Geodiidae
Genus: *Geodia*
Species: *Geodia parva*

Locality: Mohns Ridge, Greenland Sea
Depth: 1834-1863m

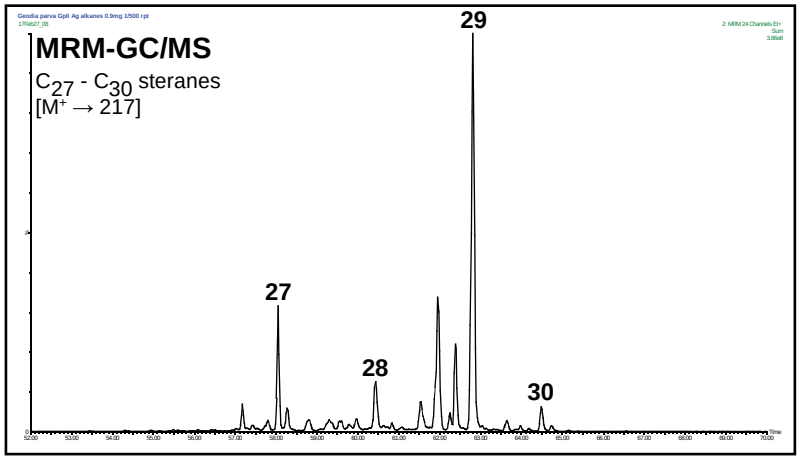

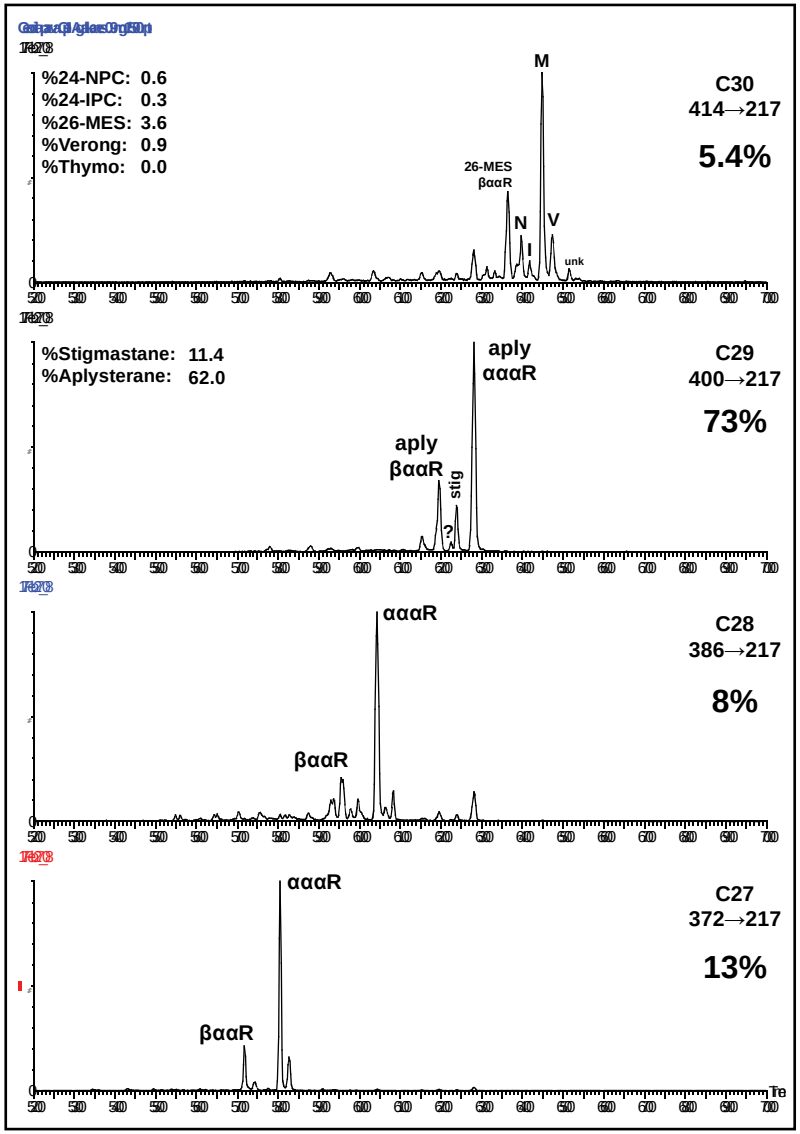

Sponge: *Geodia parva*
Lab ID: PC535

Phylum: Porifera
Class: Demospongiae
Subclass: Heteroscleromorpha
Order: Tetractinellida
Family: Geodiidae
Genus: *Geodia*
Species: *Geodia parva*

Locality: Flemish Cap, off Newfoundland, Canada
Depth: 1180m

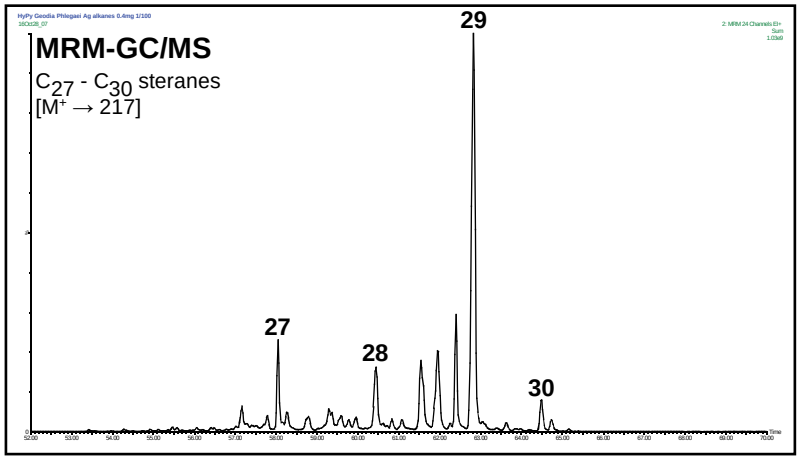

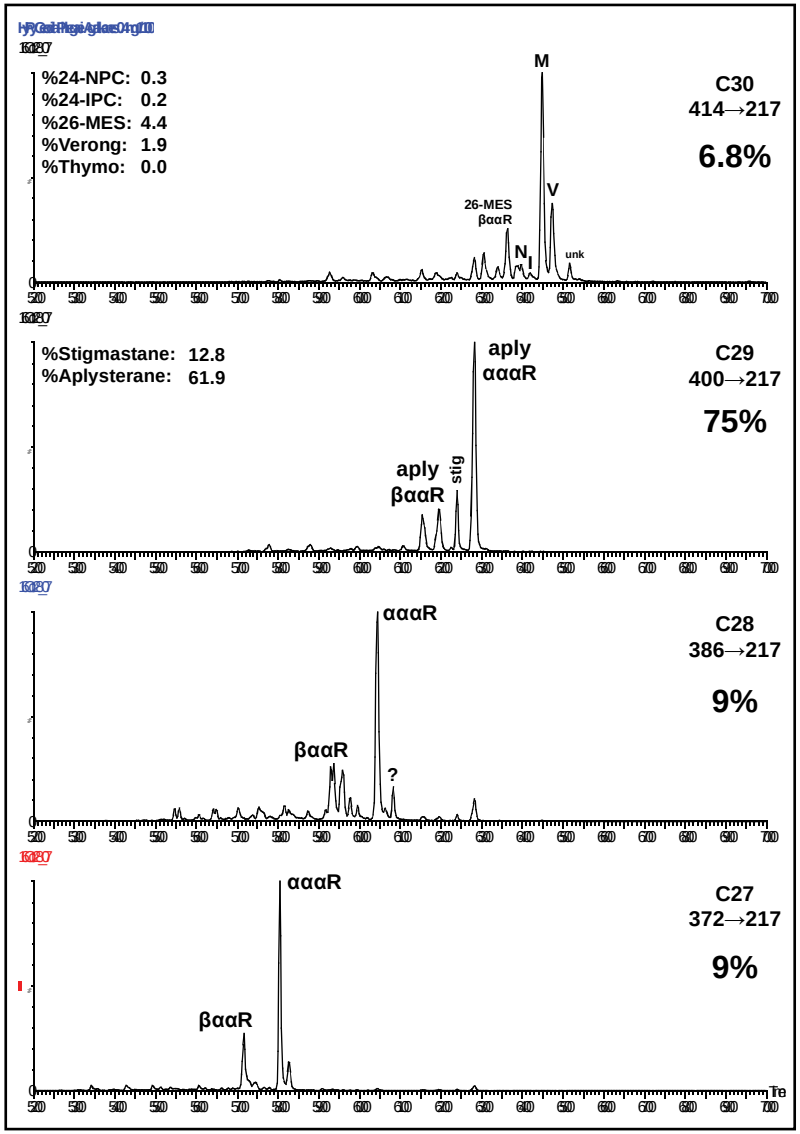

Sponge: *Geodia phlegraei*
Lab ID: PC511

Phylum: Porifera
Class: Demospongiae
Subclass: Heteroscleromorpha
Order: Tetractinellida
Family: Geodiidae
Genus: *Geodia*
Species: *Geodia phlegraei*

Locality: Svalbard, Norway
Depth: 215m

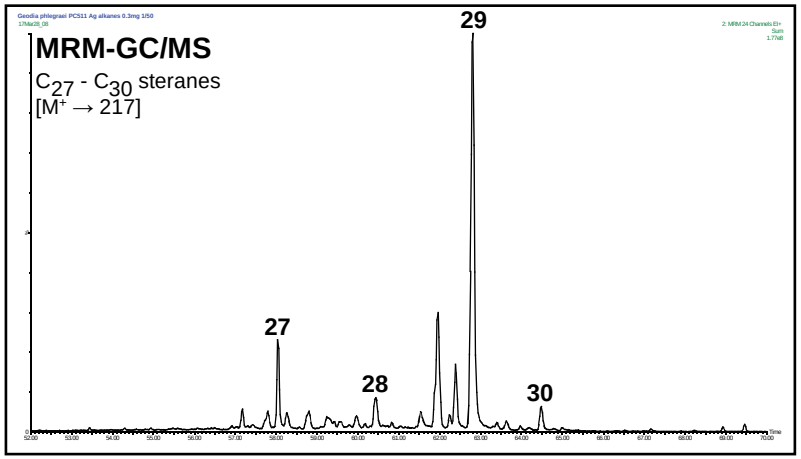

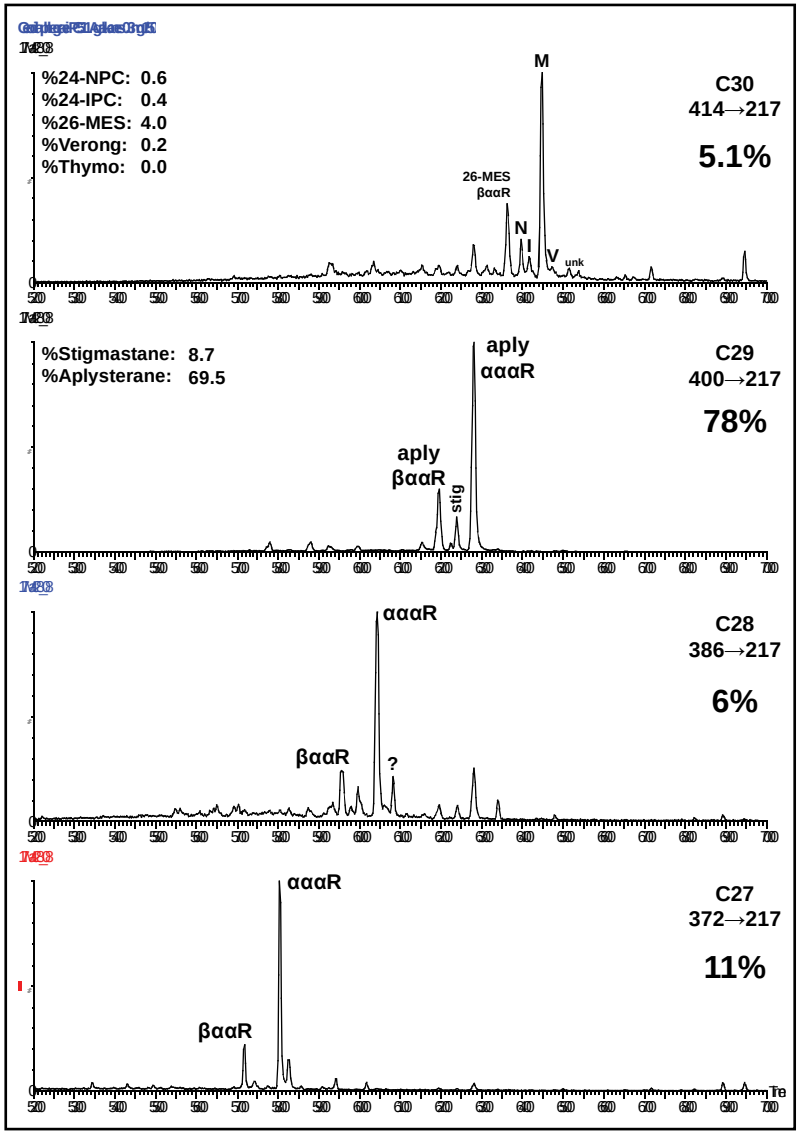

Sponge: *Geodia sp.*
Lab ID: PC567

Phylum: Porifera
Class: Demospongiae
Subclass: Heteroscleromorpha
Order: Tetractinellida
Family: Geodiidae
Genus: *Geodia*
Species: *Geodia sp.*

Locality: n/a
Depth: n/a

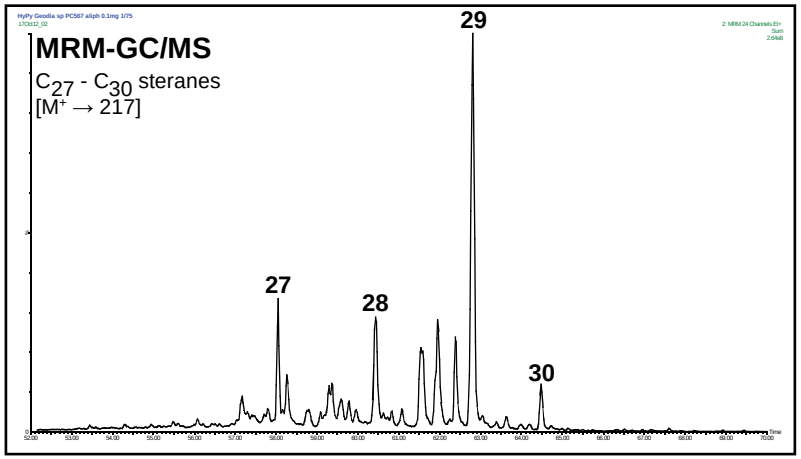

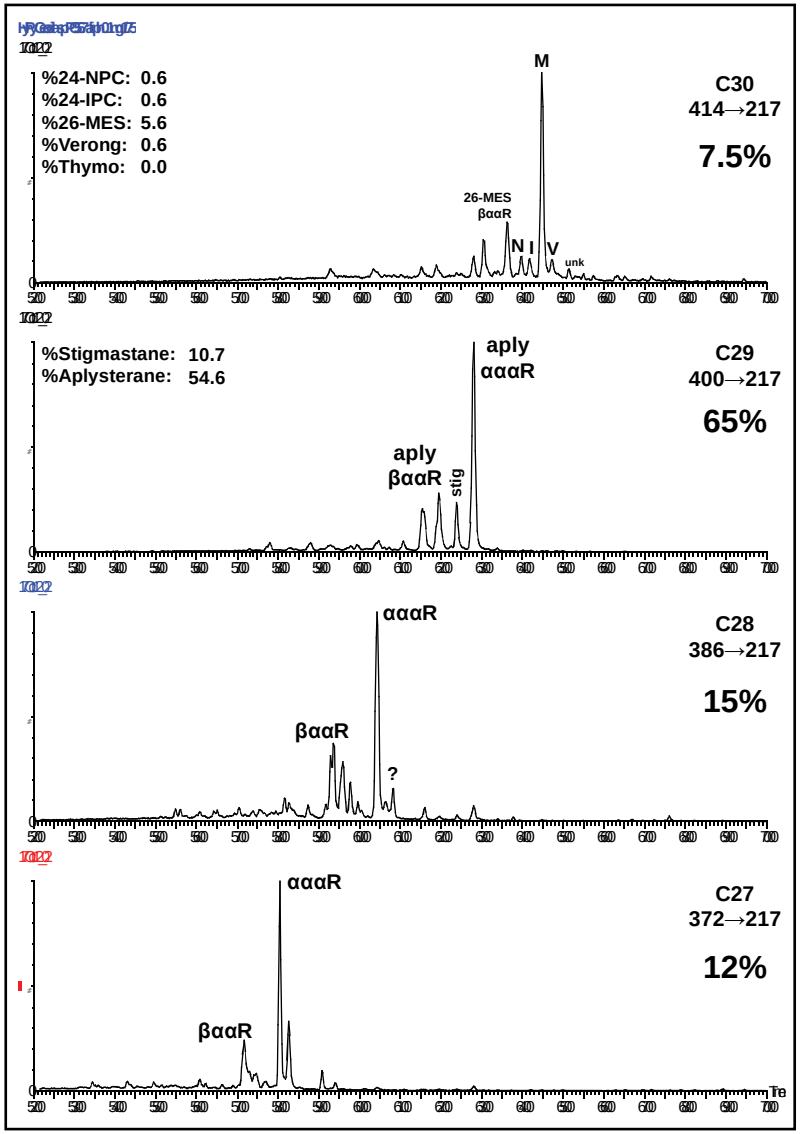

Sponge: *Halichondria sp.*
Lab ID: sponge 1

Phylum: Porifera
Class: Demospongiae
Subclass: Heteroscleromorpha
Order: Suberitida
Family: Halichondriidae
Genus: *Halichondria*
Species: *Halichondria sp.*

Locality: Marine Biological Lab, MA
Depth: shallow

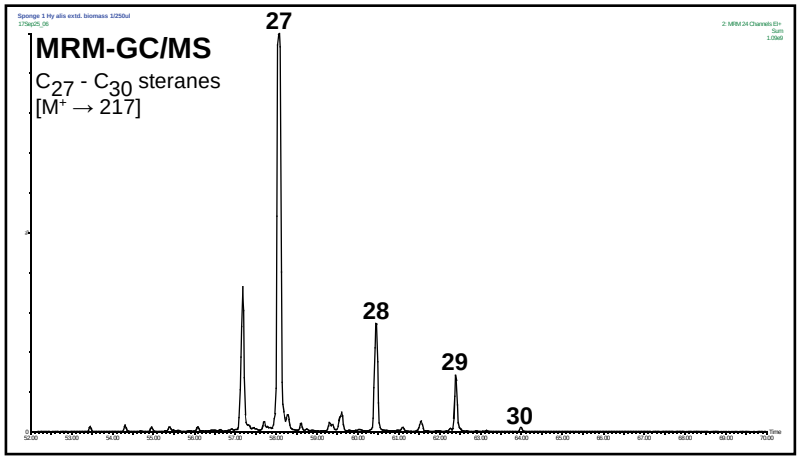

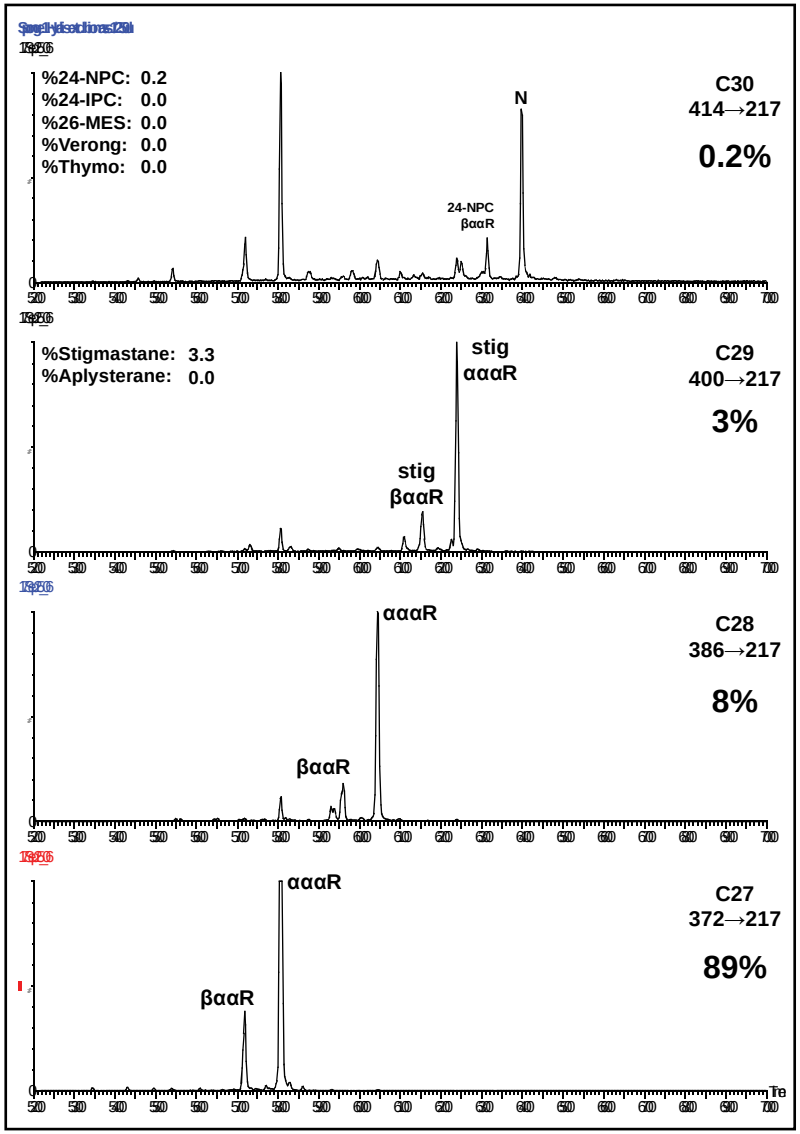

Sponge: *Petrosia (Strongylophora)* cf. *vansoesti*
Lab ID: PC982

Phylum: Porifera
Class: Demospongiae
Subclass: Heteroscleromorpha
Order: Haplosclerida
Family: Petrosiidae
Genus: *Petrosia*
Species: *Petrosia (Strongylophora)* cf. *vansoesti*

Locality: off Lagos, Portugal
Depth: 60m

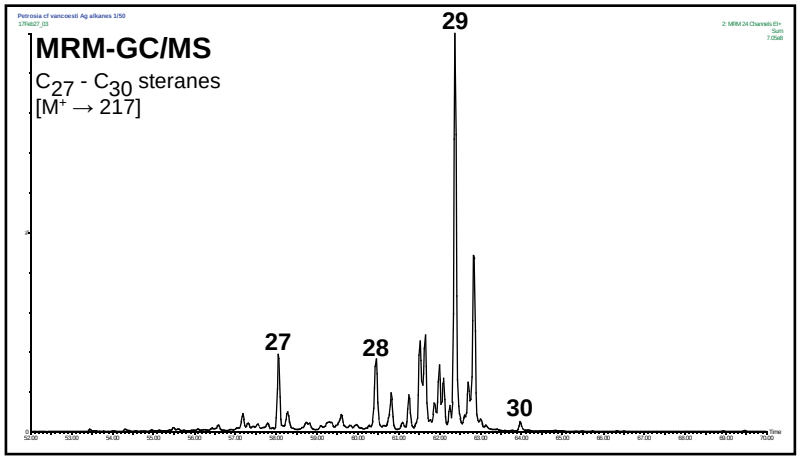

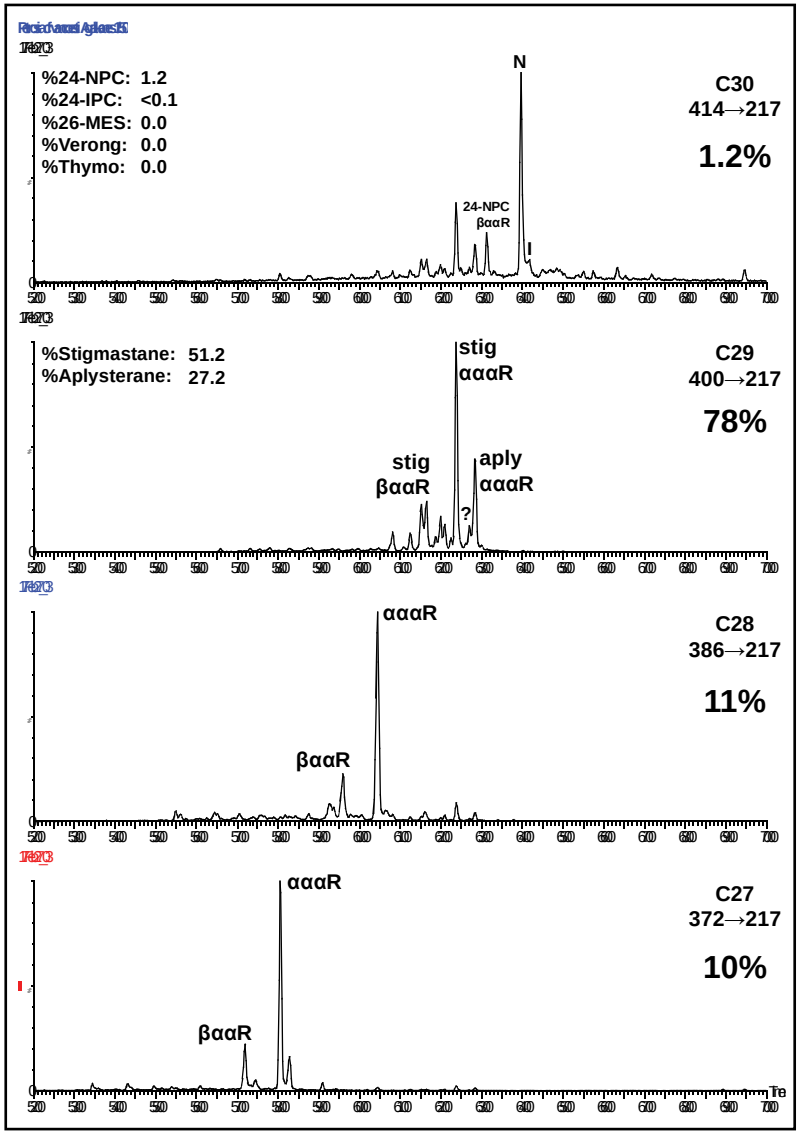

Sponge: *Petrosia (Strongylophora) durissima*
Lab ID: PC1068

Phylum: Porifera
Class: Demospongiae
Subclass: Heteroscleromorpha
Order: Haplosclerida
Family: Petrosiidae
Genus: *Petrosia*
Species: *Petrosia (Strongylophora) durissima*

Locality: North Sulawesi, Indonesia
Depth: 20m

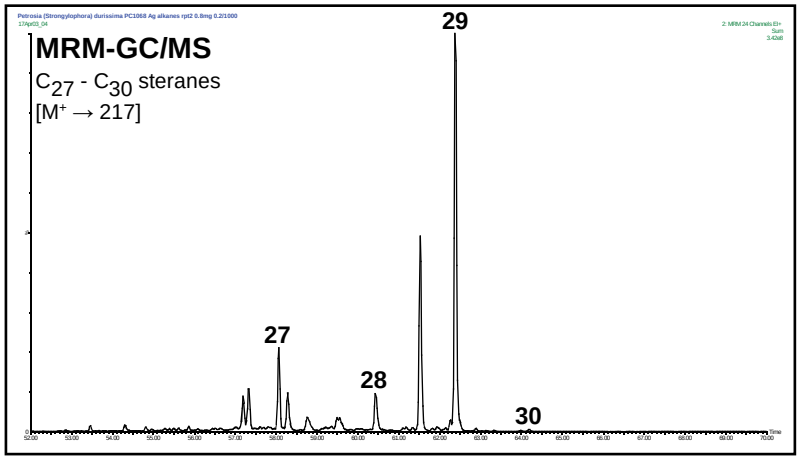

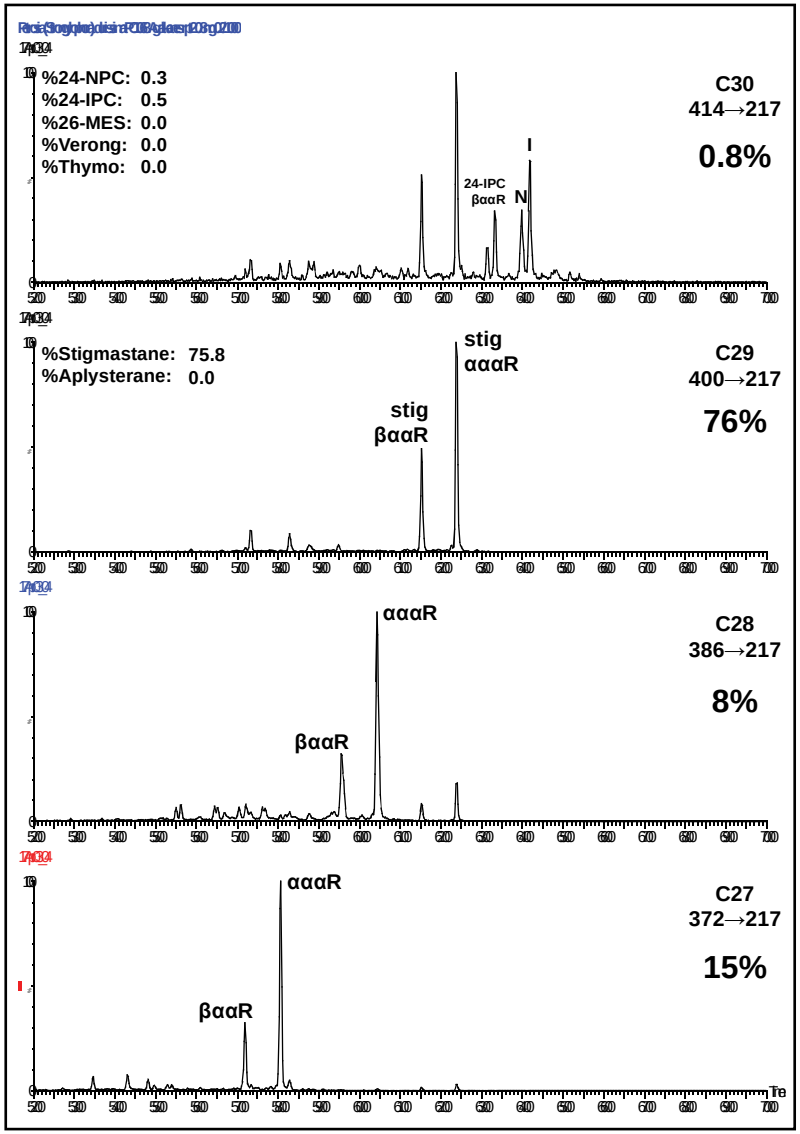

Sponge: *Phakellia ventilabrum*
Lab ID: FKOG-POR2

Phylum: Porifera
Class: Demospongiae
Subclass: Heteroscleromorpha
Order: Bubarida (Axinellida?)
Family: Bubaridae
Genus: *Phakellia*
Species: *Phakellia ventilabrum*

Locality: Tjarno, Sweden
Depth: n/a

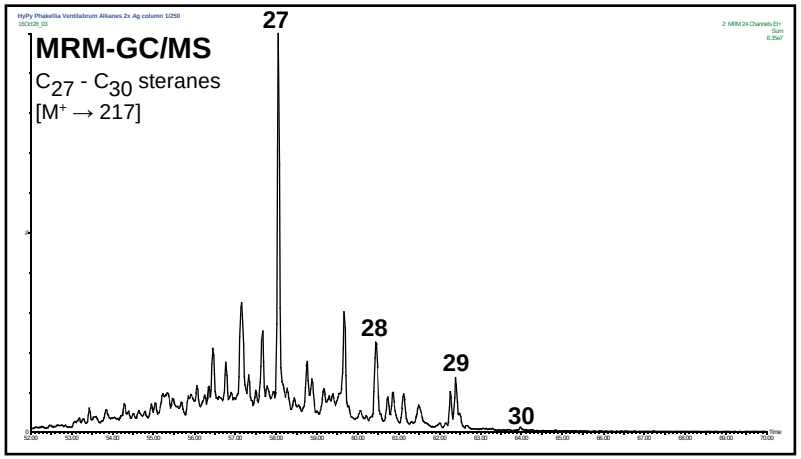

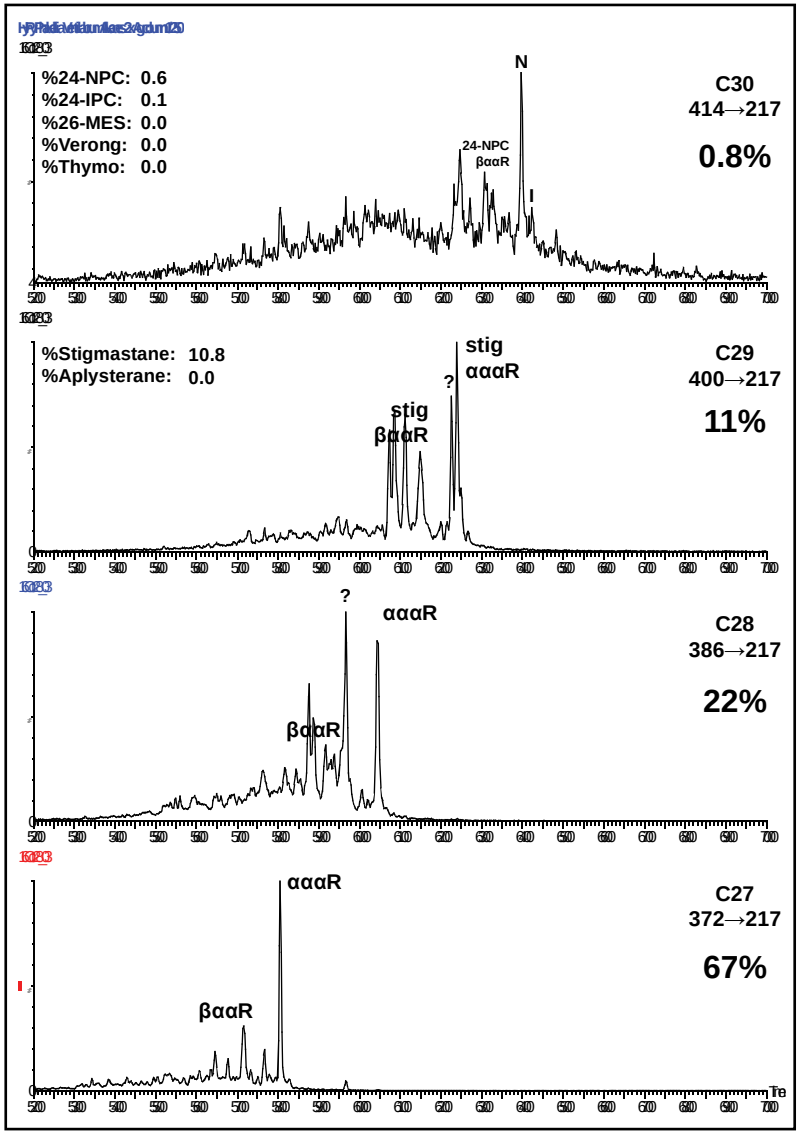

Sponge: *Plakinastrella onkodes*
Lab ID: 1133732

Phylum: Porifera
Class: Homoscleromorpha
Subclass: n/a
Order: Homosclerophorida
Family: Plakinidae
Genus: *Plakinastrella*
Species: *Plakinastrella onkodes*

Locality: off Panama, Caribbean Sea
Depth: shallow

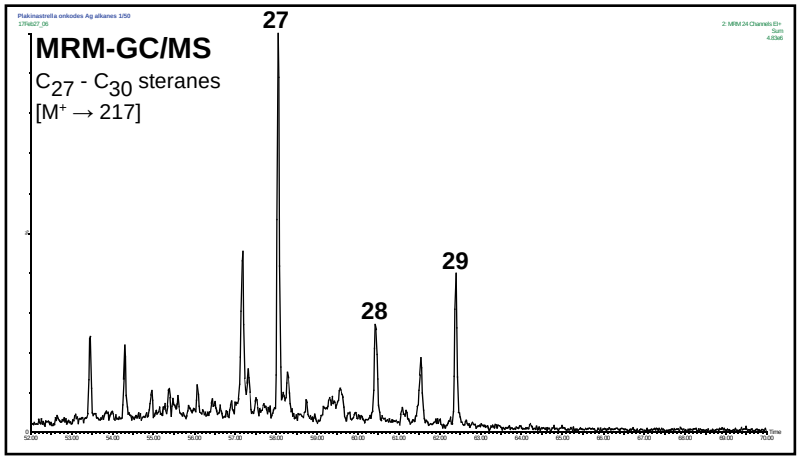

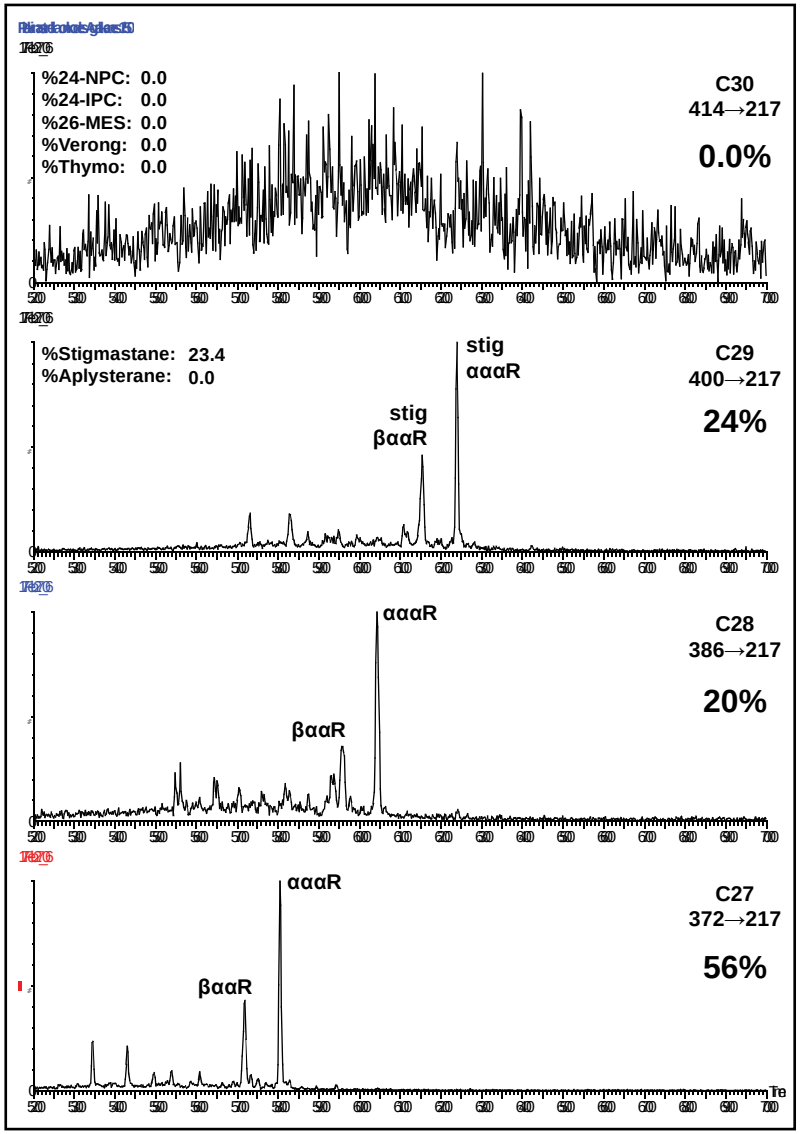

Sponge: *Plakortis halichondrioides*
Lab ID: 1133720

Phylum: Porifera
Class: Homoscleromorpha
Subclass: n/a
Order: Homosclerophorida
Family: Plakinidae
Genus: *Plakortis*
Species: *Plakortis halichondrioides*

Locality: off Panama, Caribbean Sea
Depth: shallow

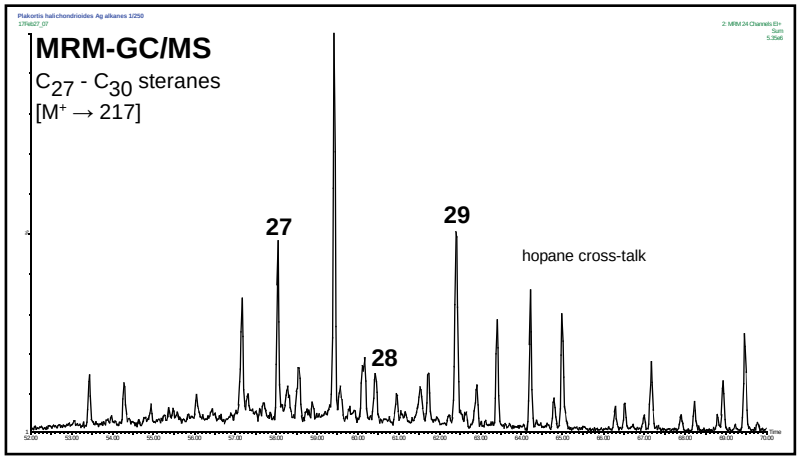

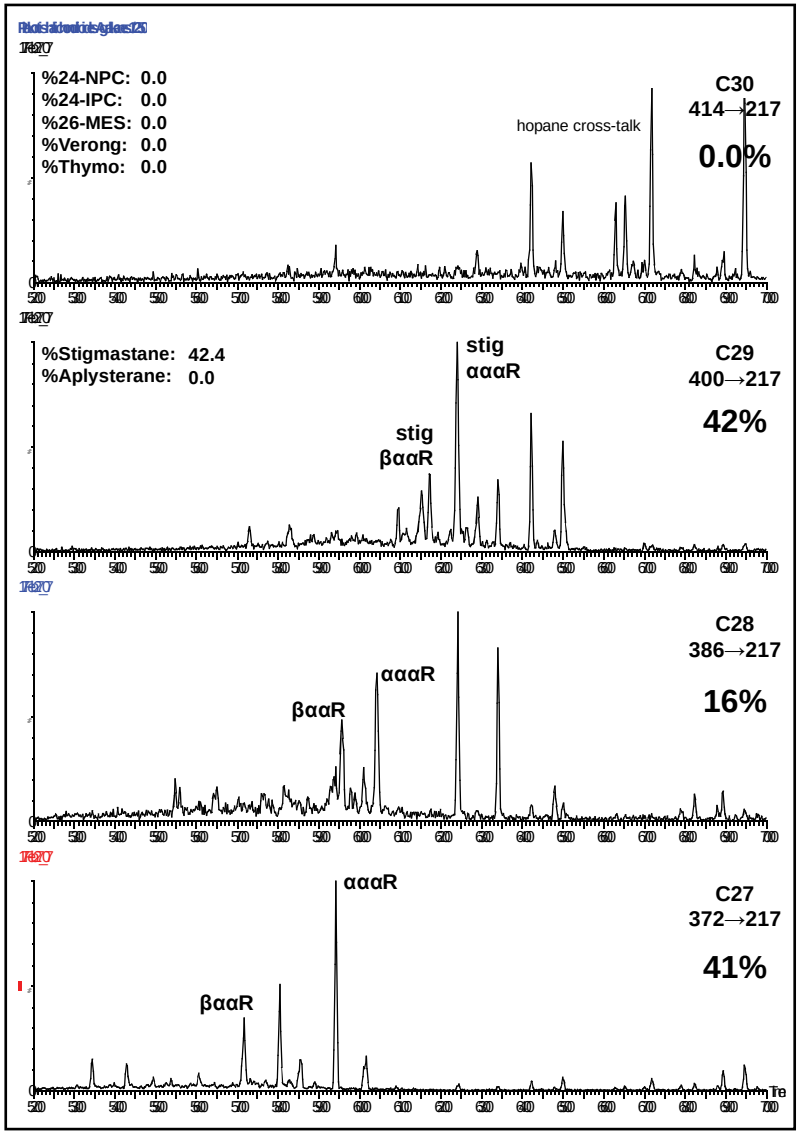

Sponge: *Rhabdastrella distincta*
Lab ID: PC1127

Phylum: Porifera
Class: Demospongiae
Subclass: Heteroscleromorpha
Order: Tetractinellida
Family: Ancorinidae
Genus: *Rhabdastrella*
Species: *Rhabdastrella distincta*

Locality: North Sulawesi, Indonesia
Depth: 27m

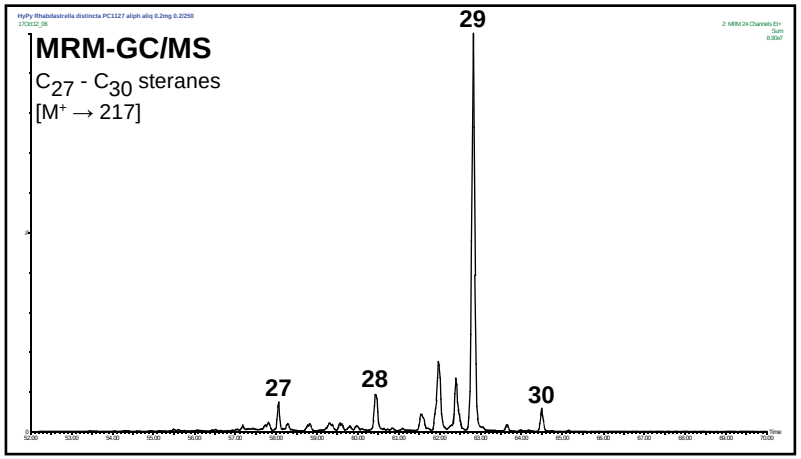

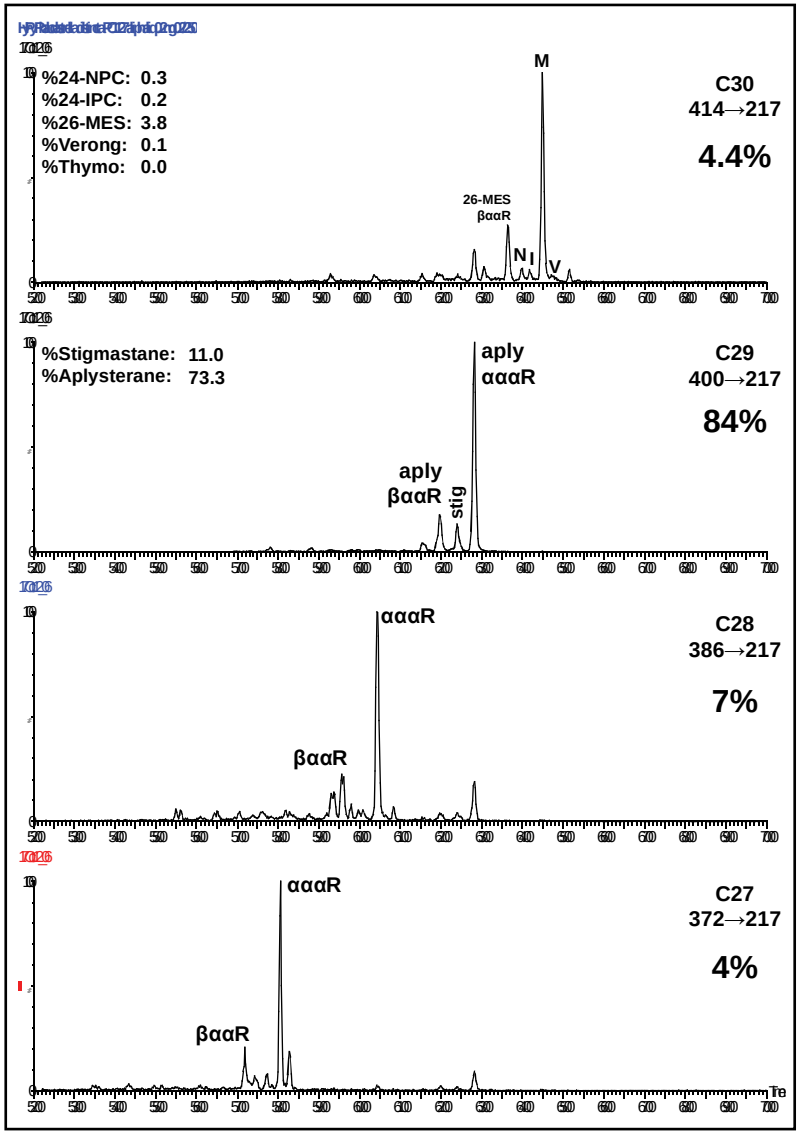

Sponge: *Rhabdastrella globostellata*
Lab ID: G317580

Phylum: Porifera
Class: Demospongiae
Subclass: Heteroscleromorpha
Order: Tetractinellida
Family: Ancorinidae
Genus: *Rhabdastrella*
Species: *Rhabdastrella globostellata*

Locality: Great Barrier Reef; Reef 21-490, Swain Reefs
Depth: 20m

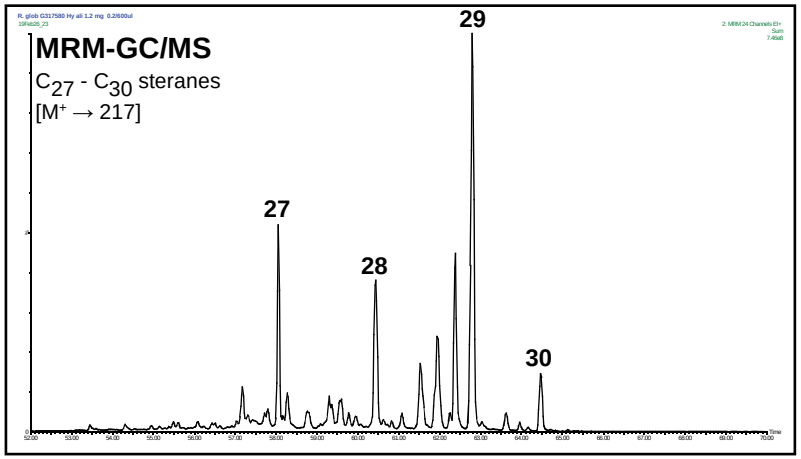

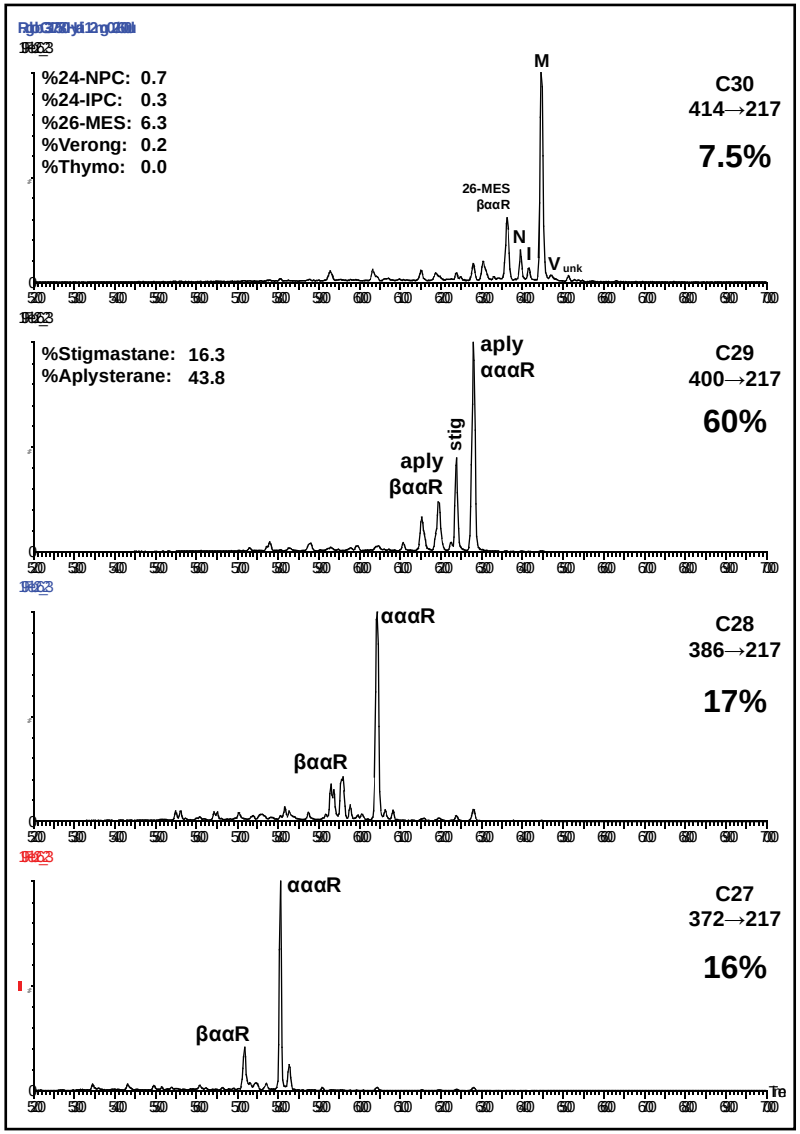

Sponge: *Rhabdastrella globostellata*
Lab ID: PC140

Phylum: Porifera
Class: Demospongiae
Subclass: Heteroscleromorpha
Order: Tetractinellida
Family: Ancorinidae
Genus: *Rhabdastrella*
Species: *Rhabdastrella globostellata*

Locality: Manus Island, Papua New Guinea
Depth: shallow

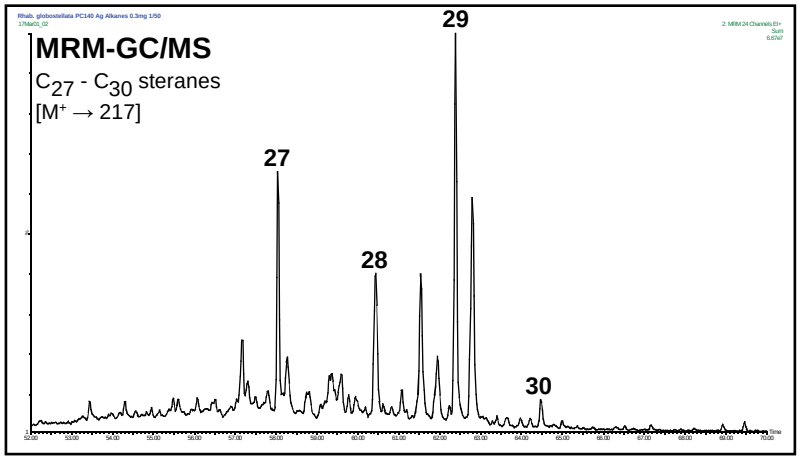

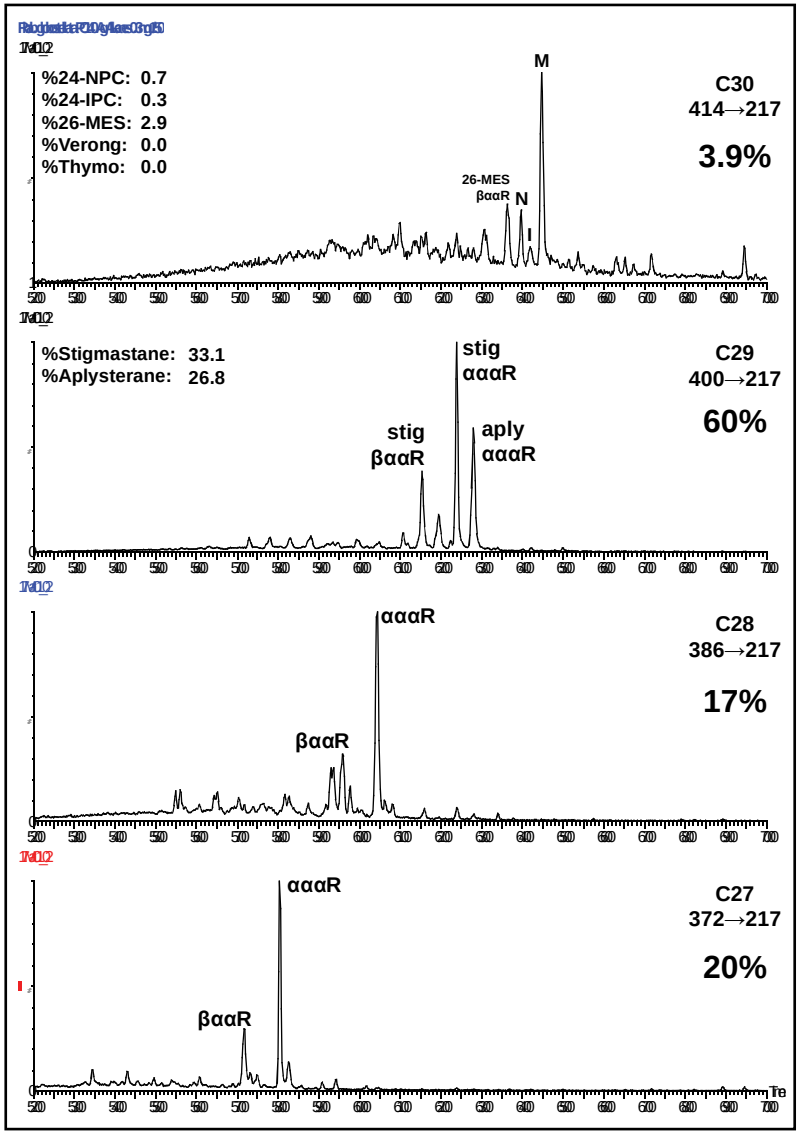

Sponge: *Rhabdastrella globostellata*
Lab ID: PC492

Phylum: Porifera
Class: Demospongiae
Subclass: Heteroscleromorpha
Order: Tetractinellida
Family: Ancorinidae
Genus: *Rhabdastrella*
Species: *Rhabdastrella globostellata*

Locality: Guam Island
Depth: shallow

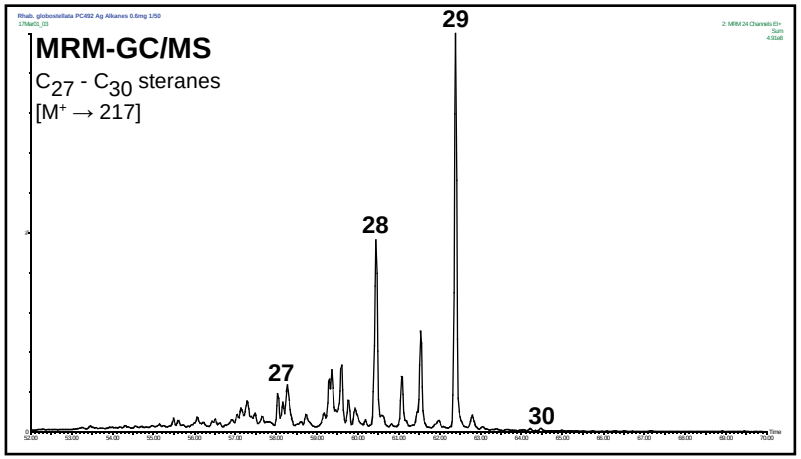

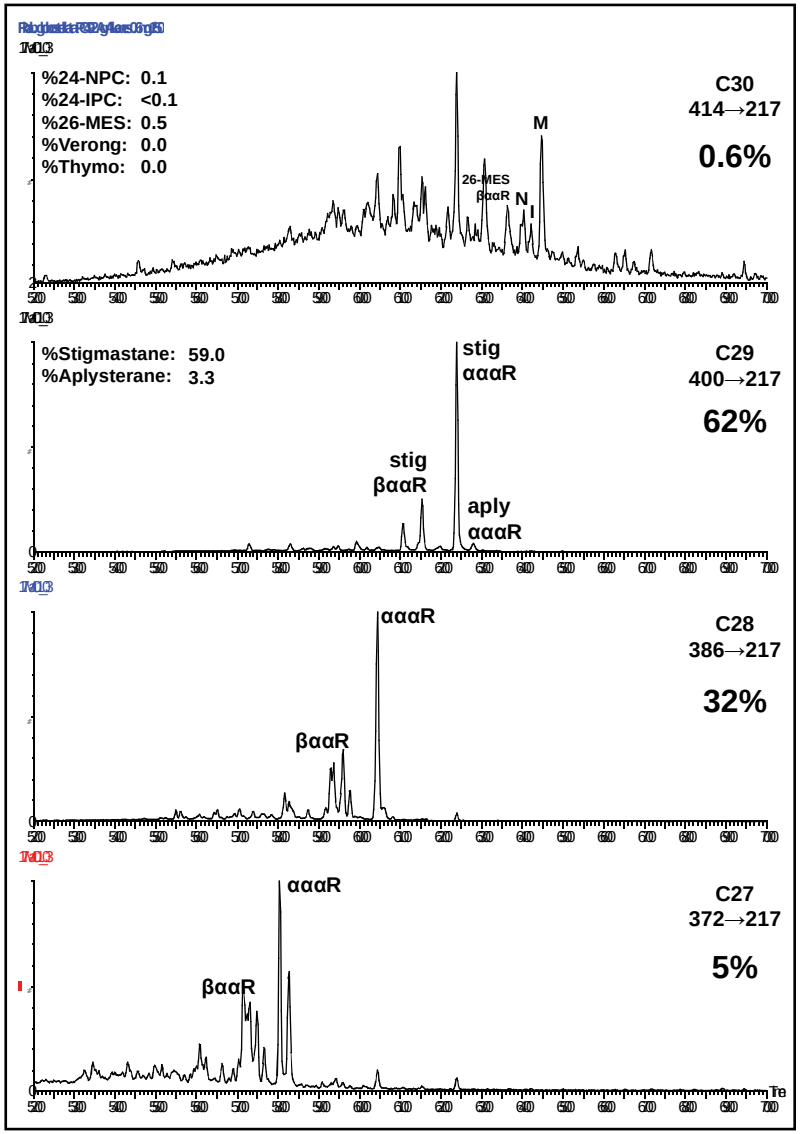

Sponge: *Rhabdastrella globostellata*
Lab ID: PC922

Phylum: Porifera
Class: Demospongiae
Subclass: Heteroscleromorpha
Order: Tetractinellida
Family: Ancorinidae
Genus: *Rhabdastrella*
Species: *Rhabdastrella globostellata*

Locality: Penghu Archipelago, Taiwan
Depth: shallow

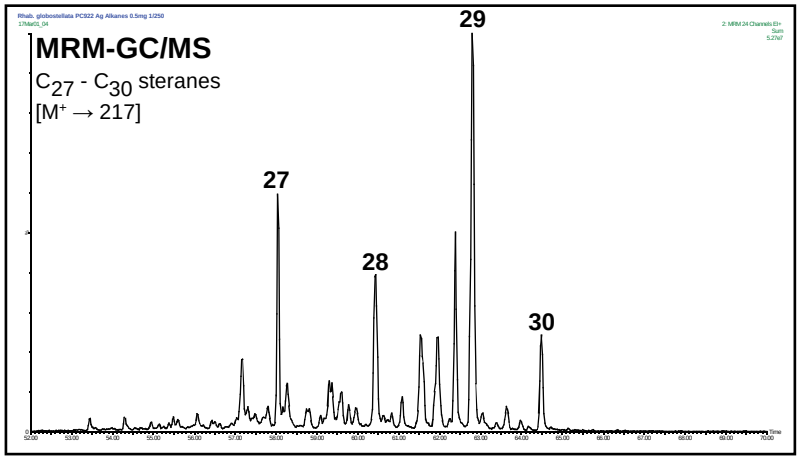

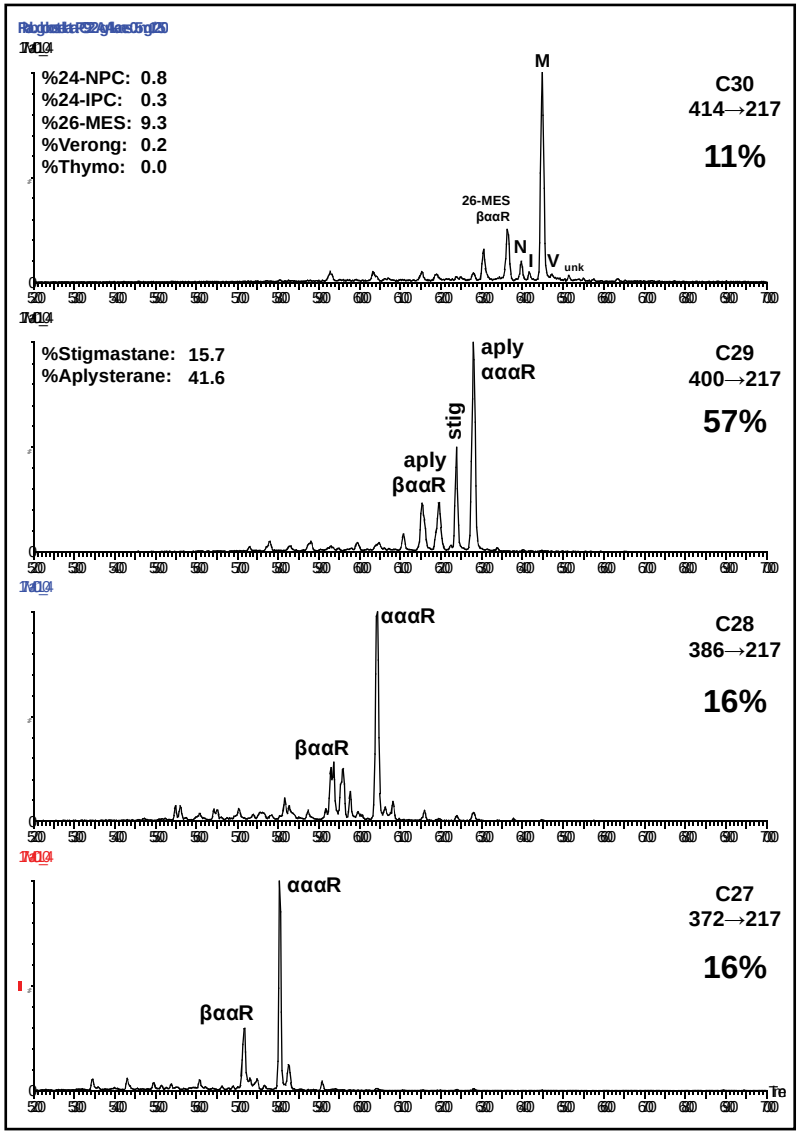

Sponge: *Rhabdastrella wondoensis*
Lab ID: PC865

Phylum: Porifera
Class: Demospongiae
Subclass: Heteroscleromorpha
Order: Tetractinellida
Family: Ancorinidae
Genus: *Rhabdastrella*
Species: *Rhabdastrella wondoensis*

Locality: Yeoseo Island, South Korea
Depth: shallow

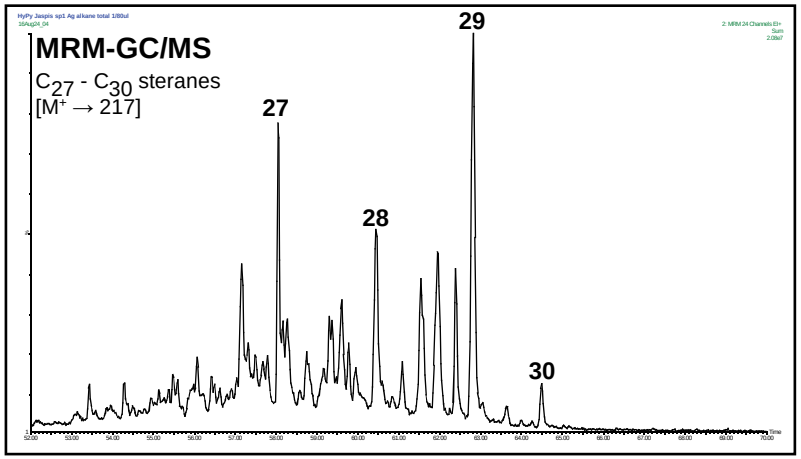

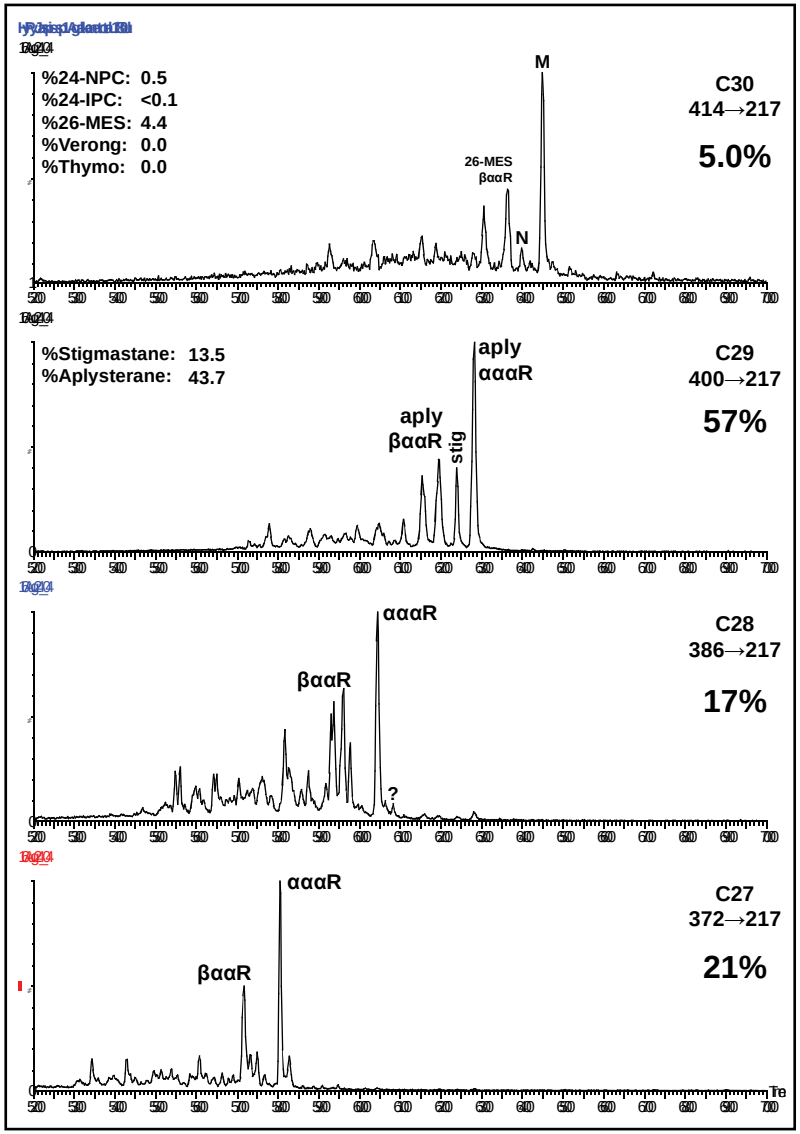

Sponge: *Rhabdastrella wondoensis*
Lab ID: PC866

Phylum: Porifera
Class: Demospongiae
Subclass: Heteroscleromorpha
Order: Tetractinellida
Family: Ancorinidae
Genus: *Rhabdastrella*
Species: *Rhabdastrella wondoensis*

Locality: Yeoseo Island, South Korea
Depth: shallow

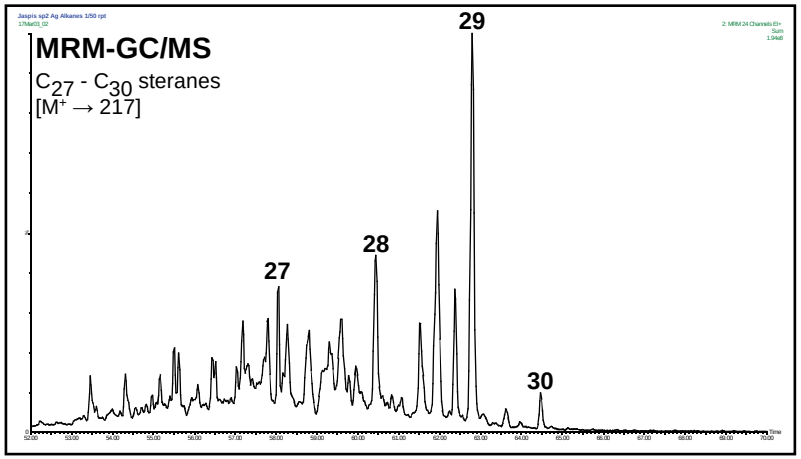

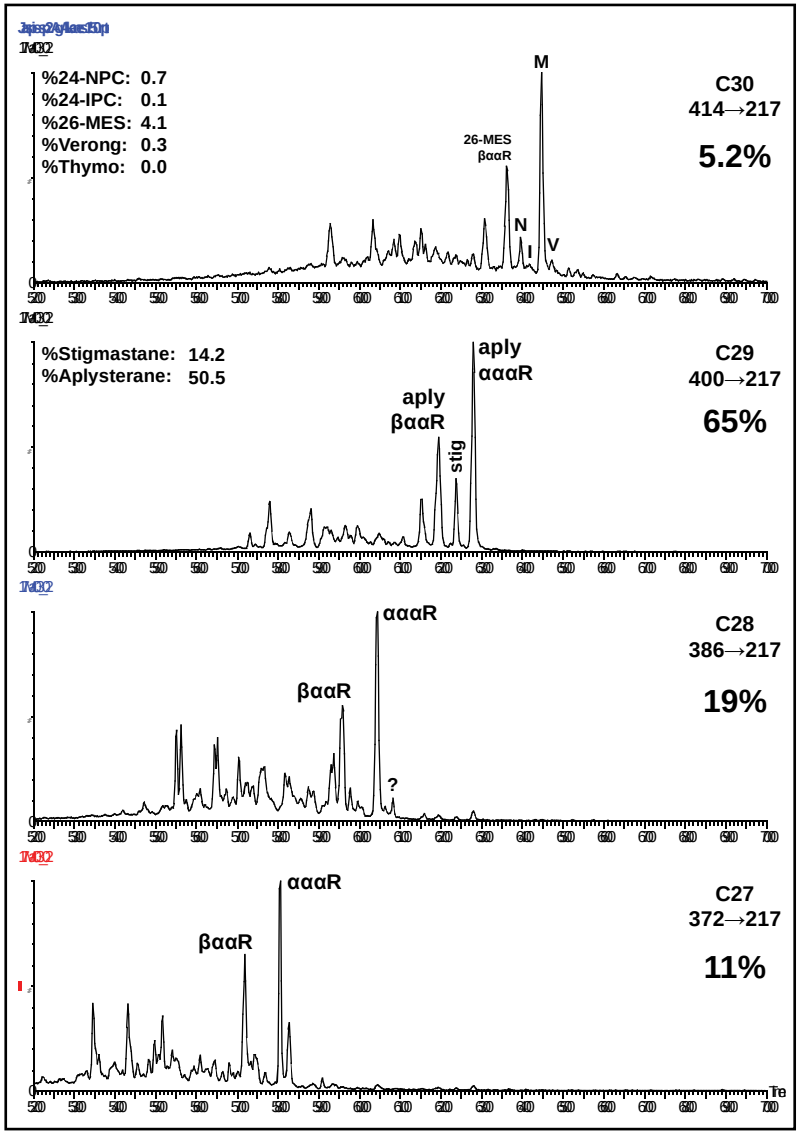

Sponge: *Stelletta tuberosa*
Lab ID: PC675

Phylum: Porifera
Class: Demospongiae
Subclass: Heteroscleromorpha
Order: Tetractinellida
Family: Ancorinidae
Genus: *Stelletta*
Species: *Stelletta tuberosa*

Locality: Flemish Cap, off Newfoundland, Canada
Depth: 1339m

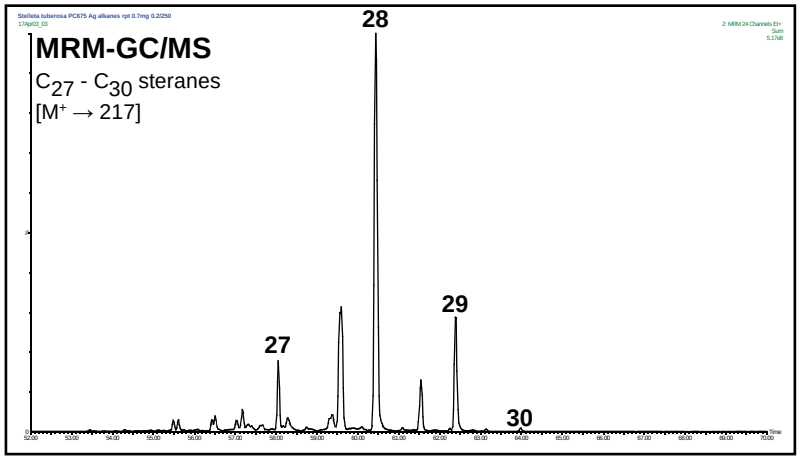

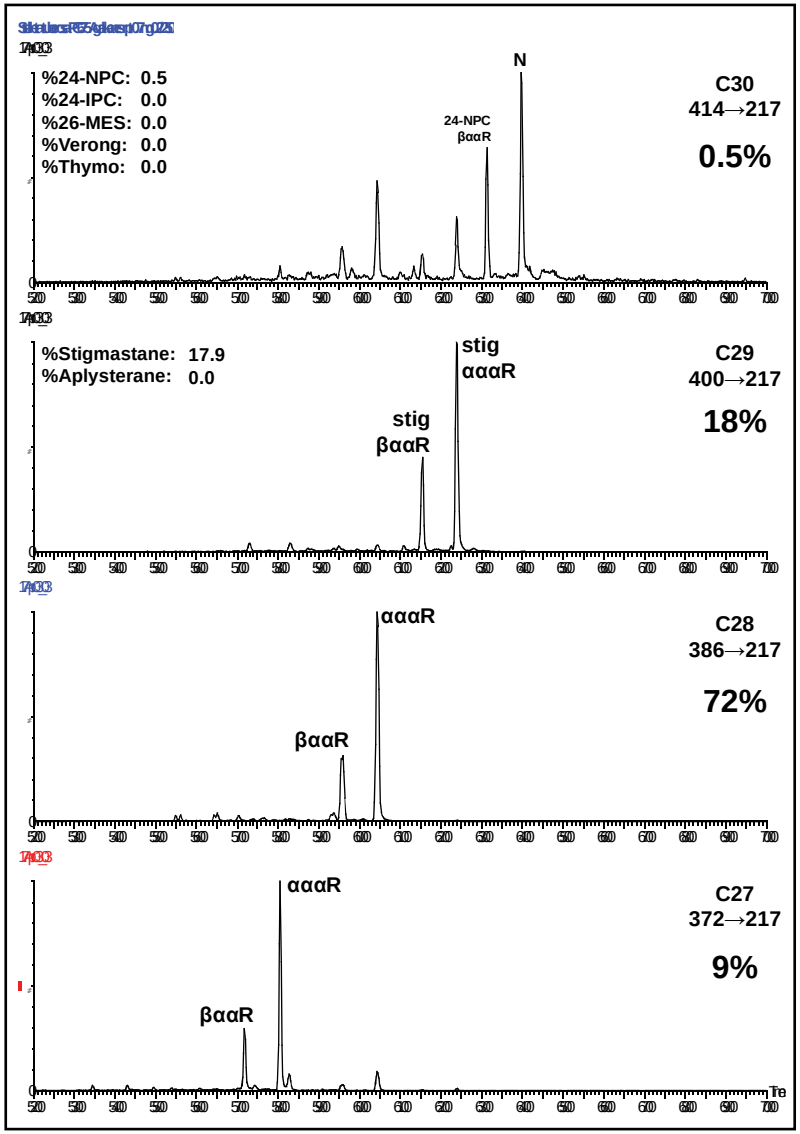

Sponge: *Suberites sp.*
Lab ID: sponge 2

Phylum: Porifera
Class: Demospongiae
Subclass: Heteroscleromorpha
Order: Suberitida
Family: Suberitidae
Genus: *Suberites*
Species: *Suberites sp.*

Locality: Marine Biological Lab, MA
Depth: shallow

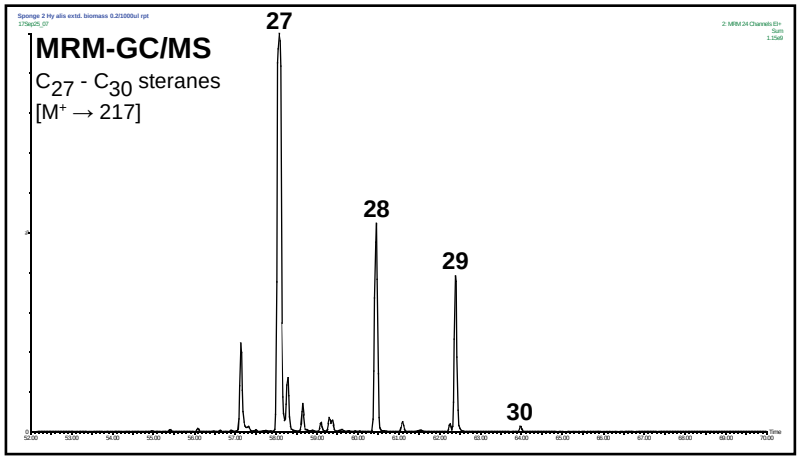

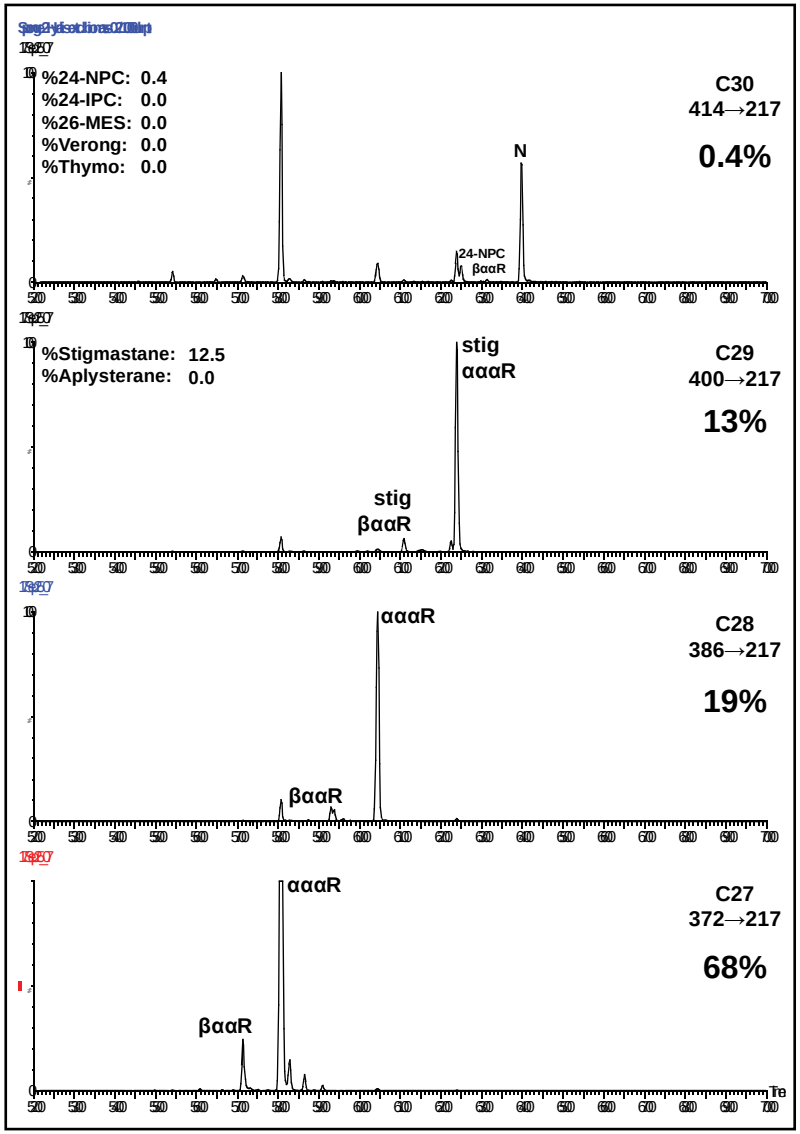

Sponge: *Thymosiopsis* cf. *cuticulatus*
Lab ID: Endoume

Phylum: Porifera
Class: Demospongiae
Subclass: Verongimorpha
Order: Chondrillida
Family: Chondrillidae
Genus: *Thymosiopsis*
Species: *Thymosiopsis* cf. *cuticulatus*

Locality: Endoume Cave, France
Depth: 7m

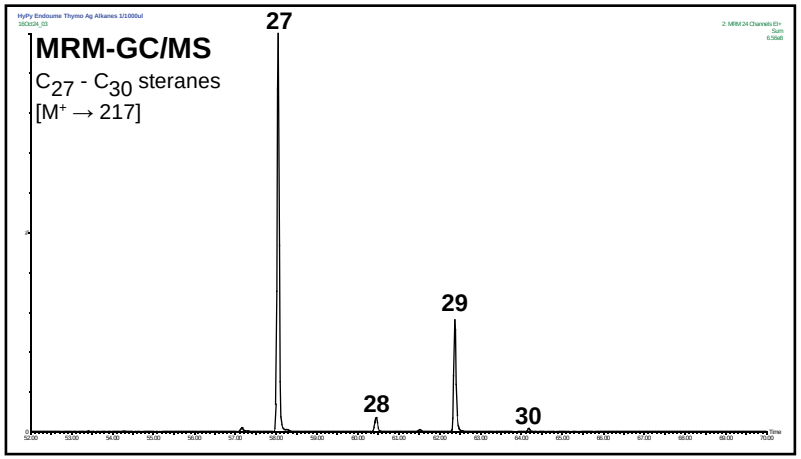

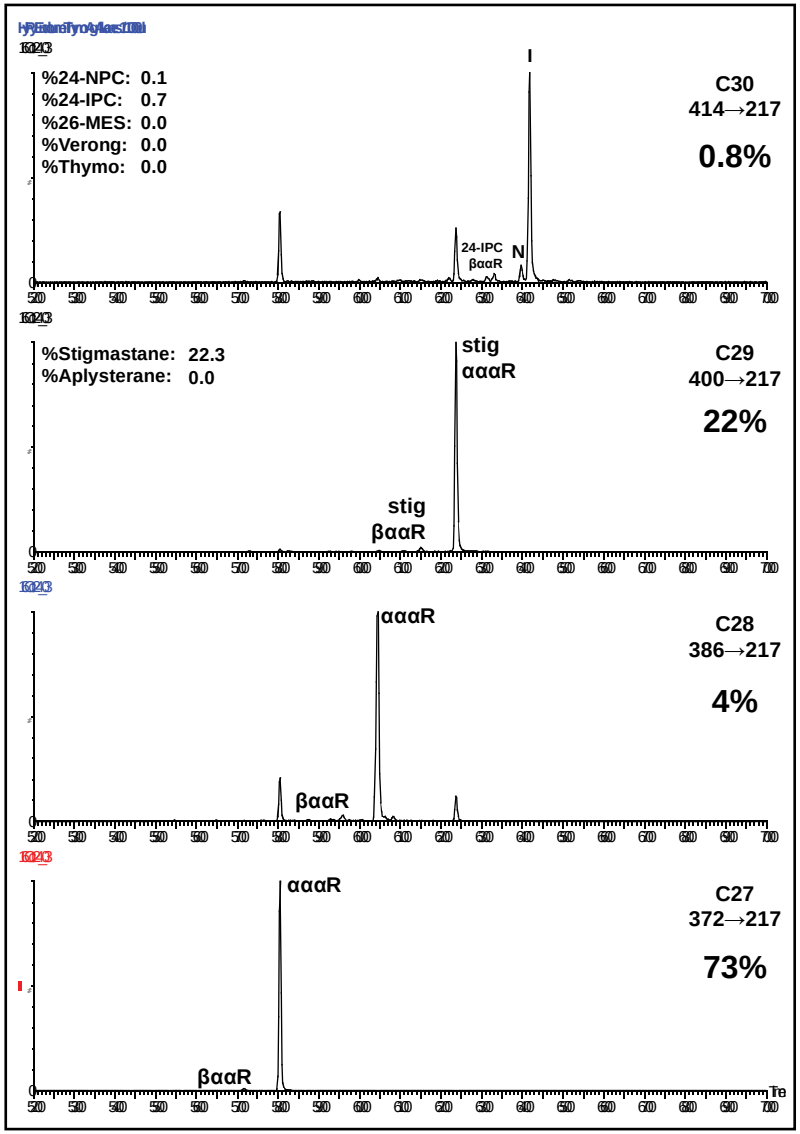

Sponge: *Thymosiopsis conglomerans*
Lab ID: Tremies

Phylum: Porifera
Class: Demospongiae
Subclass: Verongimorpha
Order: Chondrillida
Family: Chondrillidae
Genus: *Thymosiopsis*
Species: *Thymosiopsis conglomerans*

Locality: Tremies Cave, France
Depth: 12-13m

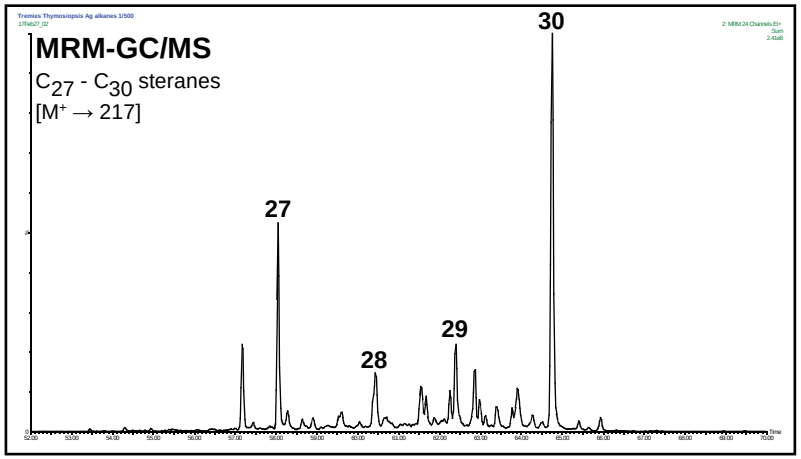

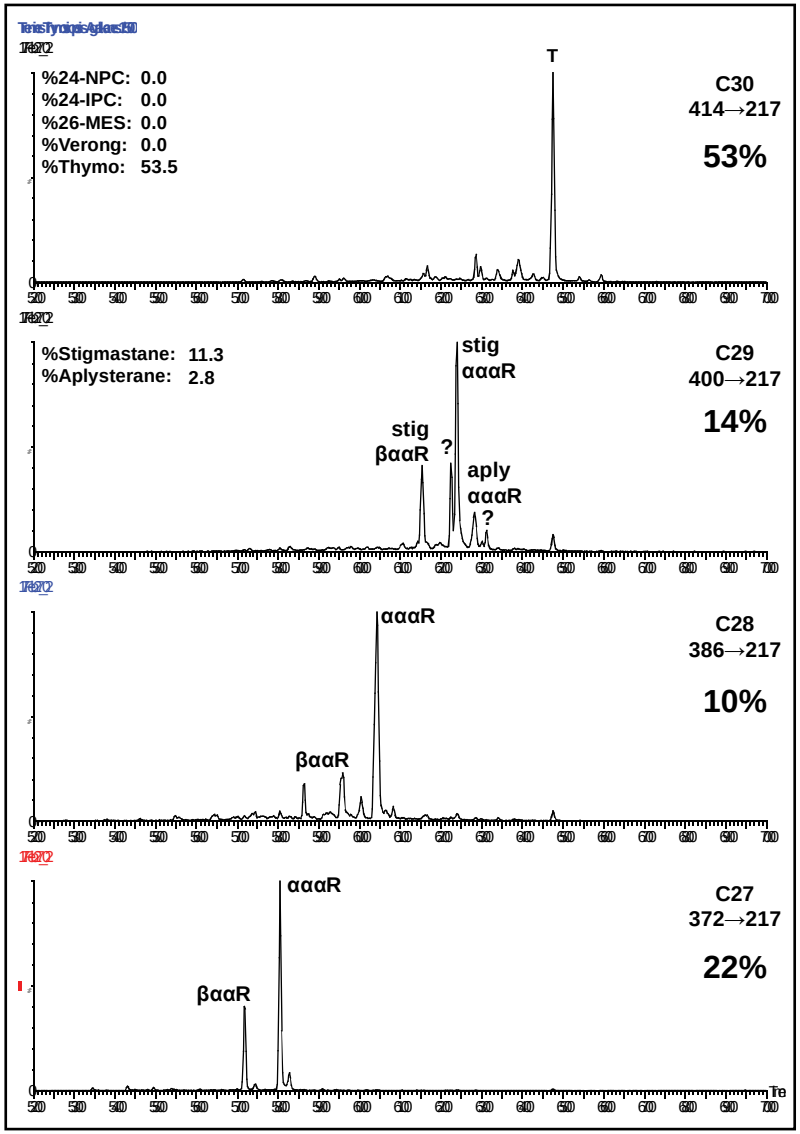

Sponge: *Vazella pourtalesii*
Lab ID: HUD16-019-B0362

Phylum: Porifera
Class: Hexactinellida
Subclass: Hexasterophora
Order: Lyssacinosida
Family: Rossellidae
Genus: *Vazella*
Species: *Vazella pourtalesii*

Locality: Emerald Basin, off Nova Scotia, Canada
Depth: 183-212m

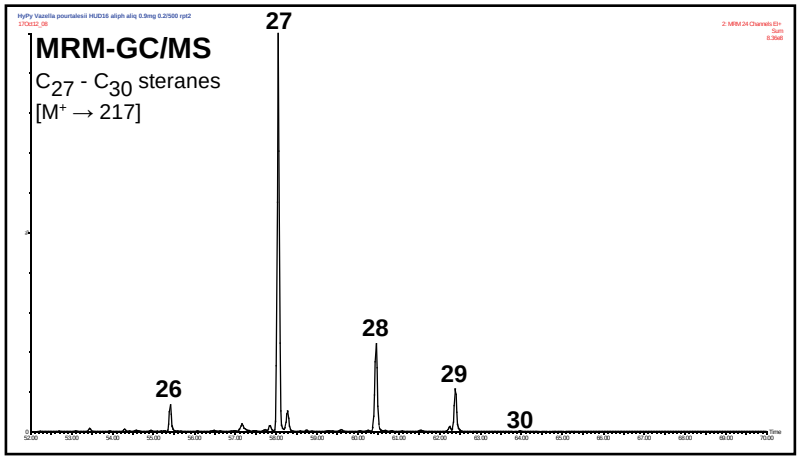

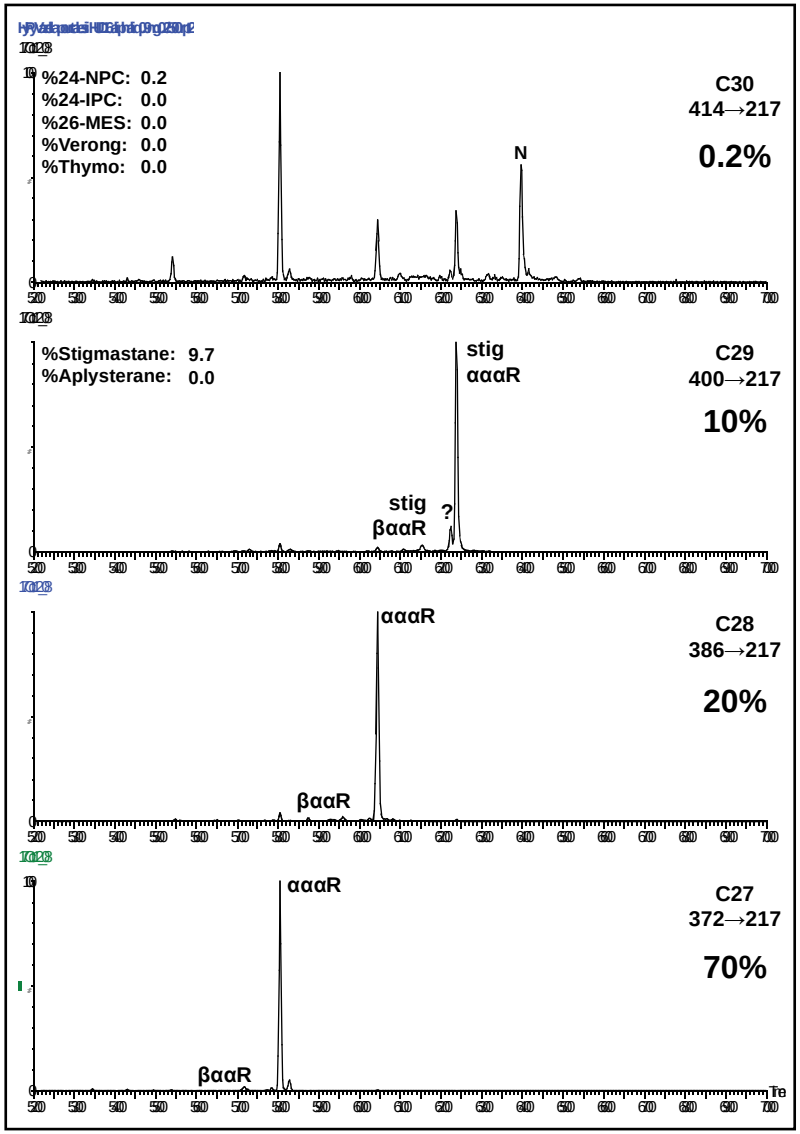

Sponge: *Verongula reiswigi*
Lab ID: BT-13

Phylum: Porifera
Class: Demospongiae
Subclass: Verongimorpha
Order: Verongiida
Family: Aplysinidae
Genus: *Verongula*
Species: *Verongula reiswigi*

Locality: Bocas del Toro, Panama
Depth: 3m

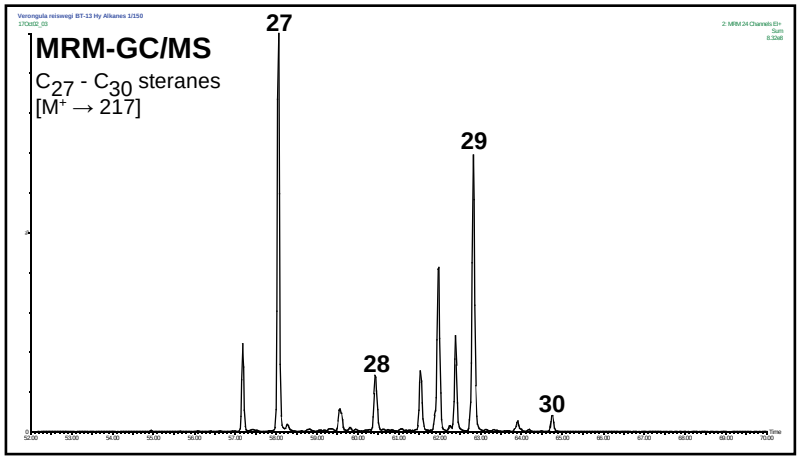

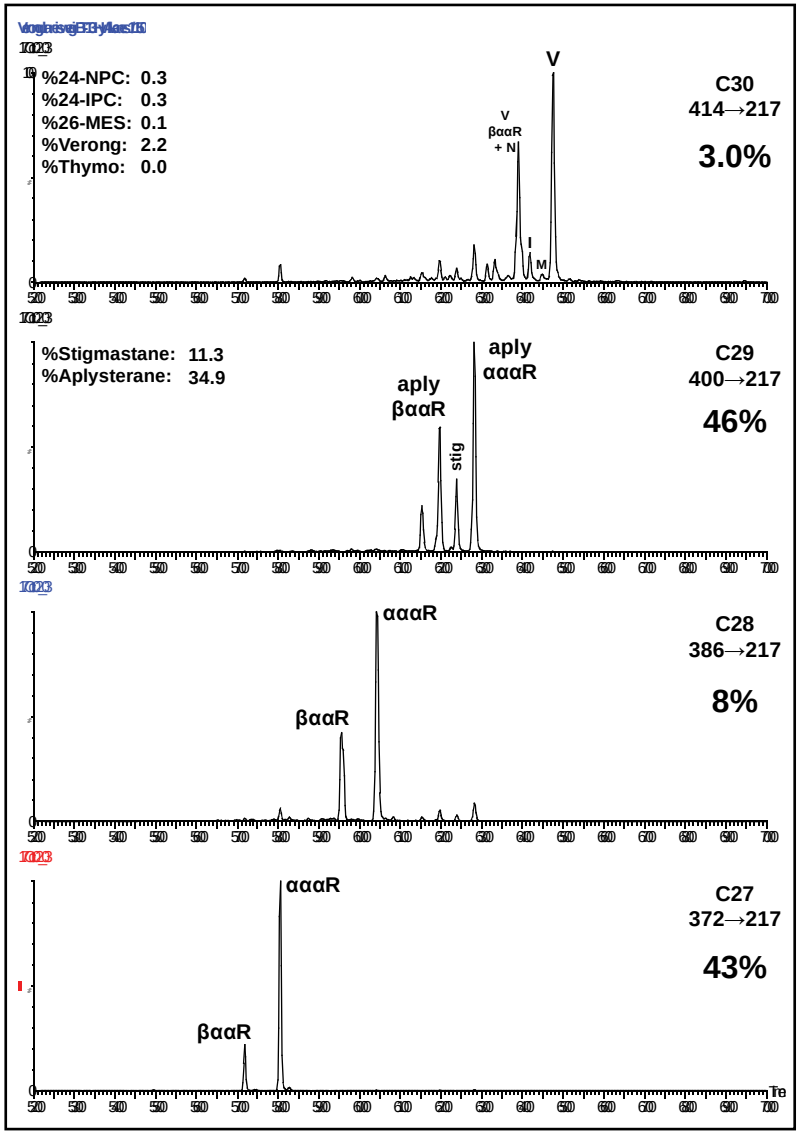

Sponge: *Verongula rigida*
Lab ID: sponge 8

Phylum: Porifera
Class: Demospongiae
Subclass: Verongimorpha
Order: Verongiida
Family: Aplysinidae
Genus: *Verongula*
Species: *Verongula rigida*

Locality: Bocas del Toro, Panama
Depth: 3m

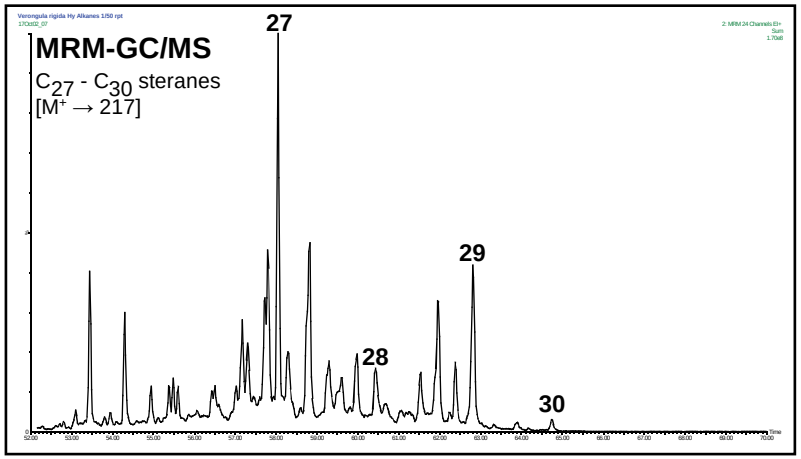

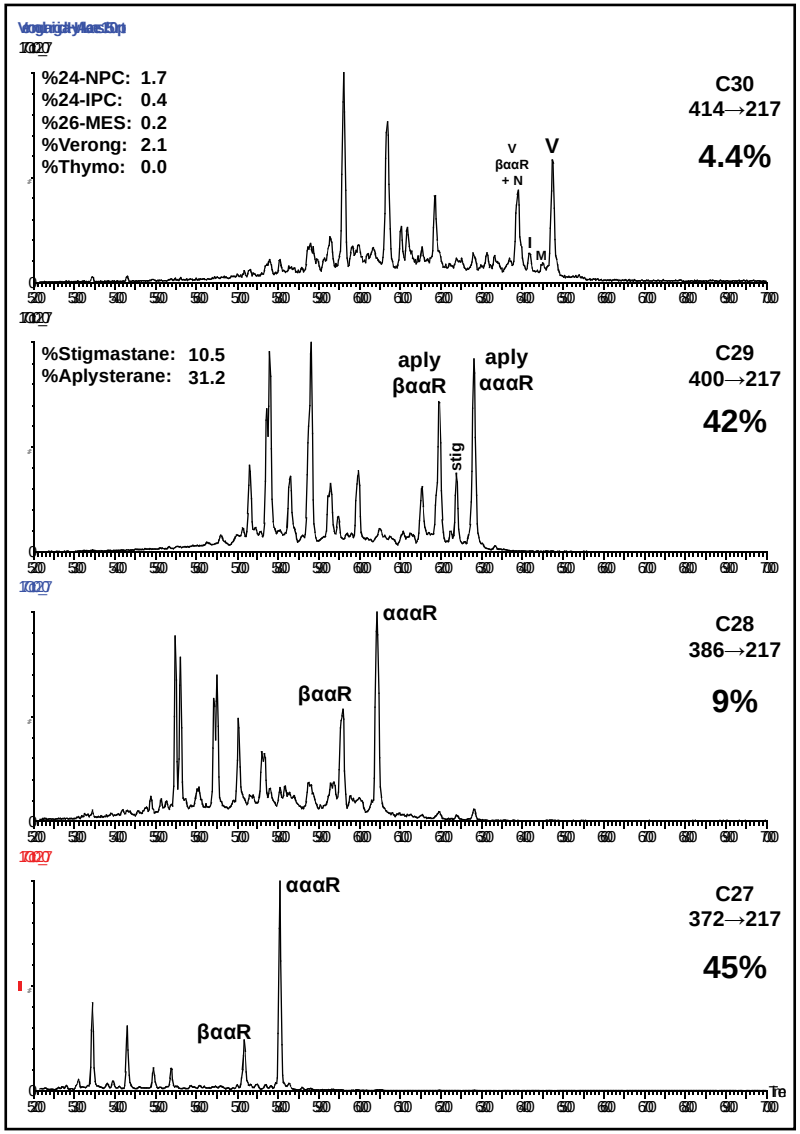

Appendix C: Sterol (TMS-ether) Distributions of Sponge Biomass

***Genus species* SpongeID**

Assignment: $C_n\Delta^x$ (n = number of total carbons; x = unsaturation site(s))

Name: Sterol Common Name

m/z: Fragment ion distributions; M+ denotes the molecular ion

%: Percent of Total Sterols

! Sponges starting with LabID MNHN-IP-2015-#### have similar sterol distributions due to a cross-contamination issue. These specimens were collected on the same cruise and added to a shared container with organic solvent (EtOH) which effectively extracted all free sterols.

***Aplysina aerophoba* TLE430**

Assignment	Name	m/z (relative abundance)	%
$C_{27}\Delta^{5,22}$	22(E/Z)-dehydrocholesterol	456(41,M^+), 441(10), 366(39), 351(18), 327(34), 255(19), 129(100)	5
$C_{27}\Delta^{5}$	cholesterol	458(38,M^+), 443(15), 368(63), 353(42), 329(91), 255(16), 129(100)	6
$C_{28}\Delta^{5,22}$	brassicasterol	470(38,M^+), 455(8), 380(42), 365(17), 341(26), 255(49), 129(100)	5
$C_{28}\Delta^{5,24}$	codisterol	470(31,M^+), 455(8), 380(38), 365(20), 341(21), 253(13), 129(100)	1
$C_{28}\Delta^{5}$	campesterol	472(36,M^+), 457(14), 382(60), 367(28), 343(77), 255(13), 129(100)	2
$C_{29}\Delta^{5,25}$	25-dehydroaplysterol isomer	484(40,M^+), 469(11), 394(38), 379(19), 355(19), 253(13), 129(100)	2
$C_{29}\Delta^{5,25}$	25-dehydroaplysterol	484(60,M^+), 469(14), 394(42), 379(42), 355(29), 255(15), 129(100)	45
$C_{29}\Delta^{5}$	aplysterol	486(43,M^+), 472(15), 396(90), 381(43), 357(80), 255(18), 129(100)	31
$C_{30}\Delta^{5,25}$	verongulasterol	498(33,M^+), 483(10), 408(34), 393(23), 369(18), 271(15), 129(100)	1

***Caminella intuta* PC1162**

Assignment	Name	m/z (relative abundance)	%
$C_{27}\Delta^{5,22}$	22(E/Z)-dehydrocholesterol	456(50,M^+), 441(13), 366(50), 351(35), 327(69), 255(50), 129(100)	1
$C_{27}\Delta^{5}$	cholesterol	458(44,M^+), 443(22), 368(89), 353(44), 329(96), 255(18), 129(100)	8
$C_{28}\Delta^{5,22}$	brassicasterol	470(41,M^+), 455(14), 380(41), 365(18), 341(25), 255(36), 129(100)	3
$C_{28}\Delta^{5,24(28)}$	24-methylenecholesterol	470(24,M^+), 455(20), 386(57), 365(24), 341(36), 296(36), 257(21), 129(100)	77
$C_{29}\Delta^{5,22}$	stigmasterol	484(43,M^+), 469(9), 394(34), 379(22), 355(27), 255(40), 129(100)	2
$C_{29}\Delta^{5,24(28)}$	fucosterol	484(9,M^+), 469(7), 396(27), 386(60), 357(27), 296(35), 255(16), 129(100)	6
$C_{29}\Delta^{5,24(28)}$	isofucosterol	484(4,M^+), 469(6), 398(9), 386(72), 371(18), 296(53), 255(19), 215(31), 129(100)	2
$C_{30}\Delta^{5,24(28)}$	24-*n*-propylcholesterol	498(5 ,M^+), 483(11), 386(100), 371(23), 296(65), 281(27), 257(24), 213(18), 129(94)	<1

***Cinachyrella kuekenthali* PC941**

Assignment	Name	m/z (relative abundance)	%
$C_{27}\Delta^{5,22}$	22(E/Z)-dehydrocholesterol	456(23,M^+), 442(6), 366(39), 351(21), 327(36), 282(34), 255(29), 129(100)	2
$C_{27}\Delta^{5}$	cholesterol	458(21,M^+), 443(12), 368(39), 353(24), 329(56), 255(12), 129(100)	14
$C_{28}\Delta^{5,22}$	brassicasterol	470(26,M^+), 455(6), 380(26), 365(13), 341(18), 255(33), 129(100)	9
$C_{28}\Delta^{5}$	campesterol	472(23,M^+), 457(7), 382(43), 367(20), 343(53), 255(10), 129(100)	14
$C_{29}\Delta^{5,22}$	stigmasterol	484(21,M^+), 469(5), 394(27), 379(10), 351(18), 255(30), 129(100)	6
$C_{29}\Delta^{5}$	sitosterol	486(26,M^+), 471(10), 396(51), 381(24), 357(57), 255(13), 129(100)	53
$C_{29}\Delta^{5,24(28)}$	isofucosterol	484(6,M^+), 469(7), 386(44), 371(9), 355(10), 296(38), 257(18), 129(100)	3

***Ciocalypta carballoi* PC1064**

Assignment	Name	m/z (relative abundance)	%
$C_{27}\Delta^{5}$	cholesterol		<1
$C_{28}\Delta^{5,22}$	brassicasterol	470(48,M^+), 455(13), 380(38), 365(23), 341(27), 255(50), 129(100)	1
$C_{29}\Delta^{5,22}$	stigmasterol	484(54,M^+), 469(12), 394(35), 379(15), 355(19), 255(54), 129(100)	4
$C_{29}\Delta^{5}$	sitosterol	486(33,M^+), 471(13), 396(58), 381(29), 357(66), 255(19), 129(100)	8
$C_{30}\Delta^{5,22}$	24-isopropyl-22-dehydrocholesterol	498(39,M^+), 483(9), 455(7), 408(30), 393(10), 365(100), 255(43), 129(81)	22
$C_{30}\Delta^{5,28(30)}$	24-isopropenylcholesterol	498(47,M^+), 483(13), 408(26), 393(17), 369(16), 253(15), 129(100)	1
$C_{30}\Delta^{5}$	24-isopropylcholesterol	500(37,M^+), 485(13), 410(83), 395(40), 371(81), 255(17), 129(100)	64

***Ciocalypta pencillius* Roscoff#1**

Assignment	Name	m/z (relative abundance)	%
$C_{27}\Delta^{5}$	cholesterol		<1
$C_{27}\Delta^{0}$	cholestanol	460(62,M^+), 445(100), 403(30), 370(32), 355(55), 305(30), 215(91)	67
$C_{28}\Delta^{5,22}$	brassicasterol	470(50,M^+), 455(11), 380(46), 365(20), 341(29), 255(49), 129(100)	5
$C_{28}\Delta^{22}$	22-dehydrocampestanol	472(100,M^+), 457(36), 374(54), 359(23), 345(71), 257(94)	1
$C_{28}\Delta^{5,24(28)}$	24-methylenecholesterol	470(13,M^+), 455(11), 386(44), 365(20), 341(13), 296(25), 253(23), 129(100)	<1
$C_{28}\Delta^{24(28)}$	24-methylenecholestanol	472(6,M^+), 457(25), 388(100), 373(32), 345(46), 255(24), 215(25)	1
$C_{28}\Delta^{0}$	campestanol	474(67,M^+), 459(100), 417(28), 384(33), 369(53), 305(28), 215(92)	3
$C_{29}\Delta^{5,22}$	stigmasterol	484(31,M^+), 469(8), 394(44), 379(13), 355(19), 255(28), 129(100)	2

$C_{29}\Delta^{5}$	sitosterol	486(26,M^+), 471(10), 396(46), 386(27), 381(20), 357(46), 296(16), 255(11), 129(100)	7
$C_{29}\Delta^{0}$	sitostanol	488(73,M^+), 473(100), 431(33), 398(33), 386(58), 215(100), 129(83)	12
$C_{29}\Delta^{24(28)}$	24(28)-dehydrositostanol	486(6,M^+), 471(9), 388(100), 373(25), 345(9), 305(12), 215(20)	1
$C_{30}\Delta^{5,24(28)}$	24-*n*-propylcholesterol	498(7,M^+), 483(5), 386(81), 371(18), 296(50), 257(21), 129(100)	1

***Cliona celata* Roscoff#12**

Assignment	Name	m/z (relative abundance)	%
$C_{27}\Delta^{5,22}$	22(E/Z)-dehydrocholesterol	456(54,M^+), 441(15), 366(62), 351(35), 327(69), 255(54), 129(100)	5
$C_{27}\Delta^{5}$	cholesterol	458(44,M^+), 443(22), 368(89), 353(44), 329(96), 255(18), 129(100)	59
$C_{27}\Delta^{0}$	cholestanol	460(50,M^+), 445(100), 403(23), 370(27), 355(43), 305(27), 215(100)	1
$C_{28}\Delta^{5,22}$	brassicasterol	470(58,M^+), 455(13), 380(66), 365(26), 341(39), 255(59), 129(100)	8
$C_{28}\Delta^{5,24(28)}$	24-methylenecholesterol	470(20,M^+), 455(19), 386(50), 365(23), 341(38), 296(29), 257(22), 129(100)	2
$C_{28}\Delta^{5}$	campesterol	472(49,M^+), 457(46), 382(86), 367(44), 343(100), 255(21), 129(97)	3
$C_{29}\Delta^{5,22}$	stigmasterol	484(57,M^+), 469(15), 394(54), 379(23), 355(34), 255(54), 129(100)	1
$C_{29}\Delta^{5}$	sitosterol	486(43,M^+), 471(13), 396(90), 381(42), 357(97), 255(20), 129(100)	19
$C_{29}\Delta^{5,24(28)}$	isofucosterol	484(8,M^+), 469(8), 386(100), 371(18), 355(8), 296(59), 257(26), 129(77)	2
$C_{30}\Delta^{5,24(28)}$	24-*n*-propylcholesterol	498(6,M^+), 483(8), 386(100), 371(21), 296(67), 257(32), 129(83)	<1

***Cymbastella* sp1 PC241**

Assignment	Name	m/z (relative abundance)	%
$C_{29}\Delta^{5,22}$	stigmasterol	484(52,M^+), 469(10), 394(38), 379(25), 355(15), 255(42), 129(100)	1
$C_{30}\Delta^{5,22}$	24-isopropyl-22-dehydrocholesterol	498(46,M^+), 483(10), 408(36), **365(100)**, 255(45), 129(68)	85
$C_{30}\Delta^{5}$	24-isopropylcholesterol	500(31,M^+), 485(12), 410(56), 395(27), 371(56), 255(13), 129(100)	14

***Cymbastella* sp2 PC852**

Assignment	Name	m/z (relative abundance)	%
$C_{29}\Delta^{5,22}$	stigmasterol	484(38,M^+), 469(11), 394(36), 379(17), 355(21), 255(43), 129(100)	2
$C_{30}\Delta^{5,22}$	24-isopropyl-22-dehydrocholesterol	498(43,M^+), 483(8), 408(35), **365(100)**, 255(44), 129(67)	68
$C_{30}\Delta^{5}$	24-isopropylcholesterol	500(32,M^+), 485(12), 410(58), 395(29), 371(58), 255(14), 129(100)	29
$C_{31}\Delta^{5,22}$	di-unsat C31 (co-occurs w/ 24-IPC)		1

***Discodermia polymorpha* PC1156**

Assignment	Name	m/z (relative abundance)	%
$C_{27}\Delta^{5,22}$	22(E/Z)-dehydrocholesterol	456(44,M^+), 441(11), 366(52), 351(22), 327(41), 255(39), 129(100)	1
$C_{27}\Delta^{5}$	cholesterol	458(38,M^+), 443(15), 368(73), 353(38), 329(82), 255(17), 129(100)	3
$C_{27}\Delta^{0}$	cholestanol	460(57,M^+), 445(100), 370(33), 355(60), 305(33), 215(86)	<1
$C_{28}\Delta^{5,22}$	brassicasterol	470(46,M^+), 455(11), 380(52), 365(23), 341(27), 255(43), 129(100)	2
$C_{28}\Delta^{5,24(28)}$	24-methylenecholesterol	470(18,M^+), 455(18), 386(48), 365(23), 341(31), 296(30), 257(18), 129(100)	7
$C_{28}\Delta^{5}$	campesterol	472(49,M^+), 457(18), 382(100), 367(44), 343(100), 255(19), 129(96)	14
$C_{29}\Delta^{5,22}$	stigmasterol	484(44,M^+), 469(27), 394(42), 379(18), 355(18), 255(38), 129(100)	1
$C_{29}\Delta^{5}$	sitosterol	486(59,M^+), 471(19), 396(100), 381(68), 357(100), 275(23), 255(31), 129(100)	72
$C_{29}\Delta^{0}$	sitostanol	488(69,M^+), 473(94), 431(32), 398(42), 383(94), 305(36), 215(100)	<1

***Erylus* sp. MNHN-IP-2015-1616**

Assignment	Name	m/z (relative abundance)	%
$C_{27}\Delta^{5,22}$	22(E/Z)-dehydrocholesterol	456(59,M^+), 441(12), 366(62), 351(32), 327(79), 255(47), 129(100)	1
$C_{27}\Delta^{5}$	cholesterol	458(48,M^+), 443(21), 368(83), 353(42), 329(100), 255(16), 129(96)	19
$C_{27}\Delta^{0}$	cholestanol	460(56,M^+), 445(83), 370(31), 355(44), 305(33), 215(100)	4
$C_{27}\Delta^{5,24}$	desmosterol	456(26,M^+), 441(14), 366(55), 351(31), 343(14), 327(33), 253(14), 129(100)	5
$C_{28}\Delta^{5,22}$	brassicasterol	470(39,M^+), 455(5), 380(48), 365(18), 341(20), 255(40), 129(100)	2
$C_{28}\Delta^{5,24}$	codisterol	470(38,M^+), 455(28), 380(41), 365(32), 341(27), 255(18), 129(100)	1
$C_{28}\Delta^{5,24(28)}$	24-methylenecholesterol	470(15,M^+), 455(16), 386(44), 380(24), 365(18), 341(35), 296(26), 253(19), 129(100)	13
$C_{28}\Delta^{5}$	campesterol	472(36,M^+), 457(15), 382(78), 367(36), 343(73), 129(100)	2
$C_{29}\Delta^{5,22}$	stigmasterol	484(31,M^+), 469(11), 394(33), 379(12), 355(23), 255(27), 129(100)	1
$C_{29}\Delta^{5}$	petrosterol [cyclopropyl]	484(41,M^+), 469(12), 394(66), 379(26), 355(55), 255(13), 129(100)	13
$C_{29}\Delta^{5}$	sitosterol	486(25,M^+), 471(8), 396(46), 381(21), 357(45), 255(15), 129(100)	22
$C_{29}\Delta^{5,24(28)}$	isofucosterol	484(14,M^+), 469(13), 386(58), 371(13), 355(48), 296(49), 257(20), 129(100)	1
$C_{30}\Delta^{5,22}$	24-isopropyl-22-dehydrocholesterol	498(30,M^+), 483(6), 408(19), 393(6), **365(68)**, 255(25), 129(100)	8
$C_{30}\Delta^{5}$	24-isopropylcholesterol	500(28,M^+), 485(8), 410(53), 395(22), 371(49), 255(9), 129(100)	8

***Geodia barretti* PC529**

Assignment	Name	m/z (relative abundance)	%
$C_{27}\Delta^{5,22}$	22(E/Z)-dehydrocholesterol	456(59,M^+), 442(17), 366(59), 351(33), 327(65), 255(67), 129(100)	2
$C_{27}\Delta^{5}$	cholesterol	458(41,M^+), 443(18), 368(75), 353(39), 329(100), 255(21), 129(90)	3
$C_{28}\Delta^{5,22}$	brassicasterol	470(47,M^+), 455(13), 380(51), 365(24), 341(36), 255(51), 129(100)	2
$C_{28}\Delta^{5,24(28)}$	24-methylenecholesterol	470(19, M^+), 455(15), 386(52), 365(25), 341(35), 296(32), 257(22), 129(100)	79
$C_{28}\Delta^{5}$	campesterol	472(41,M^+), 457(16), 382(79), 367(37), 343(100), 255(31), 129(95)	1
$C_{29}\Delta^{5,22}$	stigmasterol	484(45,M^+), 469(14), 394(43), 379(23), 355(37), 255(36), 129(100)	1
$C_{29}\Delta^{5,24(28)}$	fucosterol	486(10,M^+), 469(9), 396(20), 386(70), 371(13), 357(21), 296(43), 257(20), 129(100)	10
$C_{29}\Delta^{5,24(28)}$	isofucosterol	484(10,M^+), 469(11), 386(100), 371(23), 343(9), 296(67), 257(23), 129(97)	2
$C_{30}\Delta^{5,24(28)}$	24-*n*-propylcholesterol	498(10,M^+), 483(4), 386(98), 371(18), 343(12), 296(59), 257(18), 129(100)	<1

***Geodia barretti* PC617**

Assignment	Name	m/z (relative abundance)	%
$C_{27}\Delta^{5}$	cholesterol	458(33,M+), 443(12), 368(63), 353(47), 329(100), 129(93)	11
$C_{28}\Delta^{5,22}$	brassicasterol	470(31,M+), 455(5), 380(39), 365(23), 341(30), 255(45), 129(100)	7
$C_{28}\Delta^{5,24(28)}$	24-methylenecholesterol	470(13,M+), 455(13), 386(31), 380(25), 365(30), 341(30), 296(35), 257(20), 129(100)	58
$C_{29}\Delta^{5,24(28)}$	fucosterol	484(10,M+), 469(15), 386(60), 371(10), 355(38), 296(42), 129(100)	19
$C_{29}\Delta^{5,24(28)}$	isofucosterol	484(10,M+), 386(67), 296(50), 129(100)	5

***Geodia* cf. *vaubani* MNHN-IP-2015-1667**

Assignment	Name	m/z (relative abundance)	%
$C_{27}\Delta^{5,22}$	22(E/Z)-dehydrocholesterol	456(42,M^+), 441(10), 366(60), 351(31), 327(53), 255(56), 129(100)	2
$C_{27}\Delta^{5}$	cholesterol	458(49,M^+), 443(21), 368(89), 353(46), 329(100), 255(20), 129(92)	11
$C_{27}\Delta^{0}$	cholestanol	460(66,M^+), 445(100), 370(28), 355(59), 305(30), 215(88)	4
$C_{27}\Delta^{5,24}$	desmosterol	456(18,M^+), 441(12), 366(35), 351(19), 343(19), 327(35), 253(10), 129(100)	1
$C_{28}\Delta^{5,22}$	brassicasterol	470(57,M^+), 455(8), 380(55), 365(15), 341(30), 255(38), 129(100)	2
$C_{28}\Delta^{5,24(28)}$	24-methylenecholesterol	470(19,M^+), 455(17), 386(47), 380(27), 365(20), 341(32), 296(27), 253(17), 129(100)	17
$C_{28}\Delta^{5}$	campesterol	472(44,M^+), 457(27), 388(50), 382(82), 367(41), 343(87), 129(100)	4

$C_{29}\Delta^{5,22}$	stigmasterol	484(42,M^+), 471(10), 394(42), 379(16), 355(21), 255(37), 129(100)	2
$C_{29}\Delta^{5}$	petrosterol [cyclopropyl]	484(39,M^+), 469(12), 394(65), 379(25), 355(49), 255(18), 129(100)	5
$C_{29}\Delta^{5}$	sitosterol	486(40,M^+), 471(15), 396(80), 381(36), 357(80), 255(15), 129(100)	50
$C_{30}\Delta^{5,22}$	24-isopropyl-22-dehydrocholesterol	498(29,M^+), 483(6), 408(27), **365(71)**, 341(14), 255(29), 129(100)	1
$C_{30}\Delta^{5}$	24-isopropylcholesterol	500(28,M^+), 485(10), 410(59), 395(28), 371(53), 255(10), 129(100)	1

***Geodia hentscheli* GhII**

Assignment	Name	m/z (relative abundance)	%
$C_{27}\Delta^{5,22}$	22(E/Z)-dehydrocholesterol	456(30,M^+), 441(11), 366(51), 351(34), 327(58), 255(56), 129(100)	3
$C_{27}\Delta^{5}$	cholesterol	458(26,M^+), 443(16), 368(49), 353(41), 329(71), 255(13), 129(100)	4
$C_{28}\Delta^{5,22}$	brassicasterol	470(36,M^+), 455(11), 380(39), 365(17), 341(27), 255(50), 129(100)	5
$C_{28}\Delta^{5,24(28)}$	24-methylenecholesterol	470(15,M^+), 455(13), 386(43), 380(26), 365(19), 341(30), 296(26), 257(17), 129(100)	76
$C_{29}\Delta^{5,24(28)}$	fucosterol	486(10,M^+), 469(7), 396(15), 386(68), 371(10), 357(22), 296(34), 257(16), 129(100)	11
$C_{29}\Delta^{5,24(28)}$	isofucosterol	484(6,M^+), 469(10), 386(83), 371(13), 343(13), 296(58), 257(25), 129(100)	2
$C_{30}\Delta^{5,24(28)}$	24-*n*-propylcholesterol	498(5,M^+), 484(8), 386(89), 371(25), 343(10), 296(60), 257(28), 129(100)	<1

***Geodia pachydermata* PC681**

Assignment	Name	m/z (relative abundance)	%
$C_{27}\Delta^{5}$	cholesterol	458(30,M+), 443(30), 368(22), 353(19), 327(22), 129(100)	3
$C_{28}\Delta^{5,22}$	brassicasterol	470(48,M+), 380(24), 341(35), 129(100)	2
$C_{28}\Delta^{5,24(28)}$	24-methylenecholesterol	470(10,M+), 455(10), 386(21), 371(10), 343(21), 296(15), 129(100)	65
$C_{29}\Delta^{5,22}$	stigmasterol		<1
$C_{29}\Delta^{5,24(28)}$	fucosterol	486(17,M+), 386(53), 356(58), 296(48), 257(34), 129(100)	30
$C_{29}\Delta^{5,24(28)}$	isofucosterol		<1

***Geodia parva* GpII**

Assignment	Name	m/z (relative abundance)	%
$C_{27}\Delta^{5,22}$	22(E/Z)-dehydrocholesterol	456(50,M+), 441(23), 366(81), 351(31), 327(63), 255(48), 129(100)	1
$C_{27}\Delta^{5}$	cholesterol	458(47,M+), 443(17), 368(80), 353(40), 329(97), 255(23), 129(100)	1

$C_{28}\Delta^{5,22}$	brassicasterol	470(55,M+), 455(15), 380(71), 365(41), 341(42), 255(63), 129(100)	1
$C_{28}\Delta^{5,24}$	codisterol	470(63,M+), 455(17), 380(63), 365(23), 341(41), 255(14), 129(100)	1
$C_{28}\Delta^{5}$	campesterol		<1
$C_{29}\Delta^{5,22}$	stigmasterol	484(62,M+), 469(11), 394(39), 379(28), 351(26), 314(47), 255(49), 129(100)	1
$C_{29}\Delta^{5,24(28)}$	24(28)-dehydroaplysterol	484(13,M+), 469(13), 394(24), 386(60), 371(15), 355(28), 296(40), 257(21), 129(100)	88
$C_{30}\Delta^{5,28(30)}$	24-isopropenylcholesterol	498(35,M+), 483(10), 408(14), 386(18), 369(16), 343(16), 255(16), 129(100)	<1
$C_{30}\Delta^{5,24(28)}$	24-*n*-propylcholesterol	498(13,M+), 484(10), 386(79), 371(25), 357(25), 296(70), 257(38), 129(100)	<1
$C_{30}\Delta^{5,25}$	verongulasterol	498(31,M+), 483(6), 408(33), 394(11), 385(14), 368(17), 253(11), 129(100)	1
$C_{30}\Delta^{5,24(28)}$	isostelliferasterol	498(4,M+), 483(5), 408(4), 386(98), 371(20), 343(8), 296(56), 257(25), 129(100)	4
$C_{30}\Delta^{5,24(28)}$	xestosterol	498(11,M+), 483(8), 386(95), 371(20), 343(10), 296(71), 257(18), 129(100)	1

***Geodia parva* PC994**

Assignment	Name	m/z (relative abundance)	%
$C_{27}\Delta^{5,22}$	22(E/Z)-dehydrocholesterol		<1
$C_{27}\Delta^{5}$	cholesterol	458(37,M+), 443(12), 368(61), 353(30), 329(67), 255(18), 129(100)	1
$C_{28}\Delta^{5,22}$	brassicasterol	470(24,M+), 455(7), 380(25), 365(11), 341(16), 255(39), 129(100)	1
$C_{28}\Delta^{5,24}$	codisterol	470(45,M+), 455(13), 380(27), 365(27), 341(33), 129(100)	<1
$C_{28}\Delta^{5}$	campesterol	472(22,M+), 457(30), 382(74), 367(37), 343(86), 129(100)	<1
$C_{29}\Delta^{5,22}$	stigmasterol	484(31,M+), 469(7), 394(33), 379(9), 355(17), 255(28), 129(100)	1
$C_{29}\Delta^{5,24(28)}$	24(28)-dehydroaplysterol	484(19,M+), 469(17), 386(80), 371(18), 355(35), 296(43), 129(100)	92
$C_{30}\Delta^{5,28(30)}$	24-isopropenylcholesterol	498(53,M+), 483(8), **408(34)**, 393(17), 369(28), 129(100)	<1
$C_{30}\Delta^{5,24(28)}$	24-*n*-propylcholesterol	498(7,M+), 483(14), **386(66)**, 371(7), 356(8), 296(43), 129(100)	<1
$C_{30}\Delta^{5,25}$	verongulasterol	498(38,M+), 408(25), 368(13), 129(100)	1
$C_{30}\Delta^{5,24(28)}$	isostelliferasterol	498(3,M+), 483(4), **386(58)**, 371(12), 296(38), 257(19), 129(100)	3
$C_{30}\Delta^{5,24(28)}$	xestosterol	498(14,M+), 483(13), 408(9), **386(26)**, 371(8), 341(18), 296(18), 253(18), 129(100)	<1
$C_{31}\Delta^{5,24(28)}$	28-methylxestosterol	512(4,M+), 428(19), **386(53)**, 355(25), 296(20), 129(100)	<1

***Geodia* sp 2 MNHN-IP-2015-1649**

Assignment	Name	m/z (relative abundance)	%
$C_{27}\Delta^{5,22}$	22(E/Z)-dehydrocholesterol	456(43,M^+), 441(20), 366(56), 351(35), 327(50), 255(36), 129(100)	2
$C_{27}\Delta^{5}$	cholesterol	458(48,M^+), 443(21), 368(79), 353(45), 329(97), 255(14), 129(100)	22
$C_{27}\Delta^{5,24}$	desmosterol	456(30,M^+), 441(15), 366(53), 351(25), 343(21), 327(43), 253(10), 129(100)	7
$C_{28}\Delta^{5,22}$	brassicasterol	470(55,M^+), 455(16), 380(63), 365(22), 341(26), 255(45), 129(100)	2
$C_{28}\Delta^{5,24(28)}$	24-methylenecholesterol	470(16,M^+), 455(16), 386(44), 380(28), 365(20), 341(31), 296(24), 253(14), 129(100)	18
$C_{28}\Delta^{5}$	campesterol	472(44,M^+), 457(22), 382(81), 367(44), 343(84), 129(100)	3
$C_{29}\Delta^{5,22}$	stigmasterol		<1
$C_{29}\Delta^{5}$	petrosterol [cyclopropyl]	484(36,M^+), 469(12), 394(80), 379(29), 355(60), 255(12), 129(100)	14
$C_{29}\Delta^{5}$	sitosterol	486(30,M^+), 471(13), 396(56), 381(25), 357(57), 255(12), 129(100)	18
$C_{30}\Delta^{5,22}$	24-isopropyl-22-dehydrocholesterol	498(43,M^+), 483(11), 408(33), **365(100)**, 255(39), 129(98)	6
$C_{30}\Delta^{5}$	24-isopropylcholesterol	500(35,M^+), 485(10), 410(68), 395(30), 371(60), 255(10), 129(100)	8

***Geodia* sp 8 MNHN-IP-2015-1545**

Assignment	Name	m/z (relative abundance)	%
$C_{27}\Delta^{5,22}$	22(E/Z)-dehydrocholesterol	456(55,M^+), 441(24), 366(73), 351(30), 327(100), 255(47), 129(91)	3
$C_{27}\Delta^{5}$	cholesterol	458(46,M^+), 443(21), 368(84), 353(43), 329(77), 255(14), 129(100)	22
$C_{27}\Delta^{0}$	cholestanol	460(100,M^+), 445(69), 370(42), 355(29), 305(42), 215(92)	7
$C_{27}\Delta^{5,24}$	desmosterol	456(38,M^+), 441(21), 366(83), 351(23), 343(58), 327(79), 253(29), 129(100)	2
$C_{28}\Delta^{5,22}$	brassicasterol	470(86,M^+), 455(9), 380(100), 365(45), 341(45), 255(32), 129(91)	3
$C_{28}\Delta^{5,24(28)}$	24-methylenecholesterol	470(21,M^+), 455(26), 386(62), 380(24), 365(14), 341(26), 296(14), 253(14), 129(100)	11
$C_{28}\Delta^{5}$	campesterol	472(31,M^+), 457(21), 388(29), 382(50), 367(19), 341(50), 129(100)	5
$C_{29}\Delta^{5,22}$	stigmasterol		4
$C_{29}\Delta^{5}$	petrosterol [cyclopropyl]	484(100,M^+), 469(44), 394(79), 379(74), 355(71), 255(22), 129(47)	5
$C_{29}\Delta^{5}$	sitosterol	486(40,M^+), 471(21), 396(71), 381(26), 357(80), 255(10), 129(100)	30
$C_{30}\Delta^{5,22}$	24-isopropyl-22-dehydrocholesterol	498(87,M^+), 483(13), 408(100), **365(85)**, 341(56), 255(56), 129(56)	3
$C_{30}\Delta^{5}$	24-isopropylcholesterol	500(48,M^+), 485(6), 410(100), 395(22), 371(37), 255(12), 129(92)	4

***Halichondria lutea* 17-V-88-4-005**

Assignment	Name	m/z (relative abundance)	%
$C_{27}\Delta^{5}$	cholesterol	458(43,M^+), 443(17), 368(76), 353(43), 329(90), 255(15), 129(100)	<1
$C_{28}\Delta^{5,22}$	brassicasterol	470(53,M^+), 455(8), 380(60), 365(29), 341(17), 255(36), 129(100)	<1
$C_{29}\Delta^{5,22}$	stigmasterol	484(43,M^+), 471(14), 394(53), 379(20), 355(15), 255(39), 129(100)	<1
$C_{30}\Delta^{5,22}$	24-isopropyl-22-dehydrocholesterol	498(43,M^+), 483(9), 408(37), **365(100)**, 255(37), 129(57)	43
$C_{30}\Delta^{5}$	24-isopropylcholesterol	500(49,M^+), 485(15), 410(97), 395(43), 371(94), 255(16), 129(100)	52
$C_{31}\Delta^{5,22}$	di-unsat C31 (co-occurs w/ 24-IPC)	512(33,M^+), 497(5), 469(100), 400(7), 387(21), 357(43), 129(36)	1
$C_{31}\Delta^{5}$	mono-unsat C31 (co-occurs w/ 24-IPC)	514(100, M^+), 499(15), 424(15), 409(42), 129(45)	4

***Halichondria lutea* 17-V-88-4-007**

Assignment	Name	m/z (relative abundance)	%
$C_{27}\Delta^{5}$	cholesterol	458(38,M^+), 443(15), 368(88), 353(50), 329(100), 255(19), 129(96)	<1
$C_{28}\Delta^{5,22}$	brassicasterol	470(55,M^+), 455(18), 380(36), 365(27), 341(36), 255(55), 129(100)	<1
$C_{29}\Delta^{5,22}$	stigmasterol	484(73,M^+), 471(11), 394(61), 379(22), 355(17), 255(56), 129(100)	1
$C_{30}\Delta^{5,22}$	24-isopropyl-22-dehydrocholesterol	498(43,M^+), 483(8), 408(37), **365(100)**, 255(40), 129(71)	97
$C_{30}\Delta^{5}$	24-isopropylcholesterol	500(42,M^+), 485(15), 410(85), 395(38), 371(73), 255(9), 129(100)	2

***Hexadella dedritifera* #12**

Assignment	Name	m/z (relative abundance)	%
$C_{26}\Delta^{5,22}$	24-nor-dehydrocholestrol	442(9,M+), 427(5), 352(7), 338(7), 314(12), 255(19), 129(46), 97(100)	4
$C_{27}\Delta^{5,22}$	22(E/Z)-dehydrocholesterol	456(17,M+), 441(6), 366(16), 351(10), 327(28), 255(34), 129(100)	11
$C_{27}\Delta^{5}$	cholesterol	458(18,M^+), 443(11), 368(42), 353(16), 329(53), 129(100)	48
$C_{28}\Delta^{5,22}$	brassicasterol	470(18,M^+), 455(2), 380(19), 365(11), 341(8), 255(23), 129(100)	11
$C_{28}\Delta^{5,24(28)}$	24-methylenecholesterol	470(7,M^+), 455(7), 386(14), 365(13), 341(10), 296(10), 257(13), 129(100)	15
$C_{29}\Delta^{5}$	sitosterol	486(12,M^+), 471(5), 396(17), 381(9), 357(19), 255(5), 129(100)	12

***Hymeniacidon perlevis* Roscoff#11**

Assignment	Name	m/z (relative abundance)	%
$C_{27}\Delta^{0}$	cholestanol	460(60,M^+), 445(100), 403(31), 370(34), 355(58), 305(31), 215(88)	80
$C_{28}\Delta^{5,22}$	brassicasterol	470(51,M^+), 455(13), 380(49), 365(26), 341(28), 255(49), 129(100)	1
$C_{28}\Delta^{5,24(28)}$	24-methylenecholesterol	470(29,M^+), 455(14), 386(34), 380(27), 365(18), 343(25), 296(22), 257(15), 129(100)	<1
$C_{28}\Delta^{24(28)}$	24-methylenecholestanol	472(9,M^+), 457(28), 388(100), 373(29), 345(29), 305(16), 255(24), 215(28)	1
$C_{28}\Delta^{0}$	campestanol	474(73,M^+), 459(100), 417(27), 384(27), 369(39), 305(29), 215(97)	1
$C_{29}\Delta^{5,22}$	stigmasterol	484(37,M^+), 469(5), 394(26), 379(26), 355(13), 255(32), 129(100)	<1
$C_{29}\Delta^{5,24(28)}$	fucosterol	484(9,M^+), 469(9), 386(75), 371(13), 355(15), 296(38), 257(15), 129(100)	12
$C_{29}\Delta^{5,24(28)}$	isofucosterol	484(8,M^+), 469(8), 386(93), 371(18), 355(8), 296(59), 257(22), 129(100)	4

***Jaspis* sp. MNHN-IP-2015-1891**

Assignment	Name	m/z (relative abundance)	%
$C_{27}\Delta^{5,22}$	22(E/Z)-dehydrocholesterol	456(58,M^+), 441(19), 366(45), 351(22), 327(45), 255(31), 129(100)	1
$C_{27}\Delta^{5}$	cholesterol	458(50,M^+), 443(18), 368(81), 353(41), 329(95), 255(14), 129(100)	19
$C_{27}\Delta^{0}$	cholestanol	460(43,M^+), 445(97), 370(24), 355(48), 305(24), 215(100)	3
$C_{27}\Delta^{5,24}$	desmosterol	456(25,M^+), 441(10), 366(39), 351(21), 343(21), 327(29), 253(10), 129(100)	5
$C_{28}\Delta^{5,22}$	brassicasterol	470(40,M^+), 455(19), 380(45), 365(17), 341(31), 255(33), 129(100)	2
$C_{28}\Delta^{5,24(28)}$	24-methylenecholesterol	470(15,M^+), 455(16), 386(41), 380(24), 365(19), 341(28), 296(23), 253(23), 129(100)	13
$C_{28}\Delta^{5}$	campesterol	472(41,M^+), 457(14), 382(77), 367(29), 343(77), 255(15), 129(100)	2
$C_{29}\Delta^{5,22}$	stigmasterol	484(24,M^+), 469(5), 394(42), 379(12), 355(40), 255(40), 129(100)	1
$C_{29}\Delta^{5}$	petrosterol [cyclopropyl]	484(38,M^+), 469(12), 394(57), 379(23), 355(48), 255(13), 129(100)	11
$C_{29}\Delta^{5}$	sitosterol	486(23,M^+), 471(9), 396(39), 381(18), 357(41), 255(11), 129(100)	26
$C_{30}\Delta^{5,22}$	24-isopropyl-22-dehydrocholesterol	498(28,M^+), 483(7), 408(17), **365(63)**, 255(27), 129(100)	7
$C_{30}\Delta^{5}$	24-isopropylcholesterol	500(29,M^+), 485(5), 410(54), 395(21), 371(46), 255(10), 129(100)	9

***Pachataxa enigmatica* MNHN-IP-2015-1781**

Assignment	Name	m/z (relative abundance)	%
$C_{27}\Delta^{5}$	cholesterol	458(40,M^+), 443(18), 368(78), 353(42), 329(100), 255(17), 129(84)	20
$C_{27}\Delta^{5,24}$	desmosterol	456(33,M^+), 441(17), 366(67), 351(30), 343(28), 327(59), 129(100)	4
$C_{28}\Delta^{5,22}$	brassicasterol	470(61,M^+), 455(14), 380(67), 365(28), 341(38), 255(62), 129(100)	2
$C_{28}\Delta^{5,24(28)}$	24-methylenecholesterol	470(15,M^+), 455(14), 386(52), 365(22), 341(36), 296(30), 257(20), 129(100)	17
$C_{28}\Delta^{5}$	campesterol	472(47,M^+), 457(17), 382(87), 367(44), 343(100), 255(20), 129(98)	3
$C_{29}\Delta^{5,22}$	stigmasterol	484(55,M^+), 469(20), 394(56), 379(25), 355(24), 255(50), 129(100)	1
$C_{29}\Delta^{5}$	petrosterol [cyclopropyl]	484(47,M^+), 469(14), 394(78), 379(31), 355(72), 255(19), 129(100)	12
$C_{29}\Delta^{5}$	sitosterol	486(32,M^+), 471(12), 396(68), 381(31), 357(72), 255(20), 129(100)	24
$C_{30}\Delta^{5,22}$	24-isopropyl-22-dehydrocholesterol	498(36,M^+), 483(9), 408(30), 393(10), **365(100)**, 255(41), 129(83)	6
$C_{30}\Delta^{5}$	24-isopropylcholesterol	500(39,M^+), 485(11), 410(80), 395(31), 371(74), 255(17), 129(100)	11

***Pachymatisma johnstonia* Roscoff#4**

Assignment	Name	m/z (relative abundance)	%
$C_{27}\Delta^{5}$	cholesterol	458(67,M^+), 443(21), 368(36), 353(42), 329(36), 255(13), 129(100)	10
$C_{28}\Delta^{5,22}$	brassicasterol	470(60,M^+), 455(11), 380(35), 365(10), 341(20), 255(58), 129(100)	5
$C_{28}\Delta^{5,24(28)}$	24-methylenecholesterol	470(23,M^+), 455(10), 386(43), 365(21), 341(31), 296(22), 257(15), 129(100)	42
$C_{29}\Delta^{5,24(28)}$	fucosterol	484(5,M^+), 469(8), 386(69), 371(10), 355(10), 296(39), 257(16), 129(100)	33
$C_{29}\Delta^{5,24(28)}$	isofucosterol	484(9,M^+), 469(12), 386(84), 371(11), 355(8), 296(40), 257(27), 129(100)	9

***Pachymatisma normani* PC952**

Assignment	Name	m/z (relative abundance)	%
$C_{27}\Delta^{5,22}$	22(E/Z)-dehydrocholesterol	456(66,M+), 441(19), 366(78), 351(35), 327(64), 255(64), 129(100)	3
$C_{27}\Delta^{5}$	cholesterol	458(51,M+), 443(17), 368(81), 353(43), 329(97), 255(20), 129(100)	6
$C_{28}\Delta^{5,22}$	brassicasterol	470(54,M+), 455(17), 380(52), 365(26), 341(37), 255(65), 129(100)	3
$C_{28}\Delta^{5,24(28)}$	24-methylenecholesterol	470(18,M+), 455(16), 386(45), 365(19), 341(33), 296(27), 257(20), 129(100)	43
$C_{29}\Delta^{5,22}$	stigmasterol		<1
$C_{29}\Delta^{5,24(28)}$	fucosterol	484(8,M+), 469(8), 386(82), 371(17), 355(18), 296(45), 257(18), 129(100)	41
$C_{29}\Delta^{5,24(28)}$	isofucosterol	484(10,M+), 473(10), 386(77), 371(22), 296(50), 281(45), 257(22), 129(100)	3
$C_{30}\Delta^{5,24(28)}$	24-*n*-propylcholesterol		<1

***Petromica* sp 4-VI-88-1-003**

Assignment	Name	m/z (relative abundance)	%
$C_{30}\Delta^{5,22}$	24-isopropyl-22-dehydrocholesterol	498(42,M^+), 483(8), 408(33), **365(100)**, 255(33), 129(83)	99
$C_{30}\Delta^{5}$	24-isopropylcholesterol	500(43,M^+), 485(16), 410(95), 395(41), 371(82), 255(30), 129(100)	1

***Petrosia (Strongylophora) corticata* PC1211**

Assignment	Name	m/z (relative abundance)	%
$C_{29}\Delta^{5,25(27)}$	strongylosterol	498(62,M^+), 483(13), 408(36), 393(19), 369(22), 255(11), 129(100)	100

***Petrosia (Strongylophora)* sp1 MNHN-IP-2015-1558**

Assignment	Name	m/z (relative abundance)	%
$C_{27}\Delta^{5}$	cholesterol	458(36,M^+), 443(15), 368(53), 353(51), 329(96), 255(14), 129(100)	20
$C_{27}\Delta^{0}$	cholestanol		4
$C_{27}\Delta^{5,24}$	desmosterol	456(21,M^+), 441(16), 366(28), 351(15), 343(27), 327(24), 129(100)	5
$C_{28}\Delta^{5,22}$	brassicasterol	470(36,M^+), 455(21), 380(80), 365(29), 341(43), 255(36), 129(100)	1
$C_{28}\Delta^{5,24(28)}$	24-methylenecholesterol	470(20,M^+), 455(13), 386(32), 365(14), 341(22), 296(17), 257(14), 129(100)	12
$C_{28}\Delta^{5}$	campesterol	472(21,M^+), 457(11), 382(19), 367(26), 343(63), 255(27), 129(100)	3
$C_{29}\Delta^{5,22}$	stigmasterol		<1
$C_{29}\Delta^{5}$	petrosterol [cyclopropyl]	484(13,M^+), 469(13), **394(57)**, 379(15), 355(67), 255(7), 129(100)	14
$C_{29}\Delta^{5}$	sitosterol	486(27,M^+), 471(8), 396(47), 381(14), 357(46), 255(8), 129(100)	20
$C_{30}\Delta^{5,22}$	24-isopropyl-22-dehydrocholesterol	498(24,M^+), 483(4), 408(18), 393(7), **365(92)**, 255(24), 129(100)	9
$C_{30}\Delta^{5}$	24-isopropylcholesterol	500(20,M^+), 485(11), 410(46), 395(11), 371(38), 255(7), 129(100)	10

***Petrosia (Strongylophora)* sp2 MNHN-IP-2015-1557**

Assignment	Name	m/z (relative abundance)	%
$C_{27}\Delta^{5}$	cholesterol	458(48,M^+), 443(16), 368(62), 353(43), 329(100), 255(22), 129(93)	21
$C_{27}\Delta^{5,24}$	desmosterol	456(20,M^+), 441(13), 366(52), 351(32), 343(48), 327(10), 129(100)	4
$C_{28}\Delta^{5,22}$	brassicasterol		<1
$C_{28}\Delta^{5,24(28)}$	24-methylenecholesterol	470(30,M^+), 455(31), 386(52), 365(23), 341(24), 296(30), 257(20), 129(100)	10
$C_{28}\Delta^{5}$	campesterol		<1

$C_{29}\Delta^{5,22}$	stigmasterol		<1
$C_{29}\Delta^{5}$	petrosterol [cyclopropyl]	484(48,M^+), 469(11), **394(57)**, 379(27), 355(74), 255(16), 129(100)	17
$C_{29}\Delta^{5}$	sitosterol	486(29,M^+), 471(11), 396(53), 381(24), 357(63), 255(13), 129(100)	24
$C_{30}\Delta^{5,22}$	24-isopropyl-22-dehydrocholesterol	498(39,M^+), 483(7), 408(21), 393(14), **365(100)**, 255(46), 129(96)	10
$C_{30}\Delta^{5}$	24-isopropylcholesterol	500(35,M^+), 485(10), 410(81), 395(33), 371(74), 255(11), 129(100)	12

***Petrosia (Strongylophora)* sp2 PC1212**

Assignment	Name	m/z (relative abundance)	%
$C_{27}\Delta^{5,22}$	22(E/Z)-dehydrocholesterol	456(54,M^+), 441(10), 366(38), 351(19), 327(52), 255(29), 129(100)	1
$C_{27}\Delta^{5}$	cholesterol	458(50,M^+), 443(35), 368(86), 353(45), 329(95), 255(14), 129(100)	1
$C_{28}\Delta^{5,22}$	brassicasterol	470(26,M^+), 455(10), 380(47), 365(14), 341(25), 255(35), 129(100)	2
$C_{28}\Delta^{5,24(28)}$	24-methylenecholesterol	470(11,M^+), 455(16), 386(29), 365(14), 341(23), 296(12), 257(13), 129(100)	1
$C_{28}\Delta^{5}$	campesterol	472(51,M^+), 457(19), 382(70), 367(33), 343(77), 255(13), 129(100)	16
$C_{29}\Delta^{5,22}$	stigmasterol	484(40,M^+), 469(19), 394(25), 379(12), 355(10), 255(16), 129(100)	1
$C_{29}\Delta^{5}$	sitosterol	486(47,M^+), 471(13), 396(87), 381(37), 357(84), 255(13), 129(100)	80

***Petrosia (Strongylophora)* sp4 MNHN-IP-2015-1644**

Assignment	Name	m/z (relative abundance)	%
$C_{27}\Delta^{5}$	cholesterol	458(61,M^+), 443(18), 368(69), 353(40), 329(77), 255(15), 129(100)	20
$C_{27}\Delta^{5,24}$	desmosterol	456(21,M^+), 441(10), 366(38), 351(21), 343(10), 327(30), 129(100)	4
$C_{28}\Delta^{5,22}$	brassicasterol	470(59,M^+), 455(21), 380(60), 365(29), 341(50), 255(26), 129(100)	2
$C_{28}\Delta^{5,24(28)}$	24-methylenecholesterol	470(21,M^+), 455(19), 386(49), 365(18), 341(21), 296(19), 257(14), 129(100)	13
$C_{28}\Delta^{5}$	campesterol	472(46,M^+), 457(23), 382(82), 367(32), 343(69), 255(15), 129(100)	3
$C_{29}\Delta^{5,22}$	stigmasterol	484(88,M^+), 469(42), 394(42), 379(25), 355(45), 255(35), 129(100)	2
$C_{29}\Delta^{5}$	petrosterol [cyclopropyl]	484(53,M^+), 469(15), **394(60)**, 379(20), 355(36), 255(14), 129(100)	11
$C_{29}\Delta^{5}$	sitosterol	486(34,M^+), 471(14), 396(53), 381(25), 357(52), 255(16), 129(100)	23
$C_{30}\Delta^{5,22}$	24-isopropyl-22-dehydrocholesterol	498(29,M^+), 483(7), 408(29), 393(8), **365(58)**, 255(13), 129(100)	9
$C_{30}\Delta^{5}$	24-isopropylcholesterol	500(34,M^+), 485(11), 410(43), 395(19), 371(40), 255(7), 129(100)	13

***Petrosia (Strongylophora)* cf. *vansoesti* PC982**

Assignment	Name	m/z (relative abundance)	%
$C_{27}\Delta^{5,22}$	22(E/Z)-dehydrocholesterol	456(55,M^+), 441(15), 366(52), 352(27), 326(54), 255(44), 129(100)	3
$C_{27}\Delta^{5}$	cholesterol		<1
$C_{28}\Delta^{5,22}$	brassicasterol	470(24,M^+), 455(19), 380(38), 365(12), 341(44), 255(46), 129(100)	4
$C_{29}\Delta^{5}$	petrosterol [cyclopropyl]	484(38,M^+), 469(13), 394(48), 379(20), 355(45), 255(13), 129(100)	77
$C_{29}\Delta^{5}$	sitosterol	486(29,M^+), 471(12), 396(45), 381(20), 357(61), 255(9), 129(100)	15

***Petrosia crassa* #11**

Assignment	Name	m/z (relative abundance)	%
$C_{29}\Delta^{5,22}$	stigmasterol	484(20,M^+), 469(14), 394(47), 379(16), 355(11), 255(10), 129(100)	1
$C_{29}\Delta^{5}$	petrosterol [cyclopropyl]	484(48,M^+), 469(18), **394(93)**, 379(35), 355(68), 255(15), 129(100)	95
$C_{29}\Delta^{5}$	sitosterol	486(57,M^+), 471(26), 396(94), 381(43), 357(79), 255(21), 129(100)	4

***Petrosia crassa* #22**

Assignment	Name	m/z (relative abundance)	%
$C_{29}\Delta^{5,22}$	stigmasterol	484(28,M^+), 469(11), 394(44), 379(16), 355(21), 255(11), 129(100)	1
$C_{29}\Delta^{5}$	petrosterol [cyclopropyl]	484(57,M^+), 469(17), **394(99)**, 379(43), 355(86), 255(20), 129(100)	97
$C_{29}\Delta^{5}$	sitosterol	486(82,M^+), 471(36), 396(89), 381(44), 357(62), 255(31), 129(100)	2

***Pheronema carpenteri* BT12-809**

Assignment	Name	m/z (relative abundance)	%
$C_{26}\Delta^{0}$	24-norcholestanol	446(36,M^+), 431(100), 389(25), 356(36), 341(63), 305(25), 215(69)	1
$C_{27}\Delta^{5}$	cholesterol	458(48,M^+), 443(6), 368(97), 353(44), 329(54), 255(39), 129(100)	1
$C_{27}\Delta^{0}$	cholestanol	460(60,M^+), 445(100), 370(28), 355(59), 305(28), 215(89)	52
$C_{27}\Delta^{0}$	epi-cholestanol	460(63,M^+), 445(100), 403(33), 370(36), 355(50), 305(30), 215(87)	3
$C_{28}\Delta^{5}$	campesterol	472(29,M^+), 457(18), 382(72), 367(48), 343(92), 255(22), 129(100)	1
$C_{28}\Delta^{0}$	campestanol	474(68,M^+), 459(100), 417(30), 384(42), 369(55), 215(91)	19
$C_{29}\Delta^{5}$	sitosterol	486(34,M^+), 471(13), 396(79), 381(32), 357(59), 255(14), 129(100)	18
$C_{29}\Delta^{0}$	sitostanol	488(65,M^+), 473(82), 431(32), 398(42), 383(47), 305(25), 215(100)	5

$C_{30}\Delta^{5}$	24-*n*-propylcholesterol	500(45,M^+), 486(14), 410(63), 395(21), 371(87), 329(13), 255(17), 129(100)	2
$C_{30}\Delta^{0}$	24-*n*-propylcholestanol	502(48,M^+), 487(100), 445(43), 412(43), 397(65), 305(30), 215(64)	1

***Polymastia boletiformis* Roscoff#9**

Assignment	Name	m/z (relative abundance)	%
$C_{27}\Delta^{5,22}$	22(E/Z)-dehydrocholesterol	456(41,M^+), 441(10), 366(52), 351(24), 327(47), 255(50), 129(100)	2
$C_{27}\Delta^{5}$	cholesterol	458(51,M^+), 443(15), 368(82), 353(38), 329(89), 255(20), 129(100)	5
$C_{27}\Delta^{0}$	cholestanol	460(63,M^+), 445(100), 403(23), 370(33), 355(50), 305(33), 215(88)	26
$C_{28}\Delta^{5,22}$	brassicasterol	470(48,M^+), 455(12), 380(48), 365(21), 341(23), 255(38), 129(100)	9
$C_{28}\Delta^{5,24(28)}$	24-methylenecholesterol	470(17,M^+), 455(19), 386(49), 380(26), 365(23), 343(23), 296(25), 253(20), 129(100)	1
$C_{28}\Delta^{5}$	campesterol	472(45,M^+), 457(18), 382(84), 367(35), 343(84), 255(18), 129(100)	4
$C_{28}\Delta^{0}$	campestanol	474(70,M^+), 459(100), 417(28), 384(29), 369(53), 305(25), 215(85)	1
$C_{29}\Delta^{5,22}$	stigmasterol	484(39,M^+), 469(9), 394(33), 379(9), 355(17), 255(32), 129(100)	1
$C_{29}\Delta^{5}$	sitosterol	486(33,M^+), 471(13), 396(67), 381(30), 357(67), 255(15), 129(100)	40
$C_{29}\Delta^{5,24(28)}$	isofucosterol	484(5,M^+), 469(7), 386(83), 371(17), 355(7), 296(50), 257(23), 129(100)	11
$C_{30}\Delta^{5,24(28)}$	24-*n*-propylcholesterol	498(7,M^+), 483(13), 386(100), 371(14), 340(24), 296(71), 257(16), 129(59)	1

***Rhabdastrella globostellata* G313432**

Assignment	Name	m/z (relative abundance)	%
$C_{27}\Delta^{5,22}$	22(E/Z)-dehydrocholesterol		<1
$C_{27}\Delta^{5}$	cholesterol	458(49,M^+), 443(20), 368(73), 353(41), 329(92), 255(8), 129(100)	3
$C_{28}\Delta^{5,22}$	brassicasterol	470(46,M^+), 455(5), 380(44), 365(21), 341(23), 255(38), 129(100)	4
$C_{28}\Delta^{5,24}$	codisterol	470(63,M^+), 455(17), 380(56), 365(30), 341(23), 255(14), 129(100)	1
$C_{28}\Delta^{5}$	campesterol	472(52,M^+), 457(22), 382(83), 367(40), 343(87), 255(17), 129(100)	2
$C_{29}\Delta^{5,22}$	stigmasterol	484(43,M^+), 469(11), 394(43), 379(24), 351(15), 255(53), 129(100)	3
$C_{29}\Delta^{5,24(28)}$	24(28)-dehydroaplysterol	484(15,M^+), 469(15), 394(24), 386(61), 371(16), 355(24), 296(34), 253(17), 129(100)	80
$C_{30}\Delta^{5,25}$	stelliferasterol	498(45,M^+), 483(8), 408(34), 393(20), 369(14), 255(12), 129(100)	7
$C_{30}\Delta^{5,24(28)}$	isostelliferasterol		<1

***Rhabdastrella globostellata* G317580**

Assignment	Name	m/z (relative abundance)	%
$C_{27}\Delta^{5,22}$	22(E/Z)-dehydrocholesterol	456(59,M^+), 441(16), 366(68), 351(31), 327(55), 255(32), 129(100)	1
$C_{27}\Delta^{5}$	cholesterol	458(50,M^+), 443(17), 368(77), 353(41), 329(100), 255(16), 129(93)	3
$C_{28}\Delta^{5,22}$	brassicasterol	470(53,M^+), 455(9), 380(61), 365(21), 341(26), 255(50), 129(100)	5
$C_{28}\Delta^{5,24}$	codisterol	470(49,M^+), 455(18), 380(39), 365(26), 341(25), 255(11), 129(100)	1
$C_{28}\Delta^{5}$	campesterol	472(50,M^+), 457(8), 382(88), 367(31), 343(83), 255(13), 129(100)	1
$C_{29}\Delta^{5,22}$	stigmasterol	484(45,M^+), 469(11), 394(31), 379(10), 354(10), 255(36), 129(100)	1
$C_{29}\Delta^{5,24(28)}$	24(28)-dehydroaplysterol	484(14,M^+), 469(14), 394(29), 386(69), 371(17), 355(31), 296(38), 253(19), 129(100)	79
$C_{30}\Delta^{5,25}$	stelliferasterol	498(42,M^+), 483(12), 408(38), 393(15), 369(18), 255(10), 129(100)	8
$C_{30}\Delta^{5,24(28)}$	isostelliferasterol		<1

***Rhabdastrella globostellata* G321791**

Assignment	Name	m/z (relative abundance)	%
$C_{27}\Delta^{5,22}$	22(E/Z)-dehydrocholesterol	456(60,M^+), 441(12), 366(57), 351(23), 327(63), 255(55), 129(100)	2
$C_{27}\Delta^{5}$	cholesterol	458(52,M^+), 443(22), 368(82), 353(38), 329(92), 255(18), 129(100)	3
$C_{28}\Delta^{5,22}$	brassicasterol	470(18,M^+), 455(8), 380(48), 365(16), 341(24), 255(44), 129(100)	4
$C_{28}\Delta^{5,24}$	codisterol	470(73,M^+), 455(17), 380(40), 365(25), 341(31), 255(17), 129(100)	2
$C_{28}\Delta^{5}$	campesterol	472(73,M^+), 457(12), 382(88), 367(35), 343(97), 255(14), 129(100)	1
$C_{29}\Delta^{5,22}$	stigmasterol	484(28,M^+), 469(8), 394(30), 379(22), 354(22), 255(27), 129(100)	1
$C_{29}\Delta^{5,24(28)}$	24(28)-dehydroaplysterol	484(15,M^+), 469(15), 394(23), 386(62), 371(15), 355(27), 296(37), 253(17), 129(100)	83
$C_{30}\Delta^{5,25}$	stelliferasterol	498(47,M^+), 483(9), 408(39), 393(13), 369(17), 255(10), 129(100)	3
$C_{31}\Delta^{5,25(27)}$	26-methylstrongylosterol	512(17,M^+), 498(11), 422(40), 407(17), 383(30), 343(13), 255(13), 129(100)	2

***Rhabdastrella globostellata* PC922**

Assignment	Name	m/z (relative abundance)	%
$C_{27}\Delta^{5,22}$	22(E/Z)-dehydrocholesterol	456(45,M^+), 441(12), 429(15), 366(38), 351(23), 327(70), 255(34), 129(100)	1
$C_{27}\Delta^{5}$	cholesterol	458(29,M^+), 443(11), 368(60), 353(31), 329(77), 255(19), 129(100)	6
$C_{28}\Delta^{5,22}$	brassicasterol	470(35,M^+), 455(6), 380(43), 365(13), 341(14), 255(37), 129(100)	6

$C_{28}\Delta^{5,24}$	codisterol	470(35,M^+), 456(9), 380(49), 365(23), 340(15), 253(14), 129(100)	3
$C_{28}\Delta^{5}$	campesterol	472(21,M^+), 457(15), 382(62), 367(29), 343(61), 255(17), 129(100)	2
$C_{29}\Delta^{5,24(28)}$	24(28)-dehydroaplysterol	484(11,M^+), 469(12), 386(54), 371(11), 355(25), 296(28), 257(16), 129(100)	75
$C_{30}\Delta^{5,25}$	stelliferasterol	498(30,M^+), 483(6), 408(30), 400(7), 393(13), 368(15), 271(17), 255(13), 129(100)	5
$C_{31}\Delta^{5,25(27)}$	26-methylstrongylosterol	512(19,M^+), 498(14), 422(47), 407(15), 383(29), 325(17), 255(21), 129(100)	2

***Rhabdastrella globostellata* PC1143**

Assignment	Name	m/z (relative abundance)	%
$C_{27}\Delta^{5,22}$	22(E/Z)-dehydrocholesterol	456(42,M^+), 441(11), 366(57), 351(18), 327(45), 255(36), 129(100)	1
$C_{27}\Delta^{5}$	cholesterol	458(43,M^+), 443(20), 368(80), 353(39), 329(91), 255(16), 129(100)	3
$C_{28}\Delta^{5,22}$	brassicasterol	470(48,M^+), 455(8), 380(46), 365(22), 341(27), 255(43), 129(100)	3
$C_{28}\Delta^{5,24}$	codisterol	470(50,M^+), 456(11), 380(46), 365(21), 341(24), 255(13), 129(100)	1
$C_{28}\Delta^{5}$	campesterol	472(38,M^+), 457(17), 382(76), 367(34), 343(76), 255(14), 129(100)	1
$C_{29}\Delta^{5,22}$	stigmasterol	484(43,M^+), 469(5), 394(40), 379(16), 355(19), 255(37), 129(100)	1
$C_{29}\Delta^{5,24(28)}$	24(28)-dehydroaplysterol	484(15,M^+), 469(13), 386(72), 371(17), 355(33), 296(46), 257(22), 129(100)	85
$C_{30}\Delta^{5,25}$	stelliferasterol	498(40,M^+), 483(8), 408(40), 393(17), 369(20), 255(12), 129(100)	4
$C_{30}\Delta^{5,24(28)}$	isostelliferasterol		<1
$C_{31}\Delta^{5,25(27)}$	26-methylstrongylosterol	512(13,M^+), 498(10), 422(38), 407(18), 383(30), 343(14), 255(13), 129(100)	1

***Rhabdastrella globostellata* PC1144**

Assignment	Name	m/z (relative abundance)	%
$C_{27}\Delta^{5,22}$	22(E/Z)-dehydrocholesterol	456(42,M^+), 441(11), 366(57), 351(18), 327(45), 255(36), 129(100)	1
$C_{27}\Delta^{5}$	cholesterol	458(43,M^+), 443(20), 368(80), 353(39), 329(91), 255(16), 129(100)	3
$C_{28}\Delta^{5,22}$	brassicasterol	470(48,M^+), 455(8), 380(46), 365(22), 341(27), 255(43), 129(100)	4
$C_{28}\Delta^{5,24}$	codisterol	470(50,M^+), 456(11), 380(46), 365(21), 341(24), 255(13), 129(100)	2
$C_{28}\Delta^{5}$	campesterol	472(38,M^+), 457(17), 382(76), 367(34), 343(76), 255(14), 129(100)	1
$C_{29}\Delta^{5,22}$	stigmasterol	484(43,M^+), 469(5), 394(40), 379(16), 355(19), 255(37), 129(100)	1
$C_{29}\Delta^{5,24(28)}$	24(28)-dehydroaplysterol	484(15,M^+), 469(13), 386(72), 371(17), 355(33), 296(46), 257(22), 129(100)	76
$C_{30}\Delta^{5,25}$	stelliferasterol	498(40,M^+), 483(8), 408(40), 393(17), 369(20), 255(12), 129(100)	4

$C_{30}\Delta^{5,24(28)}$	isostelliferasterol		<1
$C_{31}\Delta^{5,25(27)}$	26-methylstrongylosterol	512(13,M^+), 498(10), 422(38), 407(18), 383(30), 343(14), 255(13), 129(100)	3

***Rhabdastrella globostellata* PC1145**

Assignment	Name	m/z (relative abundance)	%
$C_{27}\Delta^{5,22}$	22(E/Z)-dehydrocholesterol	456(42,M^+), 441(11), 366(57), 351(18), 327(45), 255(36), 129(100)	1
$C_{27}\Delta^{5}$	cholesterol	458(43,M^+), 443(20), 368(80), 353(39), 329(91), 255(16), 129(100)	2
$C_{28}\Delta^{5,22}$	brassicasterol	470(48,M^+), 455(8), 380(46), 365(22), 341(27), 255(43), 129(100)	3
$C_{28}\Delta^{5,24}$	codisterol	470(50,M^+), 456(11), 380(46), 365(21), 341(24), 255(13), 129(100)	2
$C_{28}\Delta^{5}$	campesterol	472(38,M^+), 457(17), 382(76), 367(34), 343(76), 255(14), 129(100)	1
$C_{29}\Delta^{5,22}$	stigmasterol	484(43,M^+), 469(5), 394(40), 379(16), 355(19), 255(37), 129(100)	1
$C_{29}\Delta^{5,24(28)}$	24(28)-dehydroaplysterol	484(15,M^+), 469(13), 386(72), 371(17), 355(33), 296(46), 257(22), 129(100)	79
$C_{30}\Delta^{5,25}$	stelliferasterol	498(40,M^+), 483(8), 408(40), 393(17), 369(20), 255(12), 129(100)	11
$C_{30}\Delta^{5,24(28)}$	isostelliferasterol		<1

***Rhabdastrella globostellata* NHM 31.8.4.38**

Assignment	Name	m/z (relative abundance)	%
$C_{27}\Delta^{5}$	cholesterol	458(48,M^+), 443(18), 368(66), 353(39), 329(100), 255(19), 129(83)	15
$C_{28}\Delta^{5,22}$	brassicasterol	470(47,M^+), 455(8), 380(49), 365(11), 341(33), 255(49), 129(100)	13
$C_{28}\Delta^{5}$	campesterol	472(38,M^+), 457(17), 382(68), 367(60), 343(100), 255(28), 129(100)	7
$C_{29}\Delta^{5,24(28)}$	24(28)-dehydroaplysterol	484(12,M^+), 469(14), 386(49), 371(17), 355(19), 296(24), 257(14), 129(100)	59
$C_{30}\Delta^{5,25(27)}$	durissimasterol	498(41,M^+), 482(21), 400(100), 386(33), 358(58), 250(65), 129(93)	7

***Rhabdastrella intermedia* PC399**

Assignment	Name	m/z (relative abundance)	%
$C_{27}\Delta^{5,22}$	22(E/Z)-dehydrocholesterol	456(32,M^+), 442(17), 366(64), 351(27), 327(67), 255(53), 129(100)	3
$C_{27}\Delta^{5}$	cholesterol	458(43,M^+), 443(21), 368(81), 353(53), 329(100), 255(21), 129(97)	8
$C_{28}\Delta^{5,22}$	brassicasterol	470(36,M^+), 455(14), 380(52), 365(23), 341(27), 255(53), 129(100)	7
$C_{28}\Delta^{5,24(28)}$	24-methylenecholesterol	470(18,M^+), 455(14), 386(51), 365(23), 341(34), 296(33), 257(21), 129(100)	25

$C_{28}\Delta^{5}$	campesterol	472(48,M^+), 457(12), 382(83), 367(24), 343(100), 255(17), 129(76)	1
$C_{29}\Delta^{5,22}$	stigmasterol	484(44,M^+), 469(13), 394(48), 379(18), 355(40), 255(58), 129(100)	2
$C_{29}\Delta^{5,24(28)}$	fucosterol	484(18,M^+), 469(8), 396(36), 386(52), 357(38), 296(29), 255(15), 129(100)	39
$C_{29}\Delta^{5,24(28)}$	isofucosterol	484(6,M^+), 469(6), 386(100), 371(14), 355(7), 296(62), 257(23), 129(98)	12
$C_{30}\Delta^{5,24(28)}$	24-*n*-propylcholesterol	498(14,M^+), 483(10), 386(100), 371(27), 344(15), **296(65)**, 257(37), 129(100)	1

***Stelletta normani* #12**

Assignment	Name	m/z (relative abundance)	%
$C_{28}\Delta^{5,24(28)}$	24-methylenecholesterol	470(17,M^+), 455(10), 386(25), 371(19), 341(18), 296(24), 257(23), 129(100)	82
$C_{29}\Delta^{5,24(28)}$	fucosterol	484(9,M^+), 469(5), 386(69), 355(19), 343(16), 296(50), 255(9), 129(100)	18

***Suberites ficus* Roscoff#6**

Assignment	Name	m/z (relative abundance)	%
$C_{27}\Delta^{22}$	22-dehydrocholestanol	458(33,M^+), 443(16), 374(41), 359(9), 345(26), 257(100), 217(17)	2
$C_{27}\Delta^{0}$	cholestanol	460(71,M^+), 445(100), 370(26), 355(49), 305(29), 215(97)	86
$C_{28}\Delta^{22}$	22-dehydrocampestanol	472(76,M^+), 457(24), 374(29), 359(12), 345(47), 257(100), 215(21)	2
$C_{28}\Delta^{24(28)}$	24-methylenecholestanol	472(9,M^+), 457(73), 388(100), 373(37), 345(49), 215(51)	4
$C_{28}\Delta^{0}$	campestanol	474(50,M^+), 459(59), 417(13), 384(24), 369(26), 305(21), 215(100)	1
$C_{29}\Delta^{0}$	sitostanol	488(50,M^+), 473(100), 431(20), 398(17), 383(39), 305(22), 215(98)	4

***Tethya aurantium* Roscoff#2**

Assignment	Name	m/z (relative abundance)	%
$C_{27}\Delta^{5,22}$	22(E/Z)-dehydrocholesterol	456(39,M^+), 442(17), 366(26), 351(17), 327(66), 255(37), 129(100)	4
$C_{27}\Delta^{5}$	cholesterol	458(62,M^+), 443(16), 368(75), 353(45), 329(100), 255(17), 129(100)	16
$C_{28}\Delta^{5,22}$	brassicasterol	470(56,M^+), 455(8), 380(30), 365(9), 341(17), 255(39), 129(100)	5
$C_{28}\Delta^{5,24(28)}$	24-methylenecholesterol	470(14,M^+), 455(20), 386(49), 365(22), 341(36), 296(27), 257(22), 129(100)	69
$C_{28}\Delta^{5}$	campesterol	472(63,M^+), 457(3), 382(52), 367(13), 343(53), 129(100)	1
$C_{29}\Delta^{5}$	sitosterol	486(61,M^+), 471(26), 396(28), 381(16), 357(41), 255(18), 129(100)	2
$C_{29}\Delta^{5,24(28)}$	isofucosterol	484(10,M^+), 469(16), 386(95), 371(13), 355(13), 296(33), 257(28), 129(100)	3

***Thymosiopsis conglomerans* #25914**

Assignment	Name	m/z (relative abundance)	%
$C_{27}\Delta^{5}$	cholesterol	458(35,M^+), 443(21), 368(70), 353(35), 329(70), 129(100)	4
$C_{29}\Delta^{5}$	sitosterol	486(35,M^+), 471(20), 396(56), 381(28), 357(56), 255(24), 129(100)	2
$C_{29}\Delta^{7}$	7-dehydrositostanol	486(100,M^+), 471(24), 396(7), 381(16), 345(8), 255(54), 213(27)	9
$C_{30}\Delta^{7,25(27)}$	thymosiosterol	498(13,M+), 483(22), 408(6), 393(10), 386(29), 343(100), 255(20), 213(19)	23
$C_{30}\Delta^{7}$	thymosiostanol	500(100,M+), 485(23), 410(7), 395(12), 345(9), 255(59), 213(27)	62
$C_{31}\Delta^{7,?}$	methyl-thymosiosterol		<1

***Topsentia ophiraphidites* 2-X-88-1-010**

Assignment	Name	m/z (relative abundance)	%
$C_{27}\Delta^{5}$	cholesterol		trace
$C_{28}\Delta^{5,22}$	brassicasterol		trace
$C_{28}\Delta^{5,24(28)}$	24-methylenecholesterol		trace
$C_{28}\Delta^{5}$	campesterol		trace
$C_{29}\Delta^{5,22}$	stigmasterol		<1
$C_{29}\Delta^{5}$	sitosterol	486(34,M^+), 471(14), 396(58), 381(31), 357(69), 255(14), 129(100)	2
$C_{30}\Delta^{5,22}$	24-isopropyl-22-dehydrocholesterol	498(41,M^+), 483(9), 408(30), 393(12), **365(100)**, 255(44), 129(72)	64
$C_{30}\Delta^{5}$	24-isopropylcholesterol	500(38,M^+), 485(12), 410(74), 395(35), 371(72), 255(15), 129(100)	34

***Topsentia ophiraphidites* 10-X-88-2-009**

Assignment	Name	m/z (relative abundance)	%
$C_{30}\Delta^{5,22}$	24-isopropyl-22-dehydrocholesterol	498(42,M^+), 483(13), 408(31), 393(14), **365(100)**, 255(45), 129(84)	28
$C_{30}\Delta^{5}$	24-isopropylcholesterol	500(45,M^+), 485(15), 410(87), 395(43), 371(86), 255(18), 129(100)	72

***Topsentia* sp PC1213**

Assignment	Name	m/z (relative abundance)	%
$C_{29}\Delta^{5,22}$	stigmasterol	484(56,M^+), 469(15), 394(33), 379(21), 355(22), 255(21), 129(100)	1
$C_{30}\Delta^{5,22}$	24-isopropyl-22-dehydrocholesterol	498(37,M^+), 483(8), 408(26), 393(11), **365(86)**, 255(36), 129(100)	47
$C_{30}\Delta^{5}$	24-isopropylcholesterol	500(37,M^+), 485(12), 410(68), 395(27), 371(54), 255(14), 129(100)	52

***Vazella pourtalesii* HUD16-019-B0362**

Assignment	Name	m/z (relative abundance)	%
$C_{26}\Delta^{0}$	24-norcholestanol	446(59,M+), 431(93), 389(27), 356(29), 341(47), 305(30), 215(100)	3
$C_{27}\Delta^{0}$	cholestanol	460(57,M+), 445(82), 403(27), 370(30), 355(55), 305(30), 215(100)	70
$C_{27}\Delta^{0}$	epi-cholestanol	460(58,M+), 445(85), 403(27), 370(29), 355(48), 305(29), 215(100)	3
$C_{28}\Delta^{0}$	campestanol	474(58,M+), 459(84), 417(26), 384(30), 369(56), 305(30), 215(100)	17
$C_{29}\Delta^{0}$	sitostanol	488(68,M+), 474(84), 431(28), 398(30), 383(50), 305(31), 215(100)	8
$C_{30}\Delta^{24(28)}$	24-*n*-propylcholestanol	500(11,M+), 485(10), 388(100), 373(33), 305(17), 215(33)	<1

***Verongula rigida* [sponge 8]**

Assignment	Name	m/z (relative abundance)	%
$C_{27}\Delta^{5}$	cholesterol	458(35,M+), 443(12), 368(66), 353(37), 329(86), 129(100)	7
$C_{28}\Delta^{5,22}$	brassicasterol	470(44,M+), 455(11), 380(51), 365(18), 341(36), 255(44), 129(100)	4
$C_{28}\Delta^{5,24}$	codisterol		<1
$C_{28}\Delta^{5}$	campesterol	472(21,M+), 457(13), 382(65), 367(16), 343(77), 255(24), 129(100)	3
$C_{29}\Delta^{5,25}$	25-dehydroaplysterol isomer	484(39,M+), 469(10), 394(29), 379(13), 356(16), 343(20), 129(100)	3
$C_{29}\Delta^{5,25}$	25-dehydroaplysterol	484(46,M+), 469(10), 394(36), 379(20), 355(21), 255(11), 129(100)	55
$C_{29}\Delta^{5}$	aplysterol	486(38,M+), 471(18), 396(83), 381(34), 357(79), 255(19), 129(100)	18
$C_{30}\Delta^{5,28(30)}$	24-isopropenylcholesterol	498(16,M+), 483(11), 408(11), 354(21), 343(19), 129(100)	1
$C_{30}\Delta^{5,25}$	verongulasterol	498(23,M+), 483(6), 408(33), 393(13), 369(17), 129(100)	8

***Weberella bursa* PA2013-008**

Assignment	Name	m/z (relative abundance)	%
$C_{27}\Delta^{5,22}$	22(E/Z)-dehydrocholesterol	456(50,M+), 441(13), 366(50), 351(35), 327(69), 255(50), 129(100)	3
$C_{27}\Delta^{5}$	cholesterol	458(42,M+), 443(15), 368(83), 353(42), 329(100), 255(28), 129(97)	2
$C_{27}\Delta^{0}$	cholestanol	460(63,M+), 445(80), 403(26), 370(27), 355(46), 305(29), 215(100)	44
$C_{28}\Delta^{5,22}$	brassicasterol	470(49,M+), 455(11), 380(60), 365(19), 341(34), 255(58), 129(100)	14
$C_{28}\Delta^{5,24(28)}$	24-methylenecholesterol	470(19,M+), 455(19), 386(66), 365(27), 341(30), 296(28), 257(23), 129(100)	3
$C_{28}\Delta^{24(28)}$	24-methylenecholestanol	472(28,M+), 457(32), 388(100), 367(29), 343(47), 255(29), 215(34), 129(53)	5
$C_{28}\Delta^{0}$	campestanol	474(73,M+), 459(100), 417(31), 384(33), 369(62), 306(35), 215(92)	6

$C_{29}\Delta^{5,22}$	stigmasterol	484(59,M+), 469(21), 394(59), 379(21), 351(33), 255(43), 129(100)	3
$C_{29}\Delta^{5}$	sitosterol	486(38,M+), 471(13), 396(77), 381(36), 357(83), 255(19), 129(100)	14
$C_{29}\Delta^{5,24(28)}$	isofucosterol	488(28,M+), 473(33), 386(90), 296(56), 257(35), 215(39), 129(100)	3
$C_{30}\Delta^{5,24(28)}$	24-*n*-propylcholesterol	498(9,M+), 483(7), 386(86), 371(21), 296(62), 281(68), 257(25), 129(100)	3